Consistent Dark Matter models for the Large Hadron Collider

Tunney, Patrick John

Awarding institution:
King's College London

Consistent Dark Matter Models for The Large Hadron Collider

by

Patrick John Tunney

as

A thesis presented for the degree of
Doctor of Philosophy

at

Department of Physics
King's College London
September 11, 2019

Contents

List of Figures

List of Tables

Acknowledgements

First of all I thank my parents, Gill and John, for sparking my early interest in science from a young age, by giving me many popular science books, and raising me to be curious about the world around me. I am grateful that I was lucky enough to have many great science teachers and lecturers over the years, who kept that interest going.

I thank my supervisor Malcolm who kept an eye on me, making sure I had things to do, and that I wasn't going mad. I thank John Ellis for somehow finding time to collaborate and check in with me. I am incredibly indebted to John Heal for imparting his endless wisdom relating to Pythia, making the first year of my PhD significantly less painful than it probably should have been. I am also thankful of Felix Kahlhoefer, Jose No, Jonathan Davis, and Karl Nordstrom, who as postdocs took a large role in mentoring me as well. In fact, I felt like I could approach any of them with any issue at any time. I am grateful to Rowena, Megan, Bonnie, Julia, Paul, James and Simone who keep everything running smoothly in the Physics department at KCL. I thank Tarso, David, Sreedevi, Ali, Thomas, James, Josu, Alex, Stephanie, Katia, Katy, Krzysiek, Dries, Marco, and all the other PhD students at KCL for the companionship along the way. Special condolences to Tarso for having to sit next to me for three years.

This thesis is dedicated to Elly, who has always been there to calm and reassure me when things weren't going well, and to give me confidence when things were going fine. Finally I thank my cat Otto for introducing many typesetting errors by sitting on my keyboard at the most inconvenient times.

Chapter 1

Introduction

The unexplained presence of a large component of invisible matter in our universe is a compelling mystery. This Dark Matter (DM) is needed to solve a number of puzzles on astrophysical and cosmological scales, and should be something exotic, something beyond the matter that we currently know about. A compelling answer to the DM puzzle is the idea that DM is a Weakly Interacting Massive Particle (WIMP), which is where the DM is an exotic particle that obtains its currently observed abundance by falling out of thermal equilibrium with the primordial plasma in the early universe. If the strength of the interaction is around the electroweak scale, then just the right abundance of DM is obtained. This gives a good motivation to search for GeV-TeV scale exotic particles that might make up all or part of the DM.

The Large Hadron Collider (LHC) is a machine purpose built to find new particles in this energy range. Therefore, it is inevitable to want to search for DM at the LHC, and a large number of competing theories are on the market which allow us to do so. In this thesis we will be studying consistent models for DM at the LHC. As we will explain, starting from model-independent Effective Field Theories (EFTs) of DM interactions, a framework of simplified models has been built up. We will explore the constraints LHC data impose on these simplified models, propose more consistent theories, examine the parameter space of these UV-completions, and propose a new LHC search based on an extended version of a simplified model.

The layout of this thesis is therefore as follows. In the following sections we will summarise the various evidence for DM, before describing competing candidates,

including DM EFTs and simplified models. We will then detail the calculation of thermal freeze-out which enumerates how much of the DM budget a particular candidate can account for. Then, we describe searches for DM and exotic particles at the LHC, before including a brief mention of direct and indirect detection experiments.

The subsequent chapters are based on the Refs. [1–4] of which I am an author. In Chapter 2 we will look at a combination of dijet resonance searches to place bounds on spin-one exotic particles, before applying these constraints to a simplified model at the same time as including information coming from the relic density of DM. In Chapter 3 we continue looking at the spin-one simplified models, but from a theoretical perspective. We propose extensions of these models that are free of gauge anomalies, and investigate the conventional constraints that apply to these models in Chapter 4. In contrast, in Chapter 5 we look at a different simplified model, namely one with a pseudoscalar mediator between the SM and the DM. Here we take an already proposed UV completion, which enables the theory to be fully gauge-invariant, and use this theory to propose a new search channel that can be used by the LHC collaborations to discover this kind of portal to DM. Finally, in Chapter 6 we offer some conclusions and comments on possible future directions.

1.1 Evidence for dark matter

We will start with the astronomer Fritz Zwicky, although he was not the first to use the phrase 'Dark Matter' (DM), which had already been used for some time by the community in order to refer to matter that is simply too faint to be picked up by telescopes (for a summary of the history of DM, see [26]). Zwicky, in 1933, famously studied the velocity dispersion of galaxies in the Coma cluster. In fact, Edwin Hubble and Milton Humason had already noticed this velocity dispersion to be large in their work [5] but Zwicky took their results and proceeded to use the virial theorem to estimate the expected velocity dispersion [6, 7]. He found that the expected result (based on number of galaxies, estimate for an average galaxy mass, and so on) to be around 80 km/s, much smaller than the observed 1000 km/s. He reached the conclusion:

> *"If this would be confirmed, we would get the surprising result that dark*

matter is present in much greater amount than luminous matter."

It is worth emphasising again, at this time, DM was thought of as conventional matter that lacked enough luminosity to be detected: dead stars, planets, gas, dust, etc. These explanations are commonly referred to as baryonic dark matter in the present day, and we will see later that these candidates are ruled out by experiment, such as the measurement of the primordial light element abundances. Also, the presence of invisible mass in galaxies or galaxy clusters had not been conclusively established yet.

In the 1970s, the presence of missing matter in galaxies started to become established. For some, the most convincing initial evidence was the rotational velocity curves of galaxies, which show the variation in the velocity of stars in the galaxy as you move further away from the galactic centre. One of the most well known papers is that by Rubin et al. [8], who measured the rotational velocity curve of the Andromeda galaxy (M31), providing some of the first high quality data at large radii. This sparked a series of papers (see [26] for the complete story) including a summary of the rotational curves of three galaxies: M31, M81, and M101 by Roberts et al. [9] which we display in Figure 1.1.

Assuming the rotational velocities to be explained by the visible matter present in the galaxy, one would expect from basic Newtonian physics that the velocity scales as

$$v(r) = \sqrt{\frac{GM(r)}{r}}\,, \tag{1.1}$$

such that beyond the visible extent of the galaxy the quantity $M(r)$ (which is the mass contained the the sphere of radius r) approaches the total mass of the galaxy at large r. Therefore one would expect the velocity to fall as $v(r) \propto r^{-1/2}$. Instead what we observe in Figure 1.1 is that the rotation curves are approximately flat far from the galactic centre. An additional component of mass with $M(r) \propto r$ is required to explain this discrepancy, which is what is now commonly referred to as dark matter.

Again, at this time the community was not thinking of any new particle to make up the dark matter, instead DM was thought to be conventional but unseen matter. What the rotation curves in the 1970s did was to establish the presence of this component much more definitively, since the earlier conclusions of Zwicky had not become widely accepted due to a number of technical counter arguments [26]. The work of Rubin and other scientists, then, had arguably convinced a large

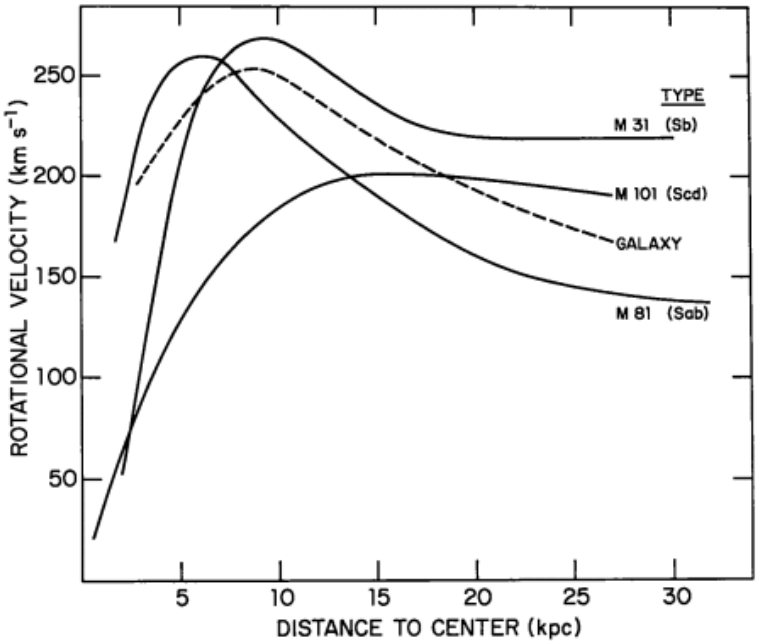

Figure 1.1: *The rotation curves of three galaxies (solid) compared to our own (dashed). The rotational velocity is shown as a function of the distance to the galactic centre. The flattish nature of the curves at large radii is an indication of additional unseen mass in the system. From ref. [9].*

portion of the community that there was a large invisible component making up the total mass of galaxies.

The evidence that DM was not baryonic came later, and came from two important sources: microlensing and the primordial element abundances. A leading hypothesis at the time was that DM was made up of Massive Astrophysical Compact Halo objects (MACHOs) which is a catch all phrase for objects similar to stars but less luminous, for example: planets, brown dwarfs, neutron stars, and black holes. Microlensing [10, 11] is a form of gravitational lensing where a single star can be enough to create a small lensing effect, as opposed to an entire ring of stars.

In 2000 the MACHO collaboration released a large data-set based on looking for microlensing events for 5 years in the Large Magellanic Cloud (LMC). Although they found a total number of events in excess to the expected background amount, they found that only 8% to 50% of the halo could be made up of MACHOs (at 95% CL) [12]. This put some pressure on the idea that MACHOs make up all of the DM, and additional results from the EROS collaboration [13] eventually, in

2006, set new limits on the mass fraction of MACHOs in the halo such that they can make up no more than 8% of the DM in the galaxy (at 95% CL) [14].

Another important indicator of the non-baryonic nature of DM came from cosmological measurements of the primordial light element abundances. According to the modern theory of Big Bang Nucleosynthesis (BBN) [15–17], one can predict the abundances of primordial Hydrogen and Helium, reaching the conclusion that they should be produced in the proportions 75% to 25% respectively, with a small amount (0.01%) of Deuterium.[1] Deuterium is particularly important since it cannot be produced in stars and so must solely be a product of BBN. This line of reasoning along with the measurements of the primordial element abundances can be used to place a bound on how much of the universe is composed of baryons. For example, one measurement in 2000 found the baryonic density to be only $\Omega_b h^2 = 0.0189 \pm 0.0019$ [18], which is not enough to explain the total matter density when combined with other observations.

In addition to Zwicky's evidence for DM coming from the Coma cluster, we must mention an additional galaxy cluster commonly known as the bullet cluster [19]. This cluster is a particularly clear piece of evidence for the presence of non-baryonic dark matter in galaxies. The bullet cluster shows two clusters of galaxies that have just collided, see Fig. 1.2. After the collision, when the images were taken, one can see that the X-ray pictures of the clusters are lagging behind the images of the clusters obtained via gravitational lensing. This means that the plasma within each cluster (which is responsible for the majority of the visible mass of a cluster, with stellar matter being a sub-dominant component) is not responsible for the majority of the mass of each cluster, giving us the conclusion that the baryons in these clusters of galaxies are not tracing the full mass distribution. Additionally, unlike the plasma components of each cluster which have collided with each other (causing them to lag behind the total mass component), the dark matter halos seem to have mainly passed through each other which can be used to set a limit on the self-interaction strength of DM.

Initially the WMAP collaboration [20], and later the Planck collaboration [21] measured with good precision the dark matter, baryonic and total matter density in the universe.[2] This was done by measuring the small anisotropies (at the level

[1] Elements heavier than Lithium are unable to be produced in BBN in any significant quantity due to a bottleneck since no stable nucleons exist with 5 or 8 nucleons.

[2] The measurements of the primordial element abundances mentioned earlier offer an inde-

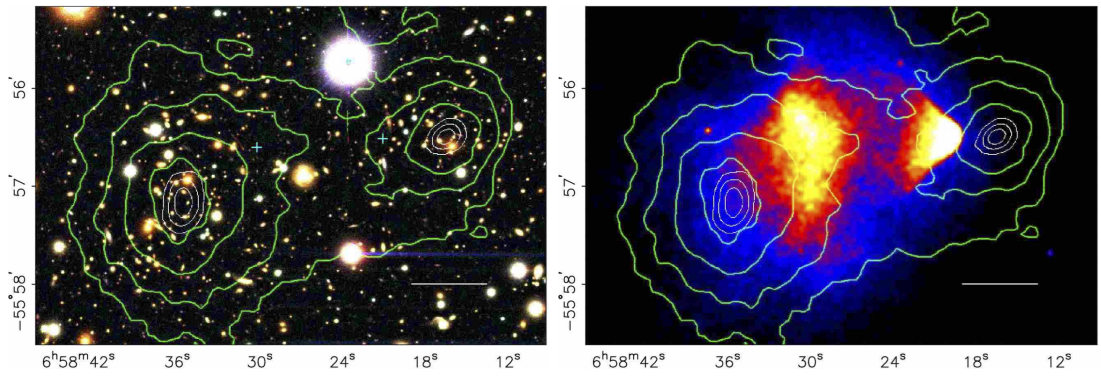

Figure 1.2: *Left: Optical picture of the bullet cluster. Right: X-ray image of the cluster, tracing the plasma within each cluster, is represented by the colour scale. In both pictures the contours of the mass distribution obtained from gravitational lensing are shown as green lines. The straight white line shows a distance of 200 kpc within the cluster. From [19].*

of 10^{-5} K) of the Cosmic Microwave Background (CMB) which is the largely uniform (temperature 2.7 K) background component of photons that have been free-streaming through the universe after decoupling from the matter-radiation plasma (this point in the early universe is called the last scattering surface). Density fluctuations undergo acoustic oscillation within this plasma, due to the opposite effects of gravitational attraction and radiation pressure. Different modes of oscillation, which are originally seeded by quantum fluctuations during inflation, enter the horizon (at superhorizon scales their evolution is frozen to a constant value) and take part in a certain number of oscillations before the photons decouple from the plasma. The first peak in the CMB power spectrum (see Fig. 1.3) corresponds to a characteristic scale whereby the mode undergoes just one half-cycle of oscillation, with later peaks corresponding to more half cycles. The power spectrum is sensitive to various cosmological parameters – in particular the ratio of the odd and even peaks are set by the baryonic density. The total mass density can be inferred from the amplitude of the peaks, and the Planck collaboration deduce from the fit to their most recent data [21] that:

$$\Omega_b h^2 = 0.0224 \pm 0.0001\,, \tag{1.2}$$

$$\Omega_c h^2 = 0.120 \pm 0.001\,, \tag{1.3}$$

pendent test of the baryonic density.

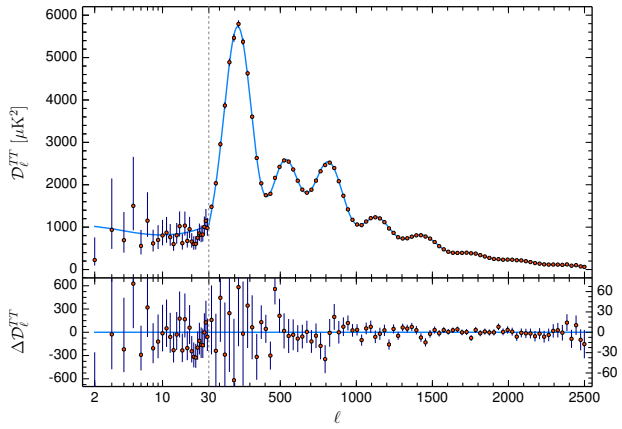

Figure 1.3: *Measurements of the CMB temperature fluctuations by the Planck collaboration, from the recent 2018 results. Qualitatively speaking, the horizontal axis represents multipole, similar to wavenumber, where a higher multipole corresponds to a smaller physical scale. The verticle axis represents the intensity of the temperature fluctuations away from the average 2.7 K. From [21].*

for the baryonic and cold dark matter densities respectively. This is perhaps the most clear evidence that DM in the universe outnumbers conventional matter by a factor of 5.

The final piece of evidence for dark matter comes from looking at the large scale structure of the universe. Galaxies in our universe are arranged into clusters, and the clusters themselves are organised along filaments of the cosmic web, with large voids in between. The filaments have an over-density of matter, while the voids have an under-density, and the pattern of filaments and voids is what we refer to as Large Scale Structure (LSS). In order to make predictions as to how dark matter seeds structure, we rely on computer simulations which are then compared to data. Taking just one example, the Millenium simulation [22] can be compared to data from the 2DFGRS collaboration [23], showing good agreement.

1.2 Candidates for dark matter

Having already explained how MACHOs and other baryonic candidates for DM are ruled out, in this section we will discuss some ideas that have been proposed to explain what DM is. We will start with the case of the SM neutrino and explain why it fails to be a good DM candidate since it is classed as hot dark matter. We

will move on to discuss the most popular candidate: Weakly Interacting Massive Particles (WIMPs) in more detail, including supersymmetry, effective field theories and simplified models. We will then finish our discussion of DM candidates with brief mentions of the axion, modified gravity and primordial black holes.

Neutrinos

The first naive candidate for DM that one could imagine is the only stable, neutral and massive particle in the Standard Model (SM): the neutrino. Unfortunately neutrinos are ruled out as DM candidates for two reasons, the first is that they simply do not make up enough of the universe's energy density to be all of the DM, and secondly they fall into a class of DM candidates now known to be unviable – hot dark matter. Firstly, it can be shown that the neutrino relic density is

$$\Omega_\nu h^2 = \frac{1}{93 \text{ eV}} \sum_i m_{\nu,i} \ , \tag{1.4}$$

and using the best laboratory limit on the neutrino mass from the Troitsk collaboration [28], $m_\nu < 2.05$ eV (95% CL), one concludes that $\Omega_\nu h^2 < 0.065$. One can obtain significantly stronger constraints from cosmology, although they assume the standard ΛCDM model.

For the second point, DM candidates can be divided into two classes: hot and cold dark matter.[3] Hot dark matter is relativistic at the time of structure formation, whereas cold dark matter is non-relativistic. We know from N-body simulations [22, 24] that cold dark matter seeds small structures first (via gravitational collapse) before merging to form larger structures. Conversely, hot dark matter has a larger free streaming length, meaning it will travel further before forming gravitationally bound structures. Therefore hot dark matter does not form structure on small scales, and since structure has been observed on these scales (by LSS surveys [23, 25]), hot dark matter candidates like the neutrino are essentially ruled out.

[3] An in-between case, warm dark matter, which is sometimes invoked to solve hotly debated core-cusp problems related to the density profile in the centre of DM halos. While we are mentioning this issue, let us comment that self-interacting DM (where the self-interaction strength does not come into conflict with limits from the Bullet cluster) has also been suggested to resolve this potential problem. However, both of these types of DM will not be mentioned again, since we will stick to the conventional paradigm of cold, non-self-interacting DM in the remainder of this thesis.

WIMPs

Weakly Interacting Massive Particles (WIMPs) have no unique definition. It was noted that one can obtain the observed abundance (relic density) of DM in the universe today by hypothesising that dark matter interacts with the standard model through some interaction strength similar to the electroweak force. The mechanism responsible for this is called thermal freeze-out and will be discussed in more detail in subsection 1.3. The observation that the relic density of DM can be obtained in this way, often called the WIMP miracle, provides dark matter candidates heavier than roughly 1 keV [34,35] in order to ensure the DM candidate is cold,[4] washing out small scale structure. There is also an upper limit on the WIMP mass coming from unitarity arguments [33]. Arbitrarily increasing the DM mass decreases the cross section, increases the relic density, and since the relic density of DM must be less than its observed value[5], the DM mass must be less than 100 TeV or so. In order to obtain the correct relic abundance the thermally averaged annihilation cross section should be roughly $\langle \sigma v \rangle \approx 3 \times 10^{-26}$ cm^3 s^{-1}, where v is the relative velocity of the annihilating DM particles.

As such, definitions of WIMPs range through a DM particle with mass in the range 1 keV [34,35] to 100 TeV [33], any particle that gets some of its relic abundance through freeze-out, a DM particle that interacts with the SM through the weak interaction, or a theory of DM with particle masses at the electroweak scale, approximately 10 GeV to 1 TeV. We will summarise a few WIMP candidates in this subsection, starting with the traditional example of SUSY particles, before describing the more model independent EFTs, their pitfalls, and the evolution towards simplified models of DM. We will then mention very briefly sterile neutrinos and extra dimensions (for a more comprehensive overview of particle DM candidates, see for example [27]).

[4] For a DM mass in the 1-100 keV scale, one would in principle need to check limits coming from small scale structure. Since we will be considering GeV-TeV scale DM in this thesis, we are guaranteed to have a cold DM candidate. Such limits can come from the Lyman-α forest, see e.g. [34,35].

[5] In the original paper [33], only $\Omega_c h^2 < 1$ is required which gives an upper bound of 340 TeV on any DM candidate. Updating this to $\Omega_c h^2 < 0.1$ makes the bound on the DM mass stronger by a factor of $\sqrt{10}$

SUSY

Supersymmetry (SUSY) is a postulated new symmetry of nature that extends the Poincaré group[6] to include additional generators, unifying fermions and bosons [36–39]. Rather than being a specific theory, it should be thought of more as a framework that contains many different theories. SUSY is of particular theoretical interest since if it exists around the electroweak scale then it can help solve the hierarchy problem related to the mass of the Higgs boson.

The hierarchy problem is a well-known fine tuning problem within our current understanding of the SM as a Quantum Field Theory (QFT). When one computes quantum corrections to the Higgs mass, one finds a quadratic divergence: such corrections should be generically proportional to the heaviest scale in the theory, and if this scale is taken to be a new physics scale such as the Planck scale, the corrections would be significantly larger than the measured Higgs mass. A huge conspiracy between different terms in the corrections to the Higgs mass (and its bare value) would be needed in order to cancel huge numbers against one another to obtain a very small value, the measured value of the Higgs mass. In SUSY the bosonic and fermionic corrections always cancel out, solving the hierarchy problem.

In addition to solving the hierarchy problem, SUSY can also help with the problem of gauge unification. Assuming only the standard model, and running its couplings up to a high scale,[7] the gauge couplings do not quite unify. Conversely, with SUSY, the gauge couplings all meet at one energy, helping the viability of Grand Unified Theories (GUTs).

Finally, and of most interest to us, SUSY can provide dark matter candidates (see [40, 41] for some early discussion of SUSY particles as cosmological relics). We will comment on one theory based on the framework of SUSY: the Minimal Supersymmetric Standard Model (MSSM) [42]. This is based on $\mathcal{N} = 1$ SUSY, where $\mathcal{N}$ is the number of fermionic generators in the symmetry group.[8] It is also minimal in the sense that the minimum number of additional fields are added to the SM, one for each fermion field, with an additional Higgs doublet included

[6] The Poincaré group is the symmetry of space-time, the symmetry group of special relativity: the group containing all Lorentz transformations and boosts.

[7] This is known as the GUT scale, a very high energy scale $\Lambda_{\mathrm{GUT}} \approx 10^{16}$ GeV, a few orders of magnitude below the Planck scale, $\Lambda_{\mathrm{Pl}} \approx 10^{19}$ GeV, which is the energy regime where quantum gravity becomes important.

[8] The bosonic generators are the standard generators of the Poincaré group.

which is necessary for anomaly cancellation.

Within the MSSM, an additional symmetry called R-parity is normally imposed. This was originally needed to avoid the violation of baryon and lepton number, which would allow the proton to decay unacceptably fast. R parity takes on the value

$$P_R \equiv (-1)^{2s+3B+L} \,, \tag{1.5}$$

for s the spin of the particle, B its baryon number and L its lepton number. The SM particles then all have $P_R = +1$ whereas the superparticles have $P_R = -1$. As a consequence superparticles can only be produced in pairs, and it is this R-parity that stabilises the DM candidates in the MSSM.

Potential DM candidates in the MSSM are the sneutrinos, the gravitino and the lightest neutralino (the neutralinos are the superpartners of the neutral gauge bosons: $\tilde{B}$, $\tilde{W}^3$, $\tilde{H}_1$ and $\tilde{H}_2$, denoting the bino, the neutral wino and the two higgsinos). The lightest neutralino, often denoted χ, is the most widely studied candidate, being a prototypical WIMP.

EFTs

Since SUSY is only one specific theory, there has recently been some interest in formulating more model independent frameworks for characterising particle DM and its interactions with the SM. Motivated in part by direct detection experiments[9] which operate in a very low energy environment, a complete set of effective operators for fermionic DM has been written down [43, 44], with this set of operators forming what we call an Effective Field Theory (EFT).

Conceptually speaking, an EFT Lagrangian has the form

$$\mathcal{L}_{\text{EFT}} = \sum_{i,j} \frac{c_{i,j}}{\Lambda^2} \bar{\chi}\, \mathcal{O}_{i,\,\mu}\, \chi \bar{q}\, \mathcal{O}_j^{\mu}\, q \,, \tag{1.6}$$

where we have taken the example of a DM fermion χ interacting with the SM quarks q, but the extension to DM particles with different spin and/or interactions with other SM particles is straightforward. $\mathcal{O}_i^{\mu} = 1, \gamma^{\mu}, \gamma^{\mu}\gamma^5$, etc. Note that since we are always use fermionic DM in this thesis, we can safely assume that dimension 5 terms are absent[10]. We also ignore operators with dimension greater

[9] We will summarise the methods of direct and indirect detection in Section 1.5.

[10] A term like $\bar{\chi}\chi H^{\dagger}H$ is dimension 5 but is essentially irrelevant for phenomenology.

than 6, since they come with additional powers of Λ, and so are expected to have a sub-leading effect.

EFT interactions are generically created when one integrates out heavy degrees of freedom (such as new mediating particles) that are only relevant at high energy scales, to create a low energy effective Lagrangian such as the one in Eq. (1.6). One then has the necessary interactions to describe all relevant phenomena in the low-energy experiment of interest. This prescription will work as long as the experiment is operating at an energy scale well below the cut-off Λ of the theory. If one tried to use the EFT to predict quantities at a higher energy scale, one would run into trouble. The cut-off Λ can also be thought of as the scale of the additional UV physics (such as that heavy mediating particle) that needs to be included in the theory for calculations to be reliable at energy scales higher than Λ.

While EFTs are fully model independent if we are guaranteed to be below the (unknown) cut-off scale Λ and if all effective operators are considered simultaneously, in high energy environments like the LHC we are at risk of the EFT losing validity unless we specify additional degrees of freedom, which we will discuss more below. For this reason, we will not consider EFTs for the rest of this thesis,[11] although for the case of direct detection experiments they are still important since the energy scale is so low it is guaranteed to be below the cut-off. As such we will use the dictionary provided in [45] to map our relativistic theory onto the non-relativistic operators relevant for direct detection [43, 44].

Simplified Models

As we have already hinted above, the EFT approach has limitations for energies above its cut-off scale, as explored in detail in [52–54]. In particular, [53] examines a monojet analysis from the LHC and compares the results of using an EFT with a so-called simplified model where the mediator is explicitly present in the Lagrangian. We will summarise some of their results here in order to provide justification for the adoption of simplified models over EFTs, before defining the four main simplified models that are currently used by the ATLAS and CMS collaborations.

[11] For a few examples of the earlier studies based on EFTs see [46–49]. See also [50, 51].

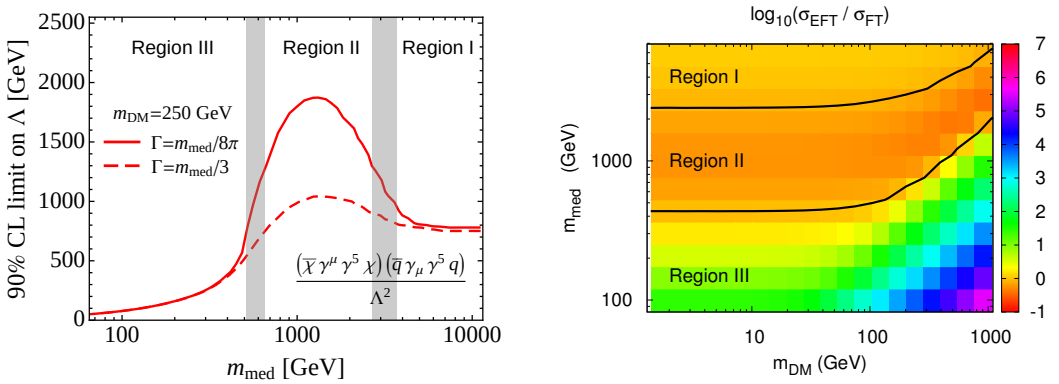

Figure 1.4: *From [53], analysis based on the CMS monojet searches [55, 56]. Left: Limit on Λ (defined in Eq. (1.9)) for the simplified model. Right: ratio of EFT to simplified model cross sections. The authors of [53] identify three regions, which we summarise in the main text.*

They compare an effective operator of the form

$$\mathcal{L}_{\text{EFT}} = \frac{1}{\Lambda^2}\bar{\chi}\gamma_\mu\gamma^5\chi\,\bar{q}\gamma^\mu\gamma^5 q\,, \tag{1.7}$$

with a simplified model

$$\mathcal{L}_{\text{AV}} = -g_\chi Z'_\mu\bar{\chi}\gamma^\mu\gamma^5\chi - g_q Z'_\mu\sum_q \bar{q}\gamma^\mu\gamma^5 q\,, \tag{1.8}$$

which is called the axial vector simplified model. In the Lagrangians above we have specified only the interaction terms and ignored the mass and kinetic terms. For the purpose of matching to the EFT

$$\Lambda \equiv \frac{m_{\text{med}}}{\sqrt{g_q g_\chi}}\,, \tag{1.9}$$

where m_{med} is the mass of Z'. Figure 1.4 shows some of the results of [53], in particular the right panel shows the ratio of the EFT cross section to the simplified model, with the authors identifying three separate regions:

Region I: Heavy mediator, EFT limit applies. Expanding the propagator in powers of $\frac{Q^2}{m^2_{\text{med}}}$

$$\frac{g_q g_\chi}{Q^2 - m^2_{\text{med}}} \approx -\frac{g_q g_\chi}{m^2_{\text{med}}}\left(1 + \frac{Q^2}{m^2_{\text{med}}} + ...\right)\,, \tag{1.10}$$

in this region the momentum transfer, Q, satisfies $Q^2 \ll m_{\text{med}}^2$ such that only the first term in the expansion above is needed, which is the EFT interaction. As such, the EFT limit is accurate here, agreeing with the simplified model.

Region II: Resonant enhancement, EFT limit too weak. In this region the mediator can be produced on-shell, giving the cross-section a resonant enhancement. This effect is not captured in the EFT, so it gives a limit that is too conservative. The left panel of Fig. 1.4 shows the resulting enhancement in the limit for region II. As would be expected, narrower resonances give a greater enhancement.

Region III: Light mediator, EFT limit too strong. In this region the light mediator causes the missing energy distribution to be softer. Therefore the missing energy cut in the CMS analysis reduces the number of simplified model events passing the cut relative to those from the EFT. As such the EFT overestimates the monojet cross section, giving a limit that is too strong.

The issues discussed above from [53], in addition to the problems highlighted in studies initially focussing on scalar mediators [52] (later extended to all s-channel interactions [54]), as well as indications of the breakdown of perturbative unitarity [57–59] led the community to adopt simplified models as the main framework for analysing DM searches at the LHC. In addition, simplified models serve as useful benchmarks that can be used to compare results coming from direct and indirect detection experiments. This was summarised in various white papers [60–64], with four s-channel simplified models emerging:

$$\mathcal{L}_S = g_q\,\phi \sum_q y_q\,\bar{q}q + g_\chi\,\phi\,\chi\bar{\chi}\,, \tag{1.11}$$

$$\mathcal{L}_P = g_q\,\phi \sum_q y_q\,\bar{q}\gamma^5 q + g_\chi\,\phi\,\chi\gamma^5\bar{\chi}\,, \tag{1.12}$$

$$\mathcal{L}_V = g_q\,Z'_\mu \sum_q \bar{q}\gamma^\mu q + g_\chi\,Z'_\mu\,\chi\gamma^\mu\bar{\chi}\,, \tag{1.13}$$

$$\mathcal{L}_{AV} = g_q\,Z'_\mu \sum_q \bar{q}\gamma^\mu\gamma^5 q + g_\chi\,Z'_\mu\,\chi\gamma^\mu\gamma^5\bar{\chi}\,, \tag{1.14}$$

known as the scalar, pseudoscalar, vector and axial-vector simplified models respectively. ϕ is a spin-zero scalar mediator whereas Z' is a spin-one vector mediator, χ is a DM fermion and q is a SM quark. Furthermore these models are known as s-channel models since when considering the characteristic monojet signature

at the LHC, the mediator is produced in the s-channel. In the spin-0 mediated models the coupling to a particular quark is assumed to be proportional to the respective yukawa coupling y_q of that quark. This is a sufficient although not necessary condition consistent with the hypothesis of Minimal Flavour Violation (MFV) [65] that allows the models to avoid generating dangerously large Flavour Changing Neutral Currents (FCNCs).

Clearly, these 4 simplified models do not encompass all possible dimension-4 Lagrangians. In particular, couplings to additional SM particles, mixtures of vector/axial couplings, generation-dependent couplings, additional dark sector particles, and t-channel interactions are ignored, to name just a few possibilities. Therefore a clear disadvantage of using simplified models already presents itself: they suffer from a higher degree of model specificity than EFTs, with it being possible to write down a huge number of simplified models. Additionally, EFTs contain as few as 2 free parameters (the coupling or cut-off scale Λ and the DM mass) whereas simplified models contain at least 4 (the coupling of the mediator to SM particles, the coupling of the mediator to DM, the mass of the mediator and the mass of the DM particle).

On the other hand, simplified models enjoy at least two significant benefits over EFTs: they provide reliable calculations above the (*a priori* unknown) cut-off scale, as well as giving a more rich and diverse phenomenology. The first advantage is clear from the discussion above, while the latter is an direct consequence of having additional dynamical particles in the theory. For example, the simplified models in Eqs. (1.11)–(1.14) give rise to resonant dijet signatures at the LHC, which are complementary to the more traditional monojet searches (more detail on LHC searches for DM will be given in Section 1.4). In fact, dijet searches will be the subject of Chapter 2 where a detailed analysis will take place based on a combination of data sets, using a simplified model that is a mixture of the conventional vector and axial vector models mentioned above.

We have already commented that the models defined above in Eqs. (1.11)–(1.14) do not represent the most general Lagrangian. In particular, a coupling to leptons is mysteriously absent, and there is also the question of whether the Lagrangians are fully gauge-invariant. We will investigate these issues in Chapter 3 for a generic spin-one mediator, and investigate the constraints on these Z' like models in Chapter 4. The quest for gauge-invariance continues in Chapter 5 where we use a more UV complete version of the pseudoscalar model, Eq. (1.12),

to propose a new search for the LHC to perform in the future. This summarises the main use of simplified models in this thesis, for a limited selection of studies involving simplified models or Z's, see [136–150, 152, 153, 158–161, 179]

We will also go beyond the simplified model framework in order to discuss consistent simplified models. We define consistency from the requirements of gauge invariance and renormalisability, such that the Lagrangian should be written down from gauge-invariant combinations of fields and that gauge-anomalies should cancel.[12] In the case of a theory with a spin-one massive Z' boson, a fully gauge-invariant theory also needs a mechanism to break the $U(1)'$ gauge symmetry and give mass to the Z' boson. Such a mechanism can be provided by an additional exotic scalar singlet, a dark Higgs, the implications of which will not be investigated in this thesis since this has been extensively investigated in previous works [169, 170, 213]

Sterile Neutrinos

We saw above that the SM neutrinos cannot be a good dark matter candidate since they would constitute hot dark matter. However, the SM does not explain how neutrino masses arise, and in addition it seems somewhat mysterious that there is a left and right-handed field for every species apart from the neutrino. The SM as such contains only a left-handed neutrino, but a hypothetical right-handed neutrino could exist. Such a particle is usually called a sterile neutrino since it is a singlet of the SM gauge group and so has no interactions with the SM particles apart from those which arise via mixing. Sterile neutrinos can constitute the DM [66–69] and depending on their mass they can either constitute warm or cold dark matter. In contrast to most other WIMPs, their interactions with the SM are so feeble that they were never in thermal equilibrium in the early universe, and so their abundance is obtained through the oscillation of other neutrino species.

Extra dimensions

Building on the initial work of Kaluza and Klein, extra-dimensional theories have been proposed in order to solve the hierarchy problem, and often the lightest excitation in such theories is a viable DM candidate. In most extra-dimensional

[12] Note in Chapter 2 we only analyse a simplified model, so these requirements will only be applied from Chapter 3 onwards.

theories, the 3+1 dimensional spacetime we live in is referred to as the brane, whereas the larger 3+δ+1 spacetime is called the bulk, with δ the number of additional spatial dimensions. The Arkani-Hamed, Dimopoulos and Dvali (ADD) proposal [70] postulates that the compactification of these extra dimensions (flat extra dimensions) within a topology (e.g. a circle) with scale R brings the Planck scale down to the electroweak scale. An alternative proposal is the Randall-Sundrum (RS) scenario [71] which introduces warped extra dimensions, where the large curvature in the extra dimensions solves the hierarchy problem.

A generic feature of these theories are the existence of Kaluza-Klein (KK) excitations which arise from decomposing Fourier modes in the compact extra dimensions. The mass of each mode is $M_n = \frac{n}{R}$ where n is the mode number and R is the size of the extra dimension. This series of excitations is called a tower of states, and the lightest one is a viable DM candidate.

Axions

Axions are particles that were originally proposed [29–32] to solve the strong CP problem in QCD. The QCD Lagrangian contains the following term:

$$\mathcal{L} \supset \bar{\Theta}\frac{g^2}{32\pi^2}G^a_{\mu\nu}\tilde{G}^{a,\mu\nu} \ , \tag{1.15}$$

where G is the field strength tensor of QCD and $\tilde{G}^{a,\mu\nu} \equiv \frac{1}{2}\epsilon^{\mu\nu\alpha\beta}G^a_{\alpha\beta}$ is its dual. This term induces CP violating effects, and measurements of the electric dipole moment constrain $\bar{\Theta} < 10^{-10}$ when according to the standard philosophy of quantum field theory we would expect $\bar{\Theta}$ to be of order one.[13] Introducing a new spontaneously broken U(1) symmetry (the Peccei-Quinn symmetry) gives a mechanism to dynamically drive $\bar{\Theta}$ to zero, solving the strong CP problem.

The associated pseudo-Nambu-Goldstone boson to this new symmetry is the axion, and if such particles are produced early in the universe, can constitute all of the DM. Thermally produced axions are under pressure from various constraints, so the production mechanism of axions is typically different to that of WIMPs

[13] There are actually two terms contributing to $\bar{\Theta}$: one is the bare term, generated by non-perturbative QCD effects, and the other comes from the determinant of the quark mass matrix, which comes from electroweak symmetry breaking. Such a conspiracy of these two different contributions to cancel (when they come from physically distinct phenomena), or for both of them to be simultaneously close to zero, gives perhaps an even stronger motivation for solving the strong CP problem.

that are produced via freeze-out. One production mechanism is based on the initial value of $\bar{\Theta}$ being larger than zero, so-called vacuum misalignment. As $\bar{\Theta}$ eventually drops to zero, the energy stored in the Peccei-Quinn field produces a population of axions. Axions then behave exactly as cold DM.

Primordial Black holes

We did not consider MACHOs or baryonic DM in this section, claiming that DM has to be non-baryonic. However there is one important exception to this statement. This is the possibility that DM is made of Primordial Black Holes (PBHs) [84] which would have to be formed before BBN and have a mass too small to be picked up in micro-lensing surveys. Additionally, PBHs can be constrained by the non-observation of Hawking radiation (see [85, 86] for a discussion of the acceptable mass range of PBHs).

Modified Gravity

So far we have talked about DM candidates that are made out of conventional or exotic matter. The alternative hypothesis is that the laws of physics should be modified, instead of postulating the existence of additional invisible matter. The first attempt at this was made by Milgrom [72–74] who proposed Modified Newtonian Dynamics (MOND) where Newton's second law is modified from $F = ma$ to

$$F = m\frac{a^2}{a_0}\,, \tag{1.16}$$

for a characteristic acceleration scale $a_0 \approx 10^{-10}\,\mathrm{ms}^{-2}$. Never supposed to be a full theory, MOND instead was imagined as a weak field limit of a UV complete theory, with Eq. (1.16) applying in the limit of weak accelerations, $a \ll a_0$.

While MOND is very successful at fitting the galactic rotation curves that we mentioned in Section 1.1 [75–77], the main issue is that in order to test it at the scale of galaxy clusters (and indeed the entire observable universe) it needs to be embedded into a fully relativistic theory. Such a completion was provided by TeVeS [78] (Tensor Vector Scalar gravity) and contains, two new fields, three free parameters, as well as a function that is free to chose. The large amount of freedom here allows TeVeS to fit various bits of data, but its predictivity becomes questionable.

Taking the example of the bullet cluster, in order for TeVeS to explain the observed data requires some of its additional degrees of freedom such as the vector field to behave like cold DM. Additionally, in order to explain the ratio of the second and third peaks of the CMB the additional fields in TeVeS have to, again, behave like cold DM. As such, one can question whether the additional fields in TeVeS (and similar modified gravity theories) are philosophically the same as postulating the existence of additional matter as is done by the conventional DM hypothesis. It is somewhat unclear whether a version of modified gravity can be made compatible with observations like the Bullet cluster and the CMB (for example see [79–83]). While we mention modified gravity as a potential candidate since it has not been explicitly excluded in all its forms, the lack of a convincing relativistic theory that explains all the phenomena we need DM for (particularly on scales larger than galaxy clusters) means modified gravity is currently a somewhat less satisfying solution to the DM problem.

1.3 Dark matter as a thermal relic

Having summarised some of the main candidates for DM, we will now describe the most widely considered production mechanism for obtaining the DM relic abundance (i.e. the fraction of the universe's energy budget that is responsible for DM: $\Omega_X h^2 \approx 0.12$), which is thermal freeze-out. Most of the WIMP candidates mentioned above obtain all or most of their relic abundance via this mechanism.

We will summarise the main steps for calculating a DM particle's relic abundance via thermal freeze-out, but the basic picture is as follows. The DM and SM particles start off in thermal equilibrium at early times, and since the temperature of this thermal bath is so high, the processes DM DM $\rightarrow$ SM SM and SM SM $\rightarrow$ DM DM occur at the same rate, where DM represents some dark matter candidate and SM is a standard model particle that the DM couples to. Both the DM and SM particles are effectively massless at this early time. As the temperature drops, the mass of the DM particles (typically heavier than the SM species) becomes relevant, meaning the DM DM $\rightarrow$ SM SM reaction is favoured and occurs as a higher rate. This causes the abundance of DM to decrease. At some point however, since the expansion of the universe is continuously acceler-

ating, the speed of expansion of the universe (H) becomes greater than the rate[14] (Γ) of DM DM $\to$ SM SM. As such, when H becomes a little higher than Γ, the abundance (defined more precisely later) becomes constant and is the value we measure today, $\Omega_X h^2 \approx 0.12$.

We will outline here the basic calculation, following some of the presentation in [27]. For the more detailed calculation see [87]. We will comment later on the caveats that need to be considered for the more detailed calculation to be important. In our discussion we will ignore the case of co-annihilations [89–91].

Starting with the most generic version of the Boltzmann equation

$$\mathbf{L}[f] = \mathbf{C}[f] \,, \tag{1.17}$$

where f is the phase-space distribution function, $\mathbf{L}$ the Liouville operator and $\mathbf{C}$ the collision operator. In it's most general form, the Boltzmann equation is a little opaque. For our purposes if we assume just one DM particle is relevant for freeze-out (other dark sector particles are assumed to be more massive, such-that co-annihilations are negligible) then the Boltzmann equation can be written in a more readable form

$$\frac{dn}{dt} + 3Hn = -\langle\sigma v\rangle(n^2 - n_{eq}^2) \,, \tag{1.18}$$

where $\langle\sigma v\rangle$ is the (thermally-averaged) product of cross-section times velocity, H is the Hubble parameter,[15] n is the particle number density and n_{eq} is the corresponding quantity while in thermal equilibrium.

Non-relativistic particles that follow the Maxwell-Boltzmann distribution satisfy

$$n_{eq} = g\left(\frac{mT}{2\pi}\right)^{3/2} e^{-m/T} \,, \tag{1.19}$$

where m is the particle mass, T the temperature and g is the number of internal (spin) degrees of freedom. It will be convenient to transform variables, so we define

$$Y \equiv \frac{n}{s} \,, \qquad\qquad Y_{eq} = \frac{n_{eq}}{s} \,, \tag{1.20}$$

[14] This Γ is representing the rate for some process, and should not be confused with a particle width.

[15] Recalling the FLRW metric for an expanding, flat universe $ds^2 = -dt^2 + a(t)^2(dx^2 + dy^2 + dz^2)$ then $H(t) = \dot{a}(t)/a(t)$, with $a(t)$ the scale factor.

where s is the entropy density

$$s = \frac{2\pi^2 g_* T^3}{45} \,, \tag{1.21}$$

for g_* the number of relativistic degrees of freedom. Since entropy is conserved in the sense that $sa^3 =$ is constant then the Boltzmann Eq. (1.18) becomes

$$s\dot{Y} = -\langle\sigma v\rangle s^2 (Y^2 - Y_{eq}^2) \,. \tag{1.22}$$

Here and throughout dotted quantities denote time derivatives. Introducing a dimensionless measure of time, $x \equiv m/T$, we can write Eq. (1.22) as

$$\frac{dY}{dx} = -\frac{\langle\sigma v\rangle s}{Hx}(Y^2 - Y_{eq}^2) \,. \tag{1.23}$$

In terms of the variable $\Delta \equiv Y - Y_{eq}$ we finally have

$$\Delta' = -Y'_{eq} - f(x)\,\Delta\,(2Y_{eq} + \Delta) \,, \tag{1.24}$$

where primes now denote derivatives with respect to x, and

$$f(x) = \sqrt{\frac{\pi g_*}{45}}\, m\, M_{pl}\, \frac{\langle\sigma v\rangle}{x^2} \,. \tag{1.25}$$

Although there are some important caveats that we will mention below, it is often possible to expand the annihilation cross section in powers of the non-relativistic velocity v

$$\langle\sigma v\rangle \approx a + b\langle v^2\rangle \approx a + 6\frac{b}{x} \,. \tag{1.26}$$

In order to obtain the present day relic density, we need to integrate Eq. (1.24) over a suitable range of x. In general, this can only be done numerically but we can make some approximations in order to get a rough analytical result. First notice that for late times $x \gg x_f$ where $x_f \equiv m/T_f$ Eq. (1.24) can be written

$$\Delta' = -f(x)\,\Delta^2 \,. \tag{1.27}$$

Integrating this between $x = x_f$ and $x = \infty$, approximating the number of relativistic degrees of freedom as constant, and using that $\Delta_{x_f} \gg \Delta_\infty$ we arrive

at

$$\frac{1}{Y_\infty} = \sqrt{\frac{\pi g_*}{45}}\, m\, M_{pl}\, \frac{a + 3b/x_f}{x_f} \,. \tag{1.28}$$

The current relic density of dark matter is expressed as the fraction of the universe's energy density,

$$\Omega_X = \frac{\rho_X}{\rho_c} \,, \tag{1.29}$$

where ρ_c is the critical energy density

$$\rho_c = \frac{3H_0^2}{8\pi G_N} \,. \tag{1.30}$$

Then using $\rho_X = m_X n_X = m_X s_0 Y_\infty$, with $s_0 \approx 3000\ \mathrm{cm}^{-3}$ the current day entropy density, we finally have

$$\Omega_X h^2 \approx \frac{1 \times 10^9 \mathrm{GeV}^{-1}}{M_{Pl}} \frac{x_f}{\sqrt{g_*}} \frac{1}{a + 3b/x_f} \,, \tag{1.31}$$

where the density of DM is expressed in terms of $h = H_0/100\,\mathrm{km\,s^{-1}\,Mpc^{-1}}$ for historical reasons. Alternatively

$$\Omega_X h^2 \approx 0.1 \left(\frac{10}{g_*}\right)^{1/2} \left(\frac{x_f}{10}\right) \frac{3 \times 10^{-10} \mathrm{GeV}^{-2}}{\langle \sigma v \rangle} \,. \tag{1.32}$$

Using estimates for $g_*(T = T_f) \approx 10$ and $x_f \approx 10$ means that we would require $\langle \sigma v \rangle \approx 3 \times 10^{-26}\,\mathrm{cm^3\,s^{-1}}$ for $\Omega h^2 \approx 0.1$.[16]

The approximations introduced above are not always justified. For example, the expansion of the annihilation cross-section in powers of v^2 breaks down on resonance and care needs to be taken near the opening of annihilation channels [87]. For this reason, we will use numerical tools such as `MicrOMEGAs` [92] when appropriate, which calculates the relic density numerically.

1.4 Dark matter at the large hadron collider

The Large Hadron Collider (LHC) is the world's most energetic hadron collider, currently able to smash protons together at a Centre-Of-Mass (COM) energy of

[16] More precisely, one finds from the Boltzmann equation that x_f is typically always order 20 [88].

13 TeV. A circular tunnel, 27 km in length, located several hundred meters under the French-Swiss border near Geneva, it is perhaps one of the most impressive feats of modern engineering.

The temperature in the underground tunnel is kept to 1.8 K, needed for the liquid helium to cool the superconducting magnets that keep the particles on their circular path. The protons are grouped up into bunches in order to provide a discrete number of collisions at the points where the counter-rotating beams are brought to collide. The main points of interest for us are the collision points which house the larger and most general-purpose detectors:[17] A Toroidal LHC ApparatuS (ATLAS) and the Compact Muon Solenoid (CMS). The crowning achievement of the LHC thus far is the discovery of the Higgs boson in 2012 [93,94].

Roughly speaking, the ATLAS and CMS detectors are built in cylindrical layers around the interaction point, where the proton collisions occur.[18] The innermost layer is the tracker, which precisely measures the paths of charged particles. The next layers are the calorimeters, the electromagnetic calorimeter which measures the energy of particles like electrons and photons, and the hadronic calorimeter which is designed to measure the energy of particles that are made up of quarks and gluons. Since muons travel through all the previously mentioned detectors in a straight line, there are large muon chambers/detectors that are dedicated to measuring the momentum of muons. Finally there is an extensive magnet system in place, which curves the path of charged particles, allowing their momentum to be measured.

The theoretical picture of particle collisions at the LHC is somewhat complicated. Starting at the interaction point, bunches of protons collide. At the high energies that these protons are being accelerated to, the basic picture of a proton being made up of 2 up quarks and 1 down quark breaks down, and the proton is more accurately described as a sea of quarks and gluons. These constituent particles are called partons,[19] having been introduced by Richard Feynman [96]. Each parton i (such as a gluon, quark, anti-quark, etc.) has its own Parton Distribution Function (PDF) $f_i(x, \mu^2)$, where f is the PDF, i labels the parton, x is

[17] The other major detectors are ALICE (A Large Ion Collider Experiment) which primarily studies heavy ion collisions and LHCb (Large Hadron Colllider Beauty, after the beauty or bottom quark) which measures many important quantities from flavour physics such as CP violation, rare b decays, etc.

[18] For a detailed description of the ATLAS detector, see [95].

[19] In principle, particles with no QCD charge such as the photon can also be partons.

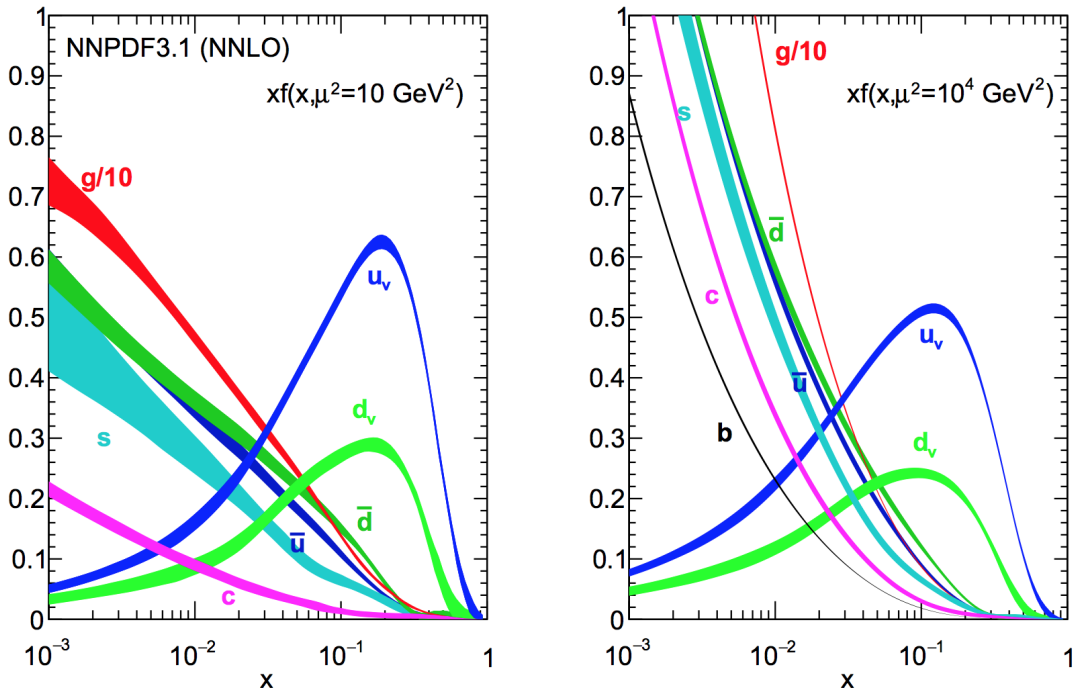

Figure 1.5: *Plots displaying the PDF values as a function of x, for two different values of μ^2. From the NNPDF collaboration [97].*

the fraction of the proton's momentum that the parton carries, and μ^2 is the momentum transferred in the interaction. Then $f_i(x, \mu^2)\,\mathrm{d}x$ is the probability of the parton carrying a fraction between x and $x + \mathrm{d}x$ of the proton's total momentum. We show some example PDFs from the NNPDF group [97] in Fig. 1.5.

One proton collision may involve Multiple Parton Interactions (MPI), where many partons take part in a perturbative process. Typically one is interested in just one hard (defined below) process, corresponding to a Feynman diagram of interest. However because of the large number of interactions taking place due to the many partons in each proton, when restricting to one process the energy and momentum of particles will not be conserved in the beam direction.[20] Instead, the transverse momentum of a particle $\vec{p_T}$ is defined as just the components of the momentum that are transverse to the beam direction, with magnitude $p_T = \sqrt{p_x^2 + p_y^2}$ where p_x and p_y are the components of the particle's momentum in the directions perpendicular to the beam. A particle with high p_T is said to be *hard* whereas a particle with low p_T is said to be *soft*. Since we are interested in DM

[20] Isolating a single hard scattering event is further complicated by Pile-Up (PU): since bunches of protons are collided, many proton collisions happen at the same time.

searches an important quantity is the missing transverse energy

$$\not{E}_T = \left| \sum_{\text{visibles}} \vec{p_T} \right| , \tag{1.33}$$

with the only known particle from the SM contributing to $\not{E}_T$ being the neutrino. The other important co-ordinates for hadron collider physics are ϕ, which is the normal azimuthal angle around the beam direction. Finally, instead of using the polar angle θ, it is far more desirable to use a quantity that is invariant under boosts along the z direction.[21] Such a quantity is the rapidity of a particle

$$y = \frac{1}{2} \ln \frac{E + p_z}{E - p_z} , \tag{1.34}$$

with the closely related quantity, the pseudo-rapidity

$$\eta = -\ln \left(\tan \frac{\theta}{2} \right) , \tag{1.35}$$

which is identical to the rapidity for massless particles. Therefore we will primarily use the co-ordinates (p_T, y, ϕ) to describe momentum 3-vectors, although η will often replace y.

Given a hard event of interest, the initial state particles must be quarks or gluons and so possess colour. Any coloured particle may at any point emit more coloured particles,[22] because of Feynman vertices such as ggg and $g\bar{q}q$ that exist within the SM. Therefore one gluon g can become two via a $g \to gg$ splitting, similarly $g \to \bar{q}q$, $q \to gq$ and other splittings can occur. This phenomenon is called *showering*, and when it originates from the initial state particle (of the hard process of interest) it is called Initial State Radiation (ISR). Conversely, Final State Radiation (FSR) is the corresponding process for final state particles. Therefore given a simple $2 \to 2$ hard process of interest, there will be a huge number of final state particles present due to ISR and FSR (the latter only when a final state is coloured).

Of course, quarks and gluons are not directly observable and the transition

[21] This is again an issue due to the unknown initial momentum along the beam direction for a particular hard process.

[22] Self-interacitons of gauge bosons such as the ggg and $gggg$ vertex in the SM are a direct consequence of the non-abelian nature of the $SU(3)_C$ gauge group.

from the perturbative to non-perturbative regime is called *hadronisation*: the mapping of quarks and gluons onto hadrons. However, individual hadrons are typically not observed by the experimental detectors, since the concentration of hadronic energy is too great to resolve each one individually. These large concentrations of hadronic energy are called jets, which have to be defined carefully in order to avoid technical problems with infra-red safety. A popular choice which will be used throughout this thesis is to define jets according to the anti-k_T algorithm [162]. A review of infra-red safety issues and a description of some modern jet finding algorithms can be found in [98].

The theoretical picture we have described above is a mixture of perturbative calculations (such as for the hard event and showering), non-perturbative models (such as for hadronisation) and quantities determined from other fits to data (such as the PDFs). There are a number of tools available that allow the user to model the phenomena described above using Monte Carlo (MC) numerical methods: `Madgraph` [99], `Pythia` [100], `CalcHEP` [101], and `Delphes` [102], to name just a few. In addition, model files can be specified in `Feynrules` [103], which allows the user to input a Lagrangian for use in the event generators specified above. Typically one then takes this model file and puts it into an event generator like `Madgraph`, which will calculate the cross section and a set of collision events at the parton level, which is essentially a list of particles in the hard process. Then one can take the outputted events from `Madgraph` and perform showering and hadronisation in `Pythia`, which includes within itself a version of the jet-finding algorithm `FastJet` [155]. This is the approach we take in this thesis, also applying analysis cuts and smearing functions to represent the effects of experimental resolution on the final states listed within `Pythia`, instead of using a more comprehensive simulation of detector effects.

Having introduced some basic concepts and variables in collider physics, we will now summarise the most generic DM search: so-called mono-X channels. We will then move on to describe a more model-specific signature: direct resonance searches. For reviews of DM at the LHC, see for example [104, 105].

Mono-X searches

If there is sufficient energy, given the simplified models introduced above, we can imagine producing DM pairs at the LHC, creating large amounts of missing energy.

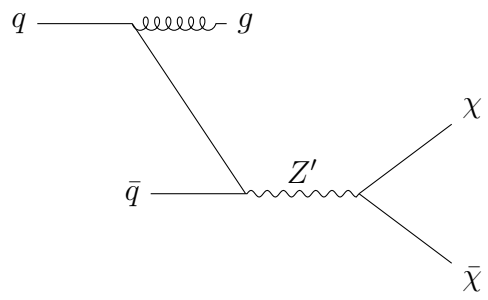

Figure 1.6: *Feynman diagram for a monojet signature in the spin-one simplified model. $\bar{q}q$ annihilation produces a Z' which decays into a pair of DM particles $\bar{\chi}\chi$. Missing energy can only be calculated by measuring visible particles, so an ISR jet is required for the trigger.*

Experimentally, missing energy can only be calculated from visible objects' p_T so the leading signature for DM at the LHC in many models is the mono-X signature. This is where $X = g, V, H, ...$ is a SM particle normally radiated as ISR. One example is a monojet signature, shown in Fig. 1.6. All Feynman diagrams in this thesis are made using `TikZ-Feynman` [106].

In order to place bounds on a model of interest (such as a simplified model), we will use the tools mentioned above to calculate the cross-section (or expected number of events) for the signal and compare it to the background prediction. For the monojet channel the main backgrounds are $Z(\to \nu\nu)+$ jets and $W(\to \ell\nu)+$ jets, where the charged lepton ℓ is misidentified by the detector or decays hadronically, creating more jets. The name mono-jet is somewhat misleading as additional jets beyond the hardest jet are allowed in an event provided there are not too many.[23] In fact, to maximise the sensitivity of a particular search channel, the LHC collaborations define a certain number of cuts, which are requirements placed on kinematic variables designed to raise the significance of a signal over the background. A simple example would be $\not{E}_T > 250$ GeV.

We show as an example the results from a recent monojet search from ATLAS [107] with an integrated luminosity of 36.1 fb^{-1} in Fig. 1.7. The typical shape of the monojet bound can be explained as follows. Firstly, the exclusion runs out of power for some fixed mediator mass $m_{\text{med}} = \text{constant}$, since the cross section becomes suppressed by a large mediator mass. On the other side of the exclusion region, $m_\chi > m_{\text{med}}/2$ is rarely probed since this would require the mediator to be

[23] More precisely, up to four jets with $p_T > 20$ GeV are allowed in a recent ATLAS search [107].

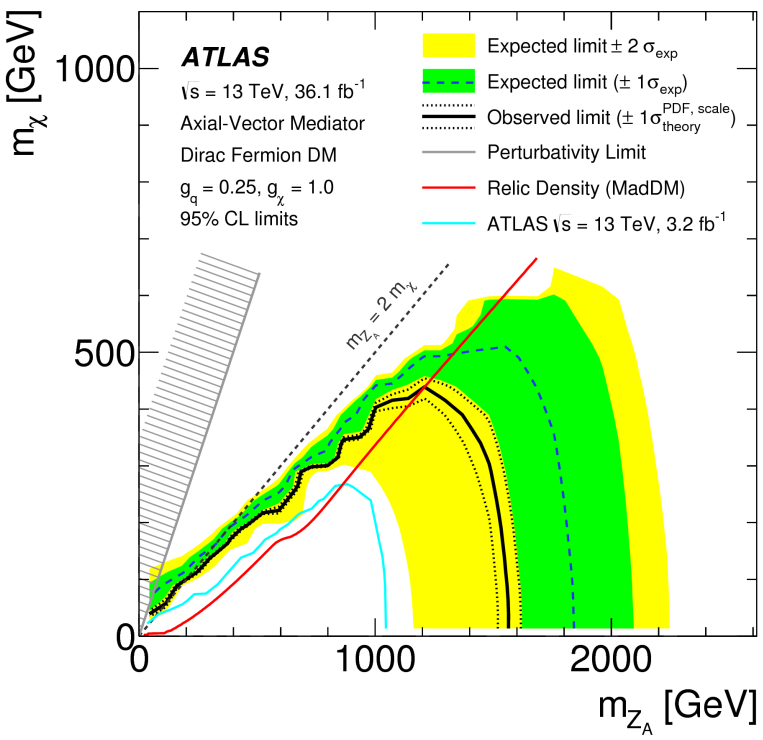

Figure 1.7: *Mono-jet bounds on the axial-vector simplified model from ATLAS [107].*

off-shell.

We note here that bounds can also be obtained by requiring the ISR particle to be a Higgs [109] or a vector boson [108], instead of a jet. Additionally, in the scalar simplified models the monojet signature is produced via a top loop due to the couplings scaling as the SM yukawas. As such alternative probes of these models can be made in the $\bar{t}tH$ channel [110]. Finally, if the DM mass is light enough measurements of the Higgs invisible width can be used to set constraints, for example ATLAS [111] find the Higgs invisible branching ratio to be less than 0.25 at 95% C.L.

Resonant searches

Given the existence of a dynamical mediator in simplified models, such as the Z', the model can also be well constrained by direct searches for the mediator. Perhaps the most basic example, a resonant diagram is displayed in Fig. 1.8.

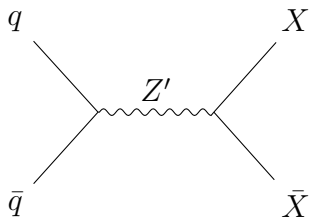

Figure 1.8: *Feynman diagram showing a resonant search for the mediator Z'. Here X are SM particles. If X is a quark, this is a dijet signature, whereas if X is a charged lepton, we have a dilepton signature.*

Dijet searches exploit the fact that if the mediator is produced via SM quarks, it can decay back into those pair of quarks, creating a pair of hard jets. Then, a dijet search involves finding the hardest pair of jets and forming a distribution of their invariant mass $m_{jj}^2 = p_{1,\mu}p_2^\mu$ where p_1 and p_2 are the momentum 4-vectors of the hardest and second hardest jet respectively. The signal will look like a resonant bump over the smoothly falling background. This gives a somewhat stronger constraint than the mono-X searches since the mono-X signal shape is also smoothly falling, making it harder to distinguish from their smoothly falling backgrounds (see Fig. 1.11 for a comparison of their relative exclusion strength).

We show in Fig. 1.9 the measured dijet invariant mass distribution, and the resulting bounds on the quark coupling in the spin-one simplified model in Fig. 1.10 from an ATLAS search [112]. Again in contrast to the monojet searches, where the background is typically calculated using MC tools (with appropriate normalisation to data), the background for the dijet resonance searches are simply obtained by a fit of a smooth function to the observed data. The function is chosen such that it cannot possess any bump-like features (which the signal is expected to have) and this approach is common in searches where the expected signal shape is distinct from the background. Dijet searches will be discussed in more detail in Chapter 2.

The main exclusion power of dijet searches come into play when the Z' resonance is not too massive, else its cross-section will be too small, and not too light, since the QCD background will become overwhelming. If the Z' resonance also couples to leptons, the conceptually similar dilepton search opens up. This signal has the advantage that the background from QED processes is significantly smaller than that of QCD processes, leading to stronger bounds from dileptons than dijets for couplings of similar magnitude. The strength of the dilepton bounds relative

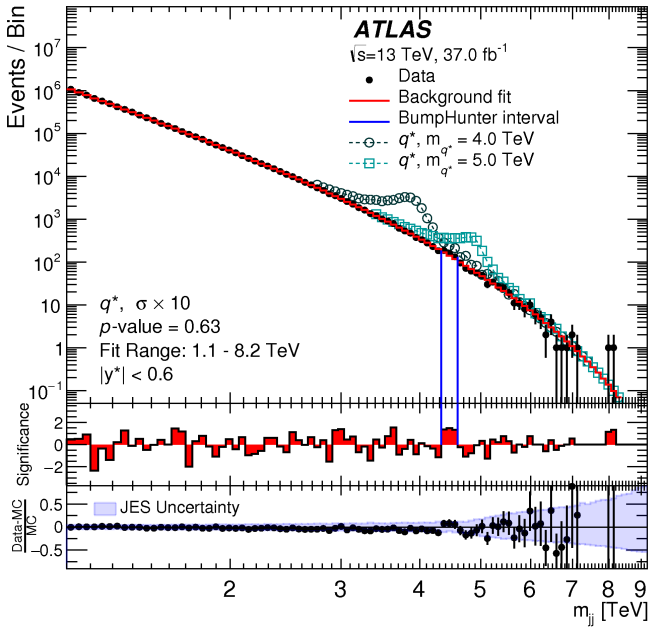

Figure 1.9: *Dijet invariant mass distribution from ATLAS [112]*

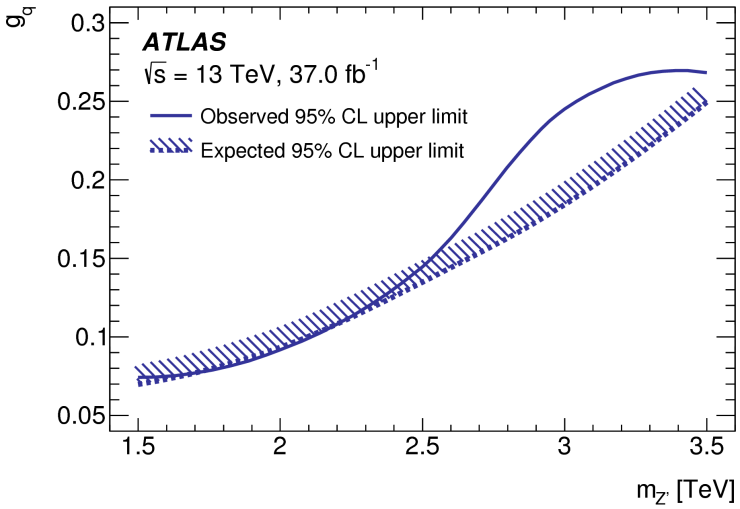

Figure 1.10: *Bounds on the quark coupling g_q in a spin-one simplified model, from ATLAS [112]*

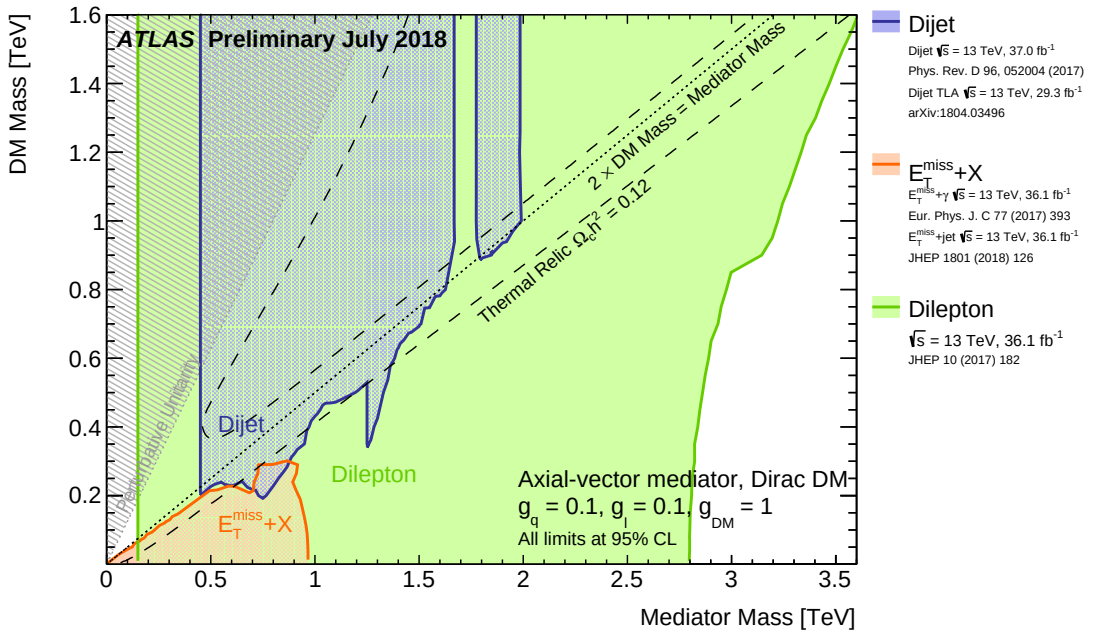

Figure 1.11: *Combination of various ATLAS searches: dijet searches [112, 113] shown in blue, a dilepton search [115] shown in green and mono-X signatures [107, 114] shown in orange. The bounds apply to the axial-vector simplified model, shown as a function of DM mass against mediator mass, for the fixed couplings shown on the plot.*

to the other discussed constraints coming from the LHC is shown in Fig. 1.11. We will introduce models that necessarily contain couplings to leptons in Chapter 3 and show the constraints that apply to them, including dileptons, dijets and monojets, in Chapter 4.

1.5 Direct and indirect detection

WIMP DM candidates enjoy a great deal of *complementarity* – the ability to be simultaneously explored by different types of experiments. As well as being probed at the LHC as mentioned in the previous section, they can also be probed by a wide range of other experiments. Having already discussed the relic density and DM at the LHC, we will now briefly summarise direct and indirect detection. Direct detection experiments search for scattering events of DM particles with nuclei, taking advantage of the DM halo in our galaxy creating a flux of DM particles

through the Earth. Indirect detection is based on the same type of particle physics process that is relevant for the relic density calculation, namely DM annihilation. Indirect detection experiments look towards parts of the sky that are expected to contain large concentrations of DM – typically the centre of galaxies. In these regions, DM is expected to annihilate into observable SM particles that would eventually be detected by a ground based or satellite telescope.

Direct detection

Direct detection was originally proposed as a way to discover DM in [116, 117]. The expected rate of scattering events in a direct detection experiment, expressed as the differential event rate per unit recoil energy, is

$$\frac{dR}{dE_R} = N_T \frac{\rho_0}{m_\chi} \int_{v_{\min}}^{v_{\text{esc}}} d^3v \, v f(v + v_E) \frac{d\sigma}{dE_R} \, , \tag{1.36}$$

where N_T is the number of targets (scattering centres) per unit mass of the detector, ρ_0 is the local density of DM, m_χ is the DM mass, v is the DM velocity (relative to the detector), v_E is the Earth's velocity (relative to the galactic rest frame), σ is the scattering cross-section, E_R is the recoil energy. $v_{\min}$ is the minimum incident velocity needed to create a scattering event with recoil energy E_R

$$v_{\min} = \frac{\sqrt{2 m_T E_R}}{2\mu_T} \, , \tag{1.37}$$

where μ_T is the WIMP-nucleus reduced mass

$$\mu_T = \frac{m_T m_\chi}{m_T + m_\chi} \, , \tag{1.38}$$

with m_T the nucleus mass. The simplest form of f, the velocity distribution of DM in the Milky Way, is based on the assumption of an isotropic, isothermal sphere, in which case f is a Maxwellian distribution

$$f(v) = C \exp\left(-\frac{v^2}{v_c^2}\right) \, , \tag{1.39}$$

with C an appropriate normalisation constant, and v_c the local circular speed. At large velocities, particles will no longer be gravitationally bound to the Milky

Way so the distribution in Eq. (1.39) must be truncated at the escape velocity $v_{\rm esc}$. Numerical values for the standard halo parameters are $\rho_0 = 0.3\,\mathrm{GeV\,cm^{-3}}$, local speed $v_c = 220\,\mathrm{km\,s^{-1}}$ and a local escape velocity $v_{\rm esc} = 544\,\mathrm{km\,s^{-1}}$. See [118] for a discussion of these values and their uncertainties.

Given a particle physics model, the calculation of the cross section for WIMP-nucleus scattering must still be calculated. This is performed in the context of non-relativistic EFT, where the operators consistent with Galilean invariance are

$$\begin{aligned}
&\mathcal{O}_1^{\rm NR} = 1\ , \\
&\mathcal{O}_3^{\rm NR} = i\,\vec{s}_N\cdot(\vec{q}\times\vec{v}^{\perp})\ , && \mathcal{O}_4^{\rm NR} = \vec{s}_\chi\cdot\vec{s}_N\ , \\
&\mathcal{O}_5^{\rm NR} = i\,\vec{s}_\chi\cdot(\vec{q}\times\vec{v}^{\perp})\ , && \mathcal{O}_6^{\rm NR} = (\vec{s}_\chi\cdot\vec{q})(\vec{s}_N\cdot\vec{q})\ , \\
&\mathcal{O}_7^{\rm NR} = \vec{s}_N\cdot\vec{v}^{\perp}\ , && \mathcal{O}_8^{\rm NR} = \vec{s}_\chi\cdot\vec{v}^{\perp}\ , \\
&\mathcal{O}_9^{\rm NR} = i\,\vec{s}_\chi\cdot(\vec{s}_N\times\vec{q})\ , && \mathcal{O}_{10}^{\rm NR} = i\,\vec{s}_N\cdot\vec{q}\ , \\
&\mathcal{O}_{11}^{\rm NR} = i\,\vec{s}_\chi\cdot\vec{q}\ , && \mathcal{O}_{12}^{\rm NR} = \vec{v}^{\perp}\cdot(\vec{s}_\chi\times\vec{s}_N)\ ,
\end{aligned} \tag{1.40}$$

where we have used the numbering in [45]. The variable $\vec{v}^{\perp} \equiv \vec{v} - \vec{q}/2\mu_N$ is used since it is hermitian[24] (in contrast to $\vec{v}$). $\vec{q}$ is the momentum transferred and $\vec{s}_N$ and $\vec{s}_\chi$ are the nucleon and DM spins respectively. This list is technically not a complete set of operators, but will be enough for the models of interest to us. For the complete set see [43].

As explained in [43–45], starting from the matrix element

$$\mathcal{M} = \sum_i c_i^N(\lambda, m_\chi)\mathcal{O}_i^{\rm NR}\ , \tag{1.41}$$

with $N = p, n$, m_χ the DM mass, and λ additional model parameters such as mediator mass and couplings. Then the spin averaged value can be written

$$\overline{|\mathcal{M}|^2} = \frac{m_T^2}{m_N^2}\sum_{i,j,N,N'} c_i^N c_j^{N'} F_{i,j}^{N,N'}\ , \tag{1.42}$$

where m_N is the nucleon mass and the form factors F encode the nuclear response,

[24] As explained in [44], taking a hermitian conjugate is equivalent to exchanging incoming and outgoing particles. For example, the momentum transfer $\vec{q}$ is anti-hermitian, so $i\vec{q}$ is preferred.

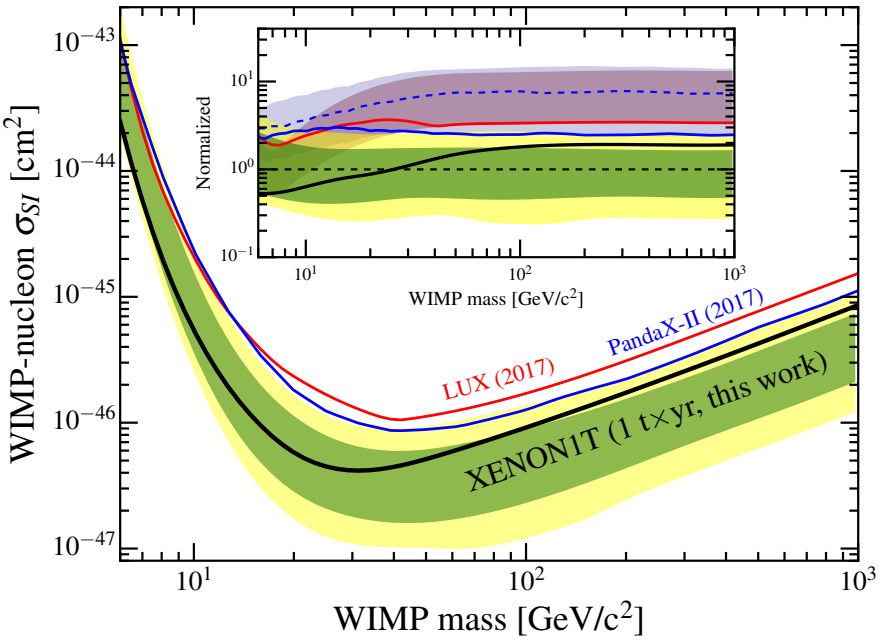

Figure 1.12: *90% C.L. bound on the spin-independent WIMP-nucleus cross-section as a function of the DM mass, from the XENON1T experiment [120]. Also shown are the results of previous experiments for comparison: PandaX-II [122] and LUX [121].*

which depends on the target material T. Then we can write

$$\frac{d\sigma}{dE_R} = \frac{1}{32\pi^2 m_\chi^2 m_T v^2} \overline{|\mathcal{M}|^2} \,. \tag{1.43}$$

All that is left is to map the simplified models and relativistic EFTs onto the non-relativistic operators in Eq. (1.40). Such a dictionary is provided for example by [45]. In principle, while performing the procedure of matching high energy theories onto low energy non-relativistic EFT, one should run the couplings of the theory. As pointed out in [119], the effect on the resulting direct detection bounds should be taken into account, however for the leading operators that result from the reduction of models we consider in this thesis, the effect from this running is always negligible.[25]

[25]The case where running has a significant effect, in the case of the spin-one simplified models, is for an axial coupling to quarks and a purely vectorial coupling to DM. Such a coupling is present for a model in Chapter 4 but the model also contains a vectorial coupling to quarks which leads to a significantly stronger bound than the contribution coming from the axial coupling to quarks (even with running taken into account).

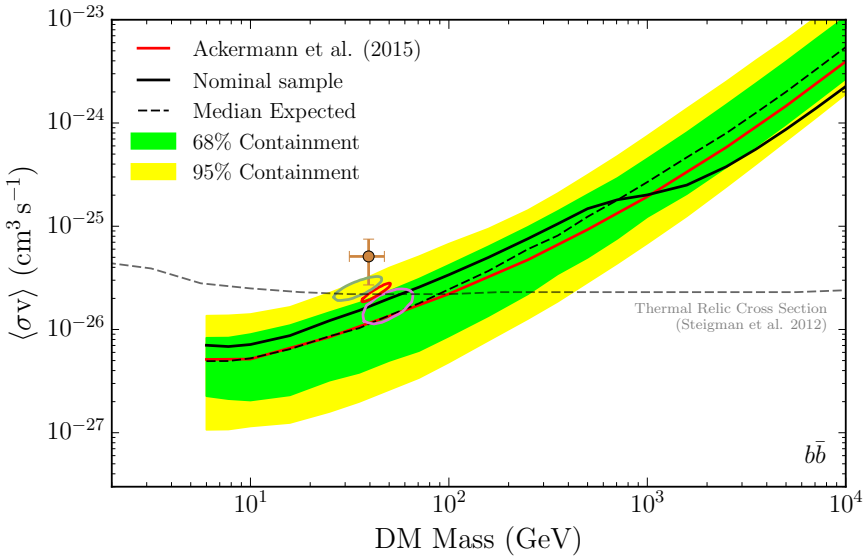

Figure 1.13: *95 % C.L. limits on the DM annihilation cross-section as a function of the DM mass, from Fermi-LAT [123], assuming the DM candidate annihilates solely into a $\bar{b}b$ final state (solid black line). Also shown is an indication of the cross-section that would allow such a DM candidate to make up all of the observed DM relic density (grey dashed line)*

As an example, we show the current leading bound on the canonical spin-independent WIMP-nucleon cross section in Fig. 1.12, from XENON1T [120]. This assumes the only non-zero operator to be $\mathcal{O}_1^{\rm NR}$, which arises from the non-relativistic limit of $\bar{\chi}\chi\,\bar{q}q$ and $\bar{\chi}\gamma_\mu\chi\,\bar{q}\gamma^\mu q$. In Chapter 4 we will use the rescaling functions from [45] (which include appropriate numerical factors which take into account the form factors, velocity integral and recoil energy integral) to rescale this bound to the relevant operators that our models of interest produce.

Indirect Detection

Indirect detection probes the opposite direction of the Feynman diagram representing DM production at the LHC. It is the same diagram as is used in the relic density calculation, but rather than applying to processes early in the universe it is applied to potential signals of DM annihilation in the nearby universe today. Indirect detection bounds will not be used in this thesis, with the exception of Chapter 5, where we will mention the Galactic Centre Excess (GCE). The GCE is a contentious possible signal of DM annihilation from our Galactic Centre, and

we will describe there the necessary requirements on our model parameters in order to fit this excess. Therefore we only give a very brief overview of indirect detection here, since it is important in the context of complementary probes of DM.

The measured flux of gamma rays from DM annihilation can be written (particles per area, time, solid angle, and energy) [27]

$$\frac{dN}{dA\,dt\,d\Omega\,dE} = \frac{\langle\sigma v\rangle}{m_\chi^2}\frac{dN}{dE}\frac{1}{4\pi}\int_{\text{l. o. s.}} ds\,\rho^2(s,\psi) \tag{1.44}$$

where $\langle\sigma v\rangle$ is the (velocity-averaged) DM annihilation cross-section, m_χ the DM mass, dN/dE is the spectrum of photons per annihilation, the integral is along the line of sight, and ψ is the angle relative to the galactic centre. The integral is known as the J-factor, $J(\psi)$, which separates the astrophysics from the particle physics in Eq. (1.44). Additionally, in Eq. (1.44) a Majorana DM candidate is assumed, where the DM particle is its own anti-particle. If instead the DM candidate is a Dirac fermion, with its anti-particle being distinct, then the right-hand side of Eq. (1.44) should be divided by 2.

We show in Fig. 1.13 the constraints on the DM annihilation cross-section as a function of the DM mass, from Fermi-LAT [123], assuming only annihilation into a $\bar{b}b$ final state. These bounds were obtained by searching for signals of DM annihilation in satellite galaxies of the Milky Way. More generally, indirect detection searches for any observable final state particles, and in any location where the current DM density is expected to peak. For example, IceCube have searched for neutrinos coming from DM annihilation in the Sun [124], which is possible if a population of DM has gradually built up in the Sun after becoming gravitationally trapped.

Chapter 2

Dijet Constraints on Z' Mediated Dark Matter Models

This Chapter is heavily based on [1] which I wrote in collaboration with Malcolm Fairbairn, John Heal and Felix Kahlhoefer. This work was published in [1].

2.1 Introduction to dijet searches

One of the most common signatures of new physics at the LHC is a resonant bump in the observed invariant mass spectrum of dijet events. This is because any new resonance formed from partons can decay back into those same particles (quarks or gluons) to form a pair of hard jets. This chapter analyses all dijet data that was available at the time of [1] appearing: the first dijet analyses at 13 TeV [125, 126] combined with the largest datasets available at 8 TeV [127, 128]. In addition we use a search that uses the tequnique of data scouting [129]. Examples of models probed by such searches are Randall-Sundrum (RS) gravitons [71], excited quarks [130, 131] and models with a leptophobic Z' [132–134] (see [135] for the implications of these searches on more generic Z' models).

As explained in Chapter 1, the case of a massive spin-one boson is of particular interest since it can provide a link between the dark and visible sectors and create a viable model of dark matter. Such a Z' can easily mediate dark matter freeze-out in the early universe to obtain the observed relic density today. Typical avenues to probe such models are direct detection experiments searching for evidence of DM-nucleus scattering and searches for missing energy at the LHC [53, 136–150].

These sort of DM models fall into the class of simplified models, which are now commonly used to optimise LHC searches for DM [61, 151].

However as mentioned by previous works [136, 147, 152, 153] an additional and highly complementary way to search for such models is not only via missing energy signatures, but via the signature the Z' mediator leaves in the dijet mass spectrum. This is normally imagined as a resonant bump which can be easily distinguished from the smoothly falling QCD background, but since the mediator can decay invisibly this resonant feature may be broadened, leaving weaker limits. The purpose of this Chapter is to describe limits that were derived using all available dijet data at the time, for generic resonance masses and widths.

Previous work has either focussed on narrow resonances [136], resonances that decay exclusively into quarks [133] or on very specific choices of couplings [147, 152]. In contrast, we take a more model-independent approach, meaning the results will be applicable to a broader selection of Z' models. We take the width of the Z' to be a free parameter, as large as $\Gamma/m_{Z'} = 0.3$. Then the dijet bounds can be applied to models where the width of the Z' is determined via its coupling to visible particles only, both visible particles and DM (as in the case of a simplified model), or a whole range of fermions as in a UV complete model. We also develop a new method of combining information from the relic abundance with dijet constraints to determine the regions where Z' mediated thermal freeze-out is compatible with LHC constraints.

This Chaper is organised as follows: First, in section 2.2 we describe our dijet analysis, and present the results as an upper limit on the Z'-quark coupling as a function of the Z' mass and width, such that the result is as model-independent as possible. We then apply these results to the case of a Z' mediated dark matter model in section 2.3, at first taking the benchmark case with fixed couplings used by the LHC collaborations before looking at only parameter points that can explain the observed relic density.

2.2 Limits on generic Z' models from dijet resonance searches at the LHC

This section describes the analysis techniques used to obtain our dijet bounds. First, we simulate dijet events from a generic Z' model in a Monte Carlo generator,

producing samples at the relevant centre-of-mass energies and applying the same selection cuts used by the experimental analyses. Next, we compare the predicted invariant mass spectrum to the data, taking the same approach to modelling the background that is used by the experimental collaborations. Finally we vary the signal strength until the combined statistical tension from all data sets gives us the appropriate limit at the 95% confidence level.

2.2.1 Dijet event generation

The first step in our analysis is to generate dijet events resulting from a new Z' mediator with mass 500 GeV $\leq m_{Z'} \leq$ 4 TeV, which interacts with the standard model quarks q via the vectorial coupling g_q. To generate this signal, we add the following terms to the SM Lagrangian:

$$\mathcal{L}_{\text{kin}} = -\frac{1}{4} F'_{\mu\nu} F'^{\mu\nu} + \frac{1}{2} m^2_{Z'} Z'_\mu Z'^\mu \,, \tag{2.1}$$

$$\mathcal{L}_{\text{int}} = -g_q Z'_\mu \sum_q \bar{q} \gamma^\mu q \,, \tag{2.2}$$

where $F'^{\mu\nu} = \partial^\mu Z'^\nu - \partial^\nu Z'^\mu$. Although we do not specify any other couplings of the Z', such couplings may in principle be present, since we are taking the total decay width Γ of the Z' to be a free parameter.

Since we treat Γ and g_q as independent parameters, and that the shape of the dijet invariant mass distribution depends only on $m_{Z'}$ and Γ, the total magnitude of the signal will scale as g^4 in regions where the intermediate Z' is produced both on and off shell. We therefore generate events across a grid of $m_{Z'}$ and Γ and a fixed value of g_q, then rescale to different values of g_q using the trivial rescaling $\sigma \propto g_q^4$.

Our simulation of dijet events is carried out using a pipeline of the publicly available software packages `FeynRules_v1.6.11` [103], `MadGraph_v3.2.2` [99], as well as `Pythia_v8.186` [100,154] and `FastJet_v3.0.5` [155]. First, we implement the model Lagrangian in `FeynRules` to calculate the Feynman rules and generate a UFO model file [156]. In `MadGraph` we then generate matrix elements for all processes involving an s-channel Z' and a pair of u, d, s, c or b quarks in the final state.

The output from `MadGraph` is interfaced with `Pythia`, which we use both as a

	R	$\|\eta\|$	$p_{T\min}$	Ref.
ATLAS 13 TeV	0.4	< 2.4	50 GeV	[125]
CMS 13 TeV	1.1	< 2.5	30 GeV	[126]
ATLAS 8 TeV	0.6	< 2.8	50 GeV	[127]
CMS 8 TeV	1.1	< 2.5	30 GeV	[128]
CMS 8 TeV (low m_{jj})	1.1	< 2.5	30 GeV	[129]

Table 2.1: *Jet parameters chosen for the anti-k_T algorithm for the five experimental searches. The radius parameter is defined as $R = \sqrt{(\Delta\eta)^2 + (\Delta\phi)^2}$ with ϕ the azimuthal angle. For the CMS analyses, jets are first reconstructed with a radius parameter of 0.5 (0.4) at 8 TeV (13 TeV) and are then combined into two fat jets with radius parameter 1.1.*

Monte Carlo event generator and to simulate showering and hadronisation. For our simulations, we use the `CTEQ5L` parton distribution function [157]. We neglect next-to-leading order corrections, which are expected to lead to somewhat larger cross sections [158], so we give a conservative bound. The resulting final states are clustered with `FastJet` using the anti-k_T algorithm [162]. We choose the jet parameters (cone-size R, maximum pseudorapidity η and minimum transverse momentum $p_{T\min}$ of the jet) to match those adopted by each experiment under consideration (see table 2.1).

Once the jets have been reconstructed, we apply the experimental selection cuts outlined in table 2.2. For each event that passes these cuts we calculate the invariant mass of the dijet system. Instead of performing a full detector simulation, we approximate the uncertainties in reconstructing the energy and momentum of the jet events arising from detector performance by applying a Gaussian smearing to the invariant dijet mass. For this purpose, we take the detector resolution in both ATLAS and CMS to be

$$\sigma(m_{jj}) = 1.8\text{GeV}\sqrt{m_{jj}/\text{GeV}}\,, \tag{2.3}$$

which was determined by fitting the smeared signals to data given by the CMS experiment [128] for a RS graviton benchmark model. The smeared invariant masses are then binned according to the bin sizes given by the different experiments and the resulting histograms are converted into differential cross sections $\mathrm{d}\sigma_{Z'}/\mathrm{d}m_{jj}$.

	m_{jj}	$\lvert\Delta\eta_{jj}\rvert$	additional	Ref.
ATLAS 13 TeV	> 1.1 TeV	< 1.2	$p_{T,j_1} > 440$ GeV and $p_{T,j_2} > 50$ GeV	[125]
CMS 13 TeV	> 1.2 TeV	< 1.3	$p_{T,j_1} > 500$ GeV or $H_T > 800$ GeV	[126]
ATLAS 8 TeV	> 250 GeV	< 1.2	-	[127]
CMS 8 TeV	> 890 GeV	< 1.3	-	[128]
CMS 8 TeV (low)	> 390 GeV	< 1.3	-	[129]

Table 2.2: *Experimental cuts adopted by the five experimental searches. p_{T,j_1} refers to the transverse momentum of the leading jet, p_{T,j_2} refers to the subleading jet. H_T is the scalar sum of all jet p_T for jets with $p_T > 40$ GeV and $|\eta| < 3$, and $\Delta\eta_{jj}$ refers to the rapidity separation of the leading and subleading jets.*

2.2.2 Compatibility of a dijet signal with LHC data

Once the dijet invariant mass distributions have been generated, the next step is to determine the compatibility of such a signal with LHC data. To do this, we follow the approach of the experimental collaborations and assume that the SM background can be described by a smooth function of the form:

$$\frac{\mathrm{d}\sigma_{\mathrm{SM}}}{\mathrm{d}m_{jj}} = \frac{P_0\,(1 - m_{jj}/\sqrt{s})^{P_1}}{(m_{jj}/\sqrt{s})^{P_2 + P_3 \log(m_{jj}/\sqrt{s})}}\,, \tag{2.4}$$

where the parameters P_i are determined by fitting the function to the data.[26] The total dijet invariant mass distribution is then given by $\mathrm{d}\sigma/\mathrm{d}m_{jj} = \mathrm{d}\sigma_{\mathrm{SM}}/\mathrm{d}m_{jj} + \mathrm{d}\sigma_{Z'}/\mathrm{d}m_{jj}$, where the first term depends on the unknown parameters P_i, while the second term depends on the assumed values for $m_{Z'}$, Γ and g_q.

To compare the model prediction to experimental data, we calculate the usual χ^2 test statistic

$$\chi^2 = \sum_i \left(\frac{d_i - s_i}{\sigma_i}\right)^2\,, \tag{2.5}$$

where the index i denotes the bin number in a given experiment, d_i is the observed differential cross section with corresponding (statistical) error σ_i and s_i is the predicted signal containing both the SM contribution and the new-physics signal , which we assume to be narrow, $\Gamma/m_{Z'} < 0.3$. We now fix the unknown parameters P_i by finding the minimum of the χ^2 distribution with respect to these parameters (called $\hat{\chi}^2$).

Now we can move on to placing an upper bound on the size of the new physics

[26] The CMS analyses at 8 and 13 TeV and the ATLAS analysis at 8 TeV allow all four parameters to vary, whereas the ATLAS analysis at 13 TeV fixes $P_3 = 0$.

contribution to the dijet signal. We use a $\Delta\chi^2$ method for this, first calculating $\hat{\chi}^2$ with no Z' contribution, $\hat{\chi}^2_0$. We then define $\Delta\chi^2(m_{Z'}, \Gamma, g_q) = \hat{\chi}^2(m_{Z'}, \Gamma, g_q) - \hat{\chi}^2_0$, the difference between the fit to data with and without the new physics contribution.

For $\Delta\chi^2 < 0$, the data would prefer a contribution from the Z' mediator. Positive values of $\Delta\chi^2$, on the other hand, are disfavoured by the data. In this case, we calculate the p-value, i.e. the probability to observe at least as large a value of $\Delta\chi^2$ from random fluctuations in the data as

$$P = 1 - \mathrm{CDF}\left(1, \Delta\chi^2\right) \tag{2.6}$$

where $\mathrm{CDF}\,(1, \chi^2)$ is the cumulative distribution function for the χ^2 distribution with one degree of freedom.[27]

As discussed above, the new-physics signal is proportional to g_q^4. As we increase g_q, keeping $m_{Z'}$ and Γ fixed, we will reach the point where $\Delta\chi^2$ becomes so large that P becomes small. For $P < 5\%$, we can exclude the corresponding value of g_q at the 95% confidence level. If $P > 5\%$, the value of g_q cannot be excluded by the experiment under consideration, but it may still be excluded by the combination of results from several experiments, explained below. Such a combination is somewhat model-dependent in the sense that it requires an assumption on the ratio of the production cross section of the resonance at 8 TeV and 13 TeV. Since we use a Z'-model to generate dijet events, our combination will surely be valid for any resonance produced dominantly from light quarks (with equal couplings to each flavour).

For a given signal hypothesis, we can follow the procedure described above to obtain a value of $\Delta\chi^2$ for each experiment under consideration, with the parameters P_i fitted independently for each experiment. Since the two CMS searches at 8 TeV are not statistically independent, we use ref [128] for $m_{Z'} \geq 1$ TeV and

[27] Technically, the $\Delta\chi^2$ test statistic as we define it does not exactly follow a χ^2-distribution. This is because we use $\hat{\chi}^2_0$ as the value of $\hat{\chi}^2$ for $g_q = 0$ rather than finding the value of g_q that actually minimises $\hat{\chi}^2$ (called $g_{q,0}$) in order to avoid the problem that the data may prefer a negative signal contribution. Since $\hat{\chi}^2(0) \geq \hat{\chi}^2(g_{q,0})$, our definition yields slightly smaller values for $\Delta\chi^2$ than the one obtained from minimising $\hat{\chi}^2$ with respect to g_q. Using a χ^2-distribution to calculate the p-value therefore means that we slightly overestimate the p-value and consequently place more conservative bounds. We have verified that the error made by this approximation is small by determining the actual distribution of $\Delta\chi^2$ from a Monte Carlo simulation for specific parameter points.

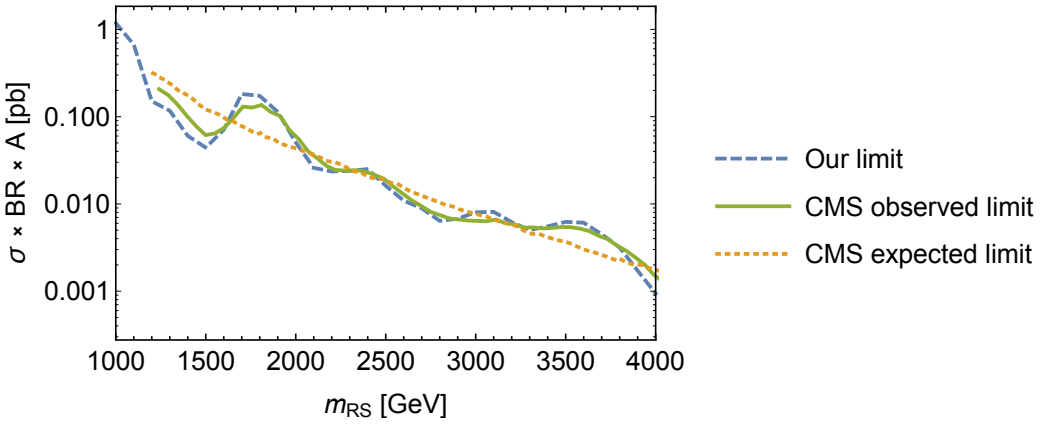

Figure 2.1: *Comparison of our method for setting limits from dijet data (blue, dashed) with those from the CMS experiment [128] (green, solid) presented in terms of the cross section times acceptance, for the benchmark model of an RS graviton [71].*

ref [129] for lower Z' masses. We can then add up the $\Delta\chi^2$ from each experiment to obtain $\Delta\chi^2_{\text{total}}$. This test statistic is expected to approximately follow a χ^2-distribution with one degree of freedom, so we can calculate the combined p-value with eq. (2.6).

Validation based on the RS-graviton model

To validate our approach, we have applied our analysis to the RS graviton model [71] used as a benchmark in the CMS analysis [128]. The model has two free parameters, the mass of the RS graviton m_{RS} and the curvature of the five-dimensional bulk $k/\tilde{M}_{\text{Pl}}$ where $\tilde{M}_{\text{Pl}}$ is the reduced Planck mass. The latter is taken to be $k = 0.1\tilde{M}_{\text{Pl}}$, which determines the relevant width and couplings needed for dijet event generation, for a given value of m_{RS}. We calculate the dijet cross section and invariant mass distributions in this model, using the distributions to find the largest rescaling factor μ which is compatible with the data. The product of μ and the dijet cross section gives the excluded cross section to 95% confidence level, shown in comparison to the published CMS result in Figure 2.1. We conclude our analysis shows good agreement with the results from the CMS collaboration, over the range of masses shown.

2.2.3 Results of dijet analysis

Now the statistical analysis has been described, we move on to presenting our results, keeping in mind the desired applicability to a broad range of Z' models. We consider $m_{Z'}$ masses between 500 GeV and 4 TeV in steps of 50 GeV. For each mediator mass, we consider six different widths: 1%, 2%, 5%, 10%, 20% and 30% (in units of $m_{Z'}$), chosen to best sample the variation in the resulting constraints for different widths. For widths smaller than 1% the dijet invariant mass distribution becomes completely dominated by detector effects. For each $m_{Z'}$ and Γ we follow the procedure described above to obtain an upper bound on g_q at the 95% confidence level, called $g_{q,95\%}$.

We find that the resulting constraints tend to vary a small amount stochastically as you vary $m_{Z'}$ due to fluctuations in the data from bin to bin. However we find that the dependence of our constraints on Γ to be much smoother, with larger values of Γ always corresponding to weaker bounds. More specifically we find that we are able to fit our constraints $g_{q,95\%}$ for fixed $m_{Z'}$ using a function of the form

$$g_{q,95\%}(m_{Z'}, \Gamma_{Z'})^4 = a(m_{Z'}) \left(\frac{\Gamma_{Z'}}{m_{Z'}} \right)^{b(m_{Z'})} + c(m_{Z'}) \,, \tag{2.7}$$

where the values of a, b and c are listed in table A.1 in appendix A.1 as a function of $m_{Z'}$. We show $g_{q,95\%}$ as a function of $m_{Z'}$ and Γ as obtained this way in the top panel of figure 2.2.

For $m_{Z'} \lesssim 1.5$ TeV dijet constraints are able to exclude values of g_q between 0.1 (for a narrow width) and 0.3 (for a broad width). For larger masses, these bounds become somewhat weaker and reach up to $g_{q,95\%} \approx 0.6$ for $m_{Z'} \sim 4$ TeV and $\Gamma/m_{Z'} > 0.2$. We observe that rather weak bounds are obtained for $m_{Z'} \approx$ 1.6–1.7 TeV. The reason is that in this mass range all four experiments see an upward fluctuation in the data, so that the observed bound is weaker than the expected one (see also [163, 164]).[28]

Since we have consistently treated Γ and g_q as independent parameters, our results can be applied to any Z' model (with universal vector-like couplings to

[28] This pattern is driven by the ATLAS 8 TeV data set and is most pronounced for very broad widths. The largest preference for a non-zero contribution from a Z' is found for $m_{Z'} = 1.7$ TeV, $\Gamma/m_{Z'} = 0.3$ and $g_q = 0.55$. The local significance of this excess is 3.3σ for ATLAS alone and 3.8σ for the combination of all data sets. Unfortunately, more recent data not included in this analysis does not show such a feature of sufficient magnitude or width [112]

quarks) by applying the following procedure:

1. For a given Z' mass and given couplings of the Z' to all other particles in the theory, calculate the total decay width Γ.

2. Look up $g_{q,95\%}$ for this value of Γ and the assumed Z' mass.

3. If $g_{q,95\%}$ is larger than the assumed Z'-quark coupling, the parameter point is allowed. Otherwise, it is excluded at 95% confidence level.

We emphasise here that since we have treated Γ as a free parameter, the bounds we obtain should only be used for physical values of Γ, that is, only values of Γ that have been calculated consistently within a specific theory. We now comment on the sorts of theories that our bounds can be applied to.

While the procedure detailed above applies to Z' models with universal vector couplings to all quarks, it is also possible for us to constrain more complicated models. For this purpose, we make use of the narrow-width approximation (NWA), which is valid as long as the width of the Z' is small compared to its mass (typically $\Gamma/m_{Z'} < 0.3$). The NWA states that the cross section for the production of dijet events via a resonance factorises into the production cross section of the resonance and the probability for this resonance to decay into a pair of jets:

$$\sigma(pp \to Z' \to jj) = \sigma(pp \to Z') \times \mathrm{BR}(Z' \to jj) \,, \tag{2.8}$$

where $\mathrm{BR}(Z' \to jj) = \Gamma(Z' \to jj)/\Gamma = 5\, g_q^2\, m_{Z'}/(4\pi\, \Gamma)$. In the model we consider the Z' production cross section is proportional to g_q^2, with a constant of proportionality that depends on the Z' mass and the centre-of-mass energy. Consequently, the dijet signal in each experiment is proportional to g_q^2 times the relevant branching ratio:

$$\sigma(pp \to jj) \propto g_q^2 \times \mathrm{BR}(Z' \to jj) \,. \tag{2.9}$$

This relation is also correct for the differential cross section, i.e. the shape of the dijet invariant mass distribution is independent of the coupling g_q for fixed mediator mass and width.

This observation allows a different way of presenting our results, by placing

an upper bound on the combination [136]

$$j \equiv g_q^2 \times \mathrm{BR}(Z' \to jj) \; . \tag{2.10}$$

As discussed above, j is proportional to g_q^4 for fixed Γ. We can then calculate the upper bound on j at 95% confidence level, called $j_{95\%}$, by evaluating j for $g_{j,95\%}$. We emphasise that it is perfectly acceptable for this calculation to yield a branching ratio larger than unity: in such a case the conclusion would simply be that the experimental bounds cannot exclude any value of g_q compatible with the chosen value of Γ.

Our results for $j_{95\%}$ are shown in the bottom panel of figure 2.2. The advantage of this approach is that $j_{95\%}$ can also be used to constrain models beyond the one considered here (Equation 2.1). In particular, our analysis can be applied to the following cases:

- For a Z' with both vector (g_q^V) and axial (g_q^A) couplings to quarks, the production cross section for a Z' is proportional to $(g_q^V)^2 + (g_q^A)^2$. In such a model, one should therefore calculate $\left[(g_q^V)^2 + (g_q^A)^2\right] \times \mathrm{BR}(Z' \to jj)$ and compare the result to $j_{95\%}$ as shown in the bottom panel of figure 2.2.[29]

- The Z' production is typically dominated by up and down quarks in the initial state. Consequently, for a Z' with different couplings to the three generations, one can obtain an approximate bound by calculating $g_1^2 \times \mathrm{BR}(Z' \to jj)$, where g_1 is the coupling to the first generation, and comparing the result to the bound on $g_q^2 \times \mathrm{BR}(Z' \to jj)$ (i.e. $j_{95\%}$) shown in figure 2.2. This approximation should hold as long as the couplings to heavier flavours are not significantly larger than those to lighter flavours.

Plain text versions of $j_{95\%}$ as a function of $m_{Z'}$ and Γ are available online in the supplementary material accompanying [1].

This concludes the description of the dijet analysis and the application of the results to generic Z' models. In the next section we move on to a specific model, a simplified DM model, in order to show how these dijet constraints can be applied and combined with information coming from the relic density.

[29] For a Z' with purely axial couplings to quarks, one can also directly compare g_q^A to $g_{q,95\%}$ shown in top panel of figure 2.2.

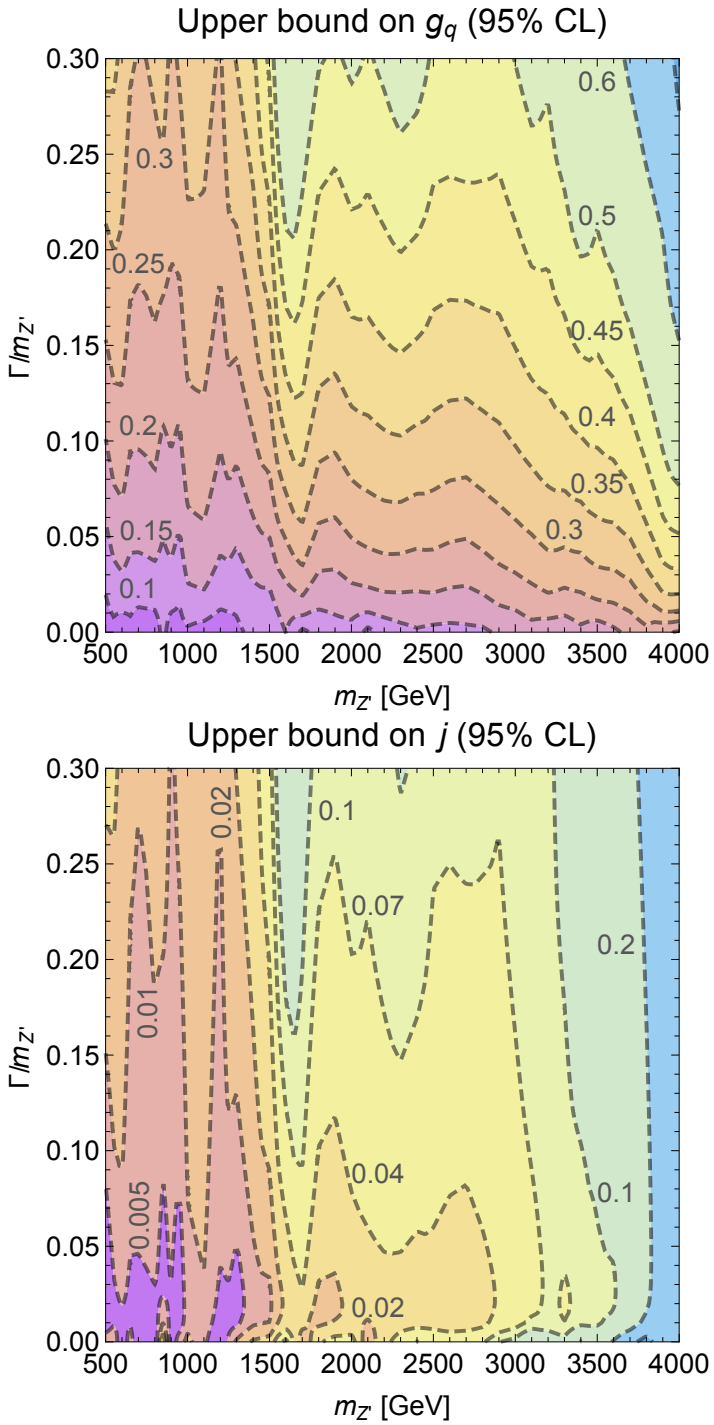

Figure 2.2: *Bounds on g_q (top) and $j \equiv g_q^2 \times BR(Z' \to jj)$ (bottom) from a combination of ATLAS and CMS dijet searches at 8 TeV and 13 TeV at 95% confidence level as a function of the Z′ mass and width.*

2.3 Constraints on a leptophobic Z' coupling to DM

We now extend the previously proposed model by allowing the Z' to couple to DM (see [165–168]) which is similar to the simplified models discussed in [61, 140, 142, 145, 148, 149, 151]. We assume DM to be a Majorana fermion, $\psi^c = \psi$, which allows us to significantly reduce bounds coming from direct detection experiments. The vectorial coupling of DM to the Z' vanishes naturally for a Majorana fermion, leaving just an axial coupling which suppresses the DM scattering cross section by powers of the non-relativistic DM velocity. Our Lagrangian is

$$\mathcal{L}_{\text{kin}} = \frac{i}{2}\bar{\psi}\gamma^\mu\partial_\mu\psi - \frac{1}{2}m_{DM}\bar{\psi}\psi - \frac{1}{4}F'_{\mu\nu}F'^{\mu\nu} + \frac{1}{2}m^2_{Z'}Z'_\mu Z'^\mu \tag{2.11}$$

$$\mathcal{L}_{\text{int}} = -\frac{1}{2}g_{DM}Z'_\mu\bar{\psi}\gamma^\mu\gamma^5\psi - g_q Z'_\mu\sum_q \bar{q}\gamma^\mu q\ . \tag{2.12}$$

For the couplings of the Z' boson to the SM quarks, in this Chapter we assume them to be entirely vectorial which is consistent with assuming the Z' does not couple to the Higgs [169]. We do not specify the additional dark Higgs necessary to generate the Z' mass and the DM mass [169], assuming that this particle is sufficiently heavy and sufficiently weakly mixed with the SM Higgs to be irrelevant for LHC phenomenology. In this Chapter we ignore the more theoretical issue of anomaly cancellation, and focus on the phenomenological problem of constraining the simplified model parameters from data. However, see Chapter 3 for a presentation of the coupling structures necessary to guarantee anomaly cancellation.

The resulting decay widths are then given by[30]

$$\Gamma(Z' \to q\bar{q}) = \frac{m_{Z'}\,g_q^2}{4\pi}\sqrt{1-\frac{4m_q^2}{m_{Z'}^2}}\left(1+2\frac{m_q^2}{m_{Z'}^2}\right) \tag{2.13}$$

$$\Gamma(Z' \to \psi\psi) = \frac{m_{Z'}}{24\pi}(g_{\text{DM}})^2\left(1-\frac{4m_{\text{DM}}^2}{m_{Z'}^2}\right)^{3/2}\ , \tag{2.14}$$

where we have assumed $m_{Z'} > 2m_t, 2m_{\text{DM}}$. The equations above enable us to calculate the total decay width Γ, which is required in order to apply the dijet

[30] The pre-factor $1/(24\pi)$ for the decay into DM results from the fact that there are two identical particles in the final state.

bounds derived above.

2.3.1 Bounds for fixed couplings

Our model has four free parameters (the two masses $m_{Z'}$ and m_{DM} and the two couplings g_q and g_{DM}). We first look at the bounds on this model for fixed couplings, which is consistent with the most common way of presenting LHC constraints on simplified models. This approach is simple, but somewhat arbitrary, so we will select couplings fixed by the relic density in the next subsection.

In principle our model is distinct from the conventional vector or axial vector simplified models which take the same type of coupling to the Z' (the SM and DM couplings are either both vectorial or both axial) whereas in our case we have an axial coupling to DM and a vectorial coupling to quarks. However, this is not expected to significantly alter the dijet bounds apart from a mild strengthening due to the invisible width of the Z' being smaller by a factor of two (a direct consequence of the Majorana nature of DM). However, the relic density calculation is altered in comparison to those that apply to the simplified models.

Following the recommendations from [63, 151], we consider the case $q_q = 0.25$, $g_{\mathrm{DM}} = 1$. For these couplings the width of the Z' varies between 2.5% (for $m_{Z'} < 2m_{\mathrm{DM}}, 2m_t$) and 4.3% (for $m'_Z \gg 2m_{\mathrm{DM}}, 2m_t$) of its mass. For each combination of $m_{Z'}$ and m_{DM}, we calculate the width Γ and then read off the largest allowed value for g_q from figure 2.2. Whenever $g_{q,95\%} < 0.25$, the parameter point is excluded by our combined dijet bounds. The results of this analysis are shown in figure 2.3 with the dijet excluded regions shown in red. We find that Z' masses between 500 GeV and 1600 GeV are excluded irrespective of the value of m_{DM}. For $m_{Z'}$ between 1600 GeV and 3 TeV, the model is excluded for heavy DM particles, such that the invisible branching ratio of the Z' is small and decays into dijets dominate. These bounds are somewhat stronger than the ones found by the individual experiments due to our combined analysis.

The region is grey is where the coupling of the DM particle to the longitudinal component of the Z' violates perturbative unitarity, $m_{DM} < \sqrt{2\pi}\frac{m_{Z'}}{g_{DM}}$,as pointed out in [147, 169]. The green lines are where the observed DM relic abundance, $\Omega h^2 = 0.12$ [171], is observed. We calculate the relic density numerically using `micrOMEGAs_v4.1.8` [172], further details of which can be found in the next subsection.

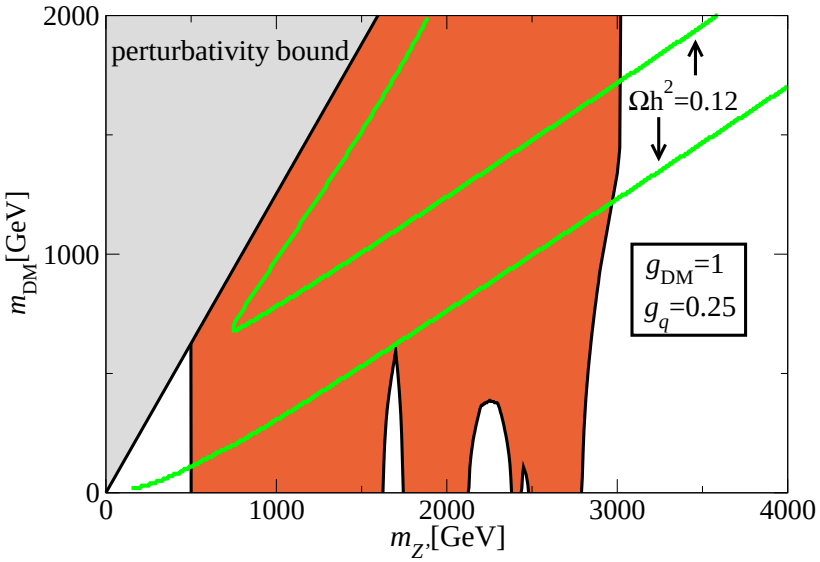

Figure 2.3: *Excluded regions of parameter space in the mass-mass plane for fixed couplings, following the recommendations of the DM LHC working group [63]. The region in red is excluded by our combined dijet analysis at the 95% confidence level while the green lines represent parameter points which reproduce the observed relic density of DM in the Universe. In the grey region perturbative unitarity is violated.*

We find that there are only two regions where the relic density is compatible with dijet constraints: A low-mass region with $m_{Z'} < 500$ GeV and $m_{\mathrm{DM}} < 150$ GeV and a high-mass region with $m_{Z'} > 3$ TeV and $m_{\mathrm{DM}} > 1200$ GeV. In reality however, the low-mass region is tightly constrained by mono-X searches, in particular searches for jets in association with missing transverse energy [173–176], although we do not discuss those further here.[31] This conclusion is, however, obviously dependent on the arbitrary choice of fixed couplings. Smaller values of g_q would reduce the production cross section of the resonance, while larger values of g_{DM} would increase the invisible branching ratio (as long as $m_{\mathrm{DM}} < m_{Z'}/2$), weakening dijet constraints.

Studying the full parameter space, including all possible values of g_q and g_{DM} in

[31] There may be additional dijet constraints from previous hadron colliders, as well as constraints from dijet resonances produced in association with SM gauge bosons [134,147]. Since this work was performed, there are now also additional dijet resonance searches at higher luminosity, and with sensitivity to low masses, using boosted ISR and data-scouting [112, 113, 214, 215].

addition to $m_{\rm DM}$ and $m_{Z'}$, would require a costly multi-dimensional scan. Instead, we take the approach that the most physically interesting choices of couplings, in the context of dark matter models, are those which accurately reproduce the DM relic density. For such a purpose, in the next subsection we develop a novel technique for systematically evaluating the compatibility of dijet searches with the relic density in this simplified model.[32]

2.3.2 Combining di-jet bounds and relic density

Out of the four-dimensional parameter space of our model, we are particularly interested in those combinations of masses and couplings for which the thermal freeze-out of the DM particle can reproduce the relic abundance

$$\Omega h^2 = 0.1188 \pm 0.0010 \tag{2.15}$$

which is the result from Planck CMB observations combined with Baryon Acoustic Oscillations, supernova data and H_0 measurements [171]. We will approximate the relic density as $\Omega h^2 = 0.12$ in the rest of this Chapter.

Before proceeding it is very important to note that that the relic density requirement can be relaxed if the dark sector consists of multiple components or if the thermal history of the Universe is non-standard. Additional annihilation channels, as well as those involving co-annihilation partners (if there are additional particles in the dark sector), could significantly affect the calculation of the relic density. For example, we later find combinations of couplings that satisfy the relic density, but in the presence of co-annihilations these couplings would be shifted to smaller values in order to reduce the overall annihilation cross-section and increase the relic density back to its observed value. Nevertheless, it is certainly of interest to consider those parameters for which the simplest assumptions are already able to match observations. If these parameters can be excluded experimentally, the model would require additional ingredients in the dark sector (such as additional annihilation channels, additional stable states or a mechanism to produce additional entropy after DM freeze-out), which by itself would be an important conclusion. Furthermore, it is certainly no worse than considering flat slices of

[32] A similar comparison between LHC searches for dilepton resonances and the DM relic abundance in the context of gauged $B - L$ has been performed in [177].

parameter space defined by fixed couplings, instead we will be taking (non-flat) slices of parameter space that have some motivation, with the important caveats mentioned above.

The layout of this subsection is as follows: we first describe some general aspects of the relic density calculation before introducing the set of free parameters we will use to conveniently combine the relic density with the dijet constraints. Finally the dijet bounds will actually be applied to constrain the hypothesis of thermal freeze-out in this model.

To first approximation, we can obtain the relic density by calculating the cross section for DM annihilation into a pair of quarks, $\sigma_{\psi\psi\to q\bar{q}}$, and expanding the result in terms of the relative velocity v of the two DM particles:

$$\sigma_{\psi\psi\to q\bar{q}}\, v \approx a + b\, v^2 + \mathcal{O}(v^4)\ . \tag{2.16}$$

The relic abundance is then approximately given by

$$\Omega\, h^2 \simeq 1.07 \times 10^9\ \text{GeV}^{-1} \frac{x_{\text{fo}}}{M_{\text{Pl}}\sqrt{g_*}\,(a + 3b/x_{\text{fo}})}\ , \tag{2.17}$$

where $x_{\text{fo}} \sim 20$–30 is the ratio of the DM mass and the freeze-out temperature and $g_* \sim 80$–90 is the number of relativistic degrees of freedom during freeze-out. For our model, we find $a = 0$ (due to the Majorana nature of DM) and

$$b = \frac{3\,(g_{\text{DM}})^2\, g_q^2}{12\pi} \frac{(m_q^2 + 2\,m_{\text{DM}}^2)(1 - m_q^2/m_{\text{DM}}^2)^{1/2}}{[(m_{Z'}^2 - 4m_{\text{DM}}^2)^2 + (\Gamma\, m_{Z'})^2]}\ . \tag{2.18}$$

For $m_{\text{DM}} \approx m_{Z'}/2$, the denominator in eq. (2.18) becomes very small and DM annihilation receives a resonant enhancement. In this case, an expansion in terms of the velocity of the two DM particles is insufficient for an accurate calculation of the relic density and numerical methods are needed. We therefore calculate the relic density using `micrOMEGAs_4.1.8` [172], including two modifications under the instruction of the authors (see appendix A.2).[33]

For given $m_{Z'}$, m_{DM} and g_{DM} we can then numerically determine the value of g_q that is required to reproduce the observed relic density.[34] As long as m_{DM}

[33] We thank Alexander Pukhov for providing us with these modifications and for his help in the implementation.

[34] The width Γ is determined internally by micrOMEGAs in a self-consistent way.

is well below the resonance region, i.e. $m_{\mathrm{DM}} \ll m_{Z'}/2$, eq. (2.18) implies that the annihilation cross section is proportional to $g_q^2\, g_{\mathrm{DM}}^2\, m_{\mathrm{DM}}^2/m_{Z'}^4$. Therefore it is always possible to fix g_q in such a way that the observed value of $\Omega\, h^2$ is matched and the solution is always unique. In the resonance region, the annihilation cross section is proportional to $g_q^2\, g_{\mathrm{DM}}^2/\Gamma$, which is still a monotonic function of g_q so that any solution is unique. However, since the expression $g_q^2\, g_{\mathrm{DM}}^2/\Gamma$ remains finite for $g_q \to \infty$, it is possible that no solution exists. In short, as long as g_{DM} is large enough, there will always be a unique value of g_q that reproduces the relic abundance.

We therefore obtain a function $g_q(m_{Z'}, m_{\mathrm{DM}}, g_{\mathrm{DM}})$, which is illustrated in figure 2.4 as a function of g_{DM} for various fixed values of $m_{Z'}$ and m_{DM}. The resulting curves have the following features:

1. Since the annihilation cross section grows monotonically with the DM mass (for fixed couplings and mediator mass), the lines for different DM masses never cross, i.e. smaller values of m_{DM} always require larger couplings.

2. For sufficiently small DM masses, the curves are hyperbolas ($g_q \propto 1/g_{\mathrm{DM}}$), whereas for larger values of m_{DM}, the curves are steeper at small g_{DM} and flatter at large g_{DM} due to the resonance effects discussed above.

We will make use of these properties below to choose a particularly convenient set of free parameters for the analysis of our model.

Relic density constraints for a fixed width

Having constructed the function $g_q(m_{Z'}, m_{\mathrm{DM}}, g_{\mathrm{DM}})$ from the relic density requirement, we could carry on and scan the remaining three-dimensional parameter space. However, the width Γ and therefore the bound from dijet constraints depends on all three parameters in a non-trivial way. For example, for fixed $m_{Z'}$ and m_{DM} one would expect stronger dijet constraints for smaller g_{DM} corresponding to larger g_q (meaning both a larger production cross section of the resonance and a larger branching fraction into dijets). However, if at the same time Γ increases, it is possible that dijet constraints are weakened enough to evade experimental bounds and that in fact larger values of g_q are less constrained than smaller couplings.

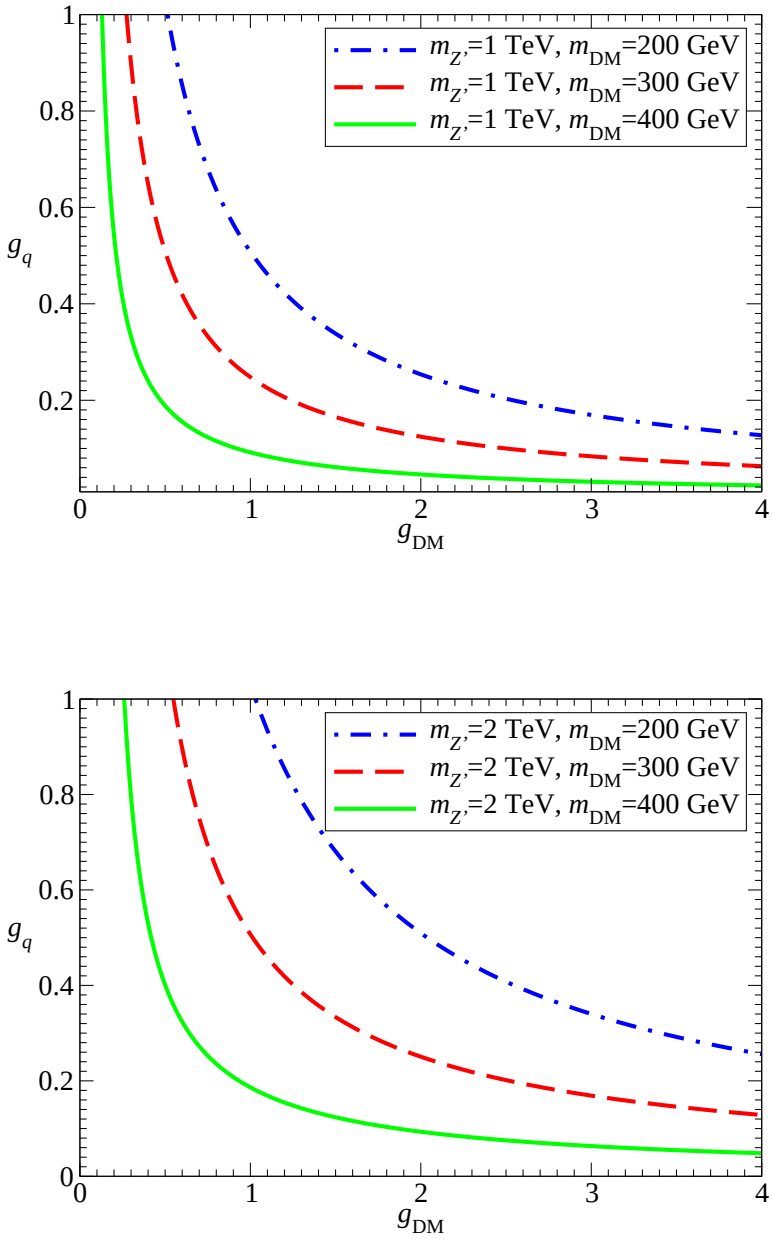

Figure 2.4: *Curves of constant relic density $\Omega h^2 = 0.12$ in the plane of the two couplings for fixed masses of the dark matter particle and a mediator mass of 1 TeV (top) and 2 TeV (bottom).*

To avoid this complication, we take both $m_{Z'}$ and Γ as free parameters. As shown in figure 2.2, for fixed values of these two parameters we can always place an upper bound on g_q. A second important advantage of this approach is that $m_{Z'}$ and Γ are the two parameters that are most directly observable at the LHC. While the DM mass is very difficult to measure at the LHC and coupling constants can only be inferred in the context of a specific model, an observation of a new resonance in the dijet channel would immediately enable us to determine the mass and the width of the mediator from the invariant mass distribution.[35] It therefore makes sense to construct all bounds in terms of these two most apparent observables.

In order to treat the width Γ as a free parameter, we need to determine the combinations of m_{DM}, g_{DM} and g_q that reproduce the observed relic density while at the same time matching the required width. For this purpose we first of all observe from eqs. (2.13)–(2.14) that for fixed $m_{Z'}$ and $m_{\mathrm{DM}} < m_{Z'}/2$ the total width Γ is an ellipse in the couplings.[36] We can now consider ellipses of constant width Γ in the same g_q-g_{DM}-plane used in figure 2.4 to study the relic density constraints. Since the relic density curve is convex while the constant-width curve is concave, the two curves will have either exactly two intersects or zero intersects.[37] In other words, for fixed values of $m_{Z'}$, Γ and m_{DM}, there is either no combination of g_q and g_{DM} that reproduces the relic density constraint or there are two separate solutions corresponding to the desired value of Γ. Whenever there are two solutions, we define Solution I to be the one with larger g_{DM} (and therefore smaller g_q) and Solution II to be the one with smaller g_{DM} (larger g_q). Two examples are shown in figure 2.5.

As noted above, increasing the value of m_{DM} will shift the relic density curve towards smaller couplings. Conversely, the constant-width curve will be shifted to larger couplings (due to the larger phase-space suppression of $Z' \to \psi\psi$). This means that for each value of $m_{Z'}$ and Γ there is a minimum value of m_{DM}, called $m_{\mathrm{DM,min}}(m_{Z'}, \Gamma)$, such that there is no solution for $m_{\mathrm{DM}} < m_{\mathrm{DM,min}}$ and two solutions for $m_{\mathrm{DM}} > m_{\mathrm{DM,min}}$. Increasing m_{DM} beyond $m_{\mathrm{DM,min}}$ will shift Solution

[35] This argument assumes that the width of the resonance is large compared to the detector resolution. For a narrow resonance it is still possible to determine the mass and place an upper bound on the width.

[36] For $m_{\mathrm{DM}} \geq m_{Z'}/2$, the total width is independent of g_{DM} and hence a straight line $g_q = \mathrm{const}$.

[37] Neglecting those special cases where the two curves just touch at exactly one point.

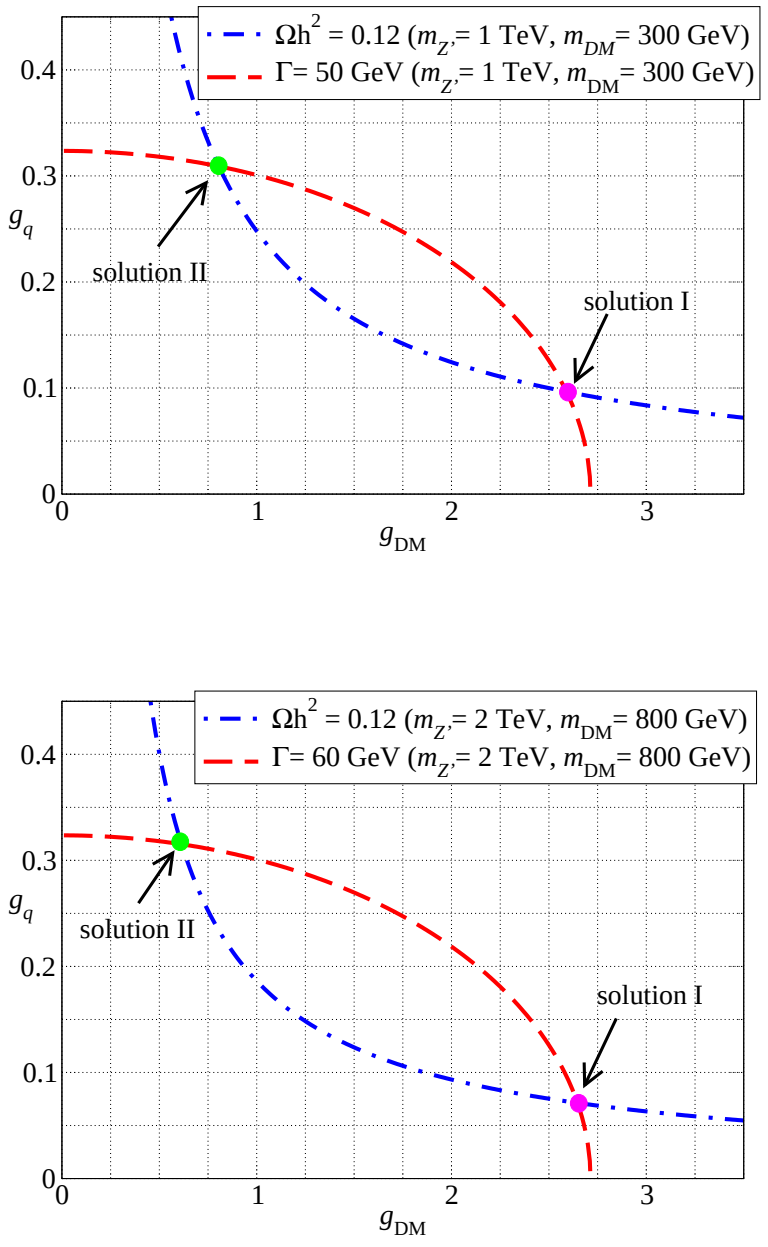

Figure 2.5: *Examples of how we find pairs of couplings that satisfy the relic density constraint (blue) for a given fixed width (red).*

I to larger values of g_{DM} and smaller values of g_q and vice versa for Solution II. As m_{DM} approaches $m_{Z'}/2$, Solution I will yield arbitrarily large values of g_{DM} and thus ultimately violate a perturbativity bound. Here and throughout, we decide to restrict all couplings to be smaller than $g < \sqrt{4\pi}$, corresponding to $\alpha = g^2/4\pi < 1$. In principle, couplings as large as $g < 4\pi$ could be allowed, since each higher order term in a perturbative expansion comes with a factor $g^2/16\pi$ which must be less than unity for the expansion to converge, with a more rigorous limit depending on the exact form of the loop corrections. We decide on the stronger requirement on g_{DM} in order to be closer to the realm of validity of perturbation theory, since a rigorous derivation of the perturbative limit is beyond the scope of this study.[38] However, in principle there is a small range of couplings we choose to exclude from our analysis, $\sqrt{4\pi} < g_{DM} \lessapprox \sqrt{8\pi}$ which still have a narrow enough Z' width $\Gamma/m_{Z'} < 0.3$. We will comment later on how our results might change with these couplings allowed. This Solution II, on the other hand, will approach a small but non-zero minimum value of g_{DM}, called $g_{\mathrm{DM,min}}$.[39] Figure 2.6 shows both $m_{\mathrm{DM,min}}$ and $g_{\mathrm{DM,min}}$ as a function of $m_{Z'}$ and Γ.

With these considerations in mind, we can now eliminate either m_{DM} or g_{DM} in favour of Γ and proceed with either ($m_{Z'}$, Γ, g_{DM}), where $g_{\mathrm{DM,min}} < g_{\mathrm{DM}} < \sqrt{4\pi}$, or with ($m_{Z'}$, Γ, m_{DM}), where $m_{\mathrm{DM,min}} < m_{\mathrm{DM}} < m_{Z'}/2$. While in the first case we find a single value of g_q for each set ($m_{Z'}$, $\Gamma\, g_{\mathrm{DM}}$) compatible with the relic density constraint and consistent with the required width, the second case yields two separate solutions as discussed above. We discuss both possibilities below, as they each offer different physical insights.

Dijet bounds on the DM coupling

We have shown above that for fixed $m_{Z'}$ and Γ smaller values of g_{DM} correspond to larger values of g_q. Using figure 2.2 to read off the upper bound on g_q from dijet searches thus allows us to place a lower bound on g_{DM}. This lower bound on g_{DM} is shown in figure 2.7. Wherever no bounds from dijet searches can be placed, we simply show the smallest value of g_{DM} for which the relic density curve and the

[38] For the widths that we are considering, $\Gamma/M_{Z'} \leq 0.3$, g_q is always less than 1, so we never run into problems with the perturbativity of g_q.

[39] Note that in fact the resonant enhancement of the annihilation cross section is maximal (and hence the coupling g_{DM} is minimal) for m_{DM} slightly below $m_{Z'}/2$. We determine the DM mass corresponding to $g_{\mathrm{DM,min}}$ numerically.

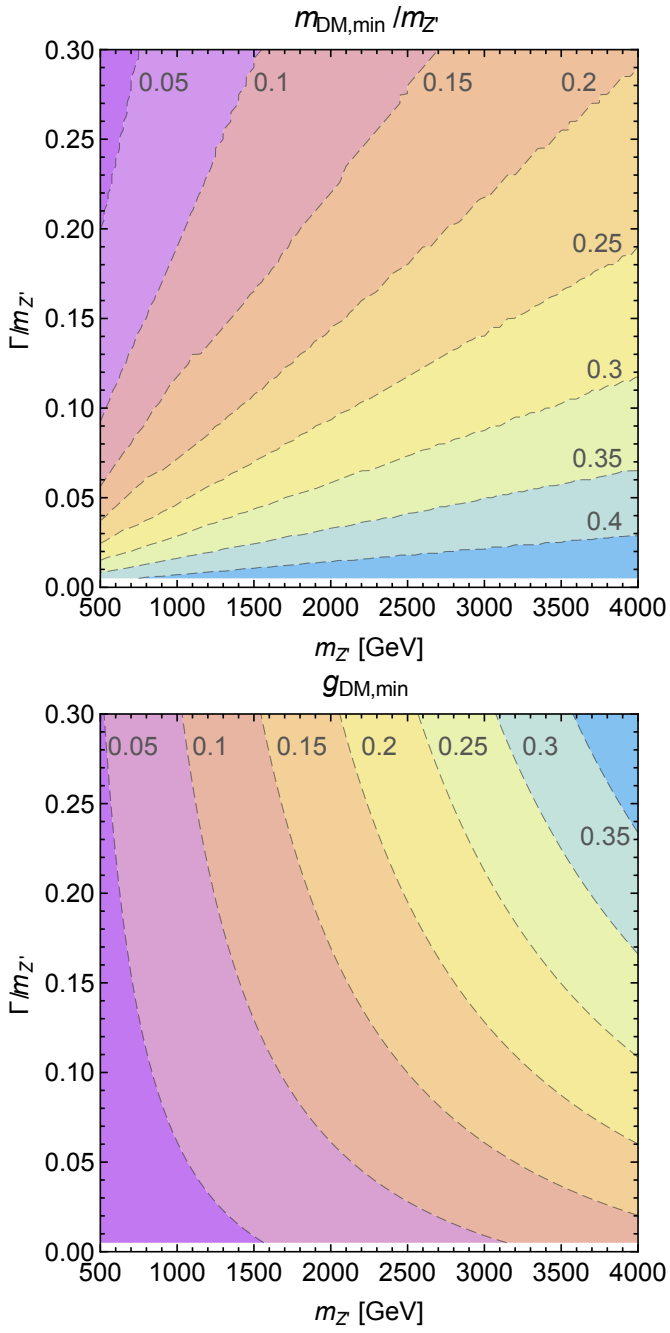

Figure 2.6: *Top: The minimum value of the DM mass (in units of $m_{Z'}$) required in order to simultaneously satisfy the relic density constraint and reproduce the assumed Z' width. For smaller DM masses, the relic density curve and the constant width curve do not intersect in the g_{DM}-g_q plane (see figure 2.5). Bottom: The smallest value of g_{DM} that can reproduce the observed relic density and the assumed width. This value corresponds to Solution II for m_{DM} slightly below $m_{Z'}/2$.*

constant-width curve intersect (called $g_{\mathrm{DM,min}}$ above). If on the other hand the lower bound from dijet searches is so strong that it requires g_{DM} to be larger than $\sqrt{4\pi}$, we conclude that it is impossible to find perturbative values of g_q and g_{DM} such that the width Γ and the relic density can be reproduced without violating dijet constraints. The corresponding regions are shaded in orange in figure 2.7.

We observe that rather large values of g_{DM} are required in order to avoid dijet constraints. While the consistency of the relic density requirement and the assumed width only required $g_{\mathrm{DM,min}} \sim 0.1$–$0.3$ (see figure 2.6), dijet constraints require $g_{\mathrm{DM}} > 1$ in almost the entire parameter space that we consider. For large Z' width, even larger values of g_{DM} are required in order to reduce the branching ratio of the Z' into dijets. For $m_{Z'} \lesssim 1.5$ TeV and $\Gamma/m_{Z'} \gtrsim 0.2$ as well as for $1.7\ \mathrm{TeV} \lesssim m_{Z'} \lesssim 3.3$ TeV and $\Gamma/m_{Z'} \gtrsim 0.25$, all perturbative values of g_{DM} that reproduce the relic abundance are excluded by dijet searches. For larger Z' masses, LHC dijet searches lose sensitivity, but significant improvements in this mass range can be expected from including more recent and future data at 13 TeV.[40]

Dijet bounds on the DM mass

Let us finally present our results from a complementary perspective by taking m_{DM} as a free parameter and determining both g_{DM} and g_q from the relic density constraint and the requirement of a constant width. As discussed above, for each value of m_{DM} we obtain two separate solutions, with Solution I (II) corresponding to larger (smaller) g_{DM}. For each of the two solutions, we can directly read off from figure 2.2 whether the parameter point is excluded by the combined dijet constraints that we have derived above. These exclusion limits in turn allow us to determine the allowed range of DM masses as a function of $m_{Z'}$ and Γ. We now discuss the two different solutions in turn.

As noted above, for Solution I (i.e. larger values of g_{DM}), the DM coupling increases with the DM mass. The requirement to have a perturbative coupling, $g_{\mathrm{DM}} < \sqrt{4\pi}$, therefore gives an upper bound on m_{DM}, called $m_{\mathrm{DM,max}}$. For some values of $m_{Z'}$ and Γ we find that Solution I yields a non-perturbative value of g_{DM} for all values of the DM mass, so for these combinations of Z' mass and width only Solution II is of interest.

[40] Recall that in this Chapter, only 13 TeV data sets of approximately 3 fb^{-1} are used.

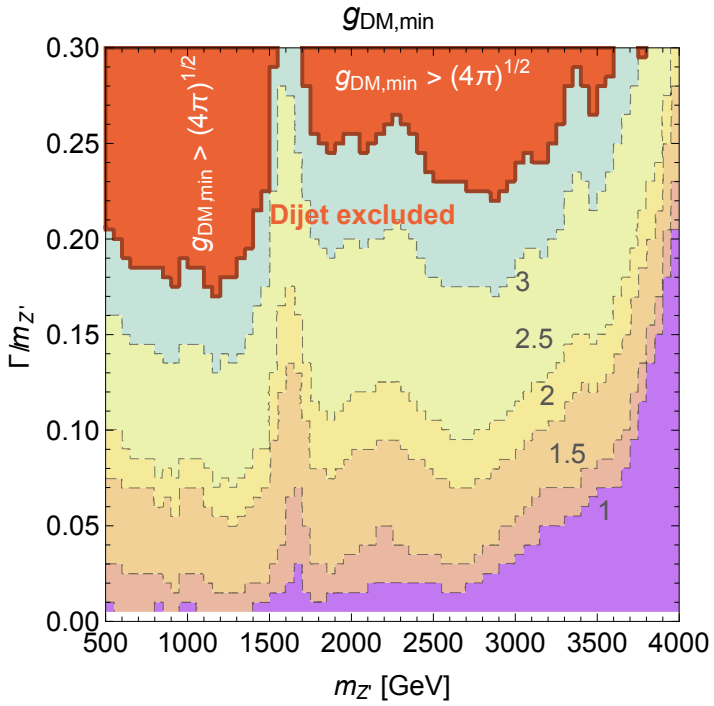

Figure 2.7: *Lower bound on the DM coupling g_{DM} from the combination of the relic density constraint and LHC dijet searches. In the orange shaded region, $g_{DM,min}$ becomes non-perturbative, i.e. all perturbative values of g_{DM} are excluded by LHC dijet searches.*

Conversely, for Solution I smaller DM masses correspond to larger values of g_q. Since large values of g_q are excluded by LHC dijet searches, we can use the LHC bounds to place a lower limit on $m_{\rm DM}$, called $m_{\rm DM,min}$.[41] The combination of the perturbativity requirement and LHC dijet searches therefore yield a range of permitted dark matter masses $[m_{\rm DM,min}, m_{\rm DM,max}]$, which satisfy all of our constraints. In other words, for $m_{\rm DM}$ in this range, it is possible to find values of g_q and $g_{\rm DM}$ that yield the observed relic abundance and are consistent with all other constraints that we consider.

Figure 2.8 shows one example, where we have fixed the Z' mass to 1 TeV and show $m_{\rm DM,min}$ (orange) and $m_{\rm DM,max}$ (blue, dashed) as a function of Γ. To illustrate the impact of dijet searches, we also show the value of $m_{\rm DM,min}$ that one obtains solely from the consistency of relic density and constant width (orange,

[41] Note that even if LHC dijet searches are not constraining, there is always a lower limit on $m_{\rm DM}$ from the requirement that the relic density curve and the constant-width curve intersect in the g_q-$g_{\rm DM}$ plane.

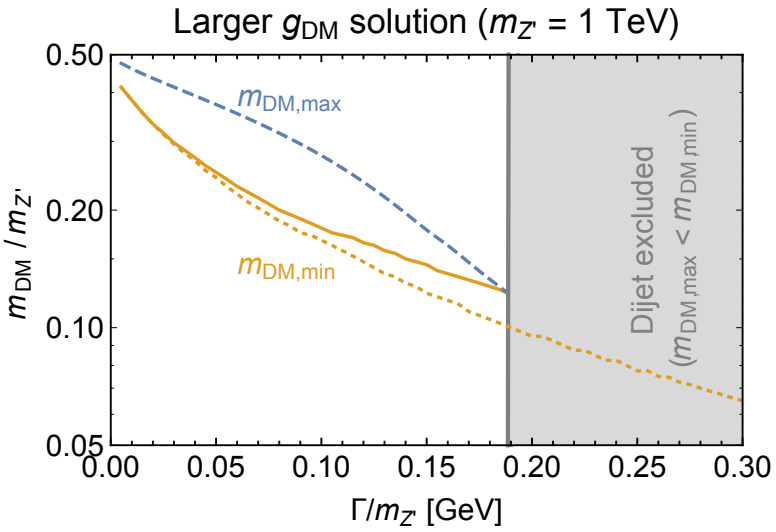

Figure 2.8: *Maximum (blue, dashed) and minimum (orange) allowed value of the DM mass as a function of the mediator width for $m_{Z'} = 1$ TeV using Solution I (larger values of g_{DM}). The dotted orange line indicates the bound on $m_{DM,min}$ in the absence of LHC dijet constraints (see figure 2.6).*

dotted). For large values of Γ we find that $m_{\mathrm{DM,max}} < m_{\mathrm{DM,min}}$, i.e. all perturbative solutions are excluded by LHC dijet searches. In the specific case under consideration, this occurs for $\Gamma/m_{Z'} \gtrsim 0.19$.

Figure 2.9 shows the largest allowed DM mass (top) and the smallest allowed DM mass (bottom) as a function of $m_{Z'}$ and Γ. The plots can be read by picking a point on the plane (i.e. fixing $m_{Z'}$ and Γ) and then reading off $m_{\mathrm{DM,max}}$ and $m_{\mathrm{DM,min}}$ from the two panels to find the range of permitted dark matter masses $[m_{\mathrm{DM,min}}, m_{\mathrm{DM,max}}]$ that satisfy all constraints. Those combinations of $m_{Z'}$ and Γ for which $m_{\mathrm{DM,max}} < m_{\mathrm{DM,min}}$ are shaded in orange. The grey region indicates those combinations of Z' mass and width for which no perturbative solutions can be found. As expected, the orange shaded region is identical to the one found in figure 2.7.

Turning now to Solution II, we note that for this solution perturbativity constraints will typically be less important (because we consider smaller values of g_{DM}), while dijet constraints will be more important (because the corresponding values of g_q are larger). Compared to the previous solution, the situation is now reversed: The requirement of perturbativity may raise $m_{\mathrm{DM,min}}$, while dijet constraints will lower $m_{\mathrm{DM,max}}$. We show the maximum and minimum allowed DM masses for Solution II in figure 2.10.

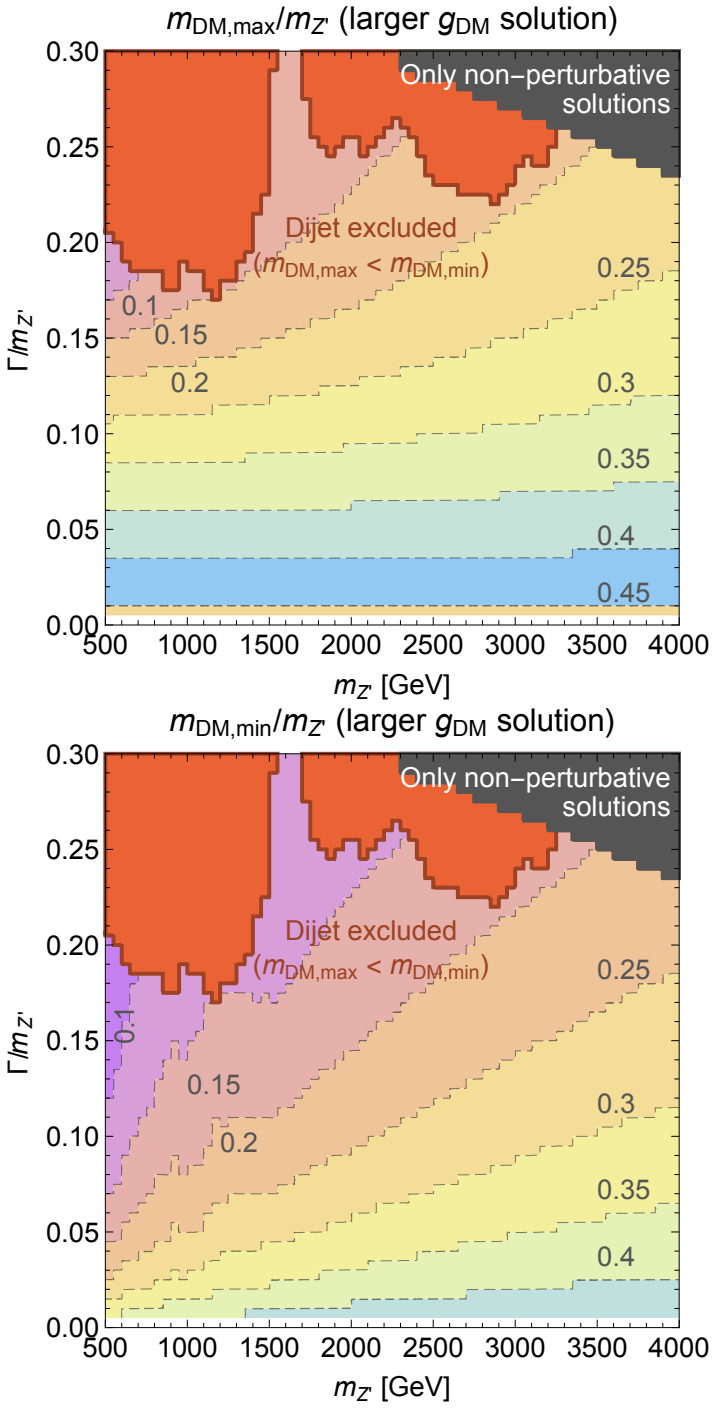

Figure 2.9: *Maximum (top) and minimum (bottom) allowed value of the DM mass as a function of the mediator mass and width using Solution I (larger values of g_{DM}).*

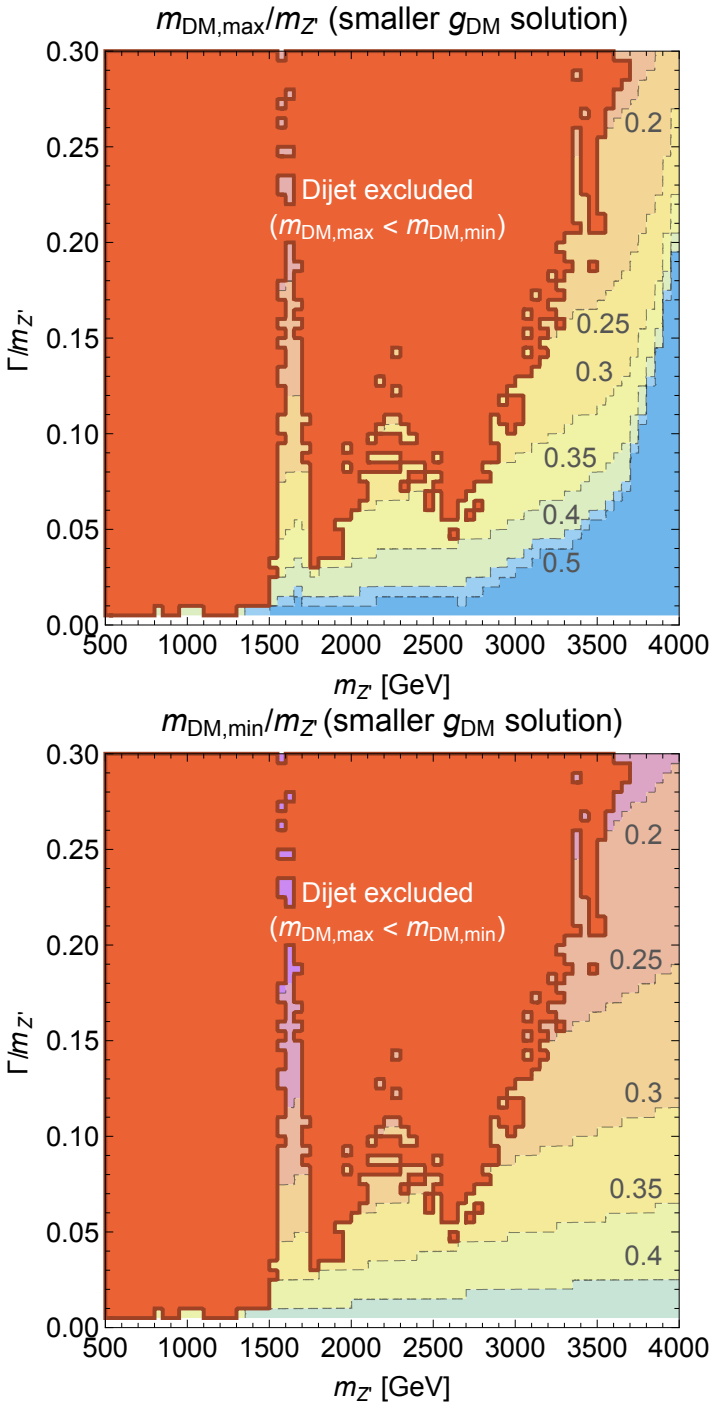

Figure 2.10: *Maximum (top) and minimum (bottom) allowed value of the DM mass as a function of the mediator mass and width using Solution II (smaller values of g_{DM}).*

As expected, we find dijet constraints (shown in orange) to be significantly stronger than for Solution I. For large width, the entire range 500 GeV $\leq m_{Z'} \leq$ 3500 GeV is excluded by dijet constraints. For $m_{Z'} \sim 1200$ GeV the dijet bounds extend down to very narrow resonances. As discussed above, dijet bounds are particularly weak around 1600 GeV, due to an upward fluctuation in the data. Finally, we note that we can always find a value of the DM mass such that Solution II corresponds to perturbative couplings (so the grey shaded region from figure 2.9 is absent).

We noted above our limit to perturbative couplings $g_{DM} < \sqrt{4\pi}$. For the reader interested in couplings close to the perturbative limit, mildly relaxing this limit by no more than a factor of $\sqrt{2}$ in g_{DM} in order to still have a narrow resonance, $\Gamma/m_{Z'} < 0.3$, would change the above results as follows. In Fig 2.7 The orange excluded region would shrink slightly, but the contours would stay the same. For Fig 2.9 $m_{DM,max}$ could increase slightly, giving a wider range of allowed m_{DM}. In Fig 2.10 $m_{DM,min}$ could instead decrease, again admitting a slightly larger range of solutions. We did not consider these solutions in the analysis above, since we wanted to be safely within the limits of perturbation theory retaining its validity.

2.4 Summary of dijet searches

We have presented a recasting and statistical combination of dijet data from both 8 and 13 TeV, allowing us to obtain constraints on models that produce a resonance that decays into a pair of jets. We presented our results in terms of a Z' model with arbitrary mass and width, which allowed the constraints to remain relatively model independent. The results are summarised in figure 2.2 and table A.1 and apply to a range of Z' models.

However, since we are interested in models of DM and in particular simplified models, we have directly applied these constraints to a simplified model with a spin-1 s-channel mediator. We first presented our results in the familiar fixed couplings plane to make contact with conventional presentations of LHC constraints on these type of models. Our results are summarised in the mass-mass plane for $g_{\rm DM} = 1$, $g_q = 0.25$, in figure 2.3 and find that dijet searches can exclude the range 500 GeV $< m_{Z'} <$ 3 TeV for most values of the DM mass.

However, since the benchmark choice of fixed couplings is somewhat arbitrary, we also investigate sets of couplings set by the relic density. This allows us to eliminate one of the free parameters of the model, using the hypothesis of thermal freeze-out. We have decided to present our bounds as a function of the Z' mass and width, the two most apparent parameters for LHC resonance searches. We've shown how the third free parameter could be chosen to be either the DM coupling or DM mass. We show the allowed range of the DM coupling in figure 2.7 and the allowed range of DM mass in figures 2.9 and 2.10. We find that regardless of the value of this third free parameter, for very broad widths ($\Gamma/m_{Z'} \gtrsim 0.25$) and Z' masses below about 3 TeV, LHC dijet searches alone already completely exclude the hypothesis that the DM particle in this theory could be completely responsible for the DM relic density.

Furthermore this approach would be very useful if any excess was observed at the LHC in the future. In this case, if the mass and width of the new resonance was able to be determined then one could take these values and read off from our plots either the allowed range of DM masses or allowed range of g_{DM} coupling. Of course, if the new resonance was in the part of our plots that was already excluded, that would be motivation to go beyond the basic simplified models of DM in order to explain the problem of DM in our universe.

In the following Chapters we will move on to consider different models of dark matter. The first will be proposed in Chapter 3 and will be natural extensions of the Z' model considered in this Chapter, motivated by anomaly-cancellation, and the wide range of constraints that apply to these models will be presented in Chapter 4. We will then explore a model with a spin-zero mediator in Chapter 5.

Chapter 3

Anomaly-free Z' Models

This Chapter is heavily based on [2] which I wrote in collaboration with John Ellis and Malcolm Fairbairn. This work was published in [2].

3.1 Introduction to anomaly-free models

As mentioned in Chapter 1, a framework of models has been built up to compare dark matter searches in collider, direct detection and astrophysical settings. These Simplified Dark Matter Models (SDMMs in this Chapter) have been motivated in part by the failings of Effective Field Theories (EFTs). In this Chapter we will attempt to extend SDMMs to more complete theories that are more theoretically consistent by virture of being anomaly-free.

It is well known that many of the simplest models in the SDMM programme are not entirely self-consistent physically. For example, models with a massive gauge boson mediator such as the one presented in Chapter 2 do not respect unitarity to arbitrarily high scales unless set within a larger theory where the mass of that boson is explained through an additonal Brout-Englert-Higgs mechanism [169]. Introducing a dark Higgs sector can make such theories more palatable, but the presence of that sector can change the phenomenology of the model [170, 213].

In this Chapter we focus on another issue, namely the fact that proposed SDMM extensions to the SM with spin-one mediators generally contain anomalies whose cancellation requires additional fermions. As pointed out in [169], the masses of the new fermions should be of the same order as the U(1)$'$ boson mass, offering additional LHC signatures that may already be constrained by the data

and should be taken into account in constraining such not-so-SDMMs.

In the case of such a spin-one intermediary particle Z', renormalizability of the SDMM requires that it be free of anomalous triangle diagrams involving any combination of the SM gauge fields, the U(1)$'$ gauge field and the graviton [180]. The requirement of anomaly freedom is understood by constructors of SDMMs [135,169], but in many cases its implications have not been pursued fully. One could, of course, take the point of view that any anomalies in the SDMM could be cancelled by some unspecified ultraviolet completion. However, in this Chapter we take the point of view that the SDMM should be self-consistent at the U(1)$'$ scale, so that one should try to construct anomaly-free SDMMs, and that it is interesting and important to understand what are the minimal such theories. [42]

There is a large literature on anomaly-free U(1)$'$ extensions of the SM with various motivations, see for example [132, 135, 166, 167, 181–196]. Among these, the closest in spirit to the models we will propose are [132, 166, 167, 189, 190], and we comment later on the relations between their papers and this work. Typical extensions of the SM with a neutral Z' particle come from GUT theories and couple to leptons as well as quarks [197]. When such a particle acts as the mediator between the SM and a DM fermion, the two strongest constraints come from dilepton events at the LHC and direct detection experiments. [43]

Models in which the Z' boson couples to leptons are very easy to constrain experimentally, since they yield dilepton events that give clear signals in hadron colliders without the QCD backgrounds that dijets would experience, see for example [139]. Depending on the model, lower bounds $m_{Z'} \gtrsim 3$ TeV [44] may be imposed by the LHC experiments [198, 199]. It therefore becomes important to try to suppress the coupling of the mediator particle to the SM leptons for couplings and masses that give rise to good relic abundance from thermal freeze-out. This is why there is an experimentally motivated preference for SDMMs containing leptophobic vector mediators that couple only to quarks.

The second very tight constraint comes from the long reach of the latest direct

[42] The information gathered in this thesis may also help to guide intuition towards an ultraviolet-complete theory, if one adopts an alternative philosophy.

[43] If one also takes the view that the specified theory should account for all of the DM in the universe, then the relic density can be a particularly strong constraint complementary to direct detection, see Chapter 4.

[44] Of course this depends also on the size of the U(1)' gauge coupling, but here we are just presenting a very rough idea of the reach of the constraints. See Chapter 4 for a detailed presentation of the constraints that apply to these models.

detection experiments – at the time of this work appearing the PandaX and LUX experiments had the leading sensitivity to spin-independent dark matter-nucleon scattering (the leader is now XENON1T, see Chapter 4), and had reached cross sections as low as 10^{-46} cm^2 for a DM particle mass of 30 GeV [121, 200]. This makes it increasingly difficult to arrange couplings and mediator masses that give good relic abundance and are not ruled out, in the case of a vector mediator interaction that would generate coherent scattering on all the nucleons in the Xenon nucleus. This coherent scattering is suppressed by the relative particle velocity if the mediator has an axial coupling to dark matter, and additionally by momentum exchange if it has only axial couplings to quarks [201] [45].

The following are the anomaly cancellation conditions involving the U(1)′ gauge field that are to be satisfied, where the trace is over all fermion species with non-trivial couplings to the corresponding gauge group factors [135]:

$$\text{(a)} \quad [SU(3)_C^2] \times [U(1)'], \text{ which implies } \mathrm{Tr}[\{\mathcal{T}^i, \mathcal{T}^j\} Y'] = 0. \tag{3.1}$$

$$\text{(b)} \quad [SU(2)_W^2] \times [U(1)'], \text{ which implies } \mathrm{Tr}[\{T^i, T^j\} Y'] = 0. \tag{3.2}$$

$$\text{(c)} \quad [U(1)_Y^2] \times [U(1)'], \text{ which implies } \mathrm{Tr}[Y^2 Y'] = 0. \tag{3.3}$$

$$\text{(d)} \quad [U(1)_Y] \times [U(1)'^2], \text{ which implies } \mathrm{Tr}[Y Y'^2] = 0. \tag{3.4}$$

$$\text{(e)} \quad [U(1)'^3], \text{ which implies } \mathrm{Tr}[Y'^3] = 0. \tag{3.5}$$

$$\text{(f)} \quad \text{Gauge-gravity, which implies } \mathrm{Tr}[Y] = \mathrm{Tr}[Y'] = 0. \tag{3.6}$$

We follow the notation in [135]: $\mathcal{T}^i$ is a generator of SU(3)$_C$, T^i is a generator of SU(2)$_W$ and Y, Y' are hypercharge and U(1)′ charge matrices respectively. The U(1) and U(1)′ charge matrices are proportional to the identity. The dimension of the identity will depend on which other groups need to be traced over. For example, we see that a field transforming under the fundamental representation of SU(3)$_C$ (such as a quark) will normally contribute a factor of 3, since we are tracing over three colours.

As we shall see, satisfying these conditions with the DM fermion χ being the only fermion beyond the SM requires that the U(1)′ boson couples to both leptons and quarks, exposing it to sensitive LHC searches, and that the DM fermion has vector-like Z' couplings, placing it within reach of direct searches

[45] However, we caution that renormalization effects below the U(1)′ mass scale may enhance significantly the scattering of a pure axial vector model [119].

for DM scattering. A purely axial $\chi - Z'$ coupling is possible only if there are additional new fermions. The intermediary boson would still have U(1)′ couplings to leptons as well as quarks if there is just one extra singlet fermion, and in a range of models with multiple new singlet fermions with identical charges. Continuing the search for a model with vanishing lepton couplings, we then consider models with extra fermions transforming non-trivially as doublets or triplets of $\mathrm{SU}(2)_W$ as well as additional exotic singlets. We find several classes of such models if the DM fermion is accompanied by two or more other new fermions with non-identical charges, generalizing a model presented in [132, 166, 167, 189].

3.2 One anomaly-free exotic fermion

We consider first that the only exotic fermions present in the SDMM are SM singlets. We assume also that the different quark and lepton generations have universal U(1)′ charges, so as to minimize flavour-changing neutral currents. In this case, the anomaly-cancellation conditions above take the forms [184]:

$$\text{(a)} \quad 3(2Y'_q - Y'_u - Y'_d) = 0\,, \tag{3.7}$$

$$\text{(b)} \quad 9Y'_q + 3Y'_l = 0\,, \tag{3.8}$$

$$\text{(c)} \quad 2Y'_q - 16Y'_u - 4Y'_d + 6\,(Y'_l - 2Y'_e) = 0\,, \tag{3.9}$$

$$\text{(d)} \quad 6\left(Y'^2_q - 2Y'^2_u + Y'^2_d\right) - 6\left(Y'^2_l - Y'^2_e\right) = 0\,, \tag{3.10}$$

$$\text{(e)} \quad 9\left(2Y'^3_q - Y'^3_u - Y'^3_d\right) + 3\left(2Y'^3_l - Y'^3_e\right) + \mathrm{Tr}_{\mathrm{BSM}}(Y'^3) = 0\,, \tag{3.11}$$

$$\text{(f)} \quad 9\left(2Y'_q - Y'_u - Y'_d\right) + 3\,(2Y'_l - Y'_e) + \mathrm{Tr}_{\mathrm{BSM}}(Y') = 0\,. \tag{3.12}$$

where the fermionic U(1)′ charges are denoted by Y'_i, with i a field label: q and l label the left-handed quark and lepton doublets, the right-handed fields are labelled u, d, e. $\mathrm{Tr}_{\mathrm{BSM}}$ denotes a trace over the additional fermions beyond the SM, which we assume in this Section and the next Section to be SM singlets [46]. We show the charge assignments of the SM fermions in Table 3.1.

In the absence of BSM particles, the anomaly cancellation conditions depend only on the Y' charges of the SM fields. The Y-sequential model [135, 183] is

[46] The anomaly-cancellation conditions for the model studied in [132, 166, 167, 189] are more complicated, as it has 2 extra U(1) gauge factors, corresponding to baryon and lepton number B and L. However, in the limit where one discards the $\mathrm{U}(1)_L$ boson it becomes a leptophobic model with a single U(1)′ equivalent to $\mathrm{U}(1)_B$, as we discuss later.

Field	SU(3)	SU(2)	$U(1)_Y$	$U(1)'_{Y'}$
Q_L	**3**	**2**	$+1/3$	Y'_q
u_R	**3**	**1**	$+4/3$	Y'_u
d_R	**3**	**1**	-2/3	Y'_d
L_L	**1**	**2**	-1	Y'_l
e_R	**1**	**1**	-2	Y'_e

Table 3.1: *Charge assignments of the SM fermions.*

a well known example of an anomaly-free $U(1)'$ theory where the Y' charge of each fermion is proportional to the SM Y hypercharge. This solution is trivially guaranteed to exist since the SM is anomaly-free, and so we expect to recover this model in our analysis when $\mathrm{Tr}_{\mathrm{BSM}}(Y') = \mathrm{Tr}_{\mathrm{BSM}}(Y'^3) = 0$. However, this model has couplings to leptons and hence is subject to the strong LHC dilepton constraints, so first we will see if it is possible to obtain an anomaly-free theory with vanishing couplings to leptons.

In addition to these anomaly cancellation conditions, gauge invariance of the SM Yukawa interactions require, if there is a single Higgs doublet,

$$Y'_H = Y'_q - Y'_u = Y'_d - Y'_q = Y'_e - Y'_l \,, \tag{3.13}$$

where Y'_H is the U(1)′ charge of the SM Higgs [47]. These relations always ensure that the first anomaly condition is satisfied, motivating the consideration of new fermions that are SU(3) singlets as the simplest possibility. If one does not want to assume a particular mass generation mechanism for the SM fields, we note that Eq. (3.13) is redundant when Eqs. (3.7)-(3.9) are solved with exotic fermions transforming trivially with respect to the SM gauge group. As such, our conclusions in this Section and in Section 3.3 are independent of the Yukawa sector, but we impose Eq. (3.13) as independent constraints in Section 3.4.

We focus first on the second anomaly condition Eq. (3.8) that involves $SU(2)_W$ gauge fields, which we rewrite as:

$$Y'_l = -3Y'_q \,. \tag{3.14}$$

[47] The conditions in Eq. (3.13) were not imposed in the models studied in [190], which would require multiple Higgs representations in order to accommodate SM fermion masses and quark mixing.

This equation implies directly that if $Y'_l = 0$, so as to avoid the strong constraints from dilepton searches at the LHC, then also $Y'_q = 0$. We then consider the second Yukawa condition in Eq. (3.13), namely $Y'_d - Y'_q = Y'_e - Y'_l$. If we now require that $Y'_e = 0$, again so as to avoid the LHC dilepton constraints, we see that also $Y'_d = 0$ and hence, via the first anomaly condition Eq. (3.7), also $Y'_u = 0$. We conclude that the boson of a U(1)′ model designed to avoid the LHC dilepton constraints would not even be produced via tree-level quark-antiquark annihilations at the LHC.

Moreover, we note that, if the DM particle χ is the only new fermion, the fifth and sixth anomaly conditions Eqs. (3.11, 3.12) require

$$3(Y'_u - 4Y'_q)^3 + Y'^3_{\chi,L} - Y'^3_{\chi,R} = 0\,, \tag{3.15}$$

$$3(Y'_u - 4Y'_q) + Y'_{\chi,L} - Y'_{\chi,R} = 0\,, \tag{3.16}$$

to which the only rational solution is $Y'_{\chi,L} = Y'_{\chi,R}$ implying that such a 'singleton' DM particle must have a vector-like U(1)′ coupling, but not constraining its magnitude. This solution also implies from Eq. (3.16) that $Y'_u = 4Y'_q$.

To summarize this Section, assuming that the U(1)′ charges of the SM fermions are generation-independent, and that any new fermions that are chirally charged under U(1)′ are singlets under the SM gauge group, we found that the intermediary U(1)′ boson must have leptonic couplings and hence be subject to LHC searches for dilepton signatures. Moreover, if the DM particle is the only such new singlet fermion, it must have a vector-like U(1)′ coupling. This would also be the case if there were other new SM-singlet fermions that are vectorial under U(1)′, since they would not contribute to any of the anomaly Eqs. (3.7)-(3.12). This benchmark model has two[48] free coupling parameters, $Y'_{\chi,L} = Y'_{\chi,R}$ and Y'_q, in terms of which the Z' couplings of the other SM fermions and the SM Higgs boson are specified as follows:

$$Y'_l = -3Y'_q, \quad Y'_e = -6Y'_q, \quad Y'_d = -2Y'_q, \quad Y'_u = 4Y'_q, \quad Y'_H = -3Y'_q\,. \tag{3.17}$$

It is possible to scale the overall couplings of the SM and dark sector to the Z' independently, although creating a large hierarchy would require accepting the

[48] However, choosing to normalise one of the Y' charges with the freedom to rescale the U(1)′ gauge coupling would leave only one free parameter

same hierarchy between U(1)′ charges.

3.3 Anomaly-free axial coupling to DM

We now study whether the DM fermion could have an axial Z' coupling if we allow extra SM-singlet fermions that possess only U(1)′ charges, in which case the constraints from experiments searching directly for DM scattering would be weaker [119]. We also recall that an axial U(1)′ is the only possibility if the DM particle is a Majorana fermion.

The constraints (3.13) and (3.14) remain valid in this case, so the anomaly conditions (3.7) to (3.10) are all satisfied automatically, and we need only consider the remaining conditions (3.11, 3.12), which we write in the forms

$$3(Y'_u - 4Y'_q)^3 + \sum_j (Y'^3_{j,L} - Y'^3_{j,R}) = 0\,, \tag{3.18}$$

$$3(Y'_u - 4Y'_q) + \sum_j (Y'_{j,L} - Y'_{j,R}) = 0\,, \tag{3.19}$$

where $Y'_{j,L/R}$ is the U(1)′ charge of the left/right-handed component of a new fermion species j.

One obvious solution has $Y'_u = 4Y'_q$ and any number of new fermions with $Y'_{j,L} = Y'_{j,R}$. In the case of a single new fermion (presumably the DM particle) this is in fact the only solution, as discussed in the previous Section. It is clear from Eqs. (3.18, 3.19) that if we require a purely axial Z' coupling of the new DM fermion χ, we will need at least one other fermion that is charged under U(1)′ in order to cancel the DM anomaly contributions.

Therefore, we consider now models that, in addition to a candidate DM particle χ with charge $Y'_{\chi,L} = -Y'_{\chi,R}$, contain a single other species A with left- and right-handed charges $Y'_{A,L}$ and $Y'_{A,R}$ under U(1)′ that is also a singlet under the SM group. Solving Eqs. (3.18) and (3.19) above, we find that that this last equation can be written as

$$Y'_u = 4Y'_q - \frac{1}{3}(Y'_{A,L} - Y'_{A,R}) - \frac{2}{3}Y'_{\chi,L}\,. \tag{3.20}$$

Substituting this condition into Eq. (3.18) gives a relatively complicated polynomial equation. Using the arbitrary normalization $Y'_{\chi,L} = 1$, the solutions we find

with U(1)′ charges that are the smallest rational numbers are

$$Y'_{A,L} = -1 \quad , \quad Y'_{A,R} = 1\,, \tag{3.21}$$

$$Y'_{A,L} = 0 \quad , \quad Y'_{A,R} = -1 \;\text{ or }\; Y'_{A,R} = 5/4\,, \tag{3.22}$$

$$Y'_{A,R} = 0 \quad , \quad Y'_{A,L} = -5/4 \;\text{ or }\; Y'_{A,L} = 1\,, \tag{3.23}$$

where the last pairs of solutions are equivalent, being mirror images.

Since the fermion species in the dark sector have different U(1)′ charges, they do not respect the Glashow-Weinberg-Paschos conditions for natural flavour conservation [202, 203], and the Z' will in general have off-diagonal interactions with the dark mass eigenstates. The heavier mass eigenstates could therefore decay into the DM particle by radiating SM $\bar{f}f$ pairs through a virtual Z' [49]. We have identified this DM particle with the χ interaction eigenstate introduced above, which would indeed be the lightest mass eigenstate in a suitable degenerate limit of the mass matrix. In this limit it would have a purely axial U(1)′ coupling, and this would also be the case for arbitrary mixing in the model defined in Eq. (3.21), where both χ and A have axial couplings. However, in the cases defined in Eq. (3.23) the coupling of the lightest mass eigenstate would not be purely axial if the mixing were non-trivial.

In general, there will be mixing between the new neutral fermions (χ, A) induced by a combination of'Majorana' mass terms that do not require U(1)′ breaking and 'Dirac' terms that involve the intervention of a Higgs vacuum expectation value (vev). As a result, the mass eigenstates will be orthogonal mixtures of the interaction eigenstates, and the lightest one should be identified as the DM particle. The pattern of mixing is quite model-dependent, being determined by the assumed pattern of Majorana-type masses that do not require a Higgs vev as well as the assumed set of Higgs representations, their vev's and the magnitudes of their couplings. For example, in the model defined in Eq. (3.21) above, there could be a 2×2 Majorana-type mass matrix for the χ_L and $\bar{\chi_R}$, and Dirac terms due to a Higgs with $Y'_H = 2$ could extend this to a full rank-4 mass matrix for $\chi_L, \bar{\chi_R}, A_L$ and $\bar{A_R}$. On the other hand, generating a full rank-4 mass matrix in

[49] This suggests the possibility of an LHC signature that complements the familiar monojet/photon/Higgs... searches, namely one in which an on-shell Z' is produced and decays into the DM particle and a heavier dark particle whose decay yields a missing energy + dijet final state. In this case there may be no need to require any initial-state boson radiation.

the first model with charges in Eq. (3.22) or the second model in Eq. (3.23) would also require a Higgs with $Y'_H = 1$, and obtaining a rank-4 matrix matrix in the other models defined in Eq. (3.22) and Eq. (3.23) would require also Higgs fields with fractional Y'

We have searched for all other solutions with rational U(1)$'$ charges of the form $p/q : |p, q| \in \mathbb{Z}$ and ≤ 100, with the following results

$$\begin{aligned} Y'_{A,L} = 2 \quad &, \quad Y'_{A,R} = -\frac{1}{2}\,, \\ Y'_{A,L} = -\frac{8}{5} \quad &, \quad Y'_{A,R} = -\frac{7}{5}\,, \\ Y'_{A,L} = \frac{25}{9} \quad &, \quad Y'_{A,R} = -\frac{29}{9} \end{aligned} \tag{3.24}$$

and equivalent mirror solutions. However, in all these cases the SM leptons have non-zero U(1)$'$ charges.

We have also explored the possibilities for two or three 'generations' of new fermions X, A with 'generation'-independent charges. In both cases the first solution in Eq. (3.23) is again valid, and in the three-'generation' case there is in addition a solution with $Y'_{A,L} = 0, Y'_{A,R} = 1$ and its mirror. We have not studied the two- and three-'generation' case thoroughly but there are, in general, fewer solutions within any fixed range of p and q than in the single-'generation' case Eqs. (3.23, 3.24), and the SM leptons again have non-zero U(1)$'$ charges.

We conclude that, if the DM particle is required to have an axial U(1)$'$ charge so as to minimize the impacts of DM search experiments, not only will the U(1)$'$ gauge boson again have leptonic couplings, but also there must be additional fermions with U(1)$'$ charges that could be produced and detected at the LHC. The simplest solutions have the following U(1)' charges (using the normalization $Y'_{\chi,L} = -Y'_{\chi,R} = 1$):

$$Y'_{A,L} = -1 \quad , \quad Y'_{A,R} = 1\,. \tag{3.25}$$

$$Y'_{A,L} = 0 \quad , \quad Y'_{A,R} = -1 \quad (\text{or} \quad Y'_{A,R} = 0\,,\ Y'_{A,L} = 1)\,. \tag{3.26}$$

These two models also have Y'_q as a free parameter, and the remaining SM U(1)$'$

charges are then related (for both models) by the following equation

$$\begin{aligned} Y'_l &= -3Y'_q, \quad Y'_u = 4Y'_q - \frac{1}{3}(Y'_{A,L} - Y'_{A,R}) - \frac{2}{3}Y'_{\chi,L}, \quad Y'_d = 2Y'_q - Y'_u, \\ Y'_e &= -2Y'_q - Y'_u, \quad Y'_H = Y'_q - Y'_u. \end{aligned} \tag{3.27}$$

DM searches at the LHC are often presented in a way that shows the complementarity between the production of DM and resonant searches for the mediator, for example when comparing missing energy and dijet searches. This presentation is only possible if one is able to treat the dark and visible couplings as independent parameters, which would be possible for Eq. (3.25) but not Eq. (3.26). This is because the anomaly cancellation in the model defined in Eq. (3.25) occurs independently in the dark and visible sectors. This allows the dark and SM couplings of the fermions to the Z' to be scaled independently, with the caveat that one would have to be prepared to accept very large or very small charges in order to create a large hierarchy between the dark and visible couplings. On the other hand, anomaly cancellation in model Eq. (3.26) relates directly the charges of the dark and visible sectors, meaning such a scaling is not possible.

Finally, we recall that only in case of Eq. (3.25) is the DM particle coupling guaranteed to be purely axial, whatever the amount of dark fermion mixing.

3.4 Anomaly-free leptophobic models

In this Section we introduce exotic fermions to cancel the anomalies present in a leptophobic theory. We first build up the minimal field content needed to obtain an anomaly-free solution, before commenting on whether there is still a viable DM candidate χ present in the theory.

We consider the possibility that there are new fermions transforming under non-trivial representations of the SM gauge group [50], in which case the question of whether the leptonic U(1)$'$ charges vanish is reopened. In such a case one would also need to ensure the cancellation of the anomalies involving only SM gauge bosons, which are not listed above. These SM anomalies would vanish if the exotic fermions are vector-like with respect to the SM gauge group, and then the new fermions would contribute only to the anomalies listed above if they are

[50] The models studied in [132,166,167,189,190] all incorporate fermions that are charged under the SM SU(3)×SU(2).

chiral with respect to the U(1)′. This option would open up possibilities for other electroweak signatures, if they are not too heavy. We therefore assume throughout that our new fermions are vector-like with respect to the SM gauge groups but chiral with respect to the U(1)′.

In order to analyse this possibility, we first repeat the anomaly conditions Eqs. (3.7) to (3.12) above, using the Yukawa conditions Eq. (3.13) to substitute Y'_u and Y'_d, and assuming that any new fermions transform in either the trivial or fundamental representations:

$$\sum_{f\in SU(3)} (Y'_{f,L} - Y'_{f,R}) = 0\,, \tag{3.28}$$

$$3Y'_l + 9Y'_q + \sum_{f\in SU(2)} (Y'_{f,L} - Y'_{f,R}) = 0\,, \tag{3.29}$$

$$-6(Y'_l + 3Y'_q) + \sum_f (Y'_{f,L}Y^2_{f,L} - Y'_{f,R}Y^2_{f,R}) = 0\,, \tag{3.30}$$

$$12(Y'_e - Y'_l)(Y'_l + 3Y'_q) + \sum_f (Y'^2_{f,L}Y_{f,L} - Y'^2_{f,R}Y_{f,R}) = 0\,, \tag{3.31}$$

$$-3\left(Y'^3_e - 2Y'^2_l(Y'_l - 9Y'_q) + 18Y'^2_e Y'_q - 36Y'_e Y'_l Y'_q\right) + \sum_f (Y'^3_{f,L} - Y'^3_{f,R}) = 0\,, \tag{3.32}$$

$$-3Y'_e + 6Y'_l + \sum_f (Y'_{f,L} - Y'_{f,R}) = 0\,. \tag{3.33}$$

Here and throughout we assume that our exotic fermions are not coloured under SU(3) such that first condition Eq. (3.28) is always satisfied. [51] As we showed in Section 3.2, vanishing couplings to leptons must imply the presence of exotic fermions transforming non-trivially under SU(2). We will therefore gradually

[51] Note that from the perspective of anomaly-cancellation it would be acceptable for the new fermions to be vector-like with respect to SU(3), but from a phenomenological perspective one would expect bounds coming from hadron colliders to strongly constrain the presence of new coloured particles. Therefore the conservative assumption is to assume that the new fermions do not possess colour.

build up the necessary field content for anomaly cancellation, checking in each case whether an SU(2) doublet or SU(3) triplet (a fermion in the adjoint representation) can solve the anomaly conditions.

We first study a single new fermion species A that transforms in the fundamental of SU(2) and has both $\mathrm{U}(1)_Y$ and $\mathrm{U}(1)'$ charges. In order not to mess up the purely SM anomaly conditions, we assume it is vector-like under both $\mathrm{SU}(2)_W$ and $\mathrm{U}(1)_Y$, so that $Y_{A,L} = Y_{A,R} = Y_A$. In this case the second and third anomaly cancellation conditions Eqs. (3.29, 3.30) take the form

$$3Y'_l + 9Y'_q + Y'_{A,L} - Y'_{A,R} = 0\,, \tag{3.34}$$

$$-6(Y'_l + 3Y'_q) + 2Y_A^2(Y'_{A,L} - Y'_{A,R}) = 0\,. \tag{3.35}$$

Eliminating Y'_q by substituting Eq. (3.34) into Eq. (3.35), we find

$$(1 + Y_A^2)(Y'_{A,L} - Y'_{A,R}) = 0\,, \tag{3.36}$$

which has only the vector-like solution $Y'_{A,L} = Y'_{A,R}$. Moreover, in this case $Y'_l + 3Y'_q = 0$, so that $Y'_l = 0$ would require $Y'_q = 0$. Implementing full leptophobia by requiring $Y'_e = 0$ would then require the SM Higgs to have $Y'_H = 0$ and hence also $Y'_u = Y'_d = 0$, again entailing vanishing couplings to quarks. The same conclusions hold for models with several new fermion 'generations' if their charges are 'generation'-independent, or if we had put A in the adjoint representation.

We are therefore led to consider adding another new fermion species B with different SM quantum numbers, imposing $Y'_l = Y'_e = 0$ in the attempt to find a non-trivial leptophobic solution. If A and B are both doublets (or both triplets) under SU(2), the only solution is the one with all SM field charges vanishing. Therefore we consider the possibility that A is a doublet under $\mathrm{SU}(2)_W$ and B is an $\mathrm{SU}(2)_W$ singlet that potentially carries SM hyper-charge Y. In this case the second anomaly Eq. (3.29) gives $Y'_q = -\frac{1}{9}(Y'_{A,L} - Y'_{A,R})$ and the sixth anomaly Eq. (3.33) gives $Y'_{B,R} = Y'_{B,L} + 2Y'_{A,L} - 2Y'_{A,R}$. Substituting these into the third anomaly Eq. (3.30) yields

$$(1 + Y_A^2 - Y_B^2)(Y'_{A,L} - Y'_{A,R}) = 0 \tag{3.37}$$

We ignore the solution $Y'_{A,L} = Y'_{A,R}$ since it would imply $Y'_q = 0$, which would

then make all SM charges vanish. Therefore we must require

$$1 + Y_A^2 - Y_B^2 = 0; \tag{3.38}$$

to which the only integer solution is $\{0, 1\}$. Since we are working in the convention where $Q = T^3 + Y/2$, this solution has half-integer electric charges for both A and B, conflicting with the integer charge quantization seen in Nature [204]. We conclude that this solution is not acceptable.

We have also looked for solutions where A is an $\mathrm{SU}(2)_W$ triplet. Equation (3.29) is modified, as we are no longer considering fermions solely in the fundamental or trivial representation, becoming

$$9Y'_q + \sum_{f\in\mathbf{2}}(Y'_{f,L} - Y'_{f,R}) + 4\sum_{f\in\mathbf{3}}(Y'_{f,L} - Y'_{f,R}) = 0 \tag{3.39}$$

where **2** and **3** label the fundamental and adjoint representations respectively. If B is again an $\mathrm{SU}(2)_W$ singlet, repeating the same steps as before we find the condition

$$8 + 3Y_A^2 - 3Y_B^2 = 0\,, \tag{3.40}$$

which has no integer solutions. Finally, in the case where A is a triplet and B is a doublet we obtain the condition

$$5 + 3Y_A^2 - 3Y_B^2 = 0\,, \tag{3.41}$$

which also has no integer solutions. Moreover, we have checked that there are still no solutions in these triplet/singlet and triplet/doublet cases when there are several 'generations' of A and B (even with different numbers of each), as long as the $\mathrm{U}(1)'$ charges are 'generation'-independent.

Since we have not found any acceptable solutions with two exotic fermions, we are therefore led to consider models with three or more species of new fermions. We show our notation and charge assignments in Table 3.2. Before proceeding we should note that the models studied in [132, 166, 167, 189, 190] all feature six new fermion species. However, as already commented, when the $\mathrm{U}(1)_L$ is discarded along with its three ν_R species, the model studied in [132, 166, 167, 189] becomes a leptophobic model with a single $\mathrm{U}(1)'$ that is equivalent to $\mathrm{U}(1)_B$. In this limit, the new fermions in the model comprise a doublet that is vector-like under SU(2)

Field	SU(3)	SU(2)	$U(1)_Y$	$U(1)'_{Y'}$
A_L	**1**	**2**	Y_A	$Y'_{A,L}$
A_R	**1**	**2**	Y_A	$Y'_{A,R}$
B_L	**1**	**1**	Y_B	$Y'_{B,L}$
B_R	**1**	**1**	Y_B	$Y'_{B,R}$
χ_L	**1**	**1**	0	$Y'_{\chi,L}$
χ_R	**1**	**1**	0	$Y'_{\chi,R}$

Table 3.2: *Charge assignments for exotic fermions added to produce the anomaly-free leptophobic models, when the exotic SU(2) multiplet is assumed to be a doublet.*

and has $Y = -1$, and two singlets with $Y = -2, 0$, respectively.[52]

We have checked the anomaly-cancellation conditions for other models containing three new fermion species with different $U(1)_Y$ charges, i.e., A, B, χ in the $(SU(2)_W,\ U(1)_Y,\ U(1)_{Y'})$ representations $(2,\ Y_A,\ Y'_{A,L/R})$, $(1,\ Y_B,\ Y'_{B,L/R})$, and $(1,\ 0,\ Y'_{\chi,L/R})$ respectively. In order to obtain a leptophobic solution with $Y'_l = Y'_e = 0$, the SM Yukawa condition Eq. (3.13) imposes $Y'_u = Y'_d = Y'_q$, so we choose Y'_q as the only remaining free SM charge. Normalizing $Y'_{\chi,L} = 1$, and noting that the SU(3) anomaly condition is satisfied automatically when the Higgs coupling constraint Eq. (3.13) is imposed, the next four anomaly-cancellation conditions yield

$$Y'_q = \frac{1}{9}\left(Y'_{A,R} - Y'_{A,L}\right)\,, \tag{3.42}$$

$$Y'_{\chi,R} = \frac{Y_B^2\left(2Y'_{A,L} - 2Y'_{A,R} + 1\right) + 2\left(Y_A^2+1\right)\left(Y'_{A,R} - Y'_{A,L}\right)}{Y_B^2}\,, \tag{3.43}$$

$$Y'_{B,L} = \frac{\left(Y_A Y_B^3 - 2\left(Y_A^2+1\right)^2\right)Y'_{A,L} + \left(Y_A Y_B^3 + 2\left(Y_A^2+1\right)^2\right)Y'_{A,R}}{2\left(Y_A^2+1\right)Y_B^2}\,, \tag{3.44}$$

$$Y'_{B,R} = \frac{\left(Y_A Y_B^3 + 2\left(Y_A^2+1\right)^2\right)Y'_{A,L} + \left(Y_A Y_B^3 - 2\left(Y_A^2+1\right)^2\right)Y'_{A,R}}{2\left(Y_A^2+1\right)Y_B^2}\,. \tag{3.45}$$

Using these expressions, the final $U(1)^3$ anomaly condition gives rise to the slightly

[52] In our convention of $Q = T_3 + Y/2$, the SM hypercharges are twice those in [132,166,167,189].

unwieldy expression:

$$
\begin{aligned}
&-\frac{1}{8\left(Y_A^2+1\right)^3 Y_B^6}\Big[-16\left(Y_A^2+1\right)^3 Y_B^6\left((Y')^3_{A,L}-(Y')^3_{A,R}\right)\\
&+\left(\left(Y_A Y_B^3+2\left(Y_A^2+1\right)^2\right)Y'_{A,L}+\left(Y_A Y_B^3-2\left(Y_A^2+1\right)^2\right)Y'_{A,R}\right)^3\\
&+\left(\left(2\left(Y_A^2+1\right)^2-Y_A Y_B^3\right)Y'_{A,L}-\left(Y_A Y_B^3+2\left(Y_A^2+1\right)^2\right)Y'_{A,R}\right)^3\\
&+8\left(Y_A^2+1\right)^3\left(Y_B^2\left(2Y'_{A,L}-2Y'_{A,R}+1\right)+2\left(Y_A^2+1\right)\left(Y'_{A,R}-Y'_{A,L}\right)\right)^3\\
&-8\left(Y_A^2+1\right)^3 Y_B^6\Big]=0\,.
\end{aligned}
\tag{3.46}
$$

This equation has a symmetry $Y_{A/B} \leftrightarrow -Y_{A/B}$, which facilitates a scan of possible solutions. We have restricted our search to positive integer values ≤ 10 for $Y_{A/B}$. The other unknowns, $Y'_{A,L/R}$, are both rational, and we have scanned irreducible rational numbers of the form $\pm p/q$ with p and q integers ≤ 10. In order to have integer charge quantisation, and recalling that our convention is $Q = T_3 + Y/2$, we further require Y_A to be odd (since its a doublet) and Y_B to be even (since its a singlet).

In certain cases Eq. (3.46) takes a relatively manageable form. One example is for $Y_A = \pm 1$ and $Y_B = \pm 2$, which is equivalent to the solution discussed in [132, 166, 167, 189]. In this case, one can either require $Y'_{A,L} = -1$ with $Y'_{A,R}$ arbitrary or $Y'_{A,R} = 1$ with $Y'_{A,L}$ arbitrary. The other case is $Y_A = \pm 7$ and $Y_B = \pm 10$, in which case one need only satisfy

$$
2Y'_{A,L} - 3Y'_{A,R} + 5 = 0 \quad \text{or} \quad 3Y'_{A,L} - 2Y'_{A,R} + 5 = 0 \tag{3.47}
$$

to obtain acceptable solutions. In addition to these 'regular' solutions with a new SU(2)-doublet fermion, we find 26 other 'exceptional' solutions that occur in 13 mirror pairs with $Y'_{A,L} \leftrightarrow -Y'_{A,R}$ that have $Y_{A/B} \leq 10$ and $Y'_{A,L/R} = \pm p/q$ with $p, q \leq 10$. The simplest of these is

$$
(Y'_{A,L}, Y'_{A,R}, Y_A, Y_B) = (1, \frac{2}{3}, 3, 2)\,, \tag{3.48}
$$

which is accompanied by its mirror solution with $Y'_{A,L} \leftrightarrow -Y'_{A,R}$.

In addition to $Y'_{\chi,L} = 1$ by definition, the benchmark solution Eq. (3.48) has

$Y_l' = Y_e' = 0$ by construction, and hence

$$Y_q' \;=\; Y_u' \;= Y_d', \quad Y_H' = 0\,, \tag{3.49}$$

where Y_q' is fixed by Eq. (3.42) and the values of $Y_{\chi,R}', Y_{B,L/R}'$ are fixed by Eqs. (3.43, 3.44) and (3.45)

$$Y_q' \;=\; -\frac{1}{27}, \quad Y_{\chi,R}' \;=\; 0, \quad Y_{B,L}' \;=\; -\frac{1}{3}, \quad Y_{B,R}' \;=\; \frac{4}{3}\,. \tag{3.50}$$

We note that this solution admits a small quark charge relative to the DM charge, implying good complementarity between dijet and missing energy searches at the LHC.

Finally, we consider the possibilities when A is in the adjoint (triplet) representation of $\mathrm{SU}(2)_W$. In this case, the first four anomaly-cancellation conditions above are modified to

$$Y_q' = -\frac{4}{9}\left(Y_{A,L}' - Y_{A,R}'\right)\,, \tag{3.51}$$

$$Y_{\chi,R}' = 3Y_{A,L}' - 3Y_{A,R}' + Y_{B,L}' - Y_{B,R}' + Y_{\chi,L}'\,, \tag{3.52}$$

$$Y_{B,L}' = \frac{\left(3Y_A Y_B^3 + \left(3Y_A^2+8\right)^2\right) Y_{A,R}' - \left(\left(3Y_A^2+8\right)^2 - 3Y_A Y_B^3\right) Y_{A,L}'}{2\left(3Y_A^2+8\right) Y_B^2}\,, \tag{3.53}$$

$$Y_{B,R}' = \frac{\left(3Y_A Y_B^3 + \left(3Y_A^2+8\right)^2\right) Y_{A,L}' - \left(\left(3Y_A^2+8\right)^2 - 3Y_A Y_B^3\right) Y_{A,R}'}{2\left(3Y_A^2+8\right) Y_B^2}\,, \tag{3.54}$$

and the $U(1)^3$ anomaly equation becomes

$$\begin{aligned}
&-\frac{1}{8\left(3Y_A^2+8\right)^3 Y_B^6}\Big[-24\left(3Y_A^2+8\right)^3 Y_B^6\left((Y')^3_{A,L} - (Y')^3_{A,R}\right)\\
&+8\left(3Y_A^2+8\right)^3\left(Y_B^2\left(3Y_{A,L}' - 3Y_{A,R}' + 1\right) - \left(3Y_A^2+8\right)\left(Y_{A,L}' - Y_{A,R}'\right)\right)^3\\
&+\left(\left(3Y_A Y_B^3 + \left(3Y_A^2+8\right)^2\right) Y_{A,L}' - \left(\left(3Y_A^2+8\right)^2 - 3Y_A Y_B^3\right) Y_{A,R}'\right)^3\\
&+\left(\left(\left(3Y_A^2+8\right)^2 - 3Y_A Y_B^3\right) Y_{A,L}' - \left(3Y_A Y_B^3 + \left(3Y_A^2+8\right)^2\right) Y_{A,R}'\right)^3\\
&-8\left(3Y_A^2+8\right)^3 Y_B^6\Big] = 0\,.
\end{aligned} \tag{3.55}$$

As before we have the symmetry $Y_{A/B} \to -Y_{A/B}$. Requiring that Y_A and Y_B are even so as to obtain integer electric charges. we identify a set of solutions defined

by $Y_A = 0$ and $Y_B = \pm 2$, which satisfy

$$Y'_{A,R} = \frac{1 + Y'_{A,L}}{1 + 3Y'_{A,L}} \,. \tag{3.56}$$

In addition to $Y'_{\chi,L} = 1$ by definition, $Y_A = 0$ and $Y_B = \pm 2$, and $Y'_{A,L}$ as a free parameter that determines $Y'_{A,R}$ via Eq. (3.56), this benchmark solution again has $Y'_l = Y'_e = 0$ by construction and the conditions (3.49) are also obeyed, where Y'_q is fixed by Eq. (3.51), and the values of $Y'_{\chi,R}, Y'_{B,L/R}$ are fixed in this case by Eqs. (3.52, 3.53) and (3.54). Choosing the positive solution $Y_B = 2$, this relates the other charges:

$$Y'_q = \frac{4 - 12Y'^2_{A,L}}{9 + 27Y'_{A,L}} \tag{3.57}$$

$$Y'_{\chi,R} = \frac{3Y'_{A,L}(1 + Y'_{A,L})}{1 + 3Y'_{A,L}} \tag{3.58}$$

$$Y'_{B,L} = \frac{1 - 3Y'^2_{A,L}}{1 + 3Y'_{A,L}} \tag{3.59}$$

$$Y'_{B,R} = -Y'_{B,L} \tag{3.60}$$

Picking a specific benchmark with $Y'_{A,L} = 1$, for example:

$$Y'_{A,R} = \frac{1}{2}, \quad Y'_q = -\frac{2}{9}, \quad Y'_{\chi,R} = \frac{3}{2}, \quad Y'_{B,L} = -\frac{1}{2}, \quad Y'_{B,R} = \frac{1}{2} \tag{3.61}$$

As in the fundamental case, there are also 'exceptional' solutions not falling into the class described above. We find 28 such solutions with $Y_{A/B} \leq 10$ and $Y'_{A,L/R} = \pm p/q$ with $p, q \leq 10$, occurring in 14 mirror pairs with $Y'_{A,L} \leftrightarrow -Y'_{A,R}$. The simplest of these is

$$(Y'_{A,L}, Y'_{A,R}, Y_A, Y_B) = (-1, -\frac{3}{2}, 2, 2) \,, \tag{3.62}$$

which is accompanied by its mirror solution.

Examining the gauge eigenstates, we find no solutions with an axial DM particle $Y'_{\chi,L} = -Y'_{\chi,R}$ in this Section. Therefore, ignoring the possible effects of mixing, we expect strong direct detection bounds to be relevant. However, based on our

results in Section 3.3, we expect that adding two SM-singlet dark fermions would allow an anomaly-free theory to exist in which one of the dark sector particles has an axial coupling.

As in the two-dark-fermion case studied in Section 3.3, the interaction eigenstates (A, B, χ) in the models studied in this Section will in general mix via a combination of 'Majorana' and 'Dirac' entries in the mass matrix, that are model-dependent. We do not discuss any details here, but note that many of the remarks made in Section 3.3 apply here also: the mixing may give the lightest mass eigenstate (the DM particle) an admixture of vector-like coupling, which would vanish in the degenerate limit in which it was much lighter than the other mass eigenstates, and the heavier mass eigenstates would, in general, decay via off-diagonal Z' couplings into lighter mass eigenstates by emitting SM $\bar{f}f$ pairs. Finally we note that, if the χ state mixes with a neutral component of A or B, then a coupling to the SM Z boson would be generated. Even without mixing between the fermions, such a coupling can also be generated via kinetic mixing of the Z and Z' bosons. Such a coupling is very heavily constrained, see, e.g., [205–207], putting pressure on the viability of χ as a DM candidate in such a case. However, please see Chapter 4 for a detailed investigations of the constraints that apply to these models.

3.5 Summary of anomaly-free models

As we have seen in this Chapter, the cancellation of anomalies is a non-trivial constraint on SDMMs with a spin-one mediator boson Z'. Our analysis has led us to consider three classes of models:

One Exotic Fermion — If the SM is supplemented by a single new fermion, a DM particle that is a singlet of the SM gauge group, the Z' cannot be leptophobic unless it also decouples from quarks. A benchmark model in this class is specified at the end of Section 3.2, see Eq. (3.17). This model contains a single vector-like fermionic DM candidate which does not contribute to any anomalies – the assigned charges of the standard model fields alone cancel all anomalies. As such, this model is the Y-sequential model [135, 183] with the addition of a DM candidate. The relative coupling of the Z' to quarks and leptons is fixed and comparable, meaning that LHC dilepton bounds would rule out much of the parameter space.

Moreover, the DM couplings to the Z' must be vectorial, meaning that the cross section for scattering off a nucleus would not be velocity suppressed and would also be coherently enhanced. Therefore an SDMM with just a DM fermion and a Z' is very strongly constrained by LHC searches [198, 199] and direct DM scattering experiments [121, 200].

Axial Dark Matter — If the DM particle is to have a purely axial U(1)$'$ coupling, which would diminish the impact of the DM scattering experiments [121, 200], then it must be accompanied by at least one other new singlet fermion. However, the U(1)$'$ charges of the SM leptons still do not vanish, no matter how many singlet fermions are added. Thus, the Z' in such a model would still be subject to strong LHC constraints [198, 199]. A benchmark model in this class is specified at the end of Section 3.3, see Eqs. (3.25) and (3.27).

Leptophobic Models — We find several anomaly free leptophobic models only if the DM fermion is accompanied by at least two other new fermions with non-identical charges, at least one of which is a non-singlet under the SM gauge group. One of these models is the model with a baryonic DM particle presented in [132, 166, 167, 189]. These models may be subject to constraints from LHC searches for new fermions with non-trivial SM quantum numbers that would need to be considered in assessing the parameter spaces of such models. A benchmark model with a new $\mathrm{SU}(2)_W$ doublet fermion is specified in Eqs. (3.48) and (3.49), and one with a new $\mathrm{SU}(2)_W$ triplet fermion is specified in Eq. (3.56). In these models the DM plays a key role since it is necessary for anomaly cancellation, leaving only one free coupling parameter in the model. The dark and visible couplings cannot be scaled independently as in the case of the simplified model, leaving certain observables such as the invisible branching ratio of the Z' fixed. [53]

Beyond the specific models presented here, we re-emphasize the general point that proponents of SDMMs should ensure that they implement the anomaly-cancellation constraints. The bad news is that the resulting models may not be so simple, but the good news is that anomaly cancellation can relate the SM and DM couplings of the Z' and furthermore the additional fermions may have novel experimental signatures.

[53] More precisely, although the branching ratios are independent of the overall U(1)$'$ gauge coupling g, and are so mostly a function of the charges in the model, there is a mild dependence on particle mass from phase-space suppression, relevant when the daughter particles are comparable in mass to $M_{Z'}/2$

We will investigate in more detail the experimental viability of the models proposed here in the next Chapter.

Chapter 4

Constraints on Anomaly-Free Models

This Chapter is based on [3], which I wrote in collaboration with John Ellis and Malcolm Fairbairn.

4.1 Overview of major phenomenological constraints

In previous Chapters we have examined simplified models of DM that feature a Z' mediator. In Chapter 2 we studied the dijet constraints that apply to these models, and in Chapter 3 we looked at the constraints on the exotic charges in these models coming from anomaly cancellation. In this Chapter we wish to examine in detail the various constraints that apply to such anomaly-free extensions of simplified models.

As we emphasised in the previous Chapter, a complete 'simplified' model of dark matter should include some mechanism for cancelling these triangle anomalies, which could in principle be achieved in different ways [135, 169]. The option we pursue is that the anomalies are cancelled by new physics at the TeV scale, which entails an interesting new set of phenomenological signatures and possible experimental constraints [54] Since there are, in total, six different gauge anomalies

[54]The alternative is to assume that the anomaly-cancellation mechanism operates at some high energy scale, generating anomalous, apparently non-renormalizable gauge-boson interactions that are also detectable in principle at lower energies [208]. See also [218, 219].

to be cancelled, the constraints on the charges of the beyond the Standard Model fermions needed to cancel them are non-trivial [2]. Consequently, the minimal 'simplified' dark matter models cannot always be as simple as those originally considered, and the phenomenological signatures are correspondingly more complex and interesting [55].

In the previous Chapter (based on [2]) we constructed systematically specific minimal anomaly-free dark matter models with a U(1)′ boson Z' whose couplings to quarks and leptons are generation-independent [56]. The simplest such models are leptophilic, and are subject to various powerful experimental constraints. In particular, the LHC constraint on resonances in dilepton mass spectra is now very strong, imposing important restrictions on U(1)′ models in which the Z' boson couples to the charged leptons e^+e^- and $\mu^+\mu^-$ [139]. Another powerful constraint comes from direct searches for dark matter scattering on nuclei, in which the market leader is now the XENON1T experiment [120]. This constraint is particularly important for U(1)′ models in which the Z' boson has vector-like couplings to Standard Model particles and/or dark matter, since coherent enhancement leads to an enhanced cross section in these situations. These considerations motivate specific studies of benchmark U(1)′ models in which the Z' boson is either leptophobic and/or has axial couplings.

We found in the previous Chapter that models with a single dark matter particle necessarily contain a leptophilic Z' with couplings to quarks and leptons that are proportional to those of the hypercharge boson of the Standard Model - such models have become known as Y-sequential models [135, 183]. In such models, $Z' - Z$ mixing is unavoidable, inducing important contributions to precision electroweak observables that impose a powerful constraint on $M_{Z'}$ [210]. Moreover, the dark matter particle must have vector-like Z' couplings. Because of these two features, the experimental constraints on this benchmark model are very strong, as we discuss in detail in Section 4.2, and only a very small region of the model's parameter space survives.

In Section 4.3 we then discuss a second Y-sequential benchmark model in which the dark matter particle has axial Z' couplings, with the aim of reducing the impact of the direct dark matter search experiments. However, the dark matter

[55] For other studies of anomaly-free Z' models, see [135, 166, 167, 181, 185, 189, 190].

[56] See [209] for the generalization to anomaly-free Z' models motivated by deviations from the Standard Model in $B \to K^{(*)}\ell^+\ell^-$ decays.

density constraint is more important in this case, the Z' is still leptophilic, and there is again an important constraint from precision electroweak data. Thus, even though the direct dark matter scattering constraint has less impact, the other constraints are still sufficiently powerful to exclude this model within the parameter range we explore [57].

Therefore, in Section 4.4 we also consider making the Z' leptophobic, which requires at least two additional particles in the dark sector, with non-zero Standard Model charges. We consider two benchmark scenarios proposed in [2], one with SU(2) doublet dark sector particles in which the Z' couplings to quarks are suppressed, and LHC monojet constraints become important, and another with SU(2) triplet dark sector particles in which the quark couplings are less suppressed, so that the LHC dijet constraints are more important. In both cases the direct dark matter search constraint is more restrictive, but allows extended regions where $\log_{10}(m_\chi/\text{GeV}) \gtrsim 3.2$. Finally, we offer some discussion in Section 4.5.

4.2 Constraints on a single dark matter particle

We consider first the possibility that the only dark sector particles are fermions that are uncharged singlets of the Standard Model gauge group. Restricting our attention to generation-independent U(1)′ charge assignments, denoting the left-handed lepton doublets by l, the right-handed lepton singlets by e, the right-handed quark singlets by u, d and the left-handed quark doublets by q, and choosing the normalisation $Y'_q = 1$, we found [2] the following unique solution which we repeat here:

$$Y'_l = -3, \quad Y'_e = -6, \quad Y'_d = -2, \quad Y'_u = 4, \quad Y'_H = -3\,, \tag{4.1}$$

which is known in the literature as the Y'-sequential model [135, 183]. Its free parameters include the U(1)′ gauge coupling g and the masses of the Z' and the dark matter particle χ. If there is a single particle in the dark sector, it must be vector-like under U(1)′: $Y'_{\chi,L} = Y'_{\chi,R}$ [2], but the magnitude of the U(1)′ charge of

[57] As discussed in [2], this axial dark matter particle must be accompanied by at least one other 'dark' particle with a U(1)′ charge, whose production offers in principle a distinctive $\not{E}_T$ signature at the LHC. However, we do not discuss this further, leaving it for a future study.

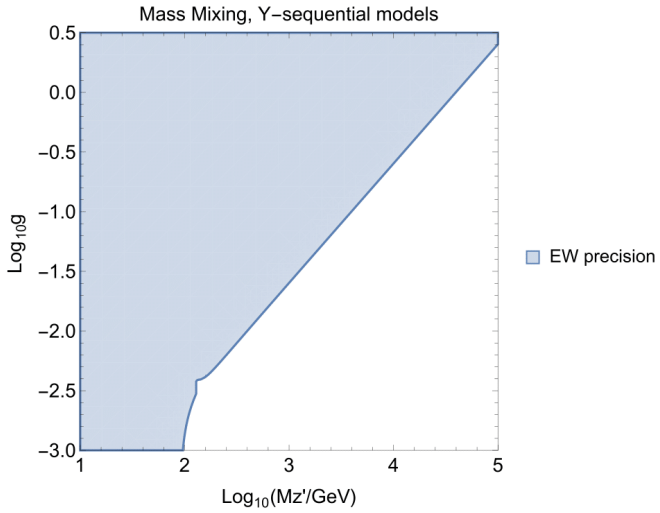

Figure 4.1: *The $(M_{Z'}, g)$ plane in the U(1)′ Y-sequential model, showing the impact of the constraints on the oblique parameters S and T imposed by precision electroweak measurements.*

this dark matter particle is arbitrary,[58] introducing a fourth parameter into this minimal model.

We consider next the constraints on the Y-sequential model that are imposed by precision electroweak measurements, specifically the constraints from the oblique parameters S and T. As seen in Eq. (4.1), this and other Y-sequential models have the feature that the Higgs doublet has a non-zero U(1)′ charge. Consequently, tree-level $Z' - Z$ mixing is unavoidable, and is calculable as a function of the U(1)′ gauge coupling g and the Z' mass, increasing as g increases and/or $M_{Z'} \to M_Z$. Therefore the precision electroweak constraint is stronger in these cases, as seen in Fig. 4.1. In this Section we neglect kinetic mixing, since mass mixing is much more important in these Y-sequential type models. The details of mass and kinetic mixing are described further in Appendix B.

If the dark sector contains more than one particle, it is possible that $Y'_{\chi,L} \neq Y'_{\chi,R}$. As already advertised, in order to minimise the impact of direct dark matter searches, the case where the dark matter particle has a purely axial Z' coupling, $Y'_{\chi,L} = -Y'_{\chi,R}$, is of particular interest. The electroweak precision constraint shown in Fig. 4.1 is applicable to that model as well as to the vector-like model, since

[58] The reason that this is not fixed by the anomaly cancellation is that the single exotic fermion does not contribute to the anomaly cancellation since it has to be vector like. This is because each anomaly has been completely cancelled by the SM fields alone.

it depends only on the coupling of the Z' to the SM Higgs. More constraints on the axial model are discussed in Section 4.3, whereas the rest of this Section is devoted to the minimal, vector-like case.

We show below the standard formulae for DM annihilation, which we reproduce here so as to illuminate the plots we show below [59]. Away from the direct-channel Z' and Z resonances, a generic $\bar{\chi}\chi \to \bar{f}f$ annihilation cross-section multiplied by the χ velocity, σv, may be expanded as a power series in v^2: $\sigma v = a + bv^2 + \mathcal{O}(v^4)$, where a and b arise from s- and p-wave annihilations respectively, and have the following leading-order expressions [147]

$$a = \frac{3m_\chi^2\sqrt{1-\frac{m_f^2}{m_\chi^2}}}{2\pi(M_{Z'}^2-4m_\chi^2)^2}\Big(g_\chi^{V^2}[g_f^{V^2}(2+\frac{m_f^2}{m_\chi^2})+2g_f^{A^2}(1-\frac{m_f^2}{m_\chi^2})] + g_\chi^{A^2}g_f^{A^2}\frac{m_f^2}{m_\chi^2}\frac{(4m_\chi^2-M_{Z'}^2)^2}{M_{Z'}^4}\Big) \tag{4.2}$$

$$b = \frac{g_\chi^{A^2}g_f^{A^2}m_\chi^2}{2\pi(M_{Z'}^2-4m_\chi^2)^2}(1-\frac{m_f^2}{m_\chi^2})^{3/2} \tag{4.3}$$

where $g_{\chi,f}^{V,A}$ are the vector and axial couplings of the dark matter particle and the final-state fermion, respectively. Close to resonance where $m_\chi \sim M_{Z'}/2$, the denominators in Eq. (4.3) are modified: $(M_{Z'}^2-4m_\chi^2)^2 \to (M_{Z'}^2-4m_\chi^2)^2 + \Gamma_{Z'}^2M_{Z'}^2$. As already mentioned, we include $Z'-Z$ mixing, and there are analogous modifications when $m_\chi \sim M_Z/2$. However care must be taken with the expansion of σv close to resonance, so we always calculate the relic density numerically with `Micromegas` [172], with model files generated with `FeynRules` [103]. The annihilation channel $\bar{\chi}\chi \to Z'Z'$ is also included consistently by `Micromegas`, which can be important when $m_\chi > M_{Z'}$.

In general, there are regions of any model's parameter space where the relic density exceeds the cold dark matter (CDM) density inferred from measurements by the Planck satellite and other experiments, $\Omega_{CDM}h^2 \simeq 0.12$. We regard these regions as excluded, while noting that modified evolution in the early Universe

[59] In models where the dark sector contains more than one particle, such as the axial Y'-sequential model discussed in Section 4.3 and the leptophobic model discussed in Section 4.4, one or more of other 'dark' particles may coannihilate with the dark matter particle. However, this complication is absent in the vector-like Y'-sequential model discussed in this Section, and we neglect it for the other models.

could change the calculation of Ω_χ so that it is $\leq \Omega_{CDM}$, in which case such models could be acceptable [211]. The other generic possibility is that $\Omega_\chi < \Omega_{CDM}$, which is acceptable if there is some other source of dark matter (for example axions, primordial black holes or sterile neutrinos). However, in this case the strength of the constraint from the direct search for dark matter scattering is reduced by the density fraction Ω_χ/Ω_{CDM}, a correction that we apply throughout this Chapter. Between these over- and under-dense regions there is a narrow boundary where $\Omega_\chi \simeq \Omega_{CDM}$, and no correction factor is needed. If $\Omega_\chi > \Omega_{CDM}$, we consider the parameter point to be excluded by the relic density, but for the sake of presenting the direct detection bound we apply no rescaling.

Fig. 4.2 displays this boundary in the $(m_\chi, M_{Z'})$ plane in the vector-like Y'-sequential model. The solid contours are at the boundaries where $\Omega_\chi = \Omega_{CDM}$, for $Y'_{\chi,L} = Y'_{\chi,R} = 1$ and fixed values of the gauge coupling $g = 0.03$ (green curve), 0.1 (orange) and 0.3 (blue).[60] The narrow-width approximation assumed in our analysis would no longer be applicable for $g > 0.3$, so we do not display results for larger g. Also shown are dashed lines where $m_\chi = M_{Z'}/2$ (red), $m_\chi = M_{Z'}$ (purple) and $m_\chi = m_t$ (brown), $m_\chi = M_Z/2$ (grey) and $M_{Z'} = M_Z$ (black).

The relic χ density is reduced below the relic CDM density by rapid annihilation $\bar{\chi}\chi \to Z' \to$ SM SM, for SM a Standard model particle, in wedge-shaped regions where $m_\chi \sim M_{Z'}/2$, whose widths increase with g. Larger values of Ω_χ arise when the dark matter annihilation rate decreases as $M_{Z'}$ increases. We note that the wedge-shaped contours exhibit outward-pointing glitches when $m_\chi \simeq M_Z/2$, where the relic density is suppressed by rapid $\chi\chi$ annihilations via the Z to Standard Model particles, and when $M_{Z'} \simeq M_Z$, where $Z' - Z$ mixing is enhanced. As already mentioned, for parameter sets inside the wedges we rescale the constraint from the direct dark matter scattering rate by a factor Ω_χ/Ω_{CDM}, whereas the regions outside these wedges are disallowed because $\Omega_\chi > \Omega_{CDM}$.

Fig. 4.3 displays $(m_\chi, M_{Z'})$ planes in the vector-like U(1)′ Y-sequential model for three selected values of the gauge coupling: $g = 0.03$ (upper left), $g = 0.1$ (upper right) and $g = 0.3$ (lower), implementing the following constraints.

In each panel the blue contour is where $\Omega_\chi = \Omega_{CDM}$ and the blue shaded regions are excluded because $\Omega_\chi > \Omega_{CDM}$. The horizontal olive lines at fixed values of $M_{Z'}$ that rise with increasing g bound the olive shaded regions at lower $M_{Z'}$

[60] The curves for other parameter choices with the same values of $g^2|Y'_{\chi,L}|$ would be identical away from resonance.

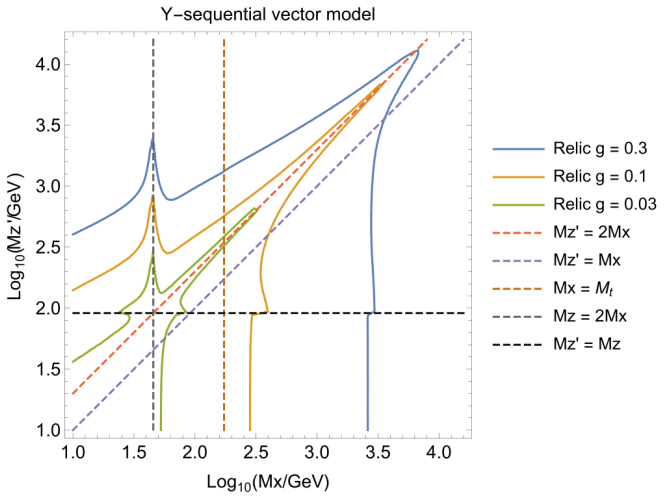

Figure 4.2: *The $(m_\chi, M_{Z'})$ plane in the U(1)′ Y-sequential model with a vector-like dark matter coupling $Y'_{\chi,L} = Y'_{\chi,R} = 1$. The solid lines are contours where $\Omega_\chi = \Omega_{CDM}$ for fixed values of the gauge coupling $g = 0.03$ (green), 0.1 (orange) and 0.3 (blue), and the red/purple/brown/grey/black dashed lines are where $m_\chi = M_{Z'}/2, m_\chi = M_{Z'}$, $m_\chi = m_t$, $m_\chi = M_Z/2$, $M_{Z'} = M_Z$, respectively.*

that are excluded by the constraints imposed by precision electroweak measurements induced by the effects of $Z' - Z$ mixing . For large $g \gtrsim 0.1$, this constraint is stronger than the ATLAS dilepton search at the LHC [199], which excludes the brown shaded regions [61]. Finally, the purple shaded regions are excluded by the direct search for the scattering of dark matter by the XENON1T experiment [120], where the appropriate reduction factor Ω_χ/Ω_{CDM} has been applied to the experimental upper limit. Here and throughout we use the form factors and rescaling functions from [45] to calculate direct detection limits. In the $g = 0.03$ and 0.1 cases there is no visible region that is allowed by all these constraints. On the other hand, when $g = 0.3$ we see a tiny region that is only just consistent with the relic density and precision electroweak constraints, while being more comfortably consistent with the dark matter scattering and ATLAS dilepton constraints.

Finally, we present in Fig. 4.4 an analysis of the vector-like U(1)′ Y-sequential model in which g is varied so as to maintain $\Omega_\chi = \Omega_{CDM}$ across the $(m_\chi, M_{Z'})$ plane. In the left panel the values of $\log_{10} g$ required by the relic density are indicated by the indicated shadings, and the red shaded regions correspond to $\Gamma_{Z'}/M_{Z'} > 0.5$ which are excluded from our analysis. The right panel of Fig. 4.4

[61] We have used `MadGraph` [99] to calculate the dilepton cross section for our signal model

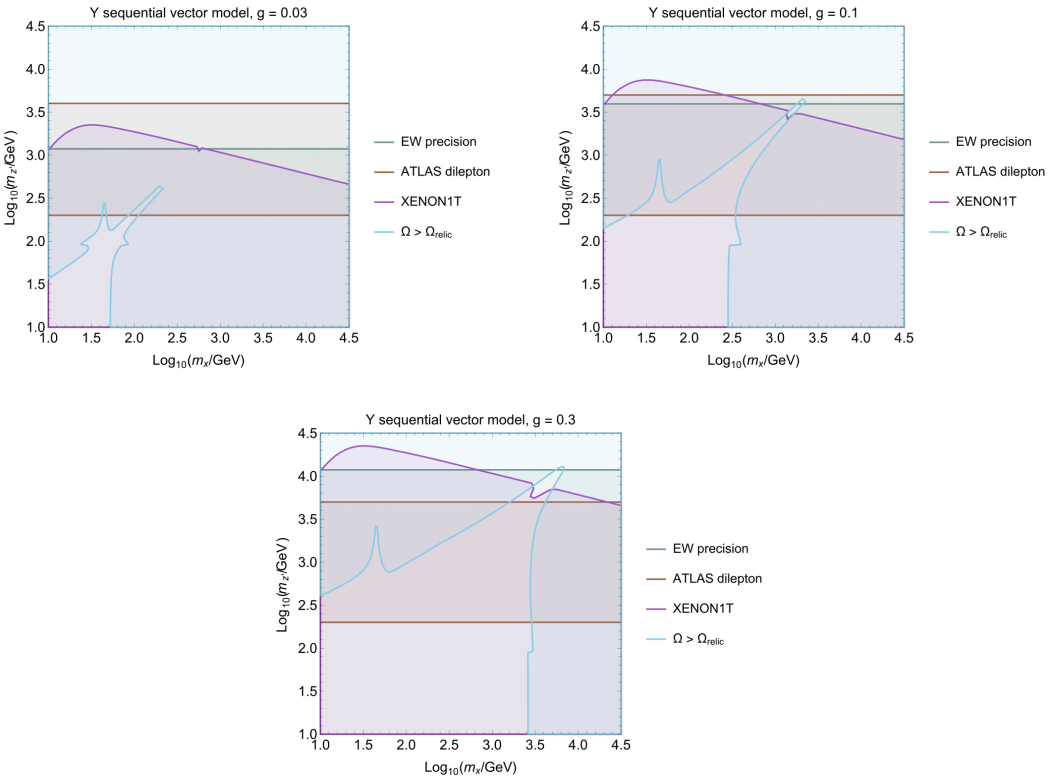

Figure 4.3: *The $(m_\chi, M_{Z'})$ planes in the U(1)′ Y-sequential model with a vector-like dark matter coupling $Y'_{\chi,L} = Y'_{\chi,R} = 1$ for a gauge coupling $g = 0.03$ (upper left), $g = 0.1$ (upper right) and $g = 0.3$ (lower). The solid blue lines are the contours where $\Omega_\chi = \Omega_{CDM}$, and $\Omega_\chi > \Omega_{CDM}$ in the regions shaded blue. The bands shaded brown are excluded by the ATLAS dilepton search [199], the regions shaded olive are excluded by precision electroweak measurements, and the direct XENON1T constraint [120] on dark matter scattering are shown as purple lines.*

shows the interplay of the LHC (brown shading) and dark matter search (purple) constraints in this plane with varying g, as well as the precision electroweak constraint (olive). As in the left panel, we exclude the red shaded regions where $\Gamma_{Z'}/M_{Z'} > 0.5$. There is a visible area where the vector-like U(1)′ Y-sequential model is compatible with all the constraints, in the high mass resonance region where $M_{Z'} \approx 2m_\chi$ around $\log_{10}(m_\chi/\text{GeV}) \gtrsim 3.3$ and $\log_{10}(M_{Z'}/\text{GeV}) \gtrsim 3.7$. This small allowed region at larger $\log_{10}(m_\chi/\text{GeV}) \sim 3.5$ and $\log_{10}(M_{Z'}/\text{GeV}) \gtrsim 3.7$ is squeezed by the requirement that $\Gamma_{Z'}/M_{Z'} < 0.5$.

In addition to this visible allowed region, there is also a narrow sliver of parameter space where $M_{Z'} \sim 2m_\chi$ that is also compatible with all the constraints,

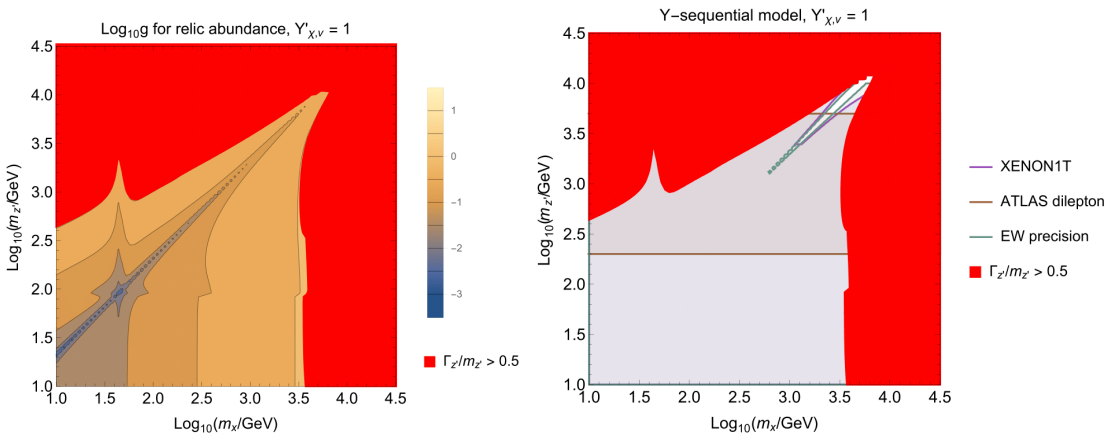

Figure 4.4: *Left panel: The $(m_\chi, M_{Z'})$ plane in the U(1)′ Y-sequential model with a vector-like dark matter coupling $Y'_{\chi,L} = Y'_{\chi,R} = 1$ and the value of the gauge coupling g allowed to vary so as to yield $\Omega_\chi = \Omega_{CDM}$ everywhere in the plane. Right panel: The same $(m_\chi, m_{Z'})$ plane with varying gauge coupling g, now showing the band excluded by the ATLAS dilepton search (shaded brown) [199], the regions excluded by the direct XENON1T search for dark matter scattering (shaded purple) [120], the region excluded by precision electroweak data (shaded olive) [210] and the regions where $\Gamma_{Z'}/M_{Z'} > 0.5$ (shaded red). Note the small allowed region with $\log_{10}(m_\chi/\text{GeV}) \gtrsim 3.3$ and $\log_{10}(M_{Z'}\text{GeV}) \gtrsim 3.7$. Note that there is a very narrow region on resonance that is not visible on this plot but is explored in Fig. 4.5*

which is invisibly thin in Fig. 4.4 [144]. The left panel of Fig. 4.5 displays the relevant constraints on the vector-like U(1)′ Y-sequential model along the line $M_{Z'} = 2m_\chi$ for a range of values of g. The relic density $\Omega_\chi = \Omega_{CDM}$ along the blue line, and the blue-shaded region below it is excluded because the relic particle is overabundant. The ATLAS dilepton constraint [199] is shown as a brown line extending over the range $2.3 \lesssim \log_{10}(M_{Z'}/\text{GeV}) \lesssim 3.7$, with the region above being excluded. The purple line shows the upper limit on g provided by direct dark matter searches as a function of $M_{Z'}$. Finally, the green line reproduces the constraint from precision electroweak data. We see that there is a region to the right of this line, below the direct search and ATLAS dilepton lines and above the blue line that is compatible with all the constraints. Points above the blue line would have $\Omega_\chi < \Omega_{CDM}$, but the relic density could be brought up to the limit $\Omega_\chi = \Omega_{CDM}$ by taking m_χ slightly below or above $M_{Z'}/2$, so that the $\chi\chi$ annihilation cross-section is suitably reduced by sliding down one of the sides of the Z' Breit-Wigner peak.

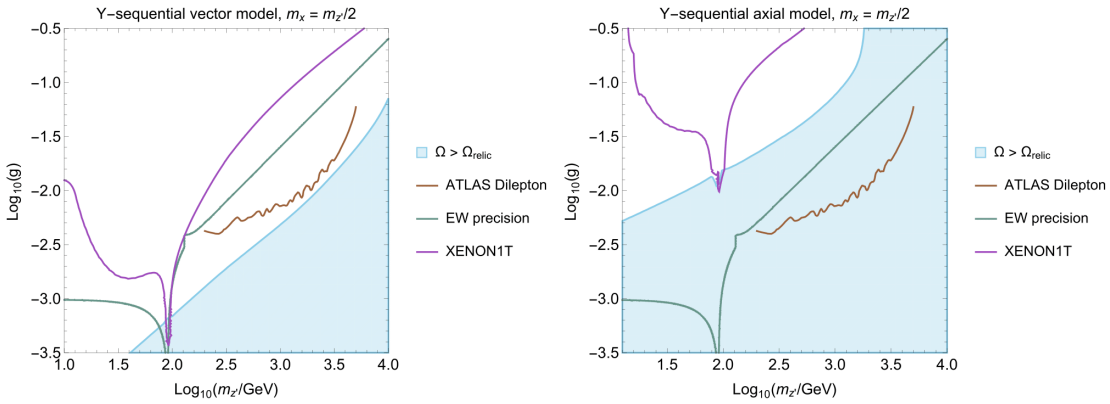

Figure 4.5: *The interplays of the constraints on the vector-like (left panel) and axial (right panel) U(1)′ Y-sequential models along the line $m_\chi = M_{Z'}/2$, for a range of values of the gauge coupling g. The relic density $\Omega_\chi = \Omega_{CDM}$ along the blue lines, and the relic density is too high in the blue-shaded region below it. The ATLAS dilepton constraint [199] is shown as brown lines: regions above are excluded. The purple lines are the upper limits on g from direct dark matter searches, and the green lines show the upper bound from precision electroweak data.*

The conclusion of this analysis of the vector-like U(1)′ Y-sequential model is similar to what was foreseen in [2]. It is very tightly constrained by the ATLAS dilepton search and direct searches for dark matter scattering, as well as the precision electroweak data, with the only allowed region (apart from the very narrow resonance region discussed in the previous paragraph) appearing when with $\log_{10}(m_\chi/\text{GeV}) \gtrsim 3.3$ and $\log_{10}(M_{Z'}\text{GeV}) \gtrsim 3.7$.

4.3 Constraints on an axial DM coupling

In this Section we consider another variant of the Y'-sequential model, assuming again that any exotic fermions are SM singlets such that the U(1)′ charges of the Standard Model particles are guaranteed to be:[62]

$$\begin{aligned} Y'_q &= 1, & Y'_l &= -3, & Y'_e &= -6, \\ Y'_d &= -2, & Y'_u &= 4, & Y'_H &= -3\,. \end{aligned} \tag{4.4}$$

[62] Up to an overall normalisation, which can be arbitrarily fixed by rescaling the overall gauge coupling g.

However, in contrast to the previous Section, we now consider a case where the dark matter particle χ has an axial U(1)$'$ coupling: $Y'_{\chi,L} = -Y'_{\chi,R}$. As in the vector-like case discussed in the previous Section, the model has as free parameters the U(1)$'$ coupling g, m_χ, $M_{Z'}$ and the magnitude of the U(1)$'$ charge of the dark matter particle. In addition, this benchmark must have at least one additional dark sector particle so as to cancel the triangle anomalies, as discussed in the previous Chapter [2]. However, here we do not discuss further the possible phenomenology of such an extended dark sector.

Fig. 4.6 displays the $(m_\chi, M_{Z'})$ plane in this model with $Y'_{\chi,L} = -Y'_{\chi,R} = 1$, analogous to the vector-like case shown in Fig. 4.2. We show as solid green (orange) (blue) lines the contours where $\Omega_\chi = \Omega_{CDM}$ for the same choices $g = 0.03(0.1)(0.3)$ considered above [63], and the relations $m_\chi = M_{Z'}/2, m_\chi = M_{Z'}$, $m_\chi = m_t$, $m_\chi = M_{Z'}/2$ and $M_{Z'} = M_Z$ are again shown by dashed lines. As in that case, the dark matter contour exhibits a wedge around $m_\chi = M_{Z'}/2$, which is asymmetric and extends to large m_χ when $\log_{10}(M_{Z'}/\mathrm{GeV}) \lesssim 2$. This extension is due to the opening of the $\chi\chi \to \bar{t}t$ threshold when $m_\chi > m_t$. Below this threshold, annihilations into pairs of Standard Model fermions are suppressed by mass factors (helicity suppressed), as can be seen in the second line of Eq. (4.3). For this reason, the dominant $\chi\chi$ annihilation channel is into pairs of mediator bosons, $Z'Z'$, when $m_t \gtrsim m_\chi \gtrsim M_{Z'}$. The relic density contours also exhibit glitches associated with enhanced annihilation when $\chi\chi \to Z$ on resonance, induced by $Z - Z'$ mixing, and when $M_{Z'} \simeq M_Z$ this mixing is enhanced.

Fig. 4.7 displays the $(m_\chi, M_{Z'})$ planes in the axial U(1)$'$ Y-sequential model for the following fixed values of g, assuming $Y'_{\chi,L} = -Y'_{\chi,R} = 1$: $g = 0.03$ (upper left), 0.1 (upper right) and 0.3 (lower). As in the vector-like case, we do not consider larger values of g, because the narrow-width approximation for the Z' breaks down. As in Fig. 4.3, the regions of the planes where $\Omega_\chi > \Omega_{CDM}$ are shaded blue, those excluded by the ATLAS dilepton search are shaded brown, those excluded by the (suitably rescaled) direct dark matter searches are shaded purple, and those excluded by precision electroweak measurements are shaded green. When $g = 0.03$ and 0.1 the dark matter density constraint is in general more powerful than the ATLAS constraint, but they are more complementary when $g = 0.3$. The direct dark matter search constraint is important at low m_χ

[63] We recall that, away from resonance, these contours would be similar for other axial models with the same value of $g^2|Y'_{\chi,L}|$.

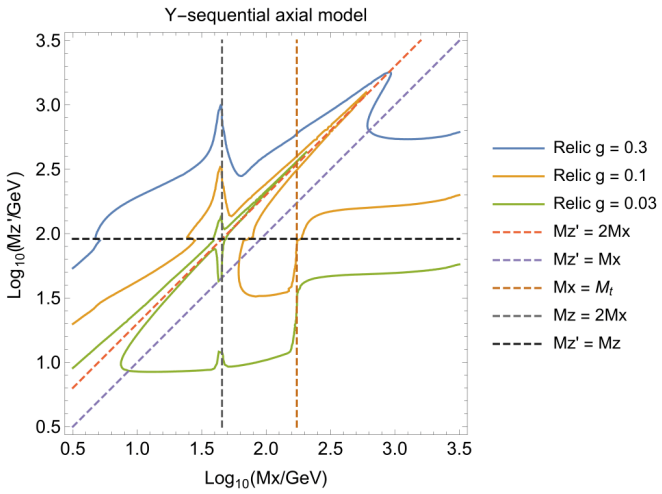

Figure 4.6: *The $(m_\chi, M_{Z'})$ plane in the U(1)′ Y-sequential model with an axial-like dark matter coupling $Y'_{\chi,L} = -Y'_{\chi,R} = 1$. The solid green (orange) (blue) lines are the contours where $\Omega_\chi = \Omega_{CDM}$ for $g = 0.03(0.1)(0.3)$, and the red/purple/brown/grey/black dashed lines are where $m_\chi = M_{Z'}/2, m_\chi = M_{Z'}$, $m_\chi = m_t$, $m_\chi = M_Z/2$ and $M_{Z'} = M_Z$, respectively.*

and $M_{Z'}$, and is relatively similar in the three panels, strengthening slightly as g increases. However, the most important constraint for $M_{Z'} \lesssim 3$ to 4 TeV is that from precision electroweak data. In combination with the relic density constraint that excludes larger $M_{Z'}$, it excludes all the displayed region of the $(m_\chi, M_{Z'})$ plane.

We show in the left panel of Fig. 4.8 the $(m_\chi, M_{Z'})$ plane in the axial U(1)′ Y-sequential model with g allowed to vary as indicated by the colour coding shown in the legend, so as to obtain $\Omega_\chi = \Omega_{CDM}$ throughout the plane. As in the vector-like case shown in the left panel of Fig. 4.4, there is a region at large $M_{Z'}$ where the required value of g becomes large and even non-perturbative. Shaded in red is the region where $\Gamma_{Z'}/M_{Z'} > 0.5$. One difference from the vector-like case is the series of 'steps' in the contours of g at $\log_{10}(m_\chi/\mathrm{GeV}) \sim 2.7$ where the onset of the $\bar{t}t$ threshold increases the annihilation rate for fixed g, so that a smaller value of g is needed to obtain $\Omega_\chi = \Omega_{CDM}$.

This feature is reflected in the right panel of Fig. 4.8, where we see that the exclusion by the direct search for dark matter scattering (purple shading) runs out of steam when $\log_{10}(m_\chi/\mathrm{GeV}) \gtrsim 3$ and g is small. For the same reason, it is also weakened along the diagonal line where $m_\chi \simeq M_{Z'}/2$. We also note the region at large $M_{Z'}$ where $\Gamma_{Z'}/M_{Z'} > 0.5$, and that the ATLAS dilepton constraint again

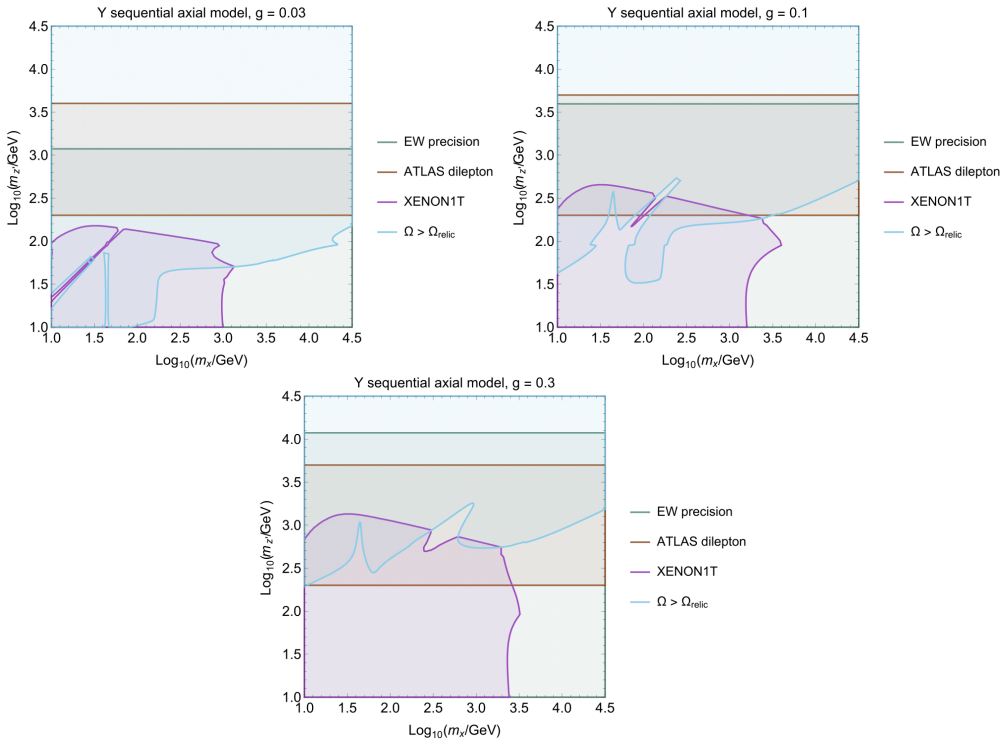

Figure 4.7: *The $(m_\chi, M_{Z'})$ planes in the U(1)′ Y-sequential model with an axial-like dark matter coupling $Y'_{\chi,L} = -Y'_{\chi,R} = 1$ for a gauge coupling $g = 0.03$ (upper left), $g = 0.1$ (upper right) and $g = 0.3$ (lower). The solid blue lines are the contours where $\Omega_\chi = \Omega_{CDM}$, and $\Omega_\chi > \Omega_{CDM}$ in the regions shaded blue. The bands shaded brown are excluded by the ATLAS dilepton search, the regions shaded purple are excluded by direct searches for dark matter scattering, and the regions shaded olive are excluded by precision electroweak data.*

enforces $\log_{10}(M_{Z'}/\text{GeV}) \lesssim 2.3$. The precision electroweak constraints rule out all of the visible plane that is compatible with a sufficiently narrow Z' width.[64]

However, we see in the right panel of Fig. 4.8 that there is no part of the displayed region of the $(m_\chi, M_{Z'})$ plane in the Y-sequential model with an axial Z' dark matter coupling that is consistent with all the constraints. In this instance, unlike in the vector-like case, there is no allowed strip when $m_\chi \simeq M_{Z'}/2$, as can be seen in the right panel of Fig. 4.5. This is mainly a result of the fact that the annihilation cross section is p-wave suppressed (resulting in a v^2 suppression), which requires the gauge coupling g to be larger to match the observed value of

[64] Even if we were to relax the requirement of a narrow width Z', one would soon run into perturbativity issues since the couplings in the region where $\Gamma_{Z'}/M_{Z'} > 0.5$ are typically unacceptably large.

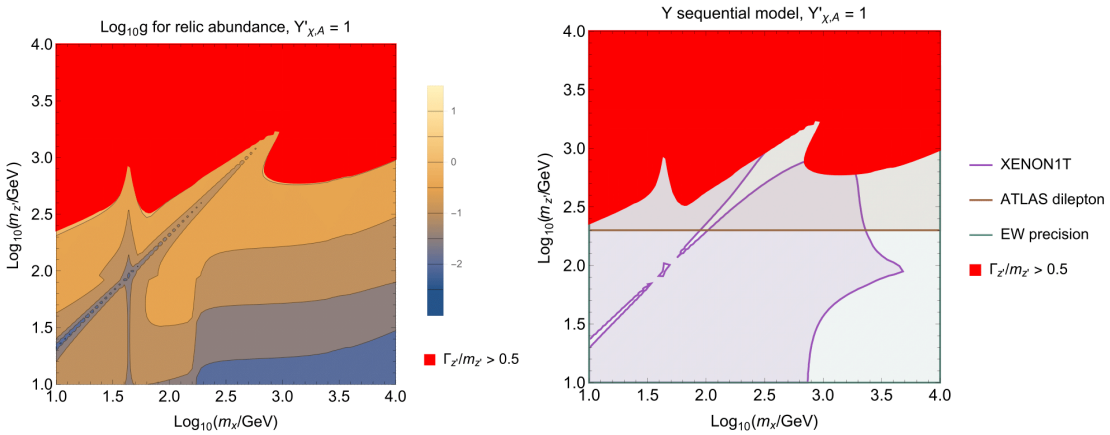

Figure 4.8: *Left panel: The $(m_\chi, M_{Z'})$ plane in the U(1)′ Y-sequential model with an axial-like dark matter coupling $Y'_{\chi,L} = -Y'_{\chi,R} = 1$ and the value of the gauge coupling g chosen to yield $\Omega_\chi = \Omega_{CDM}$. Right panel: The $(m_\chi, m_{Z'})$ plane with this varying gauge coupling g, showing the band excluded by the ATLAS dilepton search (shaded orange), the regions excluded by direct searches for dark matter scattering (shaded purple), the precision electroweak constraints (olive) and the regions where $\Gamma_{Z'}/M_{Z'} > 0.5$ (red). None of the displayed region is consistent with all the constraints since the electroweak constraints rule out all of the plane that is compatible with the narrow width requirement.*

the relic density. This larger value of g then comes into conflict with precision electroweak constraints.

4.4 Constraints on leptophobic models

We now consider two benchmark leptophobic models that were also originally proposed in [2]. By construction, they both have $Y'_l = Y'_e = 0$, which is possible only if there are additional particles beyond the dark matter particle. The first model we study contains an additional SU(2) doublet of fermions B. In the visible sector it has universal U(1)′ charges for the quarks:

$$Y'_q \;=\; Y'_u \;= Y'_d\,, \tag{4.5}$$

and hence $Y'_H = 0$. Normalizing the U(1)′ coupling so that $Y'_{\chi,L} = 1$, the following are the U(1)′ charges of the quarks and the χ_R:

$$Y'_q \;=\; -\frac{1}{27}, \quad Y'_{\chi,R} \;=\; 0\,. \tag{4.6}$$

The leptophobia of this model implies that the ATLAS dilepton search constraint is irrelevant.[65] However, one must still consider the (weaker) constraint from searches for structures in the dijet spectrum. In addition, the small size of the quark charges in Eq. (4.6) compared to the charge of the dark matter particle implies that the LHC monojet + $\not{E}_T$ constraint could be important. The absence of leptonic U(1)′ charges implies that the Higgs multiplet must also have vanishing Y', which implies that tree-level $Z - Z'$ mixing through the Higgs sector is absent. However, the presence of particles with both Standard Model and U(1)′ charges implies that kinetic $Z - Z'$ mixing is induced at the loop level, as we discuss in Appendix B.[66]

The second leptophobic Z' model that we consider contains instead an additional SU(2) triplet of fermions. It has the following universal U(1)′ charges for the quarks:

$$Y'_q = -\frac{2}{9}, \quad Y'_H \; = \; 0\,, \tag{4.7}$$

where we have again normalized the U(1)′ coupling so that $Y'_{\chi,L} = 1$, and vanishing Higgs charge. In addition, this model has $Y'_{\chi,R} = 1/2$. In this model the quark charges in Eq. (4.7) are less suppressed relative to the charge of the dark matter particle than in the first leptophobic benchmark model, so that the LHC monojet + $\not{E}_T$ constraint is correspondingly less important.

Fig. 4.9 displays in the left panel the $(m_\chi, M_{Z'})$ plane in the first leptophobic U(1)′ model with the U(1)′ charges shown in Eq. (4.6), and in the right panel the corresponding $(m_\chi, M_{Z'})$ plane in the second leptophobic U(1)′ model (Eq. (4.7)). The solid lines are contours where $\Omega_\chi = \Omega_{CDM}$ for the indicated fixed choices of the U(1)′ coupling g. The choices of g are different because the larger quark U(1)′ charges in the second model imply that its total decay width is larger than in the first model for the same value of g, causing the narrow-width approximation to break down for a smaller value of g than is the case in the first leptophobic model Eq. (4.6).

In both cases, we see the familiar feature that larger values of m_χ and $M_{Z'}$ are compatible with the $\Omega_\chi = \Omega_{CDM}$ constraint along the dashed red diagonal line where $m_\chi = M_{Z'}/2$. Below this diagonal line, the contours in the two models

[65] In principle, couplings to leptons could be induced via mixing. We checked that the resulting dilepton constraints are negligible for the two models that we consider, given our assumptions about mixing which we detail below and in Appendix B.

[66] We assume that kinetic mixing is absent at tree-level so that it is only present at loop-level.

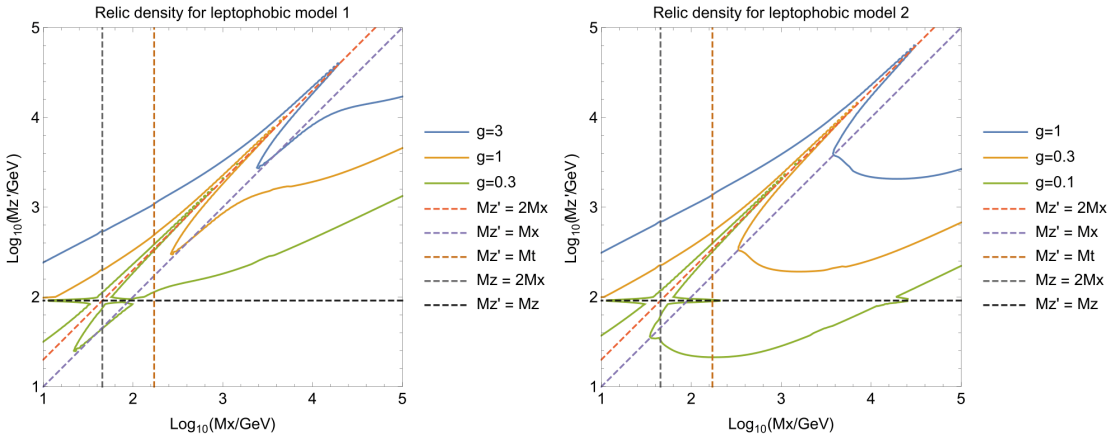

Figure 4.9: *The $(m_\chi, M_{Z'})$ planes in the leptophobic U(1)′ models (Eq. (4.6) (left panel) and Eq. (4.7) (right panel)). The solid lines are contours where $\Omega_\chi = \Omega_{CDM}$ for the indicated choices of the U(1)′ coupling g, and the red/purple/orange/-grey/black dashed lines are where $m_\chi = M_{Z'}/2, m_\chi = M_{Z'}, m_\chi = m_t, m_\chi = M_Z$ and $M_{Z'} = M_Z$, respectively.*

are quite different when $m_\chi > M_{Z'}$ (below and to the right of the diagonal purple dashed line), reflecting the greater importance of $\chi\chi$ annihilations into pairs of Z' bosons relative to annihilations into SM particles. This is because the first leptophobic model has a smaller quark U(1)′ charge (shown in Eq. (4.6)) while the dark matter charges are somewhat similar. We also note glitches in the relic density contours where $M_{Z'} = M_Z$ (black dashed lines).

This effect is also visible in Fig. 4.10, where the gauge coupling g is allowed to vary across the $(m_\chi, M_{Z'})$ planes so as to maintain $\Omega_\chi = \Omega_{CDM}$ in the leptophobic U(1)′ models with the quark charges Eq. (4.6) (left panel) and Eq. (4.7) (right panel). In the red shaded regions $\Gamma_{Z'}/M_{Z'} > 0.5$. so that the narrow-width approximation breaks down.

The upper panel of Fig. 4.11 displays the constraint imposed by precision measurements of the oblique parameters S, T in the $(M_{Z'}, \epsilon)$ plane [210], where ϵ is the magnitude of (tree-level) kinetic mixing. For our models however, we will assume that at tree level $\epsilon = 0$, but we cannot avoid generating it at loop-level. In the lower left panel of Fig. 4.11, we show the constraint in the $(M_{Z'}, g)$ plane that is imposed by the oblique parameters S, T in the first leptophobic model with $Y'_q = -1/27$ (Eq. (4.6)), and in the lower right panel the corresponding constraint in the second leptophobic model with $Y'_q = -2/9$ (Eq. (4.7)), assuming in both

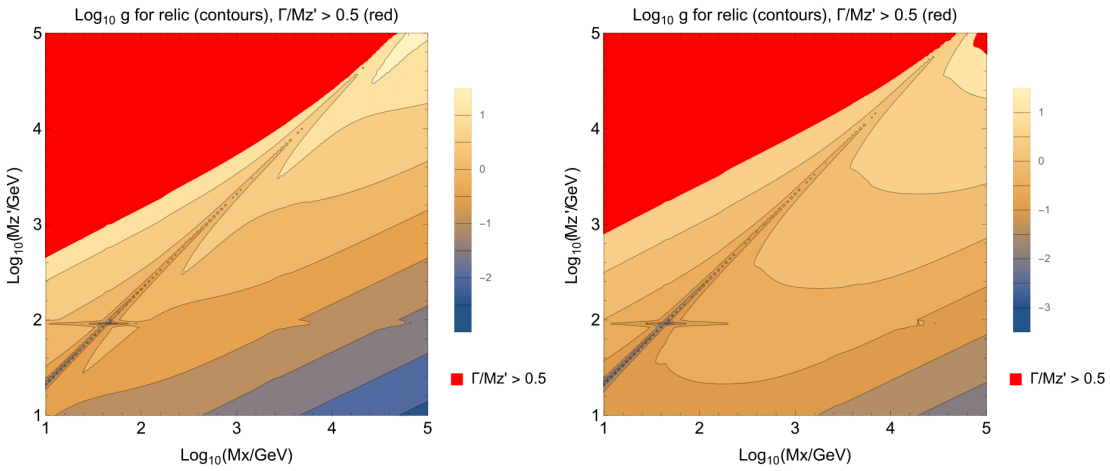

Figure 4.10: *The $(m_\chi, M_{Z'})$ planes in the leptophobic U(1)′ models Eq. (4.6) (left panel) and Eq. (4.7) (right panel), with the value of the gauge coupling g varying across the planes so as to enforce $\Omega_\chi = \Omega_{CDM}$, as indicated by the colours and solid contours.*

cases that the loop-induced mixing vanishes at the scale of 100 TeV [67]. For further details on the electroweak precision constraints, see Appendix B.

This constraint is much weaker than the mass mixing constraint in the Y'-sequential models that was shown in Fig. 4.1, due to both the loop-suppression and the small quark charges present in both models. In particular, in the case of the second leptophobic model we see in the lower right panel of Fig. 4.11 that for $M_{Z'} < M_Z$ only $g \gtrsim 0.5$ is disallowed, and that any value of $g < 1$ is allowed for $\log_{10}(M_{Z'}/\text{GeV}) \gtrsim 2.1$. Since the first leptophobic model has a smaller quark charge, namely $Y'_q = -1/27$ (Eq. (4.6)), the constraint on g for any fixed value of $M_{Z'}$ is weaker by a factor of 6, and hence of even less importance, as seen in the lower left panel of Fig. 4.11. [68]

We consider next the dijet bounds on these leptophobic models, which are shown in Fig. 4.12. This shows the constraints on the quark coupling $g \times Y'_q$ when $m_\chi > M_{Z'}/2$, so that the invisible width vanishes. When applying these bounds to parameter points with non-zero invisible width, we rescale the bounds using the

[67] For consistency, the scale at which the mixing vanishes should not lie within the range of $M_{Z'}$ displayed in the figures. By choosing the mixing to vanish at the boundary of the displayed range of $M_{Z'}$, we are applying it in the most conservative possible way.

[68] The glitches seen in the upper and lower right panels of Fig. 4.11 arise from a mismatch between our treatments of the precision electroweak constraints using S and T at large $M_{Z'}$ and the ρ parameter at smaller $M_{Z'}$.

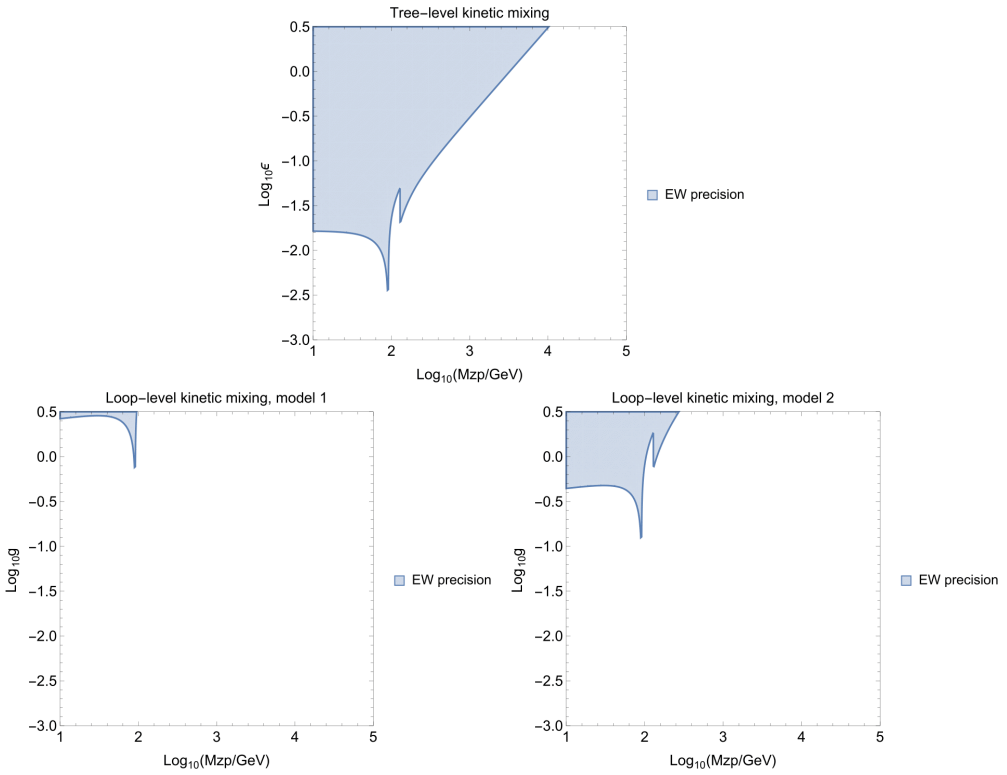

Figure 4.11: *Upper panel: The constraint on kinetic mixing ϵ as a function of $M_{Z'}$ imposed by precision measurements of the oblique parameters S and T (and ρ). Lower left panel: The kinetic mixing constraint in the $(M_{Z'}, g)$ plane in the first leptophobic model (Eq. (4.6)), taking account of the logarithmic variation of ϵ and assuming that it vanishes at a renormalization scale of* 100 *TeV. Right panel: The corresponding kinetic mixing constraint in the $(M_{Z'}, g)$ plane in the second leptophobic model (Eq. (4.7)).*

narrow width approximation. The irregularities in the limit contour arise because several different 13-TeV experimental analyses are combined:

- An ATLAS search for resonances decaying into boosted quark pairs + a γ or a jet with 36.1/fb for $M_{Z'} < 220$ GeV [214],
- An ATLAS search for dijets + an ISR γ with 15.5/fb for 220 GeV$< M_{Z'} <$ 350 GeV [215],
- An ATLAS search for dijets + an ISR jet with 15.5/fb for 350 GeV$< M_{Z'} <$ 450 GeV [215],
- An ATLAS dijet search with 3.6 to 29.7/fb for 450 GeV$< M_{Z'} <$ 1500 GeV [113],

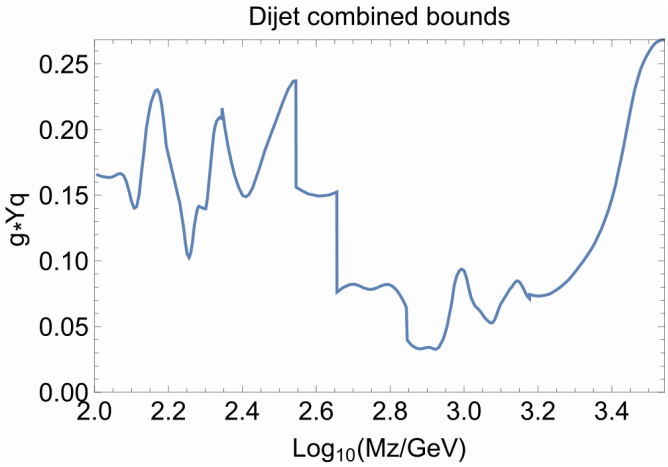

Figure 4.12: *The upper limits on the on the quark coupling $g \times Y'_q$ obtained from the LHC 13-TeV dijet searches listed in the text. The bounds displayed here are for $m_\chi > M_{Z'}/2$, such that the invisible width vanishes.*

- An ATLAS dijet search with 37.0/fb for 1.5 TeV$< M_{Z'} <$ 3.5 TeV [112].

We have also explored the constraints on the leptophobic models coming from monojet searches at the LHC. To this end, we have modelled the published results from ATLAS [107] using a rapid recasting procedure that reproduces the published experimental results within the quoted $\pm 1\sigma$ uncertainty, the main deviations being associated with binning effects in the experimental analysis and theoretical modelling. Practical details are described in Appendix C.

Next we show summary plots of all relevant constraints for fixed gauge couplings, in which we treat the relic density as an upper limit rather than a strict requirement, for leptophobic model 1 in Fig. 4.13 and for leptophobic model 2 in Fig. 4.14. We see that relic density considerations along with the direct detection constraint rule out much of the parameter space, with LHC searches being less important. In particular, the monojet constraint is unimportant for $g = 0.3$, but makes an appearance for $g = 1$ and becomes more important for $g = 3$. The scaling of the monojet sensitivity is partly due to the signal falling into different search regions at different parameter points. At low m_χ and $M_{Z'}$ the monojet signal would fall into the low $E_{T,\mathrm{miss}}$ selection, whereas at higher masses the signal is best constrained by the higher $E_{T,\mathrm{miss}}$ selection. The band structure of the region excluded by the LHC dijet searches arises because of the irregularity in the combined constraint seen in Fig. 4.12. We also recall that in these models the

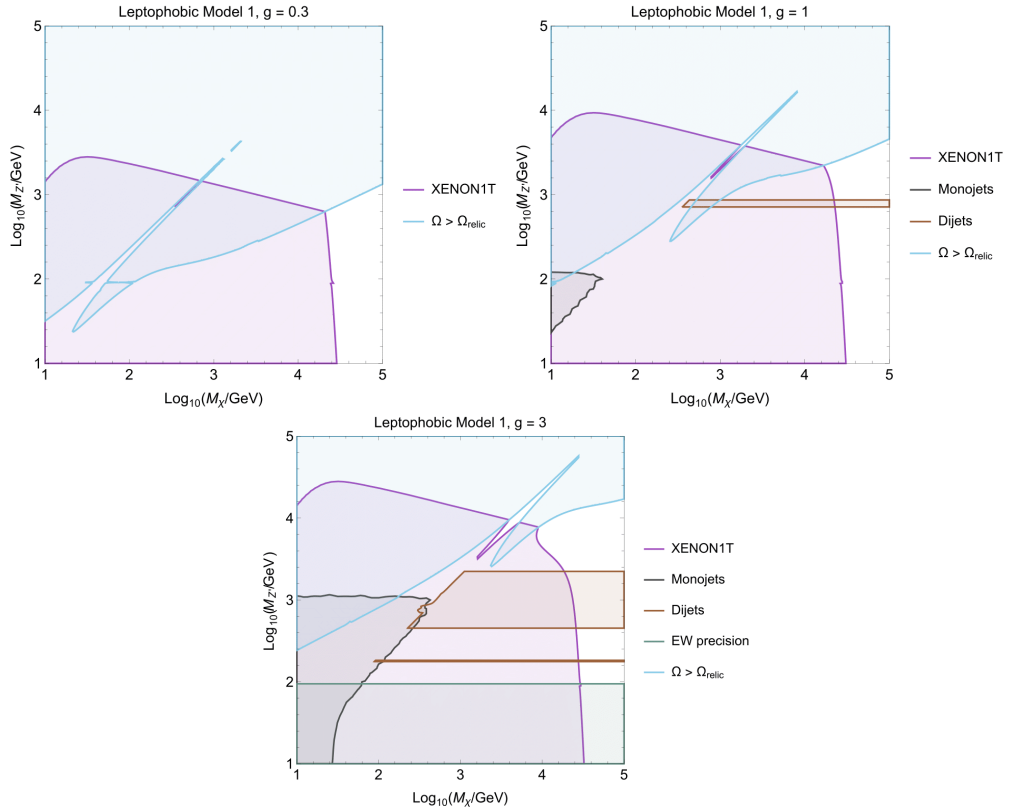

Figure 4.13: *The $(m_\chi, M_{Z'})$ planes for leptophobic model 1, for a gauge coupling $g = 0.3$ (upper left), $g = 1.0$ (upper right) and $g = 3.0$ (lower). The solid blue lines are the contours where $\Omega_\chi = \Omega_{CDM}$, and $\Omega_\chi > \Omega_{CDM}$ in the regions shaded blue. The dark grey band is excluded by the most recent ATLAS monojet search and the bands shaded brown are excluded by ATLAS dijet searches. The regions shaded purple are excluded by direct searches for dark matter scattering, and the regions shaded green are excluded by precision electroweak data.*

invisible branching ratio is typically large, such that in those regions of parameter space where the decay of the Z' into DM is kinematically allowed the bounds coming from dijet searches are weaker due to the broadening of the Z' width.

Finally, we show in the left and right panels of Fig. 4.15, respectively, compilations of the various phenomenological constraints in the $(m_\chi, M_{Z'})$ planes for the first and second leptophobic models (Eqs. (4.6, 4.7)), varying g so as to obtain the correct total cold dark matter density (see Fig. 4.10 for the required values of g). The monojet constraints (black lines and grey shading) are quite similar in the two models, despite the differences in their Z'-quark couplings,[69] and limited to

[69]This is because the gauge coupling determined via the relic density for model 1 is higher

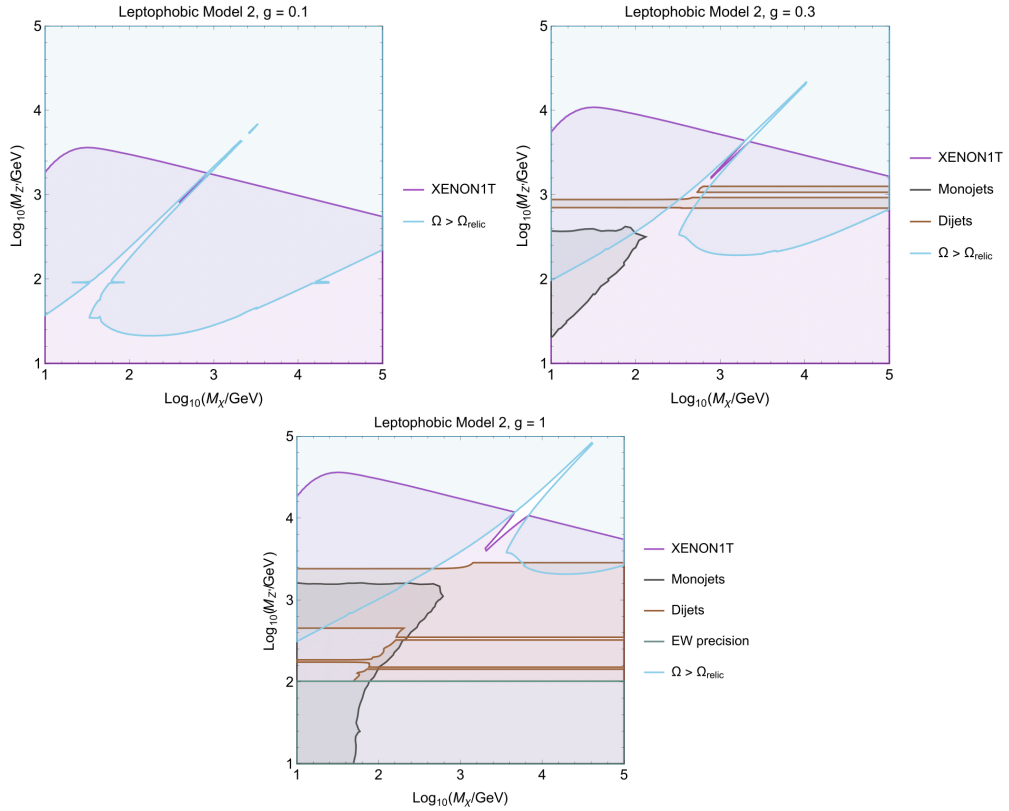

Figure 4.14: *The $(m_\chi, M_{Z'})$ planes for leptophobic model 2, for a gauge coupling $g = 0.1$ (upper left), $g = 0.3$ (upper right) and $g = 1.0$ (lower). The solid blue lines are the contours where $\Omega_\chi = \Omega_{CDM}$, and $\Omega_\chi > \Omega_{CDM}$ in the regions shaded blue. The dark grey band is excluded by the most recent ATLAS monojet search and the bands shaded brown are excluded by ATLAS dijet searches. The regions shaded purple are excluded by direct searches for dark matter scattering, and the regions shaded green are excluded by precision electroweak data.*

$\log_{10}(M_{Z'}/\text{GeV}) \lesssim 3.3$ to 3.4. We see that the dijet constraint (orange lines and shading) is generally weaker in the first model, as was to be expected in view of its smaller Z'-quark couplings. We also see that in both cases the direct DM detection constraints (purple lines and shading) are stronger than those from the dijet and monojet constraints. In the first leptophobic model, when $\log_{10}(m_\chi/\text{GeV}) \lesssim 4$ the direct DM scattering constraint enforces $\log_{10}(M_{Z'}/\text{GeV}) \gtrsim 3.2$, which is attained along the diagonal line where $M_{Z'} = 2m_\chi$ and rapid resonant annihilation requires a smaller value of the coupling g, reducing the scattering cross

than that for model 2 because it has a smaller quark charge, compensating for the smaller quark charge that enters the monojet production cross-section. In addition, model 1 has a higher invisible branching fraction.

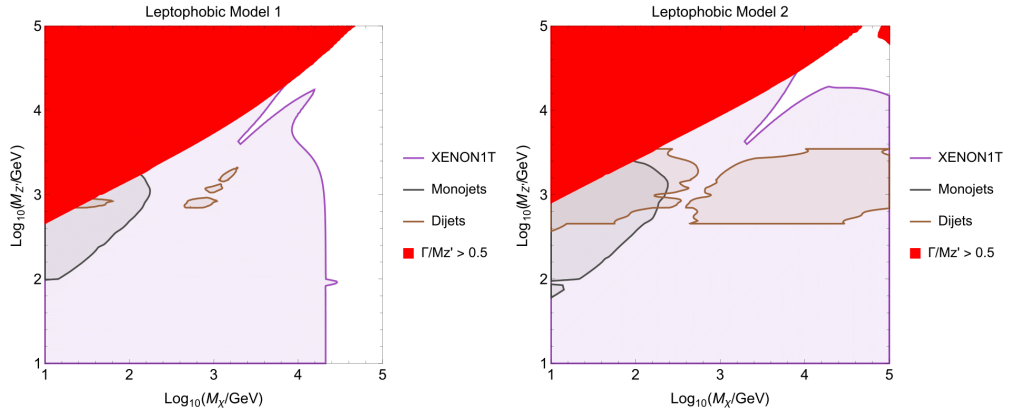

Figure 4.15: *Left panel: Compilation of constraints in the* $(m_\chi, M_{Z'})$ *plane in the first leptophobic model (Eq. (4.6)), where the coupling is varied to obtain good relic abundance. Right panel: The corresponding compilation of constraints in the* $(m_\chi, M_{Z'})$ *plane in the second leptophobic model (Eq. (4.7)).*

section. In the second leptophobic model the direct dark matter constraint imposes $\log_{10}(M_{Z'}/\text{GeV}) \gtrsim 3.2$ in all of the displayed plane.

The importance of the direct DM scattering constraint in Fig. 4.15 arises from the vector nature of the coupling of the DM particle to quarks in the two minimal leptophobic models (Eqs. (4.6, 4.7)) proposed in [2]. It would be possible to construct non-minimal leptophobic models in which the DM couplings are purely axial, by adding additional exotic SM singlet fermions, in which case the impact of the direct DM scattering constraint would be reduced.[70] However, we do not consider this case any further.

As in the previous leptophilic models, in narrow strips of resonant annihilation near the Z' peak where $m_\chi \simeq M_{Z'}/2$, the gauge coupling g may be significantly smaller while also reproducing the observed relic density. To investigate to what extent, if at all, the other experimental constraints can exclude this region, we show the $(M_{Z'}, g)$ plane for both leptophobic models in Fig. 4.16. We see that, in both cases, the correct total cold dark matter density can be obtained for any value of $M_{Z'}$ without coming into conflict with data from direct detection, the LHC and electroweak precision data. As in the case of the vector-like leptophobic model, this feature is too narrow to be visible in the $(m_\chi, M_{Z'})$ planes shown in Fig. 4.15.

[70] In this hypothetical case, indirect constraints on DM annihilations, e.g., from searches for $\chi\chi \to \gamma + \text{X}$ in dwarf spheroidal galaxies [216], would play a role for $m_\chi \lesssim 50$ GeV.

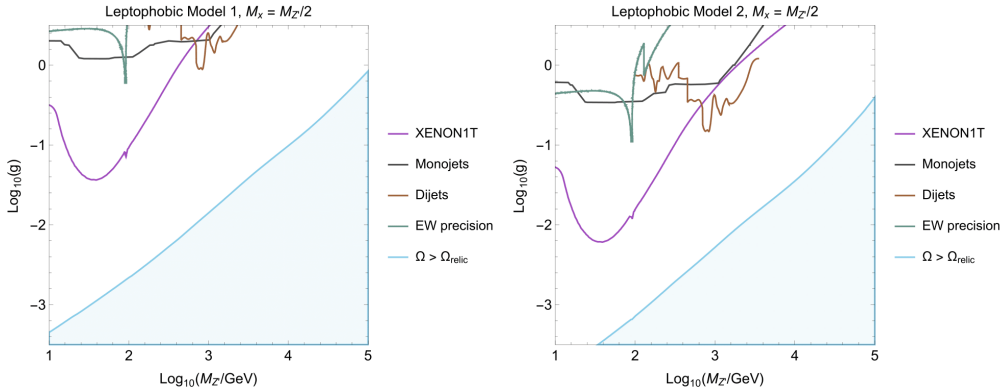

Figure 4.16: *The $(M_{Z'}, g)$ planes for leptophobic model 1 (left) and 2 (right), with $m_\chi = M_{Z'}/2$ for resonant annihilation. The solid blue lines are the contours where $\Omega_\chi = \Omega_{CDM}$, and $\Omega_\chi > \Omega_{CDM}$ in the regions shaded blue. The region above the dark grey line is excluded by the most recent ATLAS monojet search and the region above the line shaded brown is excluded by ATLAS dijet searches. The region above the purple line is excluded by direct searches for dark matter scattering, and the region above the green line is excluded by precision electroweak data.*

In this Section we have shown the impact of experimental data on the leptophobic benchmark models defined in Eqs. (4.6, 4.7). We have considered constraints coming from direct dark matter scattering, the relic density, electroweak precision data as well as monojet and dijet data coming from the LHC. As is often the case, the direct detection bound in combination with the relic density turns out to be the strongest, with the LHC searches having some relevance only on resonance. We have commented how an alternative model with a purely axial DM coupling could potentially evade this bound, although a detailed study would be needed since in this case larger gauge couplings may be required in order to obtain the relic density.[71] We now offer some final remarks and conclusions.

4.5 Viability of anomaly-free models

We have studied four benchmark models of dark matter taken from [2], whose interactions are mediated by an anomaly-free Z' boson. Two of these models

[71] We found for the Y-Sequential models in Section 4.3, that the larger gauge coupling needed to reproduce the relic density in the axial model meant that it was actually slightly more constrained than the vector model. The leptophobic models, however, have a much weaker bound coming from electroweak precision data.

are leptophilic, one with a vector-like coupling of the dark matter particle to the Z', and one with an axial coupling. The other two models are leptophobic, with the gauge anomalies cancelled by different sets of additional particles in the dark sector. We have considered the phenomenological constraints coming from the overall density of cold dark matter, direct searches for dark matter scattering, from LHC searches for dileptons, dijets and monojets, and from precision electroweak measurements.

We have found that the vector-like leptophilic model is extremely tightly constrained by direct detection and dilepton constraints, as well as modifications to the S and T electroweak parameters, which rule out almost completely the areas of parameter space where we obtain good relic abundance. There is, however, a very small region of parameter space still available where both m_χ and $M_{Z'}$ have masses of several TeV. This region may be accessible to improvements in future constraints on electroweak precision variables before future enhancements in direct detection constraints. In addition to this region, there is a continuous line of solutions constrained to a very narrow allowed strip where $m_\chi \simeq M_{Z'}/2$.

The axial leptophilic model is excluded for $M_{Z'} < 10$ TeV completely, again by direct detection, dilepton constraints and modifications to the electroweak variables. This is a consequence of the larger gauge coupling required to give a good relic abundance strengthening the other bounds. Therefore, this model requires modifications if it is to survive in the parameter range that we consider.

The two leptophobic models both have larger allowed regions of parameter space where $\log_{10}(m_\chi/\text{GeV}) \gtrsim 3.2$, as well as narrow allowed strips where $m_\chi \simeq M_{Z'}/2$. The interesting regions of these models are generally safe in terms of their effect upon electroweak precision variables, as well as evading the dilepton bounds that constrain tightly the previous models. The monojet constraints on both models are relatively weak compared to the other constraints. The leptophobic model with a triplet of 'dark' particles has a stronger Z' coupling to quarks, so that the dijet searches are stronger. However, despite this, the constraint from direct detection limits is the strongest constraint on the parameter spaces of both leptophobic models. Since the LHC centre-of-mass energy will not be increased substantially, whereas the integrated luminosity will increase by almost two orders of magnitude compared to that analyzed so far, we expect that the improvement in dijet constraints will be mainly in terms of coupling rather than Z' mass. We therefore expect future direct dark matter detection experiments to continue to

impose stronger constraints than future collider results.

We have shown that Z' models similar to the spin-one simplified models widely studied in the literature are either very strongly constrained (the Y-sequential models) or must feature exotic fermions charged under the SM gauge group (including SU(2) multiplets). In the latter case, it would be interesting in the future to study novel experimental constraints that might arise from the presence of such exotic fermions. Therefore creating an anomaly-free theory that features a purely axial coupling to dark matter would allow a greater deal of complementarity between LHC and direct detection constraints. For our benchmark models, we have found that complementarity between different experimental constraints is not so simple to achieve.

The great progress made in recent years in exploring new physics scenarios at colliders and in underground experiments still leaves uncovered regions of parameter space which will be probed by the next generation of colliders. In particular we have found that dijet and dilepton searches can set the strongest constraints when the DM annihilation is on the Z' resonance. We look forward to the continued exploration of simplified anomaly-free models of dark matter from both the theory community and future experimental data.

Having studied Z' mediated dark matter models in some detail in this Chapter and the previous Chapters, we will now move on to an alternative hypothesis. In the next Chapter, we will consider instead a spin-zero portal to dark matter. We will use a completely gauge-invariant[72] model of pseudoscalar mediators to propose a new search for DM at the LHC.

[72]The issue of gauge invariance here is more direct and not related at all to gauge anomalies.

Chapter 5

A New LHC Search for Pseudoscalar Mediated Dark Matter

This Chapter is heavily based on [4], which I wrote in collaboration with Jose Miguel No and Malcolm Fairbairn. This work was published in [4].

5.1 Introduction to the new search

In the previous Chapters we have focussed on the case of a spin-one mediator between DM and the SM. We found that these Z' models can suffer from a lack of gauge invariance unless exotic chiral fermions that are charged under the new gauge symmetry are introduced. Here we continue the quest for gauge invariant dark matter models by taking a look at the case of a spin-zero mediator between the dark and visible sectors. In terms of the simplified models introduced in Chapter 1 we will focus on a pseudoscalar mediator since the pure scalar model suffers from strong direct detection constraints. We will present a fully gauge-invariant extension of this model (already proposed by [221]) which includes a Two Higgs Doublet Model (2HDM). The main purpose of this Chapter will be to propose a new search for the LHC which will explore regions of parameter space of this model that existing searches cannot reach. In addition, it is possible to fit the Galactic Center Excess (GCE) in this model, which was already shown by [222].

The observed gamma ray excess in the Fermi-LAT space telescope observations of the Milky Way Galactic Centre [223] may be interpreted as the existence of weak-scale DM annihilating into $\bar{b}b$ pairs [224–227] (see [228] for a recent exhaustive analysis of the excess and its DM interpretation). While arguably there is some tension between the DM interpretation of the gamma ray excess at the Galactic Centre and the non-observation of emission due to DM annihilation in dwarf spheroidal galaxies [216][73], the self-annihilation cross section needed to explain the excess can be consistent with that required to generate the observed relic abundance through thermal freeze-out in the early Universe, $\langle\sigma \mathrm{v}\rangle \simeq 3 \times 10^{-26} \mathrm{cm}^3/\mathrm{s}$. The gamma ray Galactic Center Excess (GCE) can be fitted by a fermionic WIMP dark matter particle χ with mass $m_\chi \sim 45$ GeV [228], which couples to the SM via a pseudoscalar mediator with enhanced couplings to b-quarks and/or τ-leptons.

At the same time, current limits on the spin-independent DM interaction cross section with nuclei by the Large-Underground-Xenon (LUX) [121] and PandaX [200] experiments strongly constrain DM masses in the range $10 - 100$ GeV. A compelling DM interpretation of the gamma ray Galactic Centre excess (GCE) in combination with the non-observation of a signal in DM direct detection experiments is via the existence of a pseudoscalar mediator between the visible and DM sectors [222, 230, 231], which yields spin-dependent DM-nucleon interactions, for which experimental limits are much less stringent. Pseudoscalar mediated DM-nucleon interactions generally lie well below the reach of present DM direct detection experiments.

Direct and indirect probes of DM are complemented by searches at colliders, where pairs of DM particles could be produced. These escape the detector and manifest themselves as events possessing an imbalance in momentum conservation, via the presence of missing transverse momentum $\not{E}_T$ recoiling against a visible final state X. Searches for events with large $\not{E}_T$ are currently a major focus at the Large Hadron Collider (LHC) largely due to their connection to DM [232]. In this Chapter we present a new search avenue for DM at the LHC, characteristic of renormalizable, gauge invariant scenarios beyond the Standard Model with a pseudoscalar portal between the visible and dark sectors. The search is

[73] However we are also aware that the errors on the astrophysical J-factors used in [216] are somewhat small, such that allowing more freedom in the fit and adding a systematic error representing the possibility of triaxiality in the halos could reduce this disagreement somewhat [229].

characterized by a $b\bar{b}\,Z\ (Z \to \ell\ell) + \not{E}_T$ final state.

We show that this new DM search channel of a leptonically decaying Z boson, two bottom quarks and missing transverse momentum will yield a powerful probe of the region of parameter space consistent with a DM interpretation of the GCE through LHC Run 2 data. In particular, in certain regions of parameter space, this search can be stronger than Dark Matter searches via multi-jet $+\not{E}_T$, existing searches for new scalars (such as those from 2HDM models), and the important $\mathrm{Br}\,(B_s \to \mu^+\mu^-)$ bound coming from flavour physics. Additionally, we will find that it is complementary to an earlier search based on the mono-Z channel ($Z + \not{E}_T$) proposed in [233].

The layout of this Chapter is then as follows. First, in Section 5.2, we will describe the lack of gauge invariance in the standard pseudoscalar mediated DM model, introduce a gauge invariant extension of this model, include a quick review of the 2HDM features of the model, as well as describe the relic density calculation. In Section 5.3 we will describe the existing constraints applying to this model, coming from flavour physics, direct searches for 2HDM particles, and conventional missing energy channels that look for DM. Then in Section 5.4 we describe two resonant mono-Z searches that can be used to probe these sort of models: both our new search which we propose, and an existing one which we use to set constraints. Finally, we summarise the novel search described in this Chapter in Section 5.5.

5.2 The pseudoscalar portal to dark matter

We focus our analysis on scenarios with a pseudoscalar mediator between DM and the SM fermions. This can yield a compelling explanation of the GCE through DM annihilation into b-quarks (see e.g. [222, 231]). For concreteness, in this Chapter, we will consider DM to be a Dirac fermion χ with mass m_χ, singlet under the SM gauge interactions and coupling to a real singlet pseudoscalar mediator a_0 via

$$V_{\text{dark}} = \frac{m_{a_0}^2}{2}\, a_0^2 + m_\chi\, \bar{\chi}\chi + y_\chi\, a_0\, \bar{\chi}\, i\gamma^5 \chi\,. \tag{5.1}$$

However, for the pseudoscalar to be able to mediate interactions between DM and the SM fermions, $SU(2)_{\mathrm{L}} \times U(1)_{\mathrm{Y}}$ gauge invariance requires the existence of new states beyond the SM in addition to the DM particle and the pseudoscalar mediator [221, 234].

In order to identify the lack of gauge invariance in this type of pseudoscalar portal model, first consider the term $y_\chi\, a_0\, \bar{\chi}\, i\gamma^5 \chi$ in the Lagrangian above. Assuming χ to be a SM singlet, a_0 must also be a SM singlet. Then we turn to the would-be interaction of a_0 with SM quarks,[74] $y_f\, a_0\, \bar{q}\, i\gamma^5 q$, where y_f is the Yukawa coupling of the quark q. This term can only be generated from a combination of the left and right handed quarks q_L and q_R, which are chiral and so transform differently under $SU(2)_{\rm L} \times U(1)_{\rm Y}$. Since a_0 is a singlet it cannot soak up the difference in quantum numbers between q_L and q_R, meaning this term is not gauge-invariant under $SU(2)_{\rm L} \times U(1)_{\rm Y}$. Although this symmetry is broken, at higher energies it is restored and there must exist additional particles [221, 234] which are needed in order to restore gauge symmetry. These additional particles can then have an impact on the low energy phenomenology, especially if there are upper bounds on the exotic particle masses, as we will discuss later.

A possible renormalisable and gauge invariant version of the pseudoscalar portal between DM and the SM includes an extension of the SM Higgs sector with a second Higgs doublet, as first noted in [221]. The theory then contains many ingredients, including those naturally present in a two Higgs doublet model (2HDM) [221, 233–235]. We note that this also gives a preferential coupling of the pseudoscalar mediator to third generation SM fermions (b-quarks and τ-leptons), which makes it possible to explain the GCE as in the widely studied case of dominant annihilation into $\bar{b}b$ pairs.

In the following we provide a brief review of the 2HDM aspects of relevance to us (for a general review of 2HDM theory and phenomenology, see e.g. [236]): The two Higgs doublets are $H_j = \left(\phi_j^+, (v_j + h_j + i\,\eta_j)/\sqrt{2}\right)^T$, with $(j = 1, 2)$. v_j are the *vev* of the doublets ($\sqrt{v_1^2 + v_2^2} = v$ and $v_2/v_1 \equiv \tan\beta$). We consider a 2HDM scalar potential with Charge-Parity (CP) conservation and a softly broken $\mathbb{Z}_2$ symmetry. The presence of this $\mathbb{Z}_2$ symmetry in the couplings of the doublets H_j to fermions allows us to forbid dangerous tree-level flavour changing neutral currents, by forcing each fermion type to couple to one doublet only [202]. In *Type I* 2HDM all fermions couple to H_2, while for *Type II* 2HDM up-type quarks couple to H_2 and down-type quarks and leptons couple to H_1, which is the case we will consider here. The scalar spectrum of the 2HDM contains a charged scalar $H^\pm = \cos\beta\, \phi_2^\pm - \sin\beta\, \phi_1^\pm$, a neutral CP-odd scalar $A_0 = \cos\beta\, \eta_2 - \sin\beta\, \eta_1$ and two

[74] This is not written in the Lagrangian (5.1), since we will generate this term in a separate Lagrangian we introduce later.

neutral CP-even scalars $h = \cos\alpha\, h_2 - \sin\alpha\, h_1$, $H_0 = -\sin\alpha\, h_2 - \cos\alpha\, h_1$. We identify h with the 125 GeV Higgs state, which has SM-like properties when the mixing angle α in the neutral CP-even sector satisfies $\beta - \alpha = \pi/2$.

As we show now, the 2HDM allows for pseudoscalar mediated interactions between the visible sector and the DM candidate χ in (5.1). The portal between the visible and dark sectors occurs via

$$V_{\text{portal}} = i\,\kappa\, a_0\, H_1^\dagger H_2 + \text{h.c.} \tag{5.2}$$

which causes the would-be 2HDM state A_0 to mix with a_0, yielding two pseudoscalar mass eigenstates a, A: $a = c_\theta\, a_0 - s_\theta\, A_0$, $A = c_\theta\, A_0 + s_\theta\, a_0$, with $c_\theta \equiv \cos\theta$ and $s_\theta \equiv \sin\theta$. This mixing allows both a and A to couple simultaneously to DM and the SM fermions, providing the portal between visible and DM sectors. The coupling of A (a) to DM is given by $s_\theta\, y_\chi$ ($c_\theta\, y_\chi$). Regarding the pseudoscalar couplings to SM fermions, these are given by $g_{\text{SM}} \times y_f/\sqrt{2}$ (with y_f the Yukawa coupling of the fermion). We consider here a Type II 2HDM, for which the g_{SM} coupling of a (A) is given by $s_\theta \tan^{-1}\beta$ ($c_\theta \tan^{-1}\beta$) for up-type quarks and $s_\theta \tan\beta$ ($c_\theta \tan\beta$) for down-type quarks and charged leptons. To simplify the following discussion, we also restrict ourselves to $\beta - \alpha = \pi/2$ (the so-called alignment limit) where h behaves exactly as the SM Higgs [237]. We note that for a Type II 2HDM, deviations from the alignment limit are strongly constrained by LHC Higgs measurements [111].

For the rest of this Chapter, we consider the benchmark value $m_\chi = 45$ GeV which is motivated by the GCE but we emphasise that the new LHC search we will eventually propose is relevant for a wider range of parameters. For DM annihilating through a pseudoscalar mediator [228] finds, for the GCE, a preferred range $m_\chi \in [50,\, 170]$ GeV if DM annihilates into b-quark pairs, and $m_\chi \in [10,\, 20]$ GeV if it annihilates into leptons. In our case, DM annihilates dominantly into b-quarks, with a small ($\sim 10\,\%$) annihilation component into τ-leptons. We also consider the mediator A (doublet-like) to be much heavier than a (singlet-like). For $m_\chi < m_a \ll m_A$, DM annihilates primarily to SM particles through s-channel a exchange. The velocity averaged annihilation cross section for $\chi\bar{\chi} \to$ SM in the

nonrelativistic limit is

$$\langle \sigma \mathrm{v} \rangle = \frac{y_\chi^2}{2\pi} \frac{m_\chi^2}{m_a^4} s_\theta^2 c_\theta^2 \tan^2\beta \left[\left(1 - \frac{4m_\chi^2}{m_a^2} \right)^2 + \frac{\Gamma_a^2}{m_a^2} \right]^{-1} \times \sum_f N_C \frac{m_f^2}{v^2} \sqrt{1 - \frac{m_f^2}{m_a^2}} \,, \tag{5.3}$$

with Γ_a the decay width of a. The sum is over quarks ($N_C = 3$) and charged leptons ($N_C = 1$). Reproducing the observed DM relic density requires $\langle \sigma \mathrm{v} \rangle \simeq 3 \times 10^{-26} \mathrm{cm}^3/\mathrm{s}$, which favours large values of $\tan\beta$ (particularly for not too large values of y_χ). [75]

In this Section we have introduced our full model, including the 2HDM aspects, and described how the relic density is obtained. In the next Section we will move on to describe existing experimental constraints on the model, including important bounds from flavour physics, such as $B_s \to \mu^+\mu^-$. Additionally we will comment on bounds coming from direct searches for new scalars at the LHC, as well as more traditional missing energy searches for DM models with spin-0 mediators.

5.3 Existing experimental constraints on the pseudoscalar portal

In this Section we will discuss various constraints that apply to our model, but we will delay presenting them until the next Section (the eager reader can jump ahead to Figs. 5.2 and 5.3), where we will also display our new search for this pseudoscalar portal.

Flavour constraints from $\bar{B} \to X_s\gamma$ decays yield a lower bound on $m_{H^\pm}$ in Type II 2HDM, given by $m_{H^\pm} > 480$ GeV at 95% C.L. [238]. In addition, electroweak precision observables strongly constrain the splitting between the charged scalar $H^\pm$ and either of the neutral states H_0, A [239]. Combined, these yield m_A, m_{H_0}, $m_{H^\pm} \gtrsim 500$ GeV. On the other hand m_A, m_{H_0}, $m_{H^\pm}$ may not be taken arbitrarily high if s_θ and/or m_a are kept fixed due to unitarity constraints. For $m_a \sim 100$ GeV and $\theta = \pi/4$ the unitarity bounds on m_A, m_{H_0} are respectively

[75] We note that contrary to the previous Chapters we are not using numerical tools to calculate the relic density. In this Chapter we will always be picking particle masses such that the DM is annihilating away from resonance, and Eq. 5.3 remains valid.

$m_A \leq 1.4$ TeV, $m_{H_0} \leq 1$ TeV [234]. In the following we take as benchmarks $m_{H^\pm} = m_{H_0} = 600$ GeV, 800 GeV (and assume a somewhat larger m_A, such that the production cross section for H_0 dominates over that for A).

Besides the aforementioned flavour bound $m_{H^\pm} > 480$ GeV from $\bar{B} \to X_s\gamma$ decays, the existence of a light pseudoscalar a coupling to SM fermions can be probed by its contributions to the decay $B_s \to \mu^+\mu^-$ [240, 241], which for $m_a \gg m_{B_s} \simeq 5.36$ GeV may be expressed as[76]

$$\begin{aligned} &\text{Br}\left(B_s \to \mu^+\mu^-\right) \simeq \text{Br}\left(B_s \to \mu^+\mu^-\right)_{\text{SM}} \\ &\times \left(\left| 1 + x_B \tan^2\beta \frac{f(x_t, x_a, r)}{4\, Y(x_t)} \right|^2 + \left| x_B \tan^2\beta \frac{g(r)}{4\, Y(x_t)} \right|^2 \right), \end{aligned} \tag{5.4}$$

with $x_B = m_b m_{B_s}/m_W^2$, $x_t = m_t^2/m_W^2$, $x_a = m_a^2/m_A^2$, $r = m_{H^\pm}^2/m_t^2$, $r_t = x_t\, r$, $g(r) = \log(r)/(r-1)$,

$$\begin{aligned} f\left(x_t, x_a, r\right) = g(r) \;&+\; \frac{s_\theta^2}{(r-1)} \left[2c_\theta^2 (x_a + x_a^{-1} - 1) - 1 \right] \\ &\times \left(\frac{r_t \log r_t}{(r_t - 1)} - \frac{x_t \log x_t}{(x_t - 1)} \right), \end{aligned} \tag{5.5}$$

and $Y(x)$ the Inami-Lim function,

$$Y(x) = \frac{x}{8(x-1)^2} \left[4 - 5x + x^2 + 3x \log x \right]. \tag{5.6}$$

The average of the LHCb and CMS measurements of this mode from LHC 7 and 8 TeV data is $\text{Br}\left(B_s \to \mu^+\mu^-\right) = (2.9 \pm 0.7) \times 10^{-9}$ [242–244] which may be compared against the SM prediction $(3.65 \pm 0.23) \times 10^{-9}$ [245, 246].

For $m_a < m_h/2$ the presence of the decay $h \to aa$ yields stringent constraints on the model [222], and consequently we only consider here the case $m_a > m_h/2$ for which non-standard Higgs decays are suppressed (note that for $m_\chi = 45$ GeV the 3-body decay $h \to a\bar{\chi}\chi$ is also kinematically forbidden above $m_a = 35$ GeV).

LHC searches for the states H_0, A and a decaying to $\tau^+\tau^-$ also place important constraints at large $\tan\beta$ ($a \to \bar{b}b$ has also been considered, see e.g. [247]). The latest CMS search for $\bar{b}b\phi\,(\phi \to \tau^+\tau^-)$ with an integrated luminosity of 12.9

[76] We note the important $H^\pm$ contribution in the limit $s_\theta \to 0$ (see [241]) which was missed in [222].

fb^{-1} [248], for $\phi = H_0$, a, yields limits on the parameter space for m_a, m_{H_0}, s_θ, tanβ.

Finally, the pseudoscalar portal to DM can be probed at the LHC in the $\bar{t}t+\not{E}_T$ and $\bar{b}b+\not{E}_T$ channels (see [249] for a recent discussion), and in multi-jet $+\not{E}_T$ [179]. Using the results from [250] we find that $\bar{b}b + \not{E}_T$ searches at tan$\beta \gg 1$ yield significantly weaker constraints that the ones discussed above (e.g. $B_s \to \mu^+\mu^-$). At the same time, $\bar{t}t + \not{E}_T$ searches are currently only sensitive to tan$\beta < 1$. For multi-jet $+\not{E}_T$ searches, using the analysis from [179] we find that these yield an important constraint at low tanβ, while still being subdominant to those from the LHC searches discussed in the next Section.

We will now discuss the sensitivity of our new LHC search, along with the bounds coming from an existing search, and put together the constraints with the ones discussed in this Section. We will display the results of this procedure in the Figures 5.2 and 5.3.

5.4 A new probe of consistent pseudoscalar mediated dark matter

Remarkably, when $m_{H_0} \gg m_a$ the decay $H_0 \to Za$ yields a new avenue to probe DM at the LHC. For tan$\beta \gg 1$ as favoured by the GCE, a novel DM search channel presents itself: $pp \to b\bar{b}\,H_0$, $H_0 \to Z\,a$ ($Z \to \ell^+\ell^-$, $a \to \bar{\chi}\chi$). This topology for the final state $\bar{b}b\,\ell^+\ell^- + \not{E}_T$ has not yet been explored at the LHC, and we show here that this signature allows us to probe a wide range of parameter space for pseudoscalar portal scenarios, in particular within the region consistent with a DM interpretation of the GCE.

In order to study the prospects for this signature at the LHC with $\sqrt{s} = 13$ TeV c.o.m. energy, we require events with two oppositely charged electrons/muons in the invariant mass window $m_{\ell\ell} \in [76, 106]$ GeV, with $p_T^\ell > 20$ GeV and rapidity $|\eta^\ell| < 2.5$. Our event selection further requires $|p_T^{\ell\ell} - \not{E}_T|/p_T^{\ell\ell} < 0.5$ and a separation $\Delta R_{\ell\ell} > 0.4$ between the same-flavor lepton pair. We also demand at least one b-tagged jet with[77] $p_T^b > 30$ GeV.

[77] We note that a very low value of the chosen p_T^b cut (for a very high value of m_{H_0}) could result in a breakdown of the perturbative expansion [251] for the $\bar{b}b$-associated production of H_0 (we thank Richard Ruiz for pointing out this issue to us). Using SusHi [252] We have estimated our $b\bar{b}H_0$ next-to-leading-order (NLO) k-factor to be ~ 1.4, close to the perturbative expansion

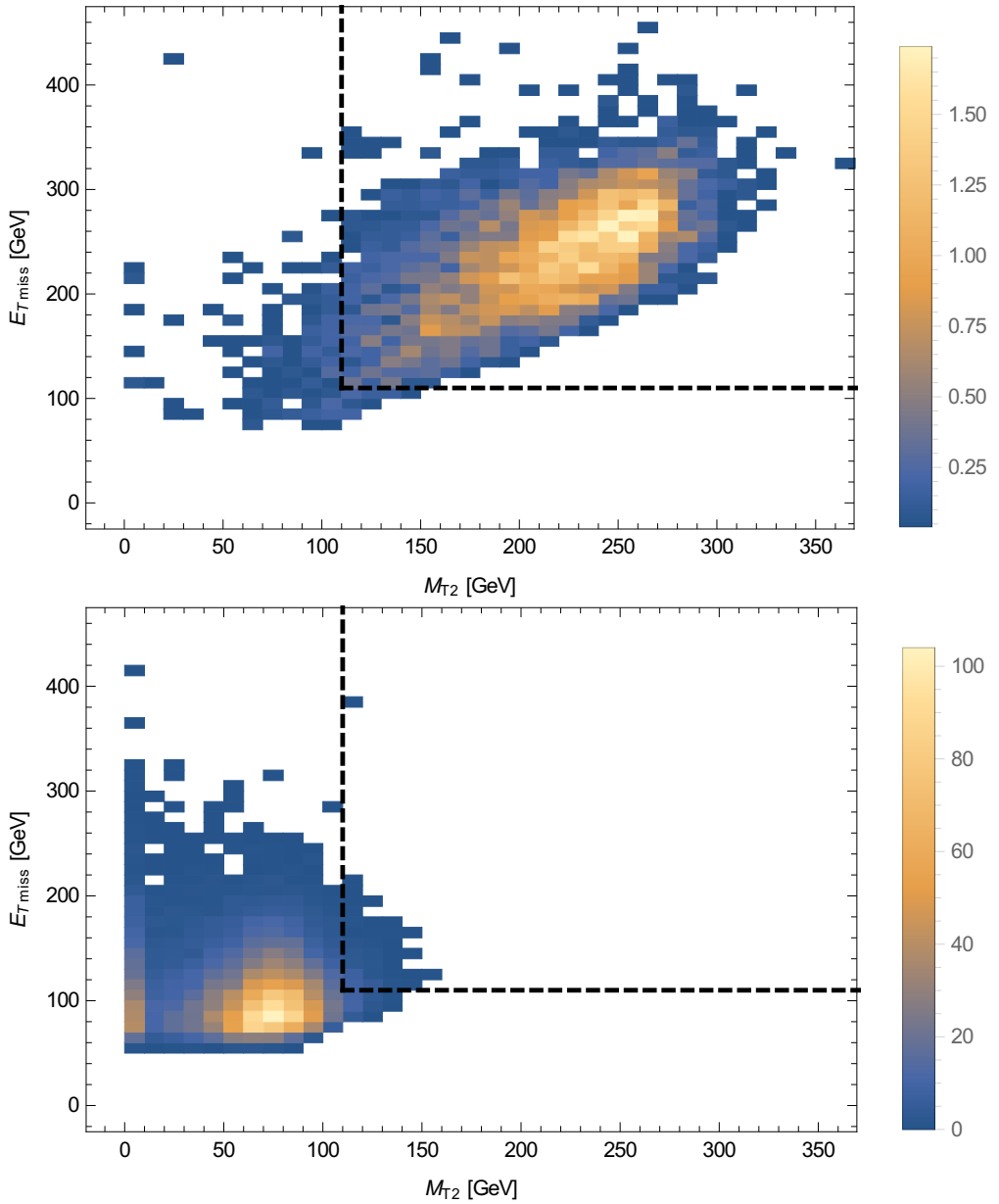

Figure 5.1: *$m_{H_0} = 600$ GeV, $m_a = 150$ GeV signal (top) and $t\bar{t}$ background (bottom) events in the (m_{T2}, $\not{E}_T$) plane, after all other cuts have been applied. The colour scale shows the expected number of events for 300 fb^{-1} of luminosity. The dashed line corresponds to the signal region $\not{E}_T$, $m_{T2} > 110$ GeV.*

The main SM backgrounds are $t\bar{t}$ and di-boson (WZ and ZZ) + jets production[78]. The requirement of one or more b-tagged jets acts as an effective suppressor of the latter, while the invariant mass window $m_{\ell\ell}$ helps diminish the $t\bar{t}$ background. In order to further reduce SM backgrounds we take advantage of the boosted configuration of the signal for $m_{H_0} \gg m_a + m_Z$, and demand the leading lepton in p_T^ℓ to satisfy $p_T^{\ell_1} > 80$ GeV as well as $p_T^{\ell_1} + p_T^{\ell_2} > 150$ GeV. Finally we use $\not{E}_T$ and the variable m_{T2} [253] to define our signal region. We calculate m_{T2} using [254] as

$$m_{T2}^2 \equiv \min_{\vec{k_T}+\vec{q_T}=\vec{p_T}} \left\{ \max \left[m_T^2(\vec{p_T^{\ell_1}}, \vec{k_T}), m_T^2(\vec{p_T^{\ell_2}}, \vec{q_T}) \right] \right\} \tag{5.7}$$

where minimisation is over all possible vectors $\vec{k_T}$ and $\vec{q_T}$ that satisfy $\vec{k_T} + \vec{q_T} = \vec{\not{p}_T}$ (with $|\vec{\not{p}_T}| = \not{E}_T$). Our signal region is defined as[79] $\not{E}_T > 110$ GeV, $m_{T2} > 110$ GeV.

We generate our signal and background event samples at LO in `MadGraph5_MC@NLO` [99] and perform showering in `Pythia 8` [100]. For the ZZ and WZ backgrounds we include up to two additional jets in the final state, matched to parton shower. We replace a full detector simulation with a Gaussian smearing of the p_T of final state paricles: We define jets, well isolated charged leptons and photons, and $\not{E}_T$ as the relevant final state objects. Jets are constructed with the `FastJet` package [155] using the anti-k_T algorithm [162] with $R = 0.4$, and are required to have $p_T > 25$ GeV and $|\eta| < 2.5$. We smear the p_T of the visible particles and calculate both the truth $\not{E}_T$ and the reconstructed value calculated from the smeared visible objects. We then smear the difference between the truth and reconstructed $\not{E}_T$. The functions for the smearing of the visible objects and $\not{E}_T$, as well as the b-tagging efficiency and mistag rates are chosen to match the ATLAS performance reported in [95] for the leptons and $\not{E}_T$, [255] for the jets and [256] for the b-tagging. We derive the projected sensitivity of our search using the CLs method [257], and assuming a conservative 20% background systematic

validity limit, but arguably safe [251].

[78] The WW diboson background is strongly suppressed by the $m_{\ell\ell}$ selection in combination with a large amount of $\not{E}_T$. Other potential backgrounds become negligible when demanding a significant amount of $\not{E}_T$ in the event.

[79] The m_{T2} cut is chosen conservatively to ensure the background prediction is not dominated by the Monte Carlo statistical uncertainty. An analysis performed by the experimental collaborations would achieve better sensitivity through a stronger cut on m_{T2}.

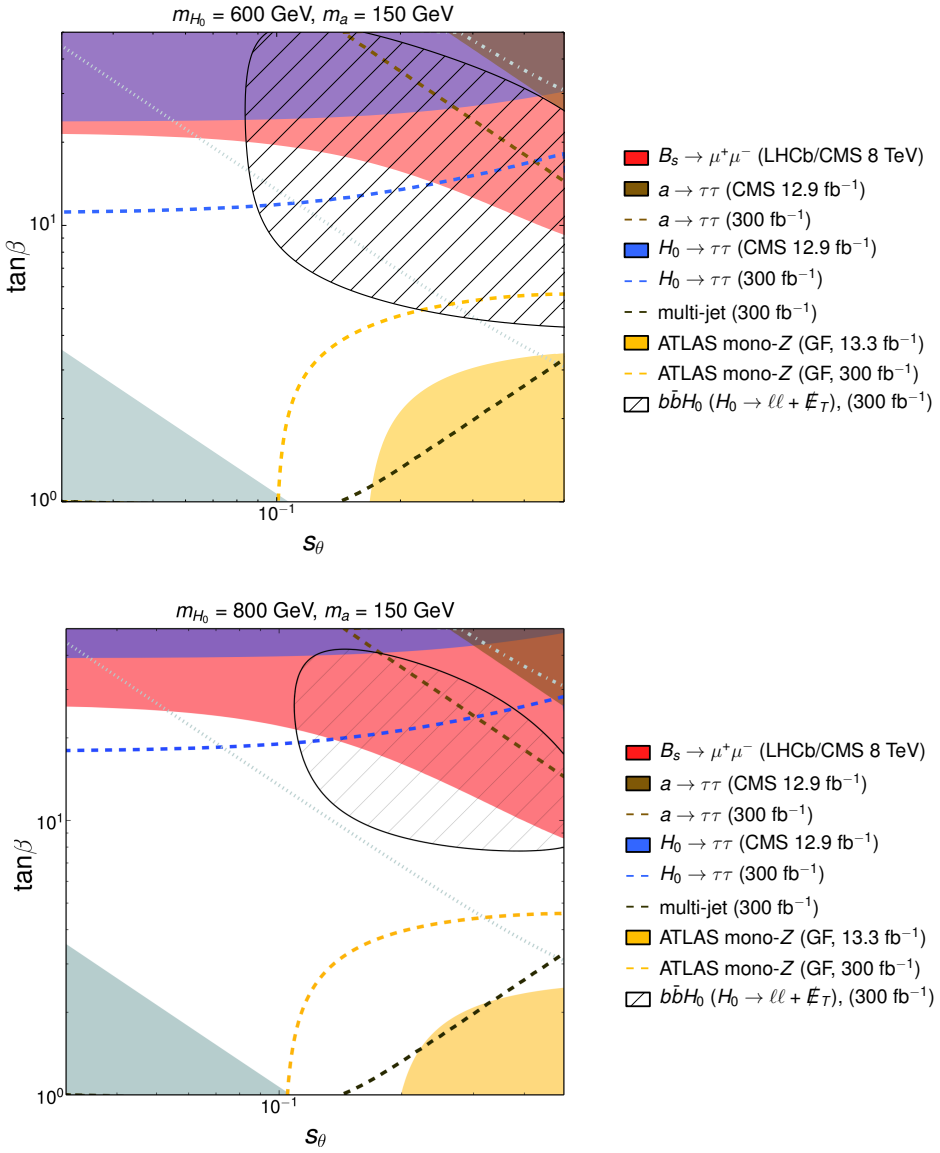

Figure 5.2: *Current and projected (with $\mathcal{L} = 300\ fb^{-1}$) LHC bounds are shown as solid regions and dashed lines respectively. The 95% C.L. exclusion regions are displayed in the (s_θ, $\tan\beta$) plane for (m_{H_0}, m_a) = (600, 150) GeV (top) and (800, 150) GeV (bottom) with a DM mass $m_\chi = 45$ GeV, from $H_0 \to \tau^+\tau^-$ (blue), $a \to \tau^+\tau^-$ (brown), multi-jet $+\not{E}_T$ (black) and ATLAS mono-Z (yellow). The $B_s \to \mu^+\mu^-$ exclusion is shown in red. The dashed region corresponds to the 95% C.L. sensitivity for our proposed search, $pp \to b\bar{b}\,\ell\ell + \not{E}_T$, with $\mathcal{L} = 300\ fb^{-1}$. The coupling y_χ is fixed at each point to match the DM relic density. The perturbativity excluded region $y_\chi > 4\pi$ is depicted in grey. Lines $y_\chi = 1$ (dotted grey), $y_\chi = 0.1$ (dot-dashed grey) are shown for guidance.*

uncertainty added in quadrature to a $1/\sqrt{N}$ Monte Carlo uncertainty (N the number of generated background Monte Carlo events in the signal region).

For a benchmark signal $m_{H_0} = 600$ GeV, $m_a = 150$ GeV, $\tan\beta = 15$, $s_\theta = 0.3$ the background and signal samples surviving event selection are shown in Figure 5.1 in the ($\not{E}_T$, m_{T2}) plane, highlighting the choice of signal region $\not{E}_T$, $m_{T2} >$ 110 GeV as tailored for a clean signal extraction. In Figure 5.2 we show the 95% C.L. sensitivity of our proposed search (hatched region) with 300 fb^{-1} of integrated luminosity in the (s_θ, $\tan\beta$) plane for (m_{H_0}, m_a) = (600, 150) GeV (top) and (800, 150) GeV (bottom), demanding $\langle\sigma v\rangle \simeq 3 \times 10^{-26}\text{cm}^3/\text{s}$ to fix y_χ in terms of $\tan\beta$ and s_θ in each case. We demand perturbativity $y_\chi < 4\pi$, and show the lines $y_\chi = 1$ (dotted grey) and $y_\chi = 0.1$ (dot-dashed grey) for guidance.

The decay $H_0 \to Za$ ($a \to \bar{\chi}\chi$) may be probed also by ATLAS/CMS mono-Z searches in the $\ell^+\ell^- + \not{E}_T$ channel [258,259], both for gluon-fusion (GF) production of H_0 and for $b\bar{b}$-associated production (if both b-jets are missed, since [258, 259] impose jet/b-jet vetoes). We follow the LHC 13 TeV analysis selection of ATLAS [258] with 13.3 fb^{-1} to derive present 95% C.L. constraints on our signal in the (s_θ, $\tan\beta$) plane, shown in Figure 5.2 for GF (yellow region) for $m_{H_0} = 600$ GeV, $m_a = 150$ GeV (top) and $m_{H_0} = 800$ GeV, $m_a = 150$ GeV (bottom). We also show the LHC projections to 300 fb^{-1} (dashed lines) using a naive $\sqrt{\mathcal{L}}$ increase in the signal cross section sensitivity (we note that even in this case, the ATLAS mono-Z search from $b\bar{b}$-associated production is not sensitive enough to provide a constraint). We emphasise again that, in both cases, the coupling y_χ is fixed at each point to match the DM relic density.

In addition, Figure 5.2 shows the present and projected to 300 fb^{-1} constraints on the dark portal discussed in the previous section: the exclusion from CMS/LHCb 8 TeV $B_s \to \mu^+\mu^-$ measurements (red), the multi-jet $+\not{E}_T$ (black), and the $\bar{b}b$-associated production of $H_0 \to \tau\tau$ (blue) and $a \to \tau\tau$ (brown). For the latter two, we use SusHi to obtain the NNLO H_0, a production cross section in association with $\bar{b}b$ at 13 TeV LHC[80]. We note that $\bar{t}t + \not{E}_T$ and $\bar{b}b + \not{E}_T$ are not sensitive enough to provide a constraint in Figure 5.2.

As Figure 5.2 highlights, the ATLAS mono-Z search will be able to probe the $\tan\beta \lesssim 5$ region (for GF production), while $B_s \to \mu^+\mu^-$ and the projected

[80] We note that by performing the analysis of mono-Z and our $\bar{b}bZ(\to \ell\ell) + \not{E}_T$ signature at LO, as compared to H_0, $a \to \tau\tau$ at NNLO, we are being conservative by underestimating the constraining power of the former two signatures.

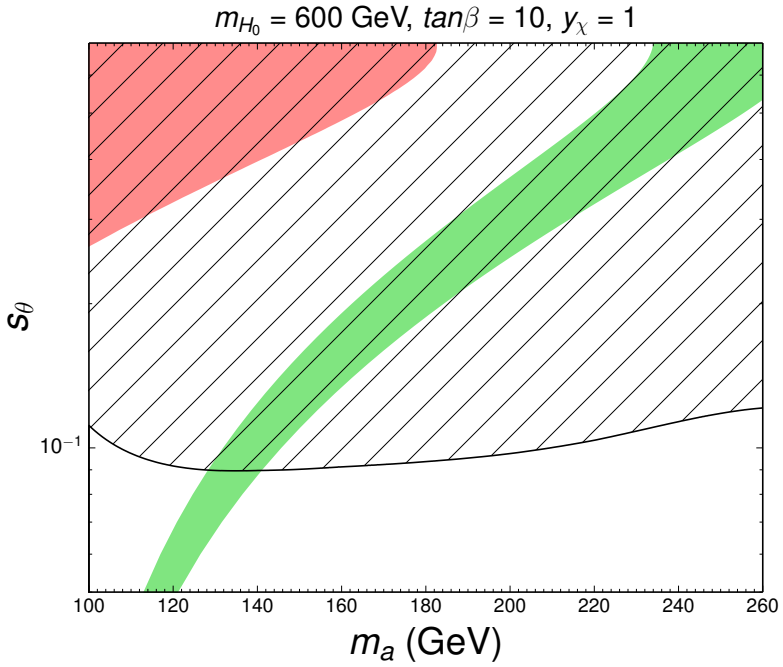

Figure 5.3: *95% C.L. sensitivity of the proposed search $pp \to b\bar{b}\,\ell\ell + \not{E}_T$ with $\mathcal{L} = 300$ fb^{-1} (dashed region) in the $(m_a,\, s_\theta)$ plane for $m_{H_0} = 600$ GeV, $\tan\beta = 10$, $y_\chi = 1$. The red region is excluded by $B_s \to \mu^+\mu^-$, while the green band yields the observed DM relic density. The DM mass is $m_\chi = 45$ GeV. All other discussed constraints are too weak to be visible on this plane.*

$H_0 \to \tau\tau$ combined could strongly constrain the very high $\tan\beta$ region ($\tan\beta > 10$ for $m_{H_0} = 600$ GeV, $\tan\beta > 20$ for $m_{H_0} = 800$ GeV); meanwhile, our proposed search $pp \to \bar{b}b\,\ell^+\ell^- + \not{E}_T$ would yield access to the intermediate $\tan\beta$ region, also probing values of the mixing down to $s_\theta \sim 0.1$.

We note that in the above analysis, we have fixed $\Gamma_{H_0 \to aa} = 0$ (as can be done by an appropriate choice of the soft $\mathbb{Z}_2$ symmetry breaking term in the 2HDM scalar potential, see e.g. [235]). A non-vanishing $\Gamma_{H_0 \to aa}$ would weaken the constraints from mono-Z, our new signature $pp \to \bar{b}b\,\ell^+\ell^- + \not{E}_T$ and from $H_0 \to \tau\tau$, but would at the same time yield new avenues to probe the pseudoscalar portal. However we do not consider this scenario here for simplicity.

Finally, in Figure 5.3 we relax the requirement of fixing y_χ via the relic density and instead show the various constraints and projected sensitivities discussed above in the $(m_a,\, s_\theta)$ plane for a benchmark $m_{H^\pm} = m_{H_0} = 600$ GeV, $\tan\beta = 10$ and $y_\chi = 1$, together with the region (in green) where the observed DM relic density is obtained, $\langle\sigma v\rangle = (2-4) \times 10^{-26}\text{cm}^3/\text{s}$. Our search is displayed by the

dashed region while $B_s \to \mu^+\mu^-$ is shown in red, with other constraints too weak to be visible in this plane. This highlights the sensitivity of the proposed search to parameter space where the correct DM relic density is not necessarily obtained, compared to other experimental probes of the pseudoscalar portal to DM. In the next and final Section, we will offer some additional discussion and Conclusions.

5.5 Summary of the new LHC search

We have discussed a gauge-invariant extension of the pseudoscalar simplified DM model which incorporates a 2HDM.[81] In Section 5.2 we introduced the relevant aspects of the model, summarising the relevant 2HDM phenomenology as well as briefly mentioning how the model can obtain the thermal relic density for DM at the same time as providing an explanation for the GCE. In addition we described how a pure pseudoscalar coupling to quarks can be generated when the pseudoscalar mediator mixes with the other pseudoscalar coming from the 2HDM.

In Section 5.3 we describe existing constraints that apply to this and similar 2HDMs, including bounds coming from flavour physics. In particular, we describe how our model gives a BSM contribution to $B_s \to \mu^+\mu^-$, which ends up giving an important bound on our model at high $\tan\beta$. We also discuss how direct searches for 2HDM scalars can constrain our model, with a CMS search for $H_0 \to \tau^+\tau^-$ again being relevant at high $\tan\beta$. Additionally we mention how $\bar{t}t + \not{E}_T$ and $\bar{b}b + \not{E}_T$ searches do not give relevant bounds, and although multijet searches can give an important constraint, they end up being weaker than the mono-Z bound introduced in Section 5.4.

Our new search, based on the $\bar{b}b + Z + \not{E}_T$ final state, is introduced in Section 5.4. We describe how we perform the event selection in order to overcome the large $\bar{t}t$ background, as well as the di-boson background. We require the presence of a b-tagged jet to eliminate the di-boson background, and use cuts on the variable m_{T2} to overcome the $t\bar{t}$ background. Furthermore, to increase the significance of the signal over the background, we use the fact that the mass of H_0 is much larger than the mass of Z and a so they are significantly boosted, giving rise to leptons with high p_T. Section 5.4 also introduces the aforementioned mono-Z

[81] If the reader is not concerned with issues of gauge-invariance, one can simply motivate the extended theory by the richer phenomenology that it offers compared to the simplified model framework.

bound, which has a similar topology to our search, based on the $Z + \not{E}_T$ state. It is distinct, however, by having the heavy Higgs particle H_0 being produced via gluon fusion (as opposed to $\bar{b}b$ associated production) which means the resulting constraints are relevant at low $\tan\beta$.

We find that a large region of parameter space which gives the observed DM relic abundance (yielding at the same time an explanation for the Galactic Centre Excess) can be explored using the proposed search (see Fig. 5.2), showing in particular that it can reach wide parts of parameter space that cannot be probed by other means, notably $B_s \to \mu^+\mu^-$ decays, heavy Higgs (H_0) decays into tau-lepton pairs, and mono-Z searches. This novel search can thus be very valuable in probing pseudoscalar portal DM scenarios at the LHC in regions of moderate $\tan\beta$, since regions of lower $\tan\beta$ ($\tan\beta \lesssim 5$) would be excluded by mono-Z searches extrapolated to a higher luminosity of 300 fb^{-1}, which is the proposed luminosity of our search. Regions of higher $\tan\beta$ ($\tan\beta \gtrsim 10$) are constrained by ditau resonance searches and $B_s \to \mu^+\mu^-$, so it is the intermediate region $5 \lesssim \tan\beta \lesssim 10$ that is uniquely probed by our search.

Finally we emphasise that the main purpose of this Chapter is to highlight a new channel for the LHC. This search can be performed regardless of whether one is concerned with explaining the GCE. For that purpose, we show in Fig. 5.3 an alternative slice of parameter space, where we relax the requirement of the DM particle being a thermal relic.[82] In this particular plane of $\sin\theta$ against the light pseudoscalar mass m_a, our novel search looks particularly promising, exploring both parameter points where DM is a thermal relic as well as regions where it would be under- or over-abundant. The only other limit visible on this plane is $B_s \to \mu^+\mu^-$, covering a small region at low m_a and high $\sin\theta$.

Summarising, DM that interacts with the visible sector via a pseudoscalar mediator is an appealing scenario, naturally avoiding the limits from DM direct detection searches while generating a rich LHC phenomenology and yielding a possible explanation for the FERMI gamma ray GCE. Generating a pseudoscalar coupling to SM fields in a consistent way implies the existence of additional BSM particles, such as in theories with a 2HDM. The additional particles in such a theory lead to a much richer phenomenology, and here we have highlighted one

[82] Recall that requiring the thermal relic cross section, $\langle\sigma v\rangle = (2-4)\times 10^{-26}\text{cm}^3/\text{s}$, gives you both the observed density of DM in the universe today at the same time as giving a good fit to the GCE.

channel that can reach parts of parameter space no other search can, both in the context of explaining the GCE, and as a way to probe more generic values of the model parameters. As such, this channel is an exciting one to be taken up by the future LHC programme.

Chapter 6

Conclusion

This thesis has examined various simplified models of dark matter, constrained them with data, proposed extensions to these models based on anomaly cancellation, and proposed a new search for the LHC. Simplified models were defined in Chapter 1 as an evolution from EFTs, and alongside other particle theories of DM that were described in Section 1.2. The evidence for DM had already been summarised by this point, in Section 1.1, from the rotation curves of galaxies, through evidence from clusters of galaxies such as the bullet cluster, to CMB measurements.

For the case of simplified models, when compared to EFTs, a much richer phenomenology is presented. Instead of being solely limited to mono-X signatures, direct searches for the mediator particle become a promising avenue. This was the subject of Chapter 2, which examined dijet resonance searches. First, in Section 2.2, a detailed recasting of various dijet searches was performed, with a statistically consistent combination of the different datasets presented in way which could be applied to a broad range of different Z' models. The results were presented in terms of the Z' mass and width, which are the only non-trivial parameters of the model that the dijet signal depends on (the couplings, apart from their impact on the width, induce a trivial overall scaling factor). The main exclusions are shown in Fig 2.2.

Then, in Section 2.3, these dijet constraints were applied to a simplified model of DM with a Z' mediator between the dark and visible sectors. We presented bounds on the model parameters by combining the requirement that the DM particle be responsible for all of the relic density with the results of our dijet

analysis. The result of this procedure is presented in Fig. 2.7 in terms of the bound on the DM coupling to the Z', and is shown in Figs. 2.9 and 2.10 in terms of the DM mass. We also showed constraints for fixed couplings, with no requirement from the relic density, in Fig. 2.3.

Additionally in Section 1.2 the basic problem with EFTs were described, that they are unreliable in high energy environments due to the unknown cut-off scale. This key theoretical issue (related to under or over estimating cross sections) motivated the introduction of additional degrees of freedom – the mediator particles in simplified models. This thesis has taken an additional step in this direction, where in Chapter 3 additional degrees of freedom are introduced to the theory in order to solve the theoretical problem relating to the presence of gauge anomalies. The constraints that apply to each of the three types of anomaly free models we introduced were then investigated in Chapter 4.

More precisely, we found that the Y-sequential model is the only model that needs no extra exotic fermions to be anomaly free. This solution was guaranteed to exist as a direct consequence of the fact that the SM is anomaly-free. This model necessarily has couplings to leptons, as well as generating a strong direct detection bound from the vectorial coupling of the Z' to both quarks and the DM particle. We then showed how the combination of direct detection, dilepton and electroweak precision measurements causes this model to be essentially excluded apart from a narrow region at high mediator mass where resonant annihilation takes place.

An axial variant of this model can be produced by adding an exotic singlet fermion (in addition to the DM particle). The resulting model still has charges to all SM fermions proportional to their hypercharge and so couplings to leptons are still present. The model has a direct detection bound that is weaker compared to the vector-like case, but if the thermal relic density of DM is required then larger gauge couplings are required in order to overcome the velocity suppression in the DM annihilation cross section. These larger couplings make the constraints coming from other observables (in particular electroweak precision) correspondingly stronger, leading us to conclude that this model is also essentially ruled out in the GeV to TeV parameter range that we considered.

We also extended the model to include additional fermions whose existence is necessary in order to perform anomaly-cancellation when the SM leptons have vanishing exotic charge. This required the existence of exotic particles trans-

forming non-trivially under the SM SU(2) group. When considering all anomaly conditions, we found that one exotic SU(2) multiplet, an exotic singlet with Y hypercharge, and an exotic singlet with no SM charges was the minimum amount of additional field content necessary to create an anomaly-free theory. The final particle is needed for cancelling the gauge anomalies, but noticing that it is an SM singlet then triggers the question of whether it could be a viable DM candidate. We picked two benchmark models from the solutions we found, one where the exotic SU(2) multiplet is a doublet, and the other where it is a triplet.

Investigating the constraints on these leptophobic models found that they are well constrained in particular by the relic density and direct detection bounds, a direct result of a non-vanishing vectorial coupling of the Z' boson to both quarks and DM. However, in comparison to the Y-sequential models, constraints coming from electroweak precision observables are significantly weakened, due to the absence of mass mixing between the Z and Z' bosons.[83]. LHC constraints were also weaker, with the strongest constraints coming from dijet searches for the two benchmark models we considered, with the monojet channel being significantly weaker.

An alternative scenario is investigated in Chapter 5, namely one with a spin-zero mediator between DM and the SM. Motivated by the strong constraints from direct detection placed on CP-even scalars, a pseudoscalar mediator was considered. A fully gauge-invariant realisation of this model necessitates the introduction of additional particles, such as those in a 2HDM model. In this model, the portal to the dark sector is opened when the pseudoscalar from the 2HDM mixes with the conventional pseudoscalar mediator from the simplified model. The purpose of our work was to propose a new search, based on the channel $\bar{b}b + Z + \not{E}_T$, that can be performed at the LHC. We present existing bounds on the model, notably from $B_s \to \mu^+\mu^-$, $H_0 \to \tau^+\tau^-$ and mono-Z ($Z + \not{E}_T$), and show that some regions of parameter space that are untouched by the existing constraints can be reached by our search. Finally, the benchmark model parameters that we select can be used to fit the GCE, but we emphasise here that this is not compulsory and the LHC search is more generic than solely probing a specific interpretation of the GCE.

[83]Kinetic mixing of the Z and Z' boson was present, but we calculated it assuming that it was only generated at loop-level, with the corresponding constraints being weaker than if it was present at tree-level.

Each of the three topics that have been investigated, namely dijet searches, anomaly-free models and the new LHC search can be extended in the future. Firstly, the dijet analysis in Chapter 2 is based on data that is now somewhat out of date, with no more than around 3 fb^{-1} of integrated luminosity at a centre of mass energy of 13 TeV, so naturally this work could be extended by simply including newer data such as [112, 113, 214, 215]. Additionally, with the complicated nature of including so many different searches, incorporating them into a coherent framework could be useful. Therefore including these dijet searches as part of a global fitting framework such as GAMBIT [260–262] could be useful for the community.

The study of anomaly-free models can be extended in many ways. We also studied anomaly-cancellation conditions on Z' models with non-universal charges motivated by recent anomalies in B meson decays [209], although this work was not included in this thesis due to having a smaller connection to DM. Restricting our discussion to the work in this thesis, in Chapter 3 we assumed that the Yukawa sector was that of the SM, that there is only one Higgs doublet. Taking instead a model with two or three Higgs doublets would remove one or both of the conditions[84] in Eq. (3.13) which would affect the anomaly-free solutions that could be found for the leptophobic models in Section 3.4. However, there would be an additional challenge in searching the space of anomaly-free solutions due to the fewer independent conditions that could be imposed on the exotic charges.

We also investigated the conventional constraints that applied to two of the benchmark leptophobic models in Chapter 4. However, although we managed to avoid the strong constraints from dilepton resonance searches, the presence of a non-zero vectorial coupling between the Z' and both the DM and quarks gave the strongest possible spin-independent direct detection signal, unsuppressed by the DM velocity. This means that not much of the parameter space remains unconstrained in these models, leaving little room for more exotic signatures to be explored. Therefore it would be of interest to search for an anomaly-free leptophobic model with a purely axial coupling to DM, and study the additional experimental signatures that might arise, e.g. via co-annihilation [89–91], or through novel LHC searches for exotic particles. In fact, this work has already been started by

[84] Recall that in Sections 3.2 and 3.3 the conditions in Eq. (3.13) were enforced by the anomaly cancellation requirements themselves, independent of any initial assumptions about the Yukawa sector.

studies that have appeared recently [263, 264].

Finally, the model we studied in Chapter 5 was a fully gauge-invariant realisation of the pseudoscalar portal, but at the cost of introducing a large number of extra parameters of the theory. Assuming one scalar particle to be the SM Higgs, there are still four exotic scalar masses in the theory as well as the DM mass. There are also at least three mixing angles, as well as a DM coupling. With such a large number of different parameters in the theory, we had to fix some of them, creating effective benchmark planes that are a two-dimensional slice of the entire parameter space. Exploring more fully the higher dimensional parameter space would necessitate some sort of global scanning framework, such as GAMBIT [260–262].

In searching for DM using the highest-energy probe that we have on our planet, basic issues such as gauge-invariance should not be ignored. The argument for the use of simpler theories proposes that they are all that is needed to describe the relevant physics in a particular channel. Yet they fail when thinking about the global picture, where additional constraints may have been ignored completely due to not including enough particles into the theory in the first place. Therefore the extension of theories such as simplified models is well motivated even if one does not care about theoretical consistency requirements such as gauge invariance, since there is always a much richer phenomenology in the extended theory. Therefore we look forward to the continued running of the LHC, recasts of the staggering amount of data currently being released by the LHC collaborations, as well as new phenomenology being opened up, including signatures inspired by fully gauge-invariant theories.

Appendix A

Dijet Bounds and Relic Density Implementation

A.1 Tabulated bounds on dijet quark coupling

We provide the numerical values of the dijet constraints obtained in section 2.2 in table A.1.

A.2 Specific modifications of micrOMEGAs

In this appendix we detail two modifications to `CalcHEP` [101], which is used by `micrOMEGAs` to calculate the cross sections for DM pair annihilation. Both modifications are necessary in order to correctly treat the width of the Z' close to the resonance (i.e. for $m_{\mathrm{DM}} \approx m_{Z'}/2$).

The first modification is necessary to avoid numerical instabilities leading to kinks in the curves of constant relic density as a function of g_{DM} and g_q for fixed m_{DM} and $m_{Z'}$ (see figure 2.4). These kinks arise due to the way the Breit-Wigner (BW) propagator is implemented in CalcHEP. The standard BW distribution for a particle with mass m and momentum q is given by

$$|\mathcal{M}|^2 \propto \frac{1}{(q^2 - m^2)^2 + m^2\Gamma^2} \,, \tag{A.1}$$

where the term involving Γ removes the divergence as the particle becomes on-shell ($q^2 \to m^2$). However, since the width is a sum of diagrams of varying orders,

its presence in eq. (A.1) can spoil gauge invariance. For this reason CalcHEP implements the BW formula as a piecewise function over three regions: Formula A.1 is used with a non-zero width for $|q^2 - m^2| < R\, m\, \Gamma$, where R is an arbitrary number that is by default fixed to 2.7. For $|q^2 - m^2| > \sqrt{R^2+1}\, m\, \Gamma$, on the other hand, the width in eq. (A.1) is set to zero. In the intermediate region the width Γ is replaced by a function of q^2 that interpolates between the two cases. For fairly large widths, as considered in the present work, this interpolation procedure can lead to kinks in the relic density calculation. To remove such kinks one can simply increase the value of R from its default value by changing the value of the variable `BWrange` [178]. We have found that $R = 100$ is sufficient to remove the kinks in our plots.[85]

Furthermore, as pointed out in ref. [152], the width Γ of the resonance depends in general on the momentum transfer q^2, i.e. $\Gamma = \Gamma(q^2)$. For the case of narrow widths ($\Gamma/m \ll 1$), eq. (A.1) gives a good approximation, because Γ is only relevant for $q^2 \approx m^2$ and one can therefore approximate $\Gamma \approx \Gamma(q^2 = m^2)$. Since we consider widths as large as 30% in this work, it is however appropriate to modify the BW formula in order to take the momentum dependence of the width into account.

Following appendix A of [152], we can approximately capture the momentum dependence by setting $\Gamma(q^2) = \frac{\sqrt{q^2}}{m}\Gamma(q^2 = m^2)$. This substitution yields

$$|\mathcal{M}|^2 \propto \frac{1}{(q^2 - m^2)^2 + \frac{(q^2)^2}{m^2}\Gamma(q^2 = m^2)^2} \tag{A.2}$$

for the shape of the BW resonance. This modification can be implemented by editing the function `prepDen` used in the `CalcHEP` code.

[85] Another effect that could lead to kinks in the relic density curves was due to a typographical mistake in `micrOMEGAs_4.1.8`, which has been fixed in the most recent version.

Table A.1: *Numerical values of the fit to the constraint on the quark coupling as a function of width outlined in eq. (2.7).*

$M_{Z'}$[GeV]	$10 \times a(M_{Z'})$	$b(M_{Z'})$	$1000 \times c(M_{Z'})$
500	2.4295	2.208	0.0588
550	1.3808	1.760	0.0712
600	0.7648	1.452	0.0000
650	0.5251	1.496	0.0584
700	0.4153	1.389	0.0000
750	0.4266	1.375	0.0000
800	0.4865	1.386	0.0000
850	1.2889	2.047	0.2376
900	0.3078	1.259	0.0000
950	0.7027	1.729	0.0540
1000	0.5892	1.341	0.0743
1100	0.4600	1.183	0.0000
1200	0.3674	1.334	0.0000
1300	1.4714	1.879	0.0809
1400	1.8096	1.723	0.1545
1500	4.4052	1.920	0.1901
1600	13.7015	1.989	0.5733
1700	5.4250	1.468	0.0000
1800	5.1603	1.729	0.2606
1900	4.8469	1.751	0.3736
2000	4.7523	1.629	0.3762
2100	3.3313	1.425	0.0000
2200	3.9147	1.458	0.1891
2300	4.9732	1.550	0.3758
2400	4.9159	1.588	0.4994
2500	3.3318	1.450	0.3996
2600	3.5345	1.509	0.3922
2700	3.9016	1.565	0.4383
2800	3.2388	1.440	0.4402
2900	2.6469	1.318	0.6291
3000	3.0428	1.315	0.7375
3100	3.5767	1.326	1.1560
3200	2.6266	1.129	0.6442
3300	4.0536	1.286	0.6851
3400	6.1825	1.421	1.3730
3500	3.7765	1.162	0.5939
3600	5.0627	1.262	1.3046
3700	6.5994	1.307	2.1257
3800	6.8087	1.191	3.0885
3900	5.6611	0.936	0.0000
4000	9.5274	1.061	0.0000

Appendix B

Z-Z' Mixing

We follow the approach in [169, 212, 213], assuming a Lagrangian with both mass and kinetic mixing:

$$\mathcal{L} = \mathcal{L}_{\rm SM} - \frac{1}{4}\hat{F}'^{\mu\nu}\hat{F}'_{\mu\nu} + \frac{1}{2}m^2_{\hat{Z}'}\hat{X}_\mu\hat{X}^\mu - \frac{1}{2}\sin\epsilon\,\hat{B}_{\mu\nu}\hat{F}'^{\mu\nu} + \delta m^2\hat{Z}_\mu\hat{X}^\mu \tag{B.1}$$

where $\hat{Z} \equiv \cos\hat{\theta}_W\hat{W}^3 - \sin\hat{\theta}_W\hat{B}$ and $\hat{F}'^{\mu\nu} \equiv \partial^\mu\hat{X}^\nu - \partial^\nu\hat{X}^\mu$.

The Lagrangian can be transformed to the mass basis, with canonical kinetic terms, via the following transformations:

$$\begin{pmatrix} \hat{B}_\mu \\ \hat{W}^3_\mu \\ \hat{X}_\mu \end{pmatrix} = \begin{pmatrix} 1 & 0 & -\tan\epsilon \\ 0 & 1 & 0 \\ 0 & 0 & 1/\cos\epsilon \end{pmatrix} \begin{pmatrix} B_\mu \\ W^3_\mu \\ X_\mu \end{pmatrix} \tag{B.2}$$

$$\begin{pmatrix} B_\mu \\ W^3_\mu \\ X_\mu \end{pmatrix} = \begin{pmatrix} \cos\hat{\theta}_W & -\sin\hat{\theta}_W\cos\xi & \sin\hat{\theta}_W\sin\xi \\ \sin\hat{\theta}_W & \cos\hat{\theta}_W\cos\xi & -\cos\hat{\theta}_W\sin\xi \\ 0 & \sin\xi & \cos\xi \end{pmatrix} \begin{pmatrix} A_\mu \\ Z_\mu \\ Z'_\mu \end{pmatrix} \tag{B.3}$$

where we identify A, Z and Z' as the physical fields, with ξ determined by

$$\tan(2\xi) = \frac{-2\cos\epsilon(\delta m^2 + m^2_{\hat{Z}}\sin\hat{\theta}_W\sin\epsilon)}{m^2_{\hat{Z}'} - m^2_{\hat{Z}}\cos\epsilon^2 + m^2_{\hat{Z}}\sin\hat{\theta}^2_W\sin\epsilon^2 + 2\,\delta m^2\,\sin\hat{\theta}_W\sin\epsilon} \tag{B.4}$$

The impact on electroweak precision observables can then be calculated using the

S and T parameters [86]:

$$\alpha\, S = 4\, \cos\theta_W^2\, \sin\theta_W\, \xi\, (\epsilon - \sin\theta_W\, \xi) \tag{B.5}$$

$$\alpha\, T = \xi^2 \left(\frac{m_{Z'}^2}{m_Z^2} - 2 \right) + 2\, \sin\theta_W\, \xi\, \epsilon \tag{B.6}$$

where $\cos\theta_W$ is the cosine of the electroweak mixing angle and $\alpha = e^2/4\pi$ is the electroweak coupling. We use for the numerical values of the S and T parameters the recent fit [210]. However, for smaller Z' masses it is more suitable to use the ρ parameter

$$\rho - 1 = \frac{\cos^2\theta_W\, \xi^2}{\cos^2\theta_W - \sin^2\theta_W} \left(\frac{m_{Z'}^2}{m_Z^2} - 1 \right) \tag{B.7}$$

and we use the ρ parameter instead of the S and T parameters when $M_{Z'} < \sqrt{2} M_Z$. The reader who is paying attention may notice glitches in some diagrams at those places in parameter space where we switch from using the S, T variables to ρ. For the value of ρ we use the most recent fit from the PDG [220].

For the Y-sequential models in Sections 4.2 and 4.3 we neglect kinetic mixing, since the effect of mass mixing is much stronger. We then find

$$\delta m^2 = \frac{1}{2} \frac{e g\, Y'_H}{\sin\theta_W \cos\theta_W} v^2 \tag{B.8}$$

where g is the $U(1)'$ gauge coupling, Y'_H is the Higgs charge under $U(1)'$, and v is the SM Higgs vev.

For the leptophobic models in Section 4.4, $Y'_H = 0$ so there is no mass mixing effect, and we also assume that kinetic mixing vanishes at tree-level. However, it is unavoidably generated at loop level since we have quarks that carry U(1)′ charge. Conservatively, we assume that $\epsilon = 0$ at $\Lambda = 100$ TeV, such that at a lower scale [217]:

$$\epsilon(\mu) = \frac{e\, g\, Y'_q}{2\pi^2\, \cos\theta_{\rm W}} \log\frac{\Lambda}{\mu} \tag{B.9}$$

In calculating our constraints we set $\mu = M_{Z'}$.

[86] To lowest order in ξ and ϵ, $\cos\hat{\theta}_W = \cos\theta_W$ and $\sin\hat{\theta}_W = \sin\theta_W$.

Appendix C

Monojet Recast

In implementing the LHC monojet constraints, we adopt the rescaling procedure proposed in [145], generating monojet samples across a grid of Z' and dark matter particle masses, and then rescaling to other points of parameter space using the narrow width approximation.

For the constraints, we use the inclusive selection of the latest ATLAS monojet search with 36.1 fb^{-1} of integrated luminosity [107]. We calculate the exclusion using each of the missing energy selections defined by ATLAS, IM1 - IM10, corresponding to various $E_{T,\text{miss}}$ cuts: $E_{T,\text{miss}} > 250$ GeV for IM1 up to $E_{T,\text{miss}} > 1000$ GeV for IM10. We calculate μ as

$$\mu = \frac{\sigma(g = 1, \Gamma = 0.01 M_{Z'})}{\sigma_{95\%}} \tag{C.1}$$

for each separate $E_{T,\text{miss}}$ cut defined in each search region, where $\sigma_{95\%}$ is the cross section excluded by ATLAS at 95% CL. We show which search region is most constraining in the left panel of Fig. C.1, and the corresponding μ factor (for leptophobic model 1) is shown in the right panel of Fig. C.1.

We then rescale this μ to different points of parameter space by a factor (for fixed charges) g^4/Γ for the on-shell region, and g^4 for the off-shell region, where Γ is the width of the Z' boson.

We note that the limit we obtain is approximate, since we do not simulate parton shower or detector effects, and we include the generation of only one hard jet at parton level in `Madgraph` [99]. However we have validated our approach by reproducing the published results from ATLAS for the axial-vector simplified

model, as seen in Fig. C.2.

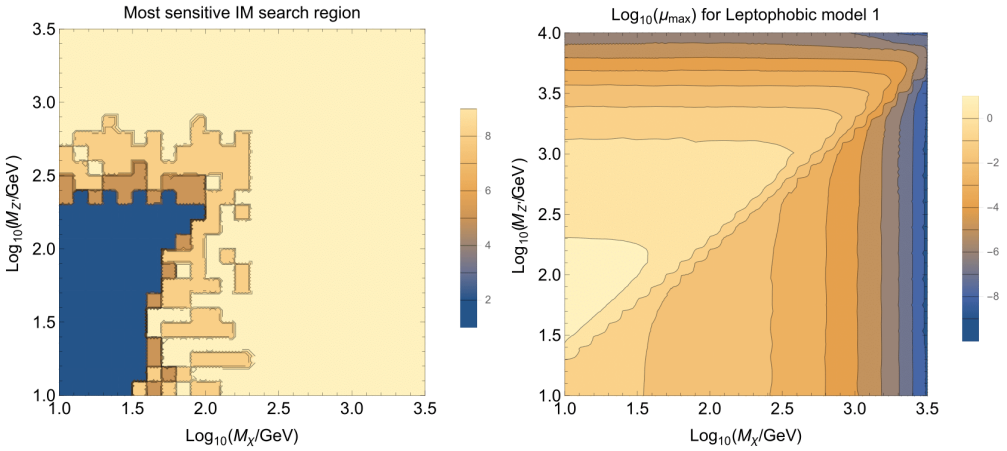

Figure C.1: *Left: the most sensitive search region, numbered 1-10 as the inclusive search regions IM1-10 defined by ATLAS [107]. The most sensitive search region is the one that gives the largest μ factor. At low masses, IM1 is the most sensitive, whereas at high masses, IM9 is the most sensitive. Right: Contours of* $\mathrm{Log}_{10}\mu$ *(see text for definitions) in the most sensitive search region.*

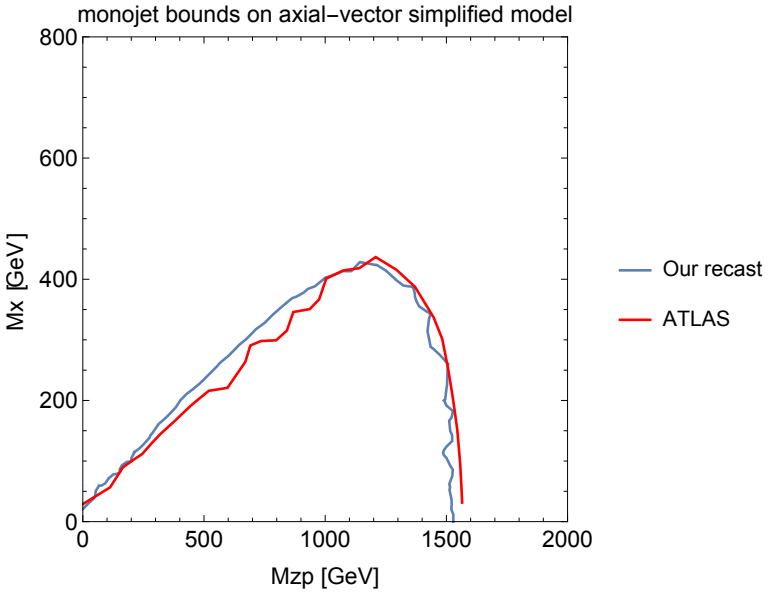

Figure C.2: *Parameter points excluded by our recast of the inclusive search (blue) compared to the published results from the exclusive monojet search [107] (red), for the axial-vector simplified model, with fixed couplings of* $g_q = 0.25$ *and* $g_{DM} = 1.0$.

Bibliography

[1] M. Fairbairn, J. Heal, F. Kahlhoefer and P. Tunney, *"Constraints on Z' models from LHC dijet searches and implications for dark matter,"* JHEP **1609** (2016) 018 doi:10.1007/JHEP09(2016)018 [arXiv:1605.07940 [hep-ph]]. 10, 45, 54

[2] J. Ellis, M. Fairbairn and P. Tunney, *"Anomaly-Free Dark Matter Models are not so Simple,"* JHEP **1708** (2017) 053 doi:10.1007/JHEP08(2017)053 [arXiv:1704.03850 [hep-ph]]. 10, 74, 95, 96, 103, 104, 107, 115, 116

[3] J. Ellis, M. Fairbairn and P. Tunney, *"Phenomenological Constraints on Anomaly-Free Dark Matter Models,"* arXiv:1807.02503 [hep-ph]. 10, 94

[4] P. Tunney, J. M. No and M. Fairbairn, *"Probing the pseudoscalar portal to dark matter via $\bar{b}bZ(\to \ell\ell) + \not{E}_T$: From the LHC to the Galactic Center excess,"* Phys. Rev. D **96** (2017) no.9, 095020 doi:10.1103/PhysRevD.96.095020 [arXiv:1705.09670 [hep-ph]]. 10, 119

[5] E. Hubble and M. L. Humason, *"The Velocity-Distance Relation among Extra-Galactic Nebulae,"* Astrophys. J. **74** (1931) 43. doi:10.1086/143323 10

[6] F. Zwicky, *"Die Rotverschiebung von extragalaktischen Nebeln,"* Helv. Phys. Acta **6** (1933) 110 [Gen. Rel. Grav. **41** (2009) 207]. doi:10.1007/s10714-008-0707-4 10

[7] F. Zwicky, *"On the Masses of Nebulae and of Clusters of Nebulae,"* Astrophys. J. **86** (1937) 217. doi:10.1086/143864 10

[8] V. C. Rubin and W. K. Ford, Jr., *"Rotation of the Andromeda Nebula from a Spectroscopic Survey of Emission Regions,"* Astrophys. J. **159** (1970) 379. doi:10.1086/150317 11

[9] M. S. Roberts and A. H. Rots, *"Comparison of Rotation Curves of Different Galaxy Types,"* Astron. & Astrophys. **26** (1973) 483. 11, 12

[10] K. Chang and S. Refsdal, *"Flux variations of QSO 0957+561 A, B and image splitting by stars near the light path,"* Nature **282** (1979) 561. doi:10.1038/282561a0 12

[11] B. Paczynski, *"Gravitational microlensing by the galactic halo,"* Astrophys. J. **304** (1986) 1. doi:10.1086/164140 12

[12] C. Alcock et al. [MACHO Collaboration], *"The MACHO project: Microlensing results from 5.7 years of LMC observations,"* Astrophys. J. **542** (2000) 281 doi:10.1086/309512 [astro-ph/0001272]. 12

[13] T. Lasserre [EROS Collaboration], *"Not enough stellar mass machos in the galactic halo,"* Astron. Astrophys. **355** (2000) L39 [astro-ph/0002253]. 12

[14] P. Tisserand et al. [EROS-2 Collaboration], *"Limits on the Macho Content of the Galactic Halo from the EROS-2 Survey of the Magellanic Clouds,"* Astron. Astrophys. **469** (2007) 387 doi:10.1051/0004-6361:20066017 [astro-ph/0607207]. 13

[15] G. Gamow, *"Expanding universe and the origin of elements,"* Phys. Rev. **70** (1946) 572. doi:10.1103/PhysRev7.0.572 13

[16] R. A. Alpher, H. Bethe and G. Gamow, *"The origin of chemical elements,"* Phys. Rev. **73** (1948) 803. doi:10.1103/PhysRev.73.803 13

[17] R. A. Alpher, J. W. Follin and R. C. Herman, *"Physical Conditions in the Initial Stages of the Expanding Universe,"* Phys. Rev. **92** (1953) 1347. doi:10.1103/PhysRev.92.1347 13

[18] S. Burles, K. M. Nollett and M. S. Turner, *"Big bang nucleosynthesis predictions for precision cosmology,"* Astrophys. J. **552** (2001) L1 doi:10.1086/320251 [astro-ph/0010171]. 13

[19] D. Clowe, M. Bradac, A. H. Gonzalez, M. Markevitch, S. W. Randall, C. Jones and D. Zaritsky, *"A direct empirical proof of the existence of dark matter,"* Astrophys. J. **648** (2006) L109 doi:10.1086/508162 [astro-ph/0608407]. 13, 14

[20] G. Hinshaw et al. [WMAP Collaboration], *"Nine-Year Wilkinson Microwave Anisotropy Probe (WMAP) Observations: Cosmological Parameter Results,"* Astrophys. J. Suppl. **208** (2013) 19 doi:10.1088/0067-0049/208/2/19 [arXiv:1212.5226 [astro-ph.CO]]. 13

[21] N. Aghanim et al. [Planck Collaboration], *"Planck 2018 results. VI. Cosmological parameters,"* arXiv:1807.06209 [astro-ph.CO]. 13, 14, 15

[22] V. Springel et al., *"Simulating the joint evolution of quasars, galaxies and their large-scale distribution,"* Nature **435** (2005) 629 doi:10.1038/nature03597 [astro-ph/0504097]. 15, 16

[23] M. Colless et al. [2DFGRS Collaboration], *"The 2dF Galaxy Redshift Survey: Spectra and redshifts,"* Mon. Not. Roy. Astron. Soc. **328** (2001) 1039 doi:10.1046/j.1365-8711.2001.04902.x [astro-ph/0106498]. 15, 16

[24] M. Davis, G. Efstathiou, C. S. Frenk and S. D. M. White, *"The Evolution of Large Scale Structure in a Universe Dominated by Cold Dark Matter,"* Astrophys. J. **292** (1985) 371. doi:10.1086/163168 16

[25] M. Davis, J. Huchra, D. W. Latham, J. Tonry *"A survey of galaxy redshifts. II - The large scale space distribution,"* Astrophys. J. **253** (1982) 423. doi:10.1086/159646 16

[26] G. Bertone and D. Hooper, *"A History of Dark Matter,"* [arXiv:1605.04909 [astro-ph.CO]]. 10, 11

[27] G. Bertone, D. Hooper and J. Silk, *"Particle dark matter: Evidence, candidates and constraints,"* Phys. Rept. **405** (2005) 279 doi:10.1016/j.physrep.2004.08.031 [hep-ph/0404175]. 17, 28, 44

[28] V. N. Aseev et al. [Troitsk Collaboration], *"An upper limit on electron antineutrino mass from Troitsk experiment,"* Phys. Rev. D **84** (2011) 112003 doi:10.1103/PhysRevD.84.112003 [arXiv:1108.5034 [hep-ex]]. 16

[29] R. D. Peccei and H. R. Quinn, *"CP Conservation in the Presence of Instantons,"* Phys. Rev. Lett. **38** (1977) 1440. doi:10.1103/PhysRevLett.38.1440 25

[30] R. D. Peccei and H. R. Quinn, *"Constraints Imposed by CP Conservation in the Presence of Instantons,"* Phys. Rev. D **16** (1977) 1791. doi:10.1103/PhysRevD.16.1791 25

[31] F. Wilczek, *"Problem of Strong p and t Invariance in the Presence of Instantons,"* Phys. Rev. Lett. **40** (1978) 279. doi:10.1103/PhysRevLett.40.279 25

[32] S. Weinberg, *"A New Light Boson?,"* Phys. Rev. Lett. **40** (1978) 223. doi:10.1103/PhysRevLett.40.223 25

[33] K. Griest and M. Kamionkowski, *"Unitarity Limits on the Mass and Radius of Dark Matter Particles,"* Phys. Rev. Lett. **64** (1990) 615. doi:10.1103/PhysRevLett.64.615 17

[34] V. K. Narayanan, D. N. Spergel, R. Dave and C. P. Ma, Astrophys. J. **543** (2000) L103 doi:10.1086/317269 [astro-ph/0005095]. 17

[35] V. Iri *et al.*, Phys. Rev. D **96** (2017) no.2, 023522 doi:10.1103/PhysRevD.96.023522 [arXiv:1702.01764 [astro-ph.CO]]. 17

[36] J. L. Gervais and B. Sakita, *"Field Theory Interpretation of Supergauges in Dual Models,"* Nucl. Phys. B **34** (1971) 632. doi:10.1016/0550-3213(71)90351-8 18

[37] Y. A. Golfand and E. P. Likhtman, *"Extension of the Algebra of Poincare Group Generators and Violation of p Invariance,"* JETP Lett. **13** (1971) 323 [Pisma Zh. Eksp. Teor. Fiz. **13** (1971) 452]. 18

[38] D. V. Volkov and V. P. Akulov, *"Possible universal neutrino interaction,"* JETP Lett. **16** (1972) 438 [Pisma Zh. Eksp. Teor. Fiz. **16** (1972) 621]. 18

[39] J. Wess and B. Zumino, *"Supergauge Transformations in Four-Dimensions,"* Nucl. Phys. B **70** (1974) 39. doi:10.1016/0550-3213(74)90355-1 18

[40] J. R. Ellis, J. S. Hagelin, D. V. Nanopoulos, K. A. Olive and M. Srednicki, *"Supersymmetric Relics from the Big Bang,"* Nucl. Phys. B **238** (1984) 453. doi:10.1016/0550-3213(84)90461-9 18

[41] H. Goldberg, *"Constraint on the Photino Mass from Cosmology,"* Phys. Rev. Lett. **50** (1983) 1419 Erratum: [Phys. Rev. Lett. **103** (2009) 099905]. doi:10.1103/PhysRevLett.103.099905, 10.1103/PhysRevLett.50.1419 18

[42] S. Dimopoulos and H. Georgi, *"Softly Broken Supersymmetry and SU(5),"* Nucl. Phys. B **193** (1981) 150. doi:10.1016/0550-3213(81)90522-8 18

[43] J. Fan, M. Reece and L. T. Wang, *"Non-relativistic effective theory of dark matter direct detection,"* JCAP **1011** (2010) 042 doi:10.1088/1475-7516/2010/11/042 [arXiv:1008.1591 [hep-ph]]. 19, 20, 41

[44] A. L. Fitzpatrick, W. Haxton, E. Katz, N. Lubbers and Y. Xu, *"The Effective Field Theory of Dark Matter Direct Detection,"* JCAP **1302** (2013) 004 doi:10.1088/1475-7516/2013/02/004 [arXiv:1203.3542 [hep-ph]]. 19, 20, 41

[45] M. Cirelli, E. Del Nobile and P. Panci, *"Tools for model-independent bounds in direct dark matter searches,"* JCAP **1310** (2013) 019 doi:10.1088/1475-7516/2013/10/019 [arXiv:1307.5955 [hep-ph]]. 20, 41, 42, 43, 100

[46] M. Beltran, D. Hooper, E. W. Kolb and Z. C. Krusberg, *"Deducing the nature of dark matter from direct and indirect detection experiments in the absence of collider signatures of new physics,"* Phys. Rev. D **80** (2009) 043509 doi:10.1103/PhysRevD.80.043509 [arXiv:0808.3384 [hep-ph]]. 20

[47] M. Beltran, D. Hooper, E. W. Kolb, Z. A. C. Krusberg and T. M. P. Tait, *"Maverick dark matter at colliders,"* JHEP **1009** (2010) 037 doi:10.1007/JHEP09(2010)037 [arXiv:1002.4137 [hep-ph]]. 20

[48] Y. Bai, P. J. Fox and R. Harnik, *"The Tevatron at the Frontier of Dark Matter Direct Detection,"* JHEP **1012** (2010) 048 doi:10.1007/JHEP12(2010)048 [arXiv:1005.3797 [hep-ph]]. 20

[49] A. L. Fitzpatrick, W. Haxton, E. Katz, N. Lubbers and Y. Xu, *"Model Independent Direct Detection Analyses,"* arXiv:1211.2818 [hep-ph]. 20

[50] A. Belyaev, L. Panizzi, A. Pukhov and M. Thomas, *"Dark Matter characterization at the LHC in the Effective Field Theory approach,"* JHEP **1704** (2017) 110 doi:10.1007/JHEP04(2017)110 [arXiv:1610.07545 [hep-ph]]. 20

[51] A. Belyaev, E. Bertuzzo, C. Caniu Barros, O. Eboli, G. Grilli Di Cortona, F. Iocco and A. Pukhov, *"Interplay of the LHC and non-LHC Dark Matter searches in the Effective Field Theory approach,"* arXiv:1807.03817 [hep-ph]. 20

[52] G. Busoni, A. De Simone, E. Morgante and A. Riotto, *"On the Validity of the Effective Field Theory for Dark Matter Searches at the LHC,"* Phys. Lett. B **728** (2014) 412 doi:10.1016/j.physletb.2013.11.069 [arXiv:1307.2253 [hep-ph]]. 20, 22

[53] O. Buchmueller, M. J. Dolan and C. McCabe, *"Beyond Effective Field Theory for Dark Matter Searches at the LHC,"* JHEP **1401** (2014) 025 doi:10.1007/JHEP01(2014)025 [arXiv:1308.6799 [hep-ph]]. 20, 21, 22, 45

[54] G. Busoni, A. De Simone, J. Gramling, E. Morgante and A. Riotto, *"On the Validity of the Effective Field Theory for Dark Matter Searches at the LHC, Part II: Complete Analysis for the s-channel,"* JCAP **1406** (2014) 060 doi:10.1088/1475-7516/2014/06/060 [arXiv:1402.1275 [hep-ph]]. 20, 22

[55] S. Chatrchyan et al. [CMS Collaboration], *"Search for dark matter and large extra dimensions in monojet events in pp collisions at* $\sqrt{s} = 7$ *TeV,"* JHEP **1209** (2012) 094 doi:10.1007/JHEP09(2012)094 [arXiv:1206.5663 [hep-ex]]. 21

[56] [CMS Collaboration], *"Search for new physics in monojet events in pp collisions at sqrt(s)= 8 TeV,"* CMS-PAS-EXO-12-048. 21

[57] I. M. Shoemaker and L. Vecchi, *"Unitarity and Monojet Bounds on Models for DAMA, CoGeNT, and CRESST-II,"* Phys. Rev. D **86** (2012) 015023 doi:10.1103/PhysRevD.86.015023 [arXiv:1112.5457 [hep-ph]]. 22

[58] P. J. Fox, R. Harnik, R. Primulando and C. T. Yu, *"Taking a Razor to Dark Matter Parameter Space at the LHC,"* Phys. Rev. D **86** (2012) 015010 doi:10.1103/PhysRevD.86.015010 [arXiv:1203.1662 [hep-ph]]. 22

[59] M. Endo and Y. Yamamoto, *"Unitarity Bounds on Dark Matter Effective Interactions at LHC,"* JHEP **1406** (2014) 126 doi:10.1007/JHEP06(2014)126 [arXiv:1403.6610 [hep-ph]]. 22

[60] S. A. Malik et al., *"Interplay and Characterization of Dark Matter Searches at Colliders and in Direct Detection Experiments,"* Phys. Dark Univ. **9-10** (2015) 51 doi:10.1016/j.dark.2015.03.003 [arXiv:1409.4075 [hep-ex]]. 22

[61] J. Abdallah et al., *"Simplified Models for Dark Matter Searches at the LHC,"* Phys. Dark Univ. **9-10** (2015) 8 doi:10.1016/j.dark.2015.08.001 [arXiv:1506.03116 [hep-ph]]. 22, 46, 56

[62] A. Albert et al., *"Towards the next generation of simplified Dark Matter models,"* Phys. Dark Univ. **16** (2017) 49 doi:10.1016/j.dark.2017.02.002 [arXiv:1607.06680 [hep-ex]]. 22

[63] A. Boveia et al., *"Recommendations on presenting LHC searches for missing transverse energy signals using simplified s-channel models of dark matter,"* arXiv:1603.04156 [hep-ex]. 22, 57, 58

[64] A. Albert et al., *"Recommendations of the LHC Dark Matter Working Group: Comparing LHC searches for heavy mediators of dark matter production in visible and invisible decay channels,"* arXiv:1703.05703 [hep-ex]. 22

[65] G. D'Ambrosio, G. F. Giudice, G. Isidori and A. Strumia, *"Minimal flavor violation: An Effective field theory approach,"* Nucl. Phys. B **645** (2002) 155 doi:10.1016/S0550-3213(02)00836-2 [hep-ph/0207036]. 23

[66] S. Dodelson and L. M. Widrow, *"Sterile-neutrinos as dark matter,"* Phys. Rev. Lett. **72** (1994) 17 doi:10.1103/PhysRevLett.72.17 [hep-ph/9303287]. 24

[67] B. W. Lee and S. Weinberg, *"Cosmological Lower Bound on Heavy Neutrino Masses,"* Phys. Rev. Lett. **39** (1977) 165. doi:10.1103/PhysRevLett.39.165 24

[68] P. Hut, *"Limits on Masses and Number of Neutral Weakly Interacting Particles,"* Phys. Lett. B **69** (1977) 85 [Phys. Lett. **69B** (1977) 85]. doi:10.1016/0370-2693(77)90139-3 24

[69] P. Hut and K. A. Olive, *"A Cosmological Upper Limit On The Mass Of Heavy Neutrinos,"* Phys. Lett. **87B** (1979) 144. doi:10.1016/0370-2693(79)90039-X 24

[70] N. Arkani-Hamed, S. Dimopoulos and G. R. Dvali, *"The Hierarchy problem and new dimensions at a millimeter,"* Phys. Lett. B **429** (1998) 263 doi:10.1016/S0370-2693(98)00466-3 [hep-ph/9803315]. 25

[71] L. Randall and R. Sundrum, *"A Large mass hierarchy from a small extra dimension,"* Phys. Rev. Lett. **83** (1999) 3370 doi:10.1103/PhysRevLett.83.3370 [hep-ph/9905221]. 25, 45, 51

[72] M. Milgrom, *"A Modification of the Newtonian dynamics as a possible alternative to the hidden mass hypothesis,"* Astrophys. J. **270** (1983) 365. doi:10.1086/161130 26

[73] M. Milgrom, *"A Modification of the Newtonian dynamics: Implications for galaxies,"* Astrophys. J. **270** (1983) 371. doi:10.1086/161131 26

[74] M. Milgrom, *"A modification of the Newtonian dynamics: implications for galaxy systems,"* Astrophys. J. **270** (1983) 384. doi:10.1086/161132 26

[75] R. H. Sanders, *"The published extended rotation curves of spiral galaxies: confrontation with modified dynamics,"* Astrophys. J. **473** (1996) 117 doi:10.1086/178131 [astro-ph/9606089]. 26

[76] M. Milgrom and R. H. Sanders, *"MOND predictions of halo phenomenology in disc galaxies,"* Mon. Not. Roy. Astron. Soc. **357** (2005) 45 doi:10.1111/j.1365-2966.2004.08578.x [astro-ph/0406487]. 26

[77] M. Milgrom and R. H. Sanders, *"MOND rotation curves of very low mass spiral galaxies,"* Astrophys. J. **658** (2007) L17 doi:10.1086/513695 [astro-ph/0611494]. 26

[78] J. D. Bekenstein, *"Relativistic gravitation theory for the MOND paradigm,"* Phys. Rev. D **70** (2004) 083509 Erratum: [Phys. Rev. D **71** (2005) 069901] doi:10.1103/PhysRevD.70.083509, 10.1103/PhysRevD.71.069901 [astro-ph/0403694]. 26

[79] B. Famaey and S. McGaugh, *"Modified Newtonian Dynamics (MOND): Observational Phenomenology and Relativistic Extensions,"* Living Rev. Rel. **15** (2012) 10 doi:10.12942/lrr-2012-10 [arXiv:1112.3960 [astro-ph.CO]]. 27

[80] C. Skordis, *"The Tensor-Vector-Scalar theory and its cosmology,"* Class. Quant. Grav. **26** (2009) 143001 doi:10.1088/0264-9381/26/14/143001 [arXiv:0903.3602 [astro-ph.CO]]. 27

[81] S. Dodelson and M. Liguori, *"Can Cosmic Structure form without Dark Matter?,"* Phys. Rev. Lett. **97** (2006) 231301 doi:10.1103/PhysRevLett.97.231301 [astro-ph/0608602]. 27

[82] C. Skordis, *"Generalizing tensor-vector-scalar cosmology,"* Phys. Rev. D **77** (2008) 123502 doi:10.1103/PhysRevD.77.123502 [arXiv:0801.1985 [astro-ph]]. 27

[83] C. Skordis, D. F. Mota, P. G. Ferreira and C. Boehm, *"Large Scale Structure in Bekenstein's theory of relativistic Modified Newtonian Dynamics,"* Phys. Rev. Lett. **96** (2006) 011301 doi:10.1103/PhysRevLett.96.011301 [astro-ph/0505519]. 27

[84] B. J. Carr and S. W. Hawking, *"Black holes in the early Universe,"* Mon. Not. Roy. Astron. Soc. **168** (1974) 399. 26

[85] J. Yokoyama, *"Cosmological constraints on primordial black holes produced in the near critical gravitational collapse,"* Phys. Rev. D **58** (1998) 107502 doi:10.1103/PhysRevD.58.107502 [gr-qc/9804041]. 26

[86] H. I. Kim, C. H. Lee and J. H. MacGibbon, *"Diffuse gamma-ray background and primordial black hole constraints on the spectral index of density fluctuations,"* Phys. Rev. D **59** (1999) 063004 doi:10.1103/PhysRevD.59.063004 [astro-ph/9901030]. 26

[87] P. Gondolo and G. Gelmini, *"Cosmic abundances of stable particles: Improved analysis,"* Nucl. Phys. B **360** (1991) 145. doi:10.1016/0550-3213(91)90438-4 28, 30

[88] G. Steigman, B. Dasgupta and J. F. Beacom, Phys. Rev. D **86** (2012) 023506 doi:10.1103/PhysRevD.86.023506 [arXiv:1204.3622 [hep-ph]]. 30

[89] P. Binetruy, G. Girardi and P. Salati, *"Constraints on a System of Two Neutral Fermions From Cosmology,"* Nucl. Phys. B **237** (1984) 285. doi:10.1016/0550-3213(84)90161-5 28, 138

[90] K. Griest and D. Seckel, *"Three exceptions in the calculation of relic abundances,"* Phys. Rev. D **43** (1991) 3191. doi:10.1103/PhysRevD.43.3191 28, 138

[91] J. Ellis, F. Luo and K. A. Olive, *"Gluino Coannihilation Revisited,"* JHEP **1509** (2015) 127 doi:10.1007/JHEP09(2015)127 [arXiv:1503.07142 [hep-ph]]. 28, 138

[92] D. Barducci, G. Belanger, J. Bernon, F. Boudjema, J. Da Silva, S. Kraml, U. Laa and A. Pukhov, *"Collider limits on new physics within micrOMEGAs_4.3,"* Comput. Phys. Commun. **222** (2018) 327 doi:10.1016/j.cpc.2017.08.028 [arXiv:1606.03834 [hep-ph]]. 30

[93] G. Aad et al. [ATLAS Collaboration], *"Observation of a new particle in the search for the Standard Model Higgs boson with the ATLAS detector at the LHC,"* Phys. Lett. B **716** (2012) 1 doi:10.1016/j.physletb.2012.08.020 [arXiv:1207.7214 [hep-ex]]. 31

[94] S. Chatrchyan et al. [CMS Collaboration], *"Observation of a new boson at a mass of 125 GeV with the CMS experiment at the LHC,"* Phys. Lett. B **716** (2012) 30 doi:10.1016/j.physletb.2012.08.021 [arXiv:1207.7235 [hep-ex]]. 31

[95] G. Aad et al. [ATLAS Collaboration], *"Expected Performance of the ATLAS Experiment - Detector, Trigger and Physics,"* arXiv:0901.0512 [hep-ex]. 31, 128

[96] R. P. Feynman, *"Very high-energy collisions of hadrons,"* Phys. Rev. Lett. **23** (1969) 1415. doi:10.1103/PhysRevLett.23.1415 31

[97] R. D. Ball et al. [NNPDF Collaboration], *"Parton distributions from high-precision collider data,"* Eur. Phys. J. C **77** (2017) no.10, 663 doi:10.1140/epjc/s10052-017-5199-5 [arXiv:1706.00428 [hep-ph]]. 32

[98] G. P. Salam, *"Towards Jetography,"* Eur. Phys. J. C **67** (2010) 637 doi:10.1140/epjc/s10052-010-1314-6 [arXiv:0906.1833 [hep-ph]]. 34

[99] J. Alwall et al., *"The automated computation of tree-level and next-to-leading order differential cross sections, and their matching to parton shower simulations,"* JHEP **1407** (2014) 079 doi:10.1007/JHEP07(2014)079 [arXiv:1405.0301 [hep-ph]]. 34, 47, 100, 128, 145

[100] T. Sjöstrand et al., *"An Introduction to PYTHIA 8.2,"* Comput. Phys. Commun. **191** (2015) 159 doi:10.1016/j.cpc.2015.01.024 [arXiv:1410.3012 [hep-ph]]. 34, 47, 128

[101] A. Belyaev, N. D. Christensen and A. Pukhov, *"CalcHEP 3.4 for collider physics within and beyond the Standard Model,"* Comput. Phys. Commun. **184** (2013) 1729 doi:10.1016/j.cpc.2013.01.014 [arXiv:1207.6082 [hep-ph]]. 34, 140

[102] J. de Favereau et al. [DELPHES 3 Collaboration], *"DELPHES 3, A modular framework for fast simulation of a generic collider experiment,"* JHEP **1402** (2014) 057 doi:10.1007/JHEP02(2014)057 [arXiv:1307.6346 [hep-ex]]. 34

[103] A. Alloul, N. D. Christensen, C. Degrande, C. Duhr and B. Fuks, *"FeynRules 2.0 - A complete toolbox for tree-level phenomenology,"* Comput. Phys. Commun. **185** (2014) 2250 doi:10.1016/j.cpc.2014.04.012 [arXiv:1310.1921 [hep-ph]]. 34, 47, 98

[104] F. Kahlhoefer, *"Review of LHC Dark Matter Searches,"* Int. J. Mod. Phys. A **32** (2017) no.13, 1730006 doi:10.1142/S0217751X1730006X [arXiv:1702.02430 [hep-ph]]. 34

[105] O. Buchmueller, C. Doglioni and L. T. Wang, *"Search for dark matter at colliders,"* Nature Phys. **13** (2017) no.3, 217. doi:10.1038/nphys4054 34

[106] J. Ellis, *"TikZ-Feynman: Feynman diagrams with TikZ,"* Comput. Phys. Commun. **210** (2017) 103 doi:10.1016/j.cpc.2016.08.019 [arXiv:1601.05437 [hep-ph]]. 35

[107] M. Aaboud et al. [ATLAS Collaboration], *"Search for dark matter and other new phenomena in events with an energetic jet and large missing transverse momentum using the ATLAS detector,"* JHEP **1801** (2018) 126 doi:10.1007/JHEP01(2018)126 [arXiv:1711.03301 [hep-ex]]. 35, 36, 39, 112, 145, 147

[108] M. Aaboud et al. [ATLAS Collaboration], *"Search for new phenomena in events with a photon and missing transverse momentum in pp collisions at $\sqrt{s}$ = 13 TeV with the ATLAS detector,"* JHEP **1606** (2016) 059 doi:10.1007/JHEP06(2016)059 [arXiv:1604.01306 [hep-ex]]. 36

[109] [CMS Collaboration], *"Search for Dark Matter Produced in Association with a Higgs Boson Decaying to Two Photons,"* CMS-PAS-EXO-16-011. 36

[110] [CMS Collaboration], *"Search for dark matter in association with a top quark pair at sqrt(s)=13 TeV,"* CMS-PAS-EXO-16-005. 36

[111] G. Aad et al. [ATLAS Collaboration], *"Constraints on new phenomena via Higgs boson couplings and invisible decays with the ATLAS detector,"* JHEP **1511** (2015) 206 doi:10.1007/JHEP11(2015)206 [arXiv:1509.00672 [hep-ex]]. 36, 123

[112] M. Aaboud et al. [ATLAS Collaboration], *"Search for new phenomena in dijet events using 37 fb^{-1} of pp collision data collected at $\sqrt{s}$ =13 TeV with the ATLAS detector,"* Phys. Rev. D **96** (2017) no.5, 052004 doi:10.1103/PhysRevD.96.052004 [arXiv:1703.09127 [hep-ex]]. 37, 38, 39, 52, 58, 112, 138

[113] M. Aaboud et al. [ATLAS Collaboration], *"Search for low-mass dijet resonances using trigger-level jets with the ATLAS detector in pp collisions at $\sqrt{s}$ = 13 TeV,"* arXiv:1804.03496 [hep-ex]. 39, 58, 111, 138

[114] M. Aaboud et al. [ATLAS Collaboration], *"Search for dark matter at $\sqrt{s}$ = 13 TeV in final states containing an energetic photon and large missing transverse momentum with the ATLAS detector,"* Eur. Phys. J. C **77** (2017) no.6, 393 doi:10.1140/epjc/s10052-017-4965-8 [arXiv:1704.03848 [hep-ex]]. 39

[115] M. Aaboud et al. [ATLAS Collaboration], *"Search for new high-mass phenomena in the dilepton final state using 36 fb^{-1} of proton-proton collision data at $\sqrt{s}$ = 13 TeV with the ATLAS detector,"* JHEP **1710** (2017) 182 doi:10.1007/JHEP10(2017)182 [arXiv:1707.02424 [hep-ex]]. 39

[116] M. W. Goodman and E. Witten, *"Detectability of Certain Dark Matter Candidates,"* Phys. Rev. D **31** (1985) 3059. doi:10.1103/PhysRevD.31.3059 40

[117] A. K. Drukier, K. Freese and D. N. Spergel, *"Detecting Cold Dark Matter Candidates,"* Phys. Rev. D **33** (1986) 3495. doi:10.1103/PhysRevD.33.3495 40

[118] A. M. Green, *"Astrophysical uncertainties on direct detection experiments,"* Mod. Phys. Lett. A **27** (2012) 1230004 doi:10.1142/S0217732312300042 [arXiv:1112.0524 [astro-ph.CO]]. 41

[119] F. D'Eramo, B. J. Kavanagh and P. Panci, *"You can hide but you have to run: direct detection with vector mediators,"* JHEP **1608** (2016) 111 doi:10.1007/JHEP08(2016)111 [arXiv:1605.04917 [hep-ph]]. 42, 76, 80

[120] E. Aprile et al. [XENON Collaboration], *"Dark Matter Search Results from a One Tonne× Year Exposure of XENON1T,"* arXiv:1805.12562 [astro-ph.CO]. 42, 43, 95, 100, 101, 102

[121] D. S. Akerib et al. [LUX Collaboration], *"Results from a search for dark matter in the complete LUX exposure,"* Phys. Rev. Lett. **118** (2017) no.2, 021303 doi:10.1103/PhysRevLett.118.021303 [arXiv:1608.07648 [astro-ph.CO]]. 42, 76, 92, 120

[122] X. Cui et al. [PandaX-II Collaboration], *"Dark Matter Results From 54-Ton-Day Exposure of PandaX-II Experiment,"* Phys. Rev. Lett. **119** (2017) no.18, 181302 doi:10.1103/PhysRevLett.119.181302 [arXiv:1708.06917 [astro-ph.CO]]. 42

[123] A. Albert et al. [Fermi-LAT and DES Collaborations], *"Searching for Dark Matter Annihilation in Recently Discovered Milky Way Satellites with Fermi-LAT,"* Astrophys. J. **834** (2017) no.2, 110 doi:10.3847/1538-4357/834/2/110 [arXiv:1611.03184 [astro-ph.HE]]. 43, 44

[124] M. G. Aartsen et al. [IceCube Collaboration], *"Search for annihilating dark matter in the Sun with 3 years of IceCube data,"* Eur. Phys. J. C **77** (2017) no.3, 146 doi:10.1140/epjc/s10052-017-4689-9 [arXiv:1612.05949 [astro-ph.HE]]. 44

[125] G. Aad et al. [ATLAS Collaboration], *"Search for new phenomena in dijet mass and angular distributions from pp collisions at* $\sqrt{s}$ =

13 TeV with the ATLAS detector," Phys. Lett. B **754** (2016) 302 doi:10.1016/j.physletb.2016.01.032 [arXiv:1512.01530 [hep-ex]]. 45, 48, 49

[126] V. Khachatryan et al. [CMS Collaboration], *"Search for narrow resonances decaying to dijets in proton-proton collisions at* $\sqrt{(s)} = 13$ *TeV,"* Phys. Rev. Lett. **116** (2016) no.7, 071801 doi:10.1103/PhysRevLett.116.071801 [arXiv:1512.01224 [hep-ex]]. 45, 48, 49

[127] G. Aad et al. [ATLAS Collaboration], *"Search for new phenomena in the dijet mass distribution using* $p - p$ *collision data at* $\sqrt{s} = 8$ *TeV with the ATLAS detector,"* Phys. Rev. D **91** (2015) no.5, 052007 doi:10.1103/PhysRevD.91.052007 [arXiv:1407.1376 [hep-ex]]. 45, 48, 49

[128] V. Khachatryan et al. [CMS Collaboration], *"Search for resonances and quantum black holes using dijet mass spectra in proton-proton collisions at* $\sqrt{s} = 8$ *TeV,"* Phys. Rev. D **91** (2015) no.5, 052009 doi:10.1103/PhysRevD.91.052009 [arXiv:1501.04198 [hep-ex]]. 45, 48, 49, 50, 51

[129] V. Khachatryan et al. [CMS Collaboration], *"Search for narrow resonances in dijet final states at* $\sqrt{(s)} = 8$ *TeV with the novel CMS technique of data scouting,"* Phys. Rev. Lett. **117** (2016) no.3, 031802 doi:10.1103/PhysRevLett.117.031802 [arXiv:1604.08907 [hep-ex]]. 45, 48, 49, 51

[130] U. Baur, I. Hinchliffe and D. Zeppenfeld, *"Excited Quark Production at Hadron Colliders,"* Int. J. Mod. Phys. A **2** (1987) 1285. doi:10.1142/S0217751X87000661 45

[131] U. Baur, M. Spira and P. M. Zerwas, *"Excited Quark and Lepton Production at Hadron Colliders,"* Phys. Rev. D **42** (1990) 815. doi:10.1103/PhysRevD.42.815 45

[132] P. Fileviez Perez and M. B. Wise, *"Baryon and lepton number as local gauge symmetries,"* Phys. Rev. D **82** (2010) 011901 Erratum: [Phys. Rev. D **82** (2010) 079901] doi:10.1103/PhysRevD.82.079901, 10.1103/PhysRevD.82.011901 [arXiv:1002.1754 [hep-ph]]. 45, 75, 77, 83, 86, 87, 88, 92

[133] B. A. Dobrescu and F. Yu, *"Coupling-mass mapping of dijet peak searches,"* Phys. Rev. D **88** (2013) no.3, 035021 Erratum: [Phys. Rev. D

90 (2014) no.7, 079901] doi:10.1103/PhysRevD.88.035021, 10.1103/PhysRevD.90.079901 [arXiv:1306.2629 [hep-ph]]. 45, 46

[134] C. W. Chiang, T. Nomura and K. Yagyu, *"Leptophobic Z' in models with multiple Higgs doublet fields,"* JHEP **1505** (2015) 127 doi:10.1007/JHEP05(2015)127 [arXiv:1502.00855 [hep-ph]]. 45, 58

[135] A. Ekstedt, R. Enberg, G. Ingelman, J. Löfgren and T. Mandal, *"Constraining minimal anomaly free* U(1) *extensions of the Standard Model,"* JHEP **1611** (2016) 071 doi:10.1007/JHEP11(2016)071 [arXiv:1605.04855 [hep-ph]]. 45, 75, 76, 77, 91, 94, 95, 96

[136] M. T. Frandsen, F. Kahlhoefer, A. Preston, S. Sarkar and K. Schmidt-Hoberg, *"LHC and Tevatron Bounds on the Dark Matter Direct Detection Cross-Section for Vector Mediators,"* JHEP **1207** (2012) 123 doi:10.1007/JHEP07(2012)123 [arXiv:1204.3839 [hep-ph]]. 24, 45, 46, 54

[137] P. J. Fox and C. Williams, *"Next-to-Leading Order Predictions for Dark Matter Production at Hadron Colliders,"* Phys. Rev. D **87** (2013) no.5, 054030 doi:10.1103/PhysRevD.87.054030 [arXiv:1211.6390 [hep-ph]]. 24, 45

[138] A. Alves, S. Profumo and F. S. Queiroz, *"The dark $Z^{'}$ portal: direct, indirect and collider searches,"* JHEP **1404** (2014) 063 doi:10.1007/JHEP04(2014)063 [arXiv:1312.5281 [hep-ph]]. 24, 45

[139] G. Arcadi, Y. Mambrini, M. H. G. Tytgat and B. Zaldivar, *"Invisible Z' and dark matter: LHC vs LUX constraints,"* JHEP **1403** (2014) 134 doi:10.1007/JHEP03(2014)134 [arXiv:1401.0221 [hep-ph]]. 24, 45, 75, 95

[140] O. Buchmueller, M. J. Dolan, S. A. Malik and C. McCabe, *"Characterising dark matter searches at colliders and direct detection experiments: Vector mediators,"* JHEP **1501** (2015) 037 doi:10.1007/JHEP01(2015)037 [arXiv:1407.8257 [hep-ph]]. 24, 45, 56

[141] O. Lebedev and Y. Mambrini, *"Axial dark matter: The case for an invisible Z',"* Phys. Lett. B **734** (2014) 350 doi:10.1016/j.physletb.2014.05.025 [arXiv:1403.4837 [hep-ph]]. 24, 45

[142] P. Harris, V. V. Khoze, M. Spannowsky and C. Williams, *"Constraining Dark Sectors at Colliders: Beyond the Effective Theory Approach,"* Phys. Rev. D **91** (2015) 055009 doi:10.1103/PhysRevD.91.055009 [arXiv:1411.0535 [hep-ph]]. 24, 45, 56

[143] G. Busoni, A. De Simone, T. Jacques, E. Morgante and A. Riotto, *"Making the Most of the Relic Density for Dark Matter Searches at the LHC 14 TeV Run,"* JCAP **1503** (2015) no.03, 022 doi:10.1088/1475-7516/2015/03/022 [arXiv:1410.7409 [hep-ph]]. 24, 45

[144] M. Fairbairn and J. Heal, *"Complementarity of dark matter searches at resonance,"* Phys. Rev. D **90** (2014) no.11, 115019 doi:10.1103/PhysRevD.90.115019 [arXiv:1406.3288 [hep-ph]]. 24, 45, 102

[145] T. Jacques and K. Nordström, *"Mapping monojet constraints onto Simplified Dark Matter Models,"* JHEP **1506** (2015) 142 doi:10.1007/JHEP06(2015)142 [arXiv:1502.05721 [hep-ph]]. 24, 45, 56, 145

[146] A. Alves, A. Berlin, S. Profumo and F. S. Queiroz, *"Dark Matter Complementarity and the Z' Portal,"* Phys. Rev. D **92** (2015) no.8, 083004 doi:10.1103/PhysRevD.92.083004 [arXiv:1501.03490 [hep-ph]]. 24, 45

[147] M. Chala, F. Kahlhoefer, M. McCullough, G. Nardini and K. Schmidt-Hoberg, *"Constraining Dark Sectors with Monojets and Dijets,"* JHEP **1507** (2015) 089 doi:10.1007/JHEP07(2015)089 [arXiv:1503.05916 [hep-ph]]. 24, 45, 46, 57, 58, 98

[148] A. De Simone and T. Jacques, *"Simplified models vs. effective field theory approaches in dark matter searches,"* Eur. Phys. J. C **76** (2016) no.7, 367 doi:10.1140/epjc/s10052-016-4208-4 [arXiv:1603.08002 [hep-ph]]. 24, 45, 56

[149] A. J. Brennan, M. F. McDonald, J. Gramling and T. D. Jacques, *"Collide and Conquer: Constraints on Simplified Dark Matter Models using Mono-X Collider Searches,"* JHEP **1605** (2016) 112 doi:10.1007/JHEP05(2016)112 [arXiv:1603.01366 [hep-ph]]. 24, 45, 56

[150] T. Jacques, A. Katz, E. Morgante, D. Racco, M. Rameez and A. Riotto, *"Complementarity of DM searches in a consistent simplified model:*

the case of Z′," JHEP **1610** (2016) 071 doi:10.1007/JHEP10(2016)071 [arXiv:1605.06513 [hep-ph]]. 24, 45

[151] D. Abercrombie et al., *"Dark Matter Benchmark Models for Early LHC Run-2 Searches: Report of the ATLAS/CMS Dark Matter Forum,"* arXiv:1507.00966 [hep-ex]. 46, 56, 57

[152] H. An, X. Ji and L. T. Wang, *"Light Dark Matter and Z′ Dark Force at Colliders,"* JHEP **1207** (2012) 182 doi:10.1007/JHEP07(2012)182 [arXiv:1202.2894 [hep-ph]]. 24, 46, 141

[153] H. An, R. Huo and L. T. Wang, *"Searching for Low Mass Dark Portal at the LHC,"* Phys. Dark Univ. **2** (2013) 50 doi:10.1016/j.dark.2013.03.002 [arXiv:1212.2221 [hep-ph]]. 24, 46

[154] T. Sjostrand, S. Mrenna and P. Z. Skands, *"A Brief Introduction to PYTHIA 8.1,"* Comput. Phys. Commun. **178** (2008) 852 doi:10.1016/j.cpc.2008.01.036 [arXiv:0710.3820 [hep-ph]]. 47

[155] M. Cacciari, G. P. Salam and G. Soyez, *"FastJet User Manual,"* Eur. Phys. J. C **72** (2012) 1896 doi:10.1140/epjc/s10052-012-1896-2 [arXiv:1111.6097 [hep-ph]]. 34, 47, 128

[156] C. Degrande, C. Duhr, B. Fuks, D. Grellscheid, O. Mattelaer and T. Reiter, *"UFO - The Universal FeynRules Output,"* Comput. Phys. Commun. **183** (2012) 1201 doi:10.1016/j.cpc.2012.01.022 [arXiv:1108.2040 [hep-ph]]. 47

[157] H. L. Lai et al. [CTEQ Collaboration], *"Global QCD analysis of parton structure of the nucleon: CTEQ5 parton distributions,"* Eur. Phys. J. C **12** (2000) 375 doi:10.1007/s100529900196 [hep-ph/9903282]. 48

[158] E. Accomando, A. Belyaev, L. Fedeli, S. F. King and C. Shepherd-Themistocleous, *"Z' physics with early LHC data,"* Phys. Rev. D **83** (2011) 075012 doi:10.1103/PhysRevD.83.075012 [arXiv:1010.6058 [hep-ph]]. 24, 48

[159] E. Accomando, D. Becciolini, A. Belyaev, S. Moretti and C. Shepherd-Themistocleous, JHEP **1310** (2013) 153 doi:10.1007/JHEP10(2013)153 [arXiv:1304.6700 [hep-ph]]. 24

[160] A. Belyaev, S. F. King and P. Svantesson, *"Little Z' models,"* Phys. Rev. D **88** (2013) no.3, 035015 doi:10.1103/PhysRevD.88.035015 [arXiv:1303.0770 [hep-ph]]. 24

[161] L. Basso, A. Belyaev, S. Moretti, G. M. Pruna and C. H. Shepherd-Themistocleous, *"Z′ discovery potential at the LHC in the minimal $B-L$ extension of the Standard Model,"* Eur. Phys. J. C **71** (2011) 1613 doi:10.1140/epjc/s10052-011-1613-6 [arXiv:1002.3586 [hep-ph]]. 24

[162] M. Cacciari, G. P. Salam and G. Soyez, *"The anti-k_t jet clustering algorithm,"* JHEP **0804** (2008) 063 doi:10.1088/1126-6708/2008/04/063 [arXiv:0802.1189 [hep-ph]]. 34, 48, 128

[163] P. S. Bhupal Dev and R. N. Mohapatra, *"Unified explanation of the eejj, diboson and dijet resonances at the LHC,"* Phys. Rev. Lett. **115** (2015) no.18, 181803 doi:10.1103/PhysRevLett.115.181803 [arXiv:1508.02277 [hep-ph]]. 52

[164] A. Das, N. Nagata and N. Okada, *"Testing the 2-TeV Resonance with Trileptons,"* JHEP **1603** (2016) 049 doi:10.1007/JHEP03(2016)049 [arXiv:1601.05079 [hep-ph]]. 52

[165] M. Duerr and P. Fileviez Perez, *"Baryonic Dark Matter,"* Phys. Lett. B **732** (2014) 101 doi:10.1016/j.physletb.2014.03.011 [arXiv:1309.3970 [hep-ph]]. 56

[166] P. Fileviez Perez, S. Ohmer and H. H. Patel, *"Minimal Theory for Lepto-Baryons,"* Phys. Lett. B **735** (2014) 283 doi:10.1016/j.physletb.2014.06.057 [arXiv:1403.8029 [hep-ph]]. 56, 75, 77, 83, 86, 87, 88, 92, 95

[167] M. Duerr and P. Fileviez Perez, *"Theory for Baryon Number and Dark Matter at the LHC,"* Phys. Rev. D **91** (2015) no.9, 095001 doi:10.1103/PhysRevD.91.095001 [arXiv:1409.8165 [hep-ph]]. 56, 75, 77, 83, 86, 87, 88, 92, 95

[168] S. Ohmer and H. H. Patel, *"Leptobaryons as Majorana Dark Matter,"* Phys. Rev. D **92** (2015) no.5, 055020 doi:10.1103/PhysRevD.92.055020 [arXiv:1506.00954 [hep-ph]]. 56

[169] F. Kahlhoefer, K. Schmidt-Hoberg, T. Schwetz and S. Vogl, *"Implications of unitarity and gauge invariance for simplified dark matter models,"* JHEP **1602** (2016) 016 doi:10.1007/JHEP02(2016)016 [arXiv:1510.02110 [hep-ph]]. 24, 56, 57, 74, 75, 94, 143

[170] M. Duerr, A. Grohsjean, F. Kahlhoefer, B. Penning, K. Schmidt-Hoberg and C. Schwanenberger, *"Hunting the dark Higgs,"* JHEP **1704** (2017) 143 doi:10.1007/JHEP04(2017)143 [arXiv:1701.08780 [hep-ph]]. 24, 74

[171] P. A. R. Ade *et al.* [Planck Collaboration], *"Planck 2015 results. XIII. Cosmological parameters,"* Astron. Astrophys. **594** (2016) A13 doi:10.1051/0004-6361/201525830 [arXiv:1502.01589 [astro-ph.CO]]. 57, 59

[172] G. Bélanger, F. Boudjema, A. Pukhov and A. Semenov, *"micrOMEGAs4.1: two dark matter candidates,"* Comput. Phys. Commun. **192** (2015) 322 doi:10.1016/j.cpc.2015.03.003 [arXiv:1407.6129 [hep-ph]]. 57, 60, 98

[173] V. Khachatryan et al. [CMS Collaboration], *"Search for dark matter, extra dimensions, and unparticles in monojet events in protonproton collisions at* $\sqrt{s} = 8$ *TeV,"* Eur. Phys. J. C **75** (2015) no.5, 235 doi:10.1140/epjc/s10052-015-3451-4 [arXiv:1408.3583 [hep-ex]]. 58

[174] G. Aad et al. [ATLAS Collaboration], *"Search for new phenomena in final states with an energetic jet and large missing transverse momentum in pp collisions at* $\sqrt{s}$ *=8 TeV with the ATLAS detector,"* Eur. Phys. J. C **75** (2015) no.7, 299 Erratum: [Eur. Phys. J. C **75** (2015) no.9, 408] doi:10.1140/epjc/s10052-015-3517-3, 10.1140/epjc/s10052-015-3639-7 [arXiv:1502.01518 [hep-ex]]. 58

[175] M. Aaboud et al. [ATLAS Collaboration], *"Search for new phenomena in final states with an energetic jet and large missing transverse momentum in pp collisions at* $\sqrt{s} = 13$ *TeV using the ATLAS detector,"* Phys. Rev. D **94** (2016) no.3, 032005 doi:10.1103/PhysRevD.94.032005 [arXiv:1604.07773 [hep-ex]]. 58

[176] [CMS Collaboration], *"Search for dark matter production in association with jets, or hadronically decaying W or Z boson at* $\sqrt{s} = 13$ *TeV,"* CMS-PAS-EXO-16-013. 58

[177] N. Okada and S. Okada, *"Z'_{BL} portal dark matter and LHC Run-2 results,"* Phys. Rev. D **93** (2016) no.7, 075003 doi:10.1103/PhysRevD.93.075003 [arXiv:1601.07526 [hep-ph]]. 59

[178] A. Pukhov, A. Belyaev and N. Christensen, *"CalcHEP User's manual for version 3.3.6,"* `http://theory.sinp.msu.ru/~pukhov/CALCHEP/calchep_man_3.3.6.pdf` 141

[179] O. Buchmueller, S. A. Malik, C. McCabe and B. Penning, *"Constraining Dark Matter Interactions with Pseudoscalar and Scalar Mediators Using Collider Searches for Multijets plus Missing Transverse Energy,"* Phys. Rev. Lett. **115** (2015) no.18, 181802 doi:10.1103/PhysRevLett.115.181802 [arXiv:1505.07826 [hep-ph]]. 24, 126

[180] M. S. Chanowitz, J. R. Ellis and M. K. Gaillard, *"The Price of Natural Flavor Conservation in Neutral Weak Interactions,"* Nucl. Phys. B **128** (1977) 506. doi:10.1016/0550-3213(77)90057-8 75

[181] S. M. Barr, B. Bednarz and C. Benesh, *"Anomaly Constraints and New U(1) Gauge Bosons,"* Phys. Rev. D **34** (1986) 235. doi:10.1103/PhysRevD.34.235 75, 95

[182] J. Erler and P. Langacker, *"Constraints on extended neutral gauge structures,"* Phys. Lett. B **456** (1999) 68 doi:10.1016/S0370-2693(99)00457-8 [hep-ph/9903476]. 75

[183] T. Appelquist, B. A. Dobrescu and A. R. Hopper, *"Nonexotic neutral gauge bosons,"* Phys. Rev. D **68** (2003) 035012 doi:10.1103/PhysRevD.68.035012 [hep-ph/0212073]. 75, 77, 91, 95, 96

[184] M. Carena, A. Daleo, B. A. Dobrescu and T. M. P. Tait, *"Z' gauge bosons at the Tevatron,"* Phys. Rev. D **70** (2004) 093009 doi:10.1103/PhysRevD.70.093009 [hep-ph/0408098]. 75, 77

[185] P. Batra, B. A. Dobrescu and D. Spivak, *"Anomaly-free sets of fermions,"* J. Math. Phys. **47** (2006) 082301 doi:10.1063/1.2222081 [hep-ph/0510181]. 75, 95

[186] D. E. Morrissey and J. D. Wells, *"The Tension between gauge coupling unification, the Higgs boson mass, and a gauge-breaking origin of the supersymmetric mu-term,"* Phys. Rev. D **74** (2006) 015008 doi:10.1103/PhysRevD.74.015008 [hep-ph/0512019]. 75

[187] C. W. Chiang, N. G. Deshpande and J. Jiang, *"Flavor changing effects in family nonuniversal Z' models,"* JHEP **0608** (2006) 075 doi:10.1088/1126-6708/2006/08/075 [hep-ph/0606122]. 75

[188] P. Langacker, *"The Physics of Heavy Z' Gauge Bosons,"* Rev. Mod. Phys. **81** (2009) 1199 doi:10.1103/RevModPhys.81.1199 [arXiv:0801.1345 [hep-ph]]. 75

[189] M. Duerr, P. Fileviez Perez and M. B. Wise, *"Gauge Theory for Baryon and Lepton Numbers with Leptoquarks,"* Phys. Rev. Lett. **110** (2013) 231801 doi:10.1103/PhysRevLett.110.231801 [arXiv:1304.0576 [hep-ph]]. 75, 77, 83, 86, 87, 88, 92, 95

[190] A. Ismail, W. Y. Keung, K. H. Tsao and J. Unwin, *"Axial vector Z' and anomaly cancellation,"* Nucl. Phys. B **918** (2017) 220 doi:10.1016/j.nuclphysb.2017.03.001 [arXiv:1609.02188 [hep-ph]]. 75, 78, 83, 86, 95

[191] D. Hooper, *"Z' Mediated Dark Matter Models for the Galactic Center Gamma-Ray Excess,"* Phys. Rev. D **91** (2015) 035025 doi:10.1103/PhysRevD.91.035025 [arXiv:1411.4079 [hep-ph]]. 75

[192] B. A. Dobrescu and C. Frugiuele, *"Hidden GeV-scale interactions of quarks,"* Phys. Rev. Lett. **113** (2014) 061801 doi:10.1103/PhysRevLett.113.061801 [arXiv:1404.3947 [hep-ph]]. 75

[193] E. Dudas, L. Heurtier, Y. Mambrini and B. Zaldivar, *"Extra U(1), effective operators, anomalies and dark matter,"* JHEP **1311** (2013) 083 doi:10.1007/JHEP11(2013)083 [arXiv:1307.0005 [hep-ph]]. 75

[194] W. Wang and Z. L. Han, *"Radiative linear seesaw model, dark matter, and $U(1)_{B-L}$,"* Phys. Rev. D **92** (2015) 095001 doi:10.1103/PhysRevD.92.095001 [arXiv:1508.00706 [hep-ph]]. 75

[195] J. M. Berryman, A. de Gouvêa, D. Hernández and K. J. Kelly, *"Imperfect mirror copies of the standard model,"* Phys. Rev. D **94** (2016) no.3, 035009 doi:10.1103/PhysRevD.94.035009 [arXiv:1605.03610 [hep-ph]]. 75

[196] A. de Gouvêa and D. Hernández, *"New Chiral Fermions, a New Gauge Interaction, Dirac Neutrinos, and Dark Matter,"* JHEP **1510** (2015) 046 doi:10.1007/JHEP10(2015)046 [arXiv:1507.00916 [hep-ph]]. 75

[197] P. Langacker, R. W. Robinett and J. L. Rosner, *"New Heavy Gauge Bosons in p p and p anti-p Collisions,"* Phys. Rev. D **30** (1984) 1470. doi:10.1103/PhysRevD.30.1470 75

[198] [CMS Collaboration], *"Search for a high-mass resonance decaying into a dilepton final state in 13 fb^{-1} of pp collisions at $\sqrt{s} = 13$ TeV,"* CMS-PAS-EXO-16-031. 75, 92

[199] [ATLAS Collaboration], *"Search for new high-mass phenomena in the dilepton final state using 36.1 fb^{-1} of proton-proton collision data at $\sqrt{s} = 13$ TeV with the ATLAS detector,"* ATLAS-CONF-2017-027. 75, 92, 100, 101, 102, 103

[200] A. Tan et al. [PandaX-II Collaboration], *"Dark Matter Results from First 98.7 Days of Data from the PandaX-II Experiment,"* Phys. Rev. Lett. **117** (2016) no.12, 121303 doi:10.1103/PhysRevLett.117.121303 [arXiv:1607.07400 [hep-ex]]. 76, 92, 120

[201] J. Kumar and D. Marfatia, *"Matrix element analyses of dark matter scattering and annihilation,"* Phys. Rev. D **88** (2013) no.1, 014035 doi:10.1103/PhysRevD.88.014035 [arXiv:1305.1611 [hep-ph]]. 76

[202] S. L. Glashow and S. Weinberg, *"Natural Conservation Laws for Neutral Currents,"* Phys. Rev. D **15** (1977) 1958. doi:10.1103/PhysRevD.15.1958 81, 122

[203] E. A. Paschos, *"Diagonal Neutral Currents,"* Phys. Rev. D **15** (1977) 1966. doi:10.1103/PhysRevD.15.1966 81

[204] M. L. Perl, E. R. Lee and D. Loomba, *"Searches for fractionally charged particles,"* Ann. Rev. Nucl. Part. Sci. **59** (2009) 47. doi:10.1146/annurev-nucl-121908-122035 86

[205] M. Escudero, A. Berlin, D. Hooper and M. X. Lin, *"Toward (Finally!) Ruling Out Z and Higgs Mediated Dark Matter Models,"* JCAP **1612** (2016) 029 doi:10.1088/1475-7516/2016/12/029 [arXiv:1609.09079 [hep-ph]]. 91

[206] G. Arcadi, Y. Mambrini and F. Richard, *"Z-portal dark matter,"* JCAP **1503** (2015) 018 doi:10.1088/1475-7516/2015/03/018 [arXiv:1411.2985 [hep-ph]]. 91

[207] J. Ellis, A. Fowlie, L. Marzola and M. Raidal, *"Statistical Analyses of Higgs- and Z-Portal Dark Matter Models,"* Phys. Rev. D **97** (2018) no.11, 115014 doi:10.1103/PhysRevD.97.115014 [arXiv:1711.09912 [hep-ph]]. 91

[208] A. Ismail, A. Katz and D. Racco, *"On dark matter interactions with the Standard Model through an anomalous Z′,"* JHEP **1710** (2017) 165 doi:10.1007/JHEP10(2017)165 [arXiv:1707.00709 [hep-ph]]. 94

[209] J. Ellis, M. Fairbairn and P. Tunney, *"Anomaly-Free Models for Flavour Anomalies,"* Eur. Phys. J. C **78** (2018) no.3, 238 doi:10.1140/epjc/s10052-018-5725-0 [arXiv:1705.03447 [hep-ph]]. 95, 138

[210] J. Ellis, C. W. Murphy, V. Sanz and T. You, *"Updated Global SMEFT Fit to Higgs, Diboson and Electroweak Data,"* JHEP **1806** (2018) 146 doi:10.1007/JHEP06(2018)146 [arXiv:1803.03252 [hep-ph]]. 95, 102, 109, 144

[211] A. Arbey, J. Ellis, F. Mahmoudi and G. Robbins, *"Dark Matter Casts Light on the Early Universe,"* arXiv:1807.00554 [hep-ph]. 99

[212] K. S. Babu, C. F. Kolda and J. March-Russell, *"Implications of generalized Z - Z-prime mixing,"* Phys. Rev. D **57** (1998) 6788 doi:10.1103/PhysRevD.57.6788 [hep-ph/9710441]. 143

[213] M. Duerr, F. Kahlhoefer, K. Schmidt-Hoberg, T. Schwetz and S. Vogl, *"How to save the WIMP: global analysis of a dark matter model with two s-channel mediators,"* JHEP **1609** (2016) 042 doi:10.1007/JHEP09(2016)042 [arXiv:1606.07609 [hep-ph]]. 24, 74, 143

[214] M. Aaboud et al. [ATLAS Collaboration], *"Search for light resonances decaying to boosted quark pairs and produced in association with a photon or*

a jet in proton-proton collisions at $\sqrt{s} = 13$ *TeV with the ATLAS detector,"* arXiv:1801.08769 [hep-ex]. 58, 111, 138

[215] [ATLAS Collaboration], *"Search for new light resonances decaying to jet pairs and produced in association with a photon or a jet in proton-proton collisions at* $\sqrt{s} = 13$ *TeV with the ATLAS detector,"* ATLAS-CONF-2016-070. 58, 111, 138

[216] M. L. Ahnen et al. [MAGIC and Fermi-LAT Collaborations], *"Limits to dark matter annihilation cross-section from a combined analysis of MAGIC and Fermi-LAT observations of dwarf satellite galaxies,"* JCAP **1602** (2016) no.02, 039 doi:10.1088/1475-7516/2016/02/039 [arXiv:1601.06590 [astro-ph.HE]]. 115, 120

[217] C. D. Carone and H. Murayama, *"Realistic models with a light U(1) gauge boson coupled to baryon number,"* Phys. Rev. D **52** (1995) 484 doi:10.1103/PhysRevD.52.484 [hep-ph/9501220]. 144

[218] J. A. Dror, R. Lasenby and M. Pospelov, *"New constraints on light vectors coupled to anomalous currents,"* Phys. Rev. Lett. **119** (2017) no.14, 141803 doi:10.1103/PhysRevLett.119.141803 [arXiv:1705.06726 [hep-ph]]. 94

[219] J. A. Dror, R. Lasenby and M. Pospelov, *"Dark forces coupled to nonconserved currents,"* Phys. Rev. D **96** (2017) no.7, 075036 doi:10.1103/PhysRevD.96.075036 [arXiv:1707.01503 [hep-ph]]. 94

[220] C. Patrignani et al. [Particle Data Group], *"Review of Particle Physics,"* Chin. Phys. C **40** (2016) no.10, 100001. doi:10.1088/1674-1137/40/10/100001 144

[221] Y. Nomura and J. Thaler, *"Dark Matter through the Axion Portal,"* Phys. Rev. D **79** (2009) 075008 doi:10.1103/PhysRevD.79.075008 [arXiv:0810.5397 [hep-ph]]. 119, 121, 122

[222] S. Ipek, D. McKeen and A. E. Nelson, *"A Renormalizable Model for the Galactic Center Gamma Ray Excess from Dark Matter Annihilation,"* Phys. Rev. D **90** (2014) no.5, 055021 doi:10.1103/PhysRevD.90.055021 [arXiv:1404.3716 [hep-ph]]. 119, 120, 121, 125

[223] M. Ajello *et al.* [Fermi-LAT Collaboration], *"Fermi-LAT Observations of High-Energy γ-Ray Emission Toward the Galactic Center,"* Astrophys. J. **819** (2016) no.1, 44 doi:10.3847/0004-637X/819/1/44 [arXiv:1511.02938 [astro-ph.HE]]. 120

[224] L. Goodenough and D. Hooper, *"Possible Evidence For Dark Matter Annihilation In The Inner Milky Way From The Fermi Gamma Ray Space Telescope,"* arXiv:0910.2998 [hep-ph]. 120

[225] D. Hooper and L. Goodenough, *"Dark Matter Annihilation in The Galactic Center As Seen by the Fermi Gamma Ray Space Telescope,"* Phys. Lett. B **697** (2011) 412 doi:10.1016/j.physletb.2011.02.029 [arXiv:1010.2752 [hep-ph]]. 120

[226] D. Hooper and T. Linden, *"On The Origin Of The Gamma Rays From The Galactic Center,"* Phys. Rev. D **84** (2011) 123005 doi:10.1103/PhysRevD.84.123005 [arXiv:1110.0006 [astro-ph.HE]]. 120

[227] K. N. Abazajian and M. Kaplinghat, *"Detection of a Gamma-Ray Source in the Galactic Center Consistent with Extended Emission from Dark Matter Annihilation and Concentrated Astrophysical Emission,"* Phys. Rev. D **86** (2012) 083511 Erratum: [Phys. Rev. D **87** (2013) 129902] doi:10.1103/PhysRevD.86.083511, 10.1103/PhysRevD.87.129902 [arXiv:1207.6047 [astro-ph.HE]]. 120

[228] C. Karwin, S. Murgia, T. M. P. Tait, T. A. Porter and P. Tanedo, *"Dark Matter Interpretation of the Fermi-LAT Observation Toward the Galactic Center,"* Phys. Rev. D **95** (2017) no.10, 103005 doi:10.1103/PhysRevD.95.103005 [arXiv:1612.05687 [hep-ph]]. 120, 123

[229] V. Bonnivard et al., *"Dark matter annihilation and decay in dwarf spheroidal galaxies: The classical and ultrafaint dSphs,"* Mon. Not. Roy. Astron. Soc. **453** (2015) no.1, 849 doi:10.1093/mnras/stv1601 [arXiv:1504.02048 [astro-ph.HE]]. 120

[230] C. Boehm, M. J. Dolan, C. McCabe, M. Spannowsky and C. J. Wallace, *"Extended gamma-ray emission from Coy Dark Matter,"* JCAP **1405** (2014) 009 doi:10.1088/1475-7516/2014/05/009 [arXiv:1401.6458 [hep-ph]]. 120

[231] E. Izaguirre, G. Krnjaic and B. Shuve, *"The Galactic Center Excess from the Bottom Up,"* Phys. Rev. D **90** (2014) no.5, 055002 doi:10.1103/PhysRevD.90.055002 [arXiv:1404.2018 [hep-ph]]. 120, 121

[232] D. E. Morrissey, T. Plehn and T. M. P. Tait, *"Physics searches at the LHC,"* Phys. Rept. **515** (2012) 1 doi:10.1016/j.physrep.2012.02.007 [arXiv:0912.3259 [hep-ph]]. 120

[233] J. M. No, *"Looking through the pseudoscalar portal into dark matter: Novel mono-Higgs and mono-Z signatures at the LHC,"* Phys. Rev. D **93** (2016) no.3, 031701 doi:10.1103/PhysRevD.93.031701 [arXiv:1509.01110 [hep-ph]]. 121, 122

[234] D. Goncalves, P. A. N. Machado and J. M. No, *"Simplified Models for Dark Matter Face their Consistent Completions,"* Phys. Rev. D **95** (2017) no.5, 055027 doi:10.1103/PhysRevD.95.055027 [arXiv:1611.04593 [hep-ph]]. 121, 122, 125

[235] M. Bauer, U. Haisch and F. Kahlhoefer, *"Simplified dark matter models with two Higgs doublets: I. Pseudoscalar mediators,"* JHEP **1705** (2017) 138 doi:10.1007/JHEP05(2017)138 [arXiv:1701.07427 [hep-ph]]. 122, 131

[236] G. C. Branco, P. M. Ferreira, L. Lavoura, M. N. Rebelo, M. Sher and J. P. Silva, *"Theory and phenomenology of two-Higgs-doublet models,"* Phys. Rept. **516** (2012) 1 doi:10.1016/j.physrep.2012.02.002 [arXiv:1106.0034 [hep-ph]]. 122

[237] J. F. Gunion and H. E. Haber, *"The CP conserving two Higgs doublet model: The Approach to the decoupling limit,"* Phys. Rev. D **67** (2003) 075019 doi:10.1103/PhysRevD.67.075019 [hep-ph/0207010]. 123

[238] M. Misiak et al., *"Updated NNLO QCD predictions for the weak radiative B-meson decays,"* Phys. Rev. Lett. **114** (2015) no.22, 221801 doi:10.1103/PhysRevLett.114.221801 [arXiv:1503.01789 [hep-ph]]. 124

[239] W. Grimus, L. Lavoura, O. M. Ogreid and P. Osland, *"A Precision constraint on multi-Higgs-doublet models,"* J. Phys. G **35** (2008) 075001 doi:10.1088/0954-3899/35/7/075001 [arXiv:0711.4022 [hep-ph]]. 124

[240] W. Skiba and J. Kalinowski, *"$B_s \to \tau^+\tau^-$ decay in a two Higgs doublet model,"* Nucl. Phys. B **404** (1993) 3. doi:10.1016/0550-3213(93)90470-A 125

[241] H. E. Logan and U. Nierste, *"$B_{s,d} \to \ell^+\ell^-$ in a two Higgs doublet model,"* Nucl. Phys. B **586** (2000) 39 doi:10.1016/S0550-3213(00)00417-X [hep-ph/0004139]. 125

[242] R. Aaij *et al.* [LHCb Collaboration], *"Measurement of the $B_s^0 \to \mu^+\mu^-$ branching fraction and search for $B^0 \to \mu^+\mu^-$ decays at the LHCb experiment,"* Phys. Rev. Lett. **111** (2013) 101805 doi:10.1103/PhysRevLett.111.101805 [arXiv:1307.5024 [hep-ex]]. 125

[243] S. Chatrchyan *et al.* [CMS Collaboration], *"Measurement of the B(s) to mu+ mu- branching fraction and search for B0 to mu+ mu- with the CMS Experiment,"* Phys. Rev. Lett. **111** (2013) 101804 doi:10.1103/PhysRevLett.111.101804 [arXiv:1307.5025 [hep-ex]]. 125

[244] [CMS and LHCb Collaborations], *"Combination of results on the rare decays $B^0_{(s)} \to \mu^+\mu^-$ from the CMS and LHCb experiments,"* CMS-PAS-BPH-13-007, LHCb-CONF-2013-012, CERN-LHCb-CONF-2013-012. 125

[245] C. Bobeth, M. Gorbahn, T. Hermann, M. Misiak, E. Stamou and M. Steinhauser, *"$B_{s,d} \to l^+l^-$ in the Standard Model with Reduced Theoretical Uncertainty,"* Phys. Rev. Lett. **112** (2014) 101801 doi:10.1103/PhysRevLett.112.101801 [arXiv:1311.0903 [hep-ph]]. 125

[246] A. J. Buras, R. Fleischer, J. Girrbach and R. Knegjens, *"Probing New Physics with the $B_s \to \mu^+\mu^-$ Time-Dependent Rate,"* JHEP **1307** (2013) 77 doi:10.1007/JHEP07(2013)077 [arXiv:1303.3820 [hep-ph]]. 125

[247] J. Kozaczuk and T. A. W. Martin, *"Extending LHC Coverage to Light Pseudoscalar Mediators and Coy Dark Sectors,"* JHEP **1504** (2015) 046 doi:10.1007/JHEP04(2015)046 [arXiv:1501.07275 [hep-ph]]. 125

[248] [CMS Collaboration], *"Search for a neutral MSSM Higgs boson decaying into $\tau\tau$ with 12.9 fb^{-1} of data at $\sqrt{s} = 13$ TeV,"* CMS-PAS-HIG-16-037. 126

[249] S. Banerjee, D. Barducci, G. Bélanger, B. Fuks, A. Goudelis and B. Zaldivar, *"Cornering pseudoscalar-mediated dark matter with the LHC*

and cosmology," JHEP **1707** (2017) 080 doi:10.1007/JHEP07(2017)080 [arXiv:1705.02327 [hep-ph]]. 126

[250] [CMS Collaboration], *"Search for Dark Matter produced in association with bottom quarks,"* CMS-PAS-B2G-15-007. 126

[251] C. Degrande, O. Mattelaer, R. Ruiz and J. Turner, *"Fully-Automated Precision Predictions for Heavy Neutrino Production Mechanisms at Hadron Colliders,"* Phys. Rev. D **94** (2016) no.5, 053002 doi:10.1103/PhysRevD.94.053002 [arXiv:1602.06957 [hep-ph]]. 126, 128

[252] R. V. Harlander, S. Liebler and H. Mantler, *"SusHi: A program for the calculation of Higgs production in gluon fusion and bottom-quark annihilation in the Standard Model and the MSSM,"* Comput. Phys. Commun. **184** (2013) 1605 doi:10.1016/j.cpc.2013.02.006 [arXiv:1212.3249 [hep-ph]]. 126

[253] C. G. Lester and D. J. Summers, *"Measuring masses of semi-invisibly decaying particles pair produced at hadron colliders,"* Phys. Lett. B **463** (1999) 99 doi:10.1016/S0370-2693(99)00945-4 [hep-ph/9906349]. 128

[254] C. G. Lester and B. Nachman, *"Bisection-based asymmetric M_{T2} computation: a higher precision calculator than existing symmetric methods,"* JHEP **1503** (2015) 100 doi:10.1007/JHEP03(2015)100 [arXiv:1411.4312 [hep-ph]]. 128

[255] G. Aad et al. [ATLAS Collaboration], *"Jet energy resolution in proton-proton collisions at $\sqrt{s} = 7$ TeV recorded in 2010 with the ATLAS detector,"* Eur. Phys. J. C **73** (2013) no.3, 2306 doi:10.1140/epjc/s10052-013-2306-0 [arXiv:1210.6210 [hep-ex]]. 128

[256] [ATLAS Collaboration], *"Expected performance of the ATLAS b-tagging algorithms in Run-2"*, ATL-PHYS-PUB-2015-022 128

[257] A. L. Read, *"Presentation of search results: The CL(s) technique,"* J. Phys. G **28** (2002) 2693. doi:10.1088/0954-3899/28/10/313 128

[258] [ATLAS collaboration], *"Search for new phenomena in the $Z(\to \ell\ell) + E_{\mathrm{T}}^{\mathrm{miss}}$ final state at $\sqrt{s} = 13$ TeV with the ATLAS detector,"* ATLAS-CONF-2016-056. 130

[259] [CMS Collaboration], *"Search for dark matter in* $\mathrm{Z} + E_{\mathrm{T}}^{\mathrm{miss}}$ *events using* 12.9 fb^{-1} *of 2016 data,"* CMS-PAS-EXO-16-038. 130

[260] P. Athron et al. [GAMBIT Collaboration], *"GAMBIT: The Global and Modular Beyond-the-Standard-Model Inference Tool,"* Eur. Phys. J. C **77** (2017) no.11, 784 Addendum: [Eur. Phys. J. C **78** (2018) no.2, 98] doi:10.1140/epjc/s10052-017-5513-2, 10.1140/epjc/s10052-017-5321-8 [arXiv:1705.07908 [hep-ph]]. 138, 139

[261] C. Balázs et al. [GAMBIT Collider Workgroup], *"ColliderBit: a GAMBIT module for the calculation of high-energy collider observables and likelihoods,"* Eur. Phys. J. C **77** (2017) no.11, 795 doi:10.1140/epjc/s10052-017-5285-8 [arXiv:1705.07919 [hep-ph]]. 138, 139

[262] T. Bringmann et al. [GAMBIT Dark Matter Workgroup], *"DarkBit: A GAMBIT module for computing dark matter observables and likelihoods,"* Eur. Phys. J. C **77** (2017) no.12, 831 doi:10.1140/epjc/s10052-017-5155-4 [arXiv:1705.07920 [hep-ph]]. 138, 139

[263] S. Caron, J. A. Casas, J. Quilis and R. Ruiz de Austri, *"Anomaly-free Dark Matter with Harmless Direct Detection Constraints,"* arXiv:1807.07921 [hep-ph]. 139

[264] S. El Hedri and K. Nordström, *"Whac-a-constraint with anomaly-free dark matter models,"* arXiv:1809.02453 [hep-ph]. 139